Dissertation

submitted to the

Combined Faculties for the Natural Sciences and for Mathematics

of the Ruperto-Carola University of Heidelberg, Germany

for the degree of

Doctor of Natural Sciences

presented by

M.Sc. Héctor Mauricio Castañeda Cortés,

born in Bogotá, Colombia.

Oral examination: February 1st, 2012

Laser assisted

α decay

Referees: **Hon.-Prof. Dr. Christoph H. Keitel**
Prof. Dr. Dirk Dubbers

Zusammenfassung

Angeregte oder kurzlebige Kerne zerfallen häufig durch die Emission von Alphateilchen. Dabei wird angenommen, dass die Alphateilchen bereits innerhalb des Mutterkerns vorgeformt vorkommen und in dessen Potentialtopf eingeschlossen sind. Der Alphazerfall wird in dieser Vorstellung als das Tunneln des Alphateilchens durch die Potentialbarriere betrachtet. In dieser Dissertation wird zum ersten Mal der Einfluss starker Laserfelder auf das Tunneln von Alphateilchen sowie auf die zugehörigen Alphazerfallsraten untersucht. Ganz allgemein kann der laser-assistierte Alphazerfall als laser-assistiertes Tunneln von quasistationären Zuständen betrachtet werden. Unsere dafür entwickelte theoretische Methode basiert auf der Komplexen-Trajektorien-Formulierung der sehr bekannten Strong-Field Approximation, die sonst vor allem für die Beschreibung der laser-induzierten Ionisation verwendet wird. Eine Erweiterung der Methode auf quasistationäre Zustände wird hier implementiert. Die Auswirkungen von sowohl statischen als auch monochromatischen Feldern im optischen und Röntgen Bereich auf die Kernlebensdauer und Emissionsspektren werden für eine Auswahl von alpha-zerfallenden Kernen untersucht. Unsere Ergebnisse zeigen, dass selbst für sehr starke Laserintensitäten die Zunahme des Zerfalls vernachlässigbar ist. Die relative Änderung befindet sich in einer Größenordnung von 10^{-3} für statische Felder mit elektrischen Feldstärken von 10^{15} V/m, von bis zu 10^{-8} für optische Felder mit Laserintensitäten von 10^{22} W/cm^2, bzw. von 10^{-6} für Röntgen Felder mit Laserintensitäten von 10^{24} W/cm^2. Dennoch hat der Laser einen großen Einfluss auf das Spektrum der Alphateilchen. Insbesondere kann es für starke Laserfelder mit optischen Frequenzen und Intensitäten von ca. 6×10^{22} W/cm^2 zur Rückstreuung der getunnelten Teilchen mit Potentialbarriere kommen. Die Dynamik des Alphateilchens in Laserfeldern mit Intensitäten unterhalb des Rückstreu-Grenzfalles wird untersucht.

Abstract

Excited or short-lived nuclei often decay by emitting alpha particles that are assumed to be preformed inside the nucleus and confined in the nuclear potential well. In this picture, α decay refers to the tunneling of the alpha particle through the potential barrier. In this thesis we investigate for the first time how strong laser fields can assist the tunneling of the alpha particle and thus influence the nuclear decay. Generally speaking, laser-assisted α decay can be described as laser-assisted tunneling of a quasistationary state, i.e, a slowly decaying state. Our theoretical treatment is developed starting from the complex trajectory formulation of the well-known strong-field approximation used to describe laser-induced ionization. We extend this formulation and develop a method to treat the decay of quasistationary states. The effect of both static and optical and x-ray monochromatic fields on the lifetimes and α-particle emission spectra are investigated for a number of α-emitting nuclei. We find that even at strong intensities, the laser-induced acceleration of the α decay is negligible, ranging from a relative modification in the decay rate of 10^{-3} for static fields of electric field strengths of 10^{15} V/m, to 10^{-8} for strong optical fields with intensities of 10^{22} W/cm^2, and to 10^{-6} for strong x-ray fields with laser intensities around 10^{24} W/cm^2. However, the effect of the external field is visible in the spectrum of emitted α particles, leading in the case of optical fields even to rescattering phenomena for intensities approaching 6×10^{22} W/cm^2. The dynamics of the alpha particle in laser fields of intensities below the rescattering limit is investigated.

In connection with work performed during the thesis, the following paper was published in a refereed journal:

Chapters 3 and 4:

- H. M. Castañeda Cortés, S. V. Popruzhenko, D. Bauer and A. Pálffy, *Laser assisted decay of quasistationary states*, New J. Phys. **13, 063007(2011).**

The following paper is to be submitted after completion of the thesis (November 2011):

Chapter 5:

- H. M. Castañeda Cortés, A. Pálffy and C. H. Keitel, *Laser assisted α decay.*

CONTENTS

CHAPTER 1

INTRODUCTION

1.1. The theory of α decay

Among the variety of channels in which a nucleus decays, the emission of α particles by the nucleus has been one of the most studied. The α decay channel in heavy and super heavy nuclei has provided information on the fundamental properties of nuclei far from stability, such as their ground state energies, the structure of their nuclear levels, shell effects, identification of new α emitting nuclei by the observation of the α decay chain and formation of clusters in the nucleus from microscopic considerations. Of all the fundamental properties of an α emitting nucleus, the α decay lifetime is one of the most important and, since the discovery of radioactivity in 1899 by Rutherford [Rut99], has been the focus of much theoretical modeling.

The model proposed by Gamow [Gam28] and Condon and Gurney [GC29] was the first successful description of this process by a quantum mechanism, namely the decay of quasistationary states (QS) via tunneling through a potential barrier. A QS state is defined as a long-lived state that eventually decays. The authors considered the parent nucleus as a system composed of a preformed α particle and a daughter nucleus. Initially, the preformed α cluster oscillates in the potential well formed by the nuclear interaction. The decay occurs when the particle tunnels through the potential barrier formed by the Coulomb interaction between the protons and the α particle and the daughter nucleus. Since the tunneling probability of the α particle is not zero, the initial state before the decay is considered to be QS. Using the tunneling mechanism, Gamow, Condon and Gurney calculated the penetrability of the tunneling α particle through the Coulomb barrier, finding the lifetimes of some α emitting nuclei. The main success of this model was the reproduction of the semi-empirical Geiger-Nuttall law that expresses the lifetimes of the α emitters in terms of the energies of the released α particles [GN11, GN12]. While these phenomenological models were successful in the reproduction of the experimental lifetimes, they did not provide a framework in which the formation of the α cluster in the parent nucleus could be understood. The necessity of finding a theory that described the microscopic interactions between the nucleons of the α particle and the daughter nucleus was pointed out by Preston in his work [Pre47].

The first model that took into account the microscopic features of the α decay came in 1954 by Thomas [Tho54] using the time-independent R matrix formalism proposed by Wigner and Eisenbud [WE47]. In the R-matrix formalism, the total configuration space is divided in two by the introduction of a spherical region. Its radius is the distance between the centers of mass of the α cluster and the daughter nucleus. The strong nuclear interactions between the nucleons dominate inside the spherical region, whereas the long-ranged Coulomb force between the protons of both systems dominates at long distances. Within this approach, the α decay is considered a two-step process. Firstly, the α particle is formed inside the region where the strong force dominates. The microscopic interactions between the nucleons of the parent nucleus play a significant role in the formation of the α cluster. While in the phenomenological model, the probability of formation of an α cluster in the parent nucleus is one, the preformation probability can be found from the microscopic considerations of the physical states before and after the decay. In that sense, the preformation probability is defined as the projection of the wavefunction of the parent nucleus upon the antisymmetric product of the wavefunction of the α cluster-daughter nucleus composed system. Subsequently the α particle may tunnel outside the nucleus. The penetrability through the Coulomb barrier is the tunneling probability of the α particle. In consequence, the nuclear width is the product of the formation amplitude and the penetrability.

Since this first microscopic model was proposed, several authors have improved this picture by including a wavefunction analysis, [Man57, Man60]. In particular, the model of Varga *et al.* showed using microscopic arguments, the necessity of a cluster being preformed inside the nucleus before the α decay can occur [VLL92]. Semiclassical methods like the Wentzel-Krammers-Brillouin (WKB) [Wen26, Kra26, Jef25, GP90] and the Two Potential Approach (TPA) [GK87] have also been used to find the lifetimes of unstable nuclei. These techniques have the advantage that they can be easily applied to more complex nuclei, provided that the tunneling barrier follows the semiclassical conditions. The WKB and TPA methods allow the lifetimes of α emitting nuclei to be calculated when the tunneling barrier includes microscopic interactions between the nucleons of the α cluster, and the daughter nucleus.

For example, in their work, Poenaru *et al.* used the WKB method to find the penetrability of the α particle and resulting lifetimes of α emitters, [PISG84]. Poenaru generalized existing fission theories to include α decay and cluster radioactivity, a development which became known as the Super Asymmetric Fission Model (SAFM) [PISG84]. In the frame of SFAM, the parent nucleus is formed by two asymmetric clusters which overlap. The interaction between the two asymmetric clusters follows a parabolic function in the overlapping region. In order to avoid the overestimation of the barrier heights and calculate accurately the penetrability through the barrier, a correction on the energy of the α cluster was introduced by Poenaru *et al.* [PISG84]. This correction is called the "zero vibration energy", and is found empirically. For more details of the validity of the WKB and TPA in the calculation of the lifetimes of α emitting nuclei and a critical view of the fitted values in SFAM, see [KCn07].

Basu further advanced the semiclassical description of alpha decay by including a more realistic mean-field nuclear potential. Basu [Bas03] assumed the parent nucleus to contain a preformed α particle that interacts with the spherical daughter nucleus, in a similar way to Gamow's phenomenological model [Bas03]. However,

unlike Gamow, the description of the mean-field nuclear potential takes into account the microscopic interactions between the nucleons. The nuclear potential is given by an effective interaction in which the matter densities of the spherical α particle and daughter nucleus are integrated together with the microscopic Michigan 3 Yukawa (M3Y) term. The M3Y term takes the form of two Yukawa-like potentials. The matter density of the α particle is represented by an exponential distribution, determined from $\alpha - \alpha$ scattering processes [SL79]. The daughter nucleus matter density is a Fermi distribution, characteristic of the liquid drop model.

Following the SFAM and the calculation of the preformation probability of the α cluster, Buck *et al.* [BJMP96, BMP92] proposed the precluster model, in which the α particle is moving around the daughter nucleus in orbits determined by the global quantum number. Similarly to the aforementioned phenomenological models, the α particle tunnels through tunneling barrier formed by the Coulomb and the nuclear potentials. The α decay lifetimes are calculated via the semiclassical limit of TPA. This model can be adapted to a wide range of nuclei and a variety of nuclear potentials, achieving a good agreement with the experimental lifetimes. Even as simplistic as it seems, the precluster model offers a transparent description of the α decay mechanism from a phenomenological point of view. Therefore, we adopted this as our fiducial model in the present work on laser-assisted α decays. A further description of this model as used in our method will be outlined in Chapter 2.

In summary, there is within the literature a well studied family of semiclassical methods, which have been effectively used to model α decay. The predicted lifetimes of these models have been verified by comparison with available experimental data [BMP91, CL10, Tul05]. Semiclassical techniques are therefore a valid method that can be used to investigate any potential variations in α decay rates.

1.2. Controlling the lifetimes of nuclear decays

Some long-lived α emitting actinides, such as ^{241}Am and several isotopes of Pu, have been found in transuranium nuclear waste [EWL04]. It would be of tremendous benefit if a method could be found to enhance the decay rate of such radioactive materials, and speed up their transition to less harmful materials. Several proposal and methods have been discussed in order to control the decay of radioactive isotopes.

One method that has been considered to alter nuclear lifetimes is screening from the cloud of electrons surrounding the nucleus. One of the first authors who worked on electronic screening was Salpeter, who found that when the nucleus is much smaller than the electron cloud, the cloud behaves as a weakly bound plasma [Sal54, RVB$^+$08]. For electrons described by the Debye-Drude model the screening is shown to have a strong dependance on the temperature of the weakly bound plasma. As the plasma of electrons cools down, it contracts, and the dependence on the temperature becomes weaker. In the limit of a strong bound plasma, the screening is completely independent of the temperature [RVB$^+$08].

Emery [Eme75] found that induced changes in the electronic cloud by chemical or environmental effects can alter the tunneling barrier, affecting the α decay lifetimes. As an example, the change in the decay rate of a stable α emitter, ^{226}Ra, whose lifetime is around 1600 years was calculated due to screening. However, the results

show that the calculated change in lifetime due to screening effects was negligible compared with the measured lifetime. After those disappointing results, the screening of the electrons was forgotten for a long time. It was brought back by Rolfs *et al.* [SRSC01, KBSR06, ALR87] in a slightly different context. Rolfs and his collaborators proposed that the influence of the screening in the change of the α decay lifetimes is magnified in a cold metallic environment. Following the work of Salpeter [Sal54], the quasi-free metallic electron cloud was treated as a Debye gas. The lifetimes of ^{210}Po and ^{226}Ra seemed to be reduced by several orders of magnitude in the cold metallic environment, a remarkable and exciting result found by Rolfs and his collaborators [KBSR06]. However, a huge controversy was generated with different arguments supporting and dismissing their result.

For instance, Zinner [Zin07] argued that the results obtained by Rolfs *et al.* in their work could not be correct, because the screening not only lowers the tunneling barrier, but also corrects the energy of α particles traversing through the barrier. The corrections to the energy and the tunneling barrier cancel each other and consequently the penetrability through the barrier remains unchanged. If the screening potential is not constant rather than changes over the radius scale of the outer turning point, the calculated change in the α decay lifetimes is considerably small.

Furthermore, Eliezer [EMVP09] found that the results by Rolfs *et al.* were not justified in the context of the Debye model. Following the Debye plasma model suggested by Rolfs *et al.* for α emitting nuclei in a cold metallic environment, Eliezer was able to determine some change in the α decay lifetimes of ^{212}Po and ^{236}Ra. Nevertheless, the results were far from the ones that Rolfs *et al.* found in his work. Experimental results by Jeppesen *et al.* [JBNW$^+$07] on ^{221}Fr, Stone *et al.* [SSL$^+$07] on the ^{224}Rn, ^{225}Ra and ^{227}Ac α decay chain, Su *et al.* [SLZ$^+$10] on ^{147}Sm and Wauters *et al.* on ^{221}Fr [WVB$^+$10] confirmed the negligible effect of the screening.

Another potential method of altering nuclear α decay rates is via the interaction with a strong laser field. For a long time, the possibility of inducing nuclear processes by the interaction with a laser was considered unthinkable. The experimental intensities were not strong enough to excite directly the nucleus, and the available photon energies were small compared to the characteristic energies of the nuclear transitions. Consequently, the nucleus-laser interaction matrix elements were too small to be significant [S.98]. In recent years, the possibility of affecting the nuclear reactions indirectly has been proposed by some authors [SAAH$^+$08], due to the continuous progress in the development of experimental laser facilities. Phenomena like photo-transmutation of nuclei were considered as a mechanism to alter nuclear properties by indirect interaction with a strong laser field.

Experiments of photo-transmutation of elements were performed by the groups of Magill and Ledingham. In their works, Magill *et al.* [MSE$^+$03] and Ledingham *et al.* [LMM$^+$03] used high energetic γ rays produced by bremmstrahlung of accelerated electrons in an ultra intense laser beam as sources to drive nuclear photo-transmutation of ^{129}I, which has a very long lifetime of million years. The laser field irradiated gold sample, driving the electrons into relativistic energies. Afterwards, the electrons were stopped in the gold target, generating γ bremmstrahlung radiation. This additional radiation helped catalyze the transmutation reaction of ^{129}I into another isotope of iodine with a lifetime of 25 minutes, ^{128}I via the emission of a neutron [LMM$^+$03].

With new experimental facilities like the Extreme Light Infrastructure (ELI) [Taj09] or the European X-Ray Free Electron Laser (XFEL [AP06, Alt97]), the direct interaction between strong lasers and nuclei can open new perspectives to explore nuclear properties and primarily establish the new field of Nuclear Quantum Optics, [BEK06, PEK08]. Furthermore, the control of nuclear reactions via direct interaction with strong laser fields would offer an alternative to change fundamental nuclear properties. Research towards these fields is supported by the recent significant increase in the available intensities and photon energies.

In particular, no theoretical work has described the direct influence of a strong laser field on spontaneous α decay so far. The interaction of α emitters with a strong laser field becomes feasible in new experimental laser facilities like ELI or XFEL, with higher peak power and higher photon energies, reaching regimes that were unthinkable some years ago. Therefore, the direct interaction with a strong laser is now an exciting new possibility which may alter α decay lifetimes.

1.3. Aims of this thesis

In the present work, *we aim to investigate whether the direct interaction with a strong laser field can affect the rate of spontaneous α decay and the momentum distribution of α emitting nuclei.* If such an effect were possible, it would have profound implications both for treatment of transuranic nuclear waste in which long-lived α emitters are present as well as for our understanding of nuclear processes.

It is well understood that lasers with lower intensities do not have enough power to modify the dynamics of the α particle during the tunneling through the Coulomb barrier. However, at large intensities, the laser may assist the α decay by altering the field-free dynamics of the α particle.

The laser-assisted tunneling (LAT) of the α particle can affect the spontaneous decays in two different ways, by modifying the field-free dynamics of the α particle in the classically forbidden region or by altering the dynamics once the α particle has left the barrier. In the first case, the values of the α decay lifetimes are modified by the direct interaction with the laser field. In the second case, the dynamics inside the barrier remain unchanged and there is no modification of the lifetimes. But due to the interaction with the external field, the momentum distribution of the α particle measured once the tunneling has taken place can be altered.

In the present work, we develop a general method to study the laser-assisted decay of a QS state in the multiphoton regime and apply it to the study of laser-assisted α decay processes. Our method is based on a well known non-perturbative approach for nonlinear ionization, proposed by Keldysh [Kel65]. This formalism, meanwhile known in its different realizations as the Keldysh-Faisal-Reiss model [Fai73, Rei80] or the Strong-Field Approximation (SFA) [Rei80] (for the present status of the SFA and its implementations see [Pop04, MPBB06]), is a well-established tool in strong-field atomic physics. The SFA allows to determine in a non-perturbative way the transition amplitude between an initial bound state and a final state, corresponding to the interaction between the tunneling particle and an electromagnetic wave. While the plain formulation of SFA is quite accurate to describe the dynamics of laser-induced processes in short range potentials, it fails when it comes to study potentials

with a long range tail, like the Coulomb barrier the α particle tunnels through in α decay. Plain SFA also fails to describe laser-assisted phenomena involving QS initial states, rather than bound states.

A formulation of the SFA in terms of complex classical trajectories, known as the Imaginary Time Method (ITM) brings a deeper understanding of the tunneling process in the presence of strong fields, and works very well in the semiclassical regime. Within the ITM, the tunneling particle follows a trajectory in complex times during its subbarrier motion, and in real time afterwards. Using the saddle-point method, the transition amplitude described by the plain SFA formulation can be expressed in terms of the classical action evaluated on the trajectories of the particle while is traversing the tunneling barrier and after leaving the classically forbidden region [Pop04, PP67].

In the dynamics of ionization, the ITM formulation of the SFA was used efficiently to introduce corrections on the transition amplitude by cause of the long-range interaction. By the introduction of the Coulomb corrections via the ITM on the transition amplitude, the ionization decay rates [PP67, PMPB08, PMPB09] and the photoelectron momentum distributions [PPB08, PB08, HRG$^+$11, YPVB10] are calculated accurately in the multiphoton regime.

Due to the asymptotic behavior of the QS wavefunction at large distances, the definition of the transition amplitude by the plain SFA and its ITM formulation fail to give an appropriate description of processes that involve the interaction between strong laser fields and QS states. Therefore, the ITM version of the transition amplitude must be modified. In this thesis, *we develop a method to include the characteristics of the QS state and the prefactor of the field-free decay in the ITM formulation of the transition amplitude to describe the laser-assisted decay of QS states.* The formalism we develop to study LAT of QS states in the presence of strong laser fields is detailed in the Chapter 3 of this thesis. In the form presented in the present work, restricted to the nonrelativistic limit, our method should be equally applicable to descriptions of different physical systems under standard semiclassical conditions.

Since the spontaneous α decay rates can be calculated using semiclassical methods like WKB or TPA, we can assure that the tunneling barrier the α particle traverses follows the semiclassical conditions. For an incoming laser field with an optical wavelength, the number of photons that the α particle absorbs or emits during a pulse is large and thus the conditions required by SFA are completely fulfilled. Consequently, the laser-assisted α decay can be studied by the implementation of the method we develop to study laser-assisted decay of QS states. The laser-assisted α decay lifetimes are calculated with our method and compared with the field-free lifetimes. We find that for static electric fields of high intensities, the laser-assisted α decay lifetime can decrease by 10^{-4}, while for monochromatic fields the relative change is much smaller, on the order of 10^{-8} for intensities close to the recollision threshold. The spectrum of the emitted α particles, on the other hand, is strongly affected by a monochromatic laser field, leading to a broad energy distribution at the detector. Furthermore, for optical fields, with increasing intensities recollisions of the emitted α particles with the daughter nucleus can occur. We investigate here qualitatively the recollision threshold for various α emitters and determine the behaviour of the tunneling exponent.

1.4. Structure of this thesis

In order to achieve our aim of the present work, we start in Chapter 2 by presenting the framework necessary to understand the α decay mechanism. We review the phenomenological model by Condon and Gamow and Gurney [Gam28, GC29] proposed to describe the spontaneous α decay. The calculations of the field-free decay rates from the time-independent Schrödinger equation are presented. In the same Chapter, an overview of some of the semiclassical methods which have been used by several authors to obtain the lifetimes of the α emitters is given. Finally, the most important aspects of the precluster model, proposed by Buck *et al.* [BMP90a, BMP91] are discussed extensively, since this is the model that we consider to characterize the field-free tunneling barrier in our theoretical study of laser-assisted α decay. The decay rate found by Buck *et al.* in [BMP90a] is later used as field-free benchmark, necessary to calculate the transition amplitude and the laser-assisted α decay rates.

In Chapter 3, we review the most important aspects of the SFA in the case of laser-induced processes and the modification of SFA implemented for processes that involve an initial QS state. As a next step, the foundations of ITM are reviewed and the ITM formulation of SFA is reviewed in detail. Finally, at the end of the Chapter, our new method is developed based on the ITM formulation of SFA that considers the characteristics of the initial QS state. With our new method, we are able to describe several laser-assisted processes, most importantly, the laser-assisted α decay.

In Chapter 4, a test case for our newly developed method is studied, namely the LAT through a one-dimensional rectangular barrier. As external field we consider both the case of a static electric field as well as of monochromatic and short-pulse laser fields. For various barrier parameters, our results reproduce an important qualitative conclusion of earlier studies [NR64, BMSS83, BSS84a, BSS84b], namely that depending on the parameters, two different regimes of decay are realized (i) when the spectrum is strongly affected without a modification of the total decay rate and (ii) when the rate of decay is also affected. These two regimes are also referred to as "exclusive" and "inclusive", respectively. In addition, the LAT probabilities in the presence of a short pulse are compared with the numerical solution of the time-dependent Schrödinger equation. We find a remarkable agreement in the qualitative and quantitative behavior of the momentum distribution.

In Chapter 5, we study the laser-assisted α decay of some medium-mass and heavy nuclear resonances, applying the method we have developed in Chapter 3. We investigate the cases of ^{106}Te, ^{162}W, ^{212}Po, ^{150}Dy, ^{238} U and ^{244}Cm. The parent nucleus is described in the frame of the precluster model, proposed by Buck *et al.* [BMP90a] and discussed in Chapter 2. We compare the results obtained by the implementation of our method in the limit of low-frequency laser field, i.e. static field, with results obtained using the WKB method. The calculated lifetime by ITM is in perfect agreement with the theoretical lifetime calculated using semiclassical methods like WKB in the low-frequency limit, showing the consistency of ITM. Next, we considered the laser-assisted α decay in the presence of a monochromatic laser field. We study the dynamics of the α particle during its subbarrier motion and once it leaves the barrier. The laser-assisted decay rates and lifetimes as well as the energy spectra of the tunneled particles for the case of a monochromatic laser field are calculated. We find that for the typical α decay parameters, we are deeply within the exclusive regime, for which the effect of the field on the lifetimes of α emitters is negligible. The spec-

trum however is strongly affected by the laser field, which modifies the dynamics of the α particle after the tunneling. With increasing intensities, recollisions with the daughter nucleus may occur. Although the effects of recollision are not fully taken into account in the development of our method, the laser-field threshold intensity at which the recollision effects become significant is found. Qualitatively, the influence of the recollision in the dynamics of the α particle is demonstrated by determining the behavior of the imaginary part of the semiclassical action.

Conclusions and Outlook are presented in Chapter 6. Atomic units are used throughout this thesis in Chapters 3 and 4 as specified. We detail our choice of units in Appendix A.

CHAPTER 2

α CLUSTERING IN NUCLEI

The α emission from unstable nuclei has allowed us to study interesting properties of the structure of the light and heavy nucleus. Recently, the experimental observation of α decay has been used to find exotic nuclei in the superheavy regime, and extract information about the drip lines of heavy and superheavy nuclear resonances. The first theoretical model that described the α emission in nuclei was proposed by Gamow and by Condon and Gurney [Gam28, GC29]. The connection between the tunneling through a potential barrier and the emission of an α particle has been used used in several approaches after Gamow and Condon's work. The lifetimes of the α decay channel have been calculated using different approaches, using either phenomenological or microscopical models to characterize the nuclear interaction. In this chapter, we review some phenomenological methods that have been proposed to describe the dynamics of the α decay via tunneling through the Coulomb barrier. In addition, we review two of the most used semiclassical methods for the calculation of spontaneous α decay rates. Finally, we describe the precluster model proposed by Buck et al. *[BMP90a, BMP91], which is the approach taken in the present work to characterize the α cluster-daughter nucleus system and the tunneling barrier in the laser-assisted α decay.*

The nuclear α decay process was one of the first nuclear phenomena observed experimentally. In 1899, Ernest Rutherford discovered that there were three types of radioactive emission from nuclei, namely, α, β and γ radiation. Rutherford was able to demonstrate the composition of the emitted α particles, and later on, introduced the concept of half life to describe the nature of the nuclear decay. The half life is defined as the time over which the number of radioactive nuclei decays to half of their original number [Raz03]. Following its discovery, the α emission from nuclear resonances was actively studied. Most of the nuclear α emitters are medium-mass, heavy and superheavy nuclei. The medium-mass nuclei are characterized by proton number between $50 \leq Z \leq 82$ and mass number $A \geq 100$. The heavy nuclei have proton numbers in the range of $82 < Z \leq 96$ and number of nucleons $A \geq 208$. The superheavy nuclei have a number of protons greater than a hundred. The medium-mass and heavy α decaying nuclei found in nature are organized in three naturally

radioactive chains of nuclear α emitters, known as the uranium, actinium and thorium series, [PB75]. The three chains start in isotopes of uranium, actinium and thorium elements (^{238}U, ^{235}U and ^{232}Th). After a limited number of radioactive transmutations, they become stable isotopes of Pb. However, the medium and heavy α emitting nuclei are not the only ones that undergo α decay, as there is evidence of the existence of light α emitter nuclei such as ^{5}Li, ^{8}Be and ^{12}C, [HDWW53, GMN01].

The dynamics of the nucleons of the parent nucleus are well described by the microscopic models of the nuclear structure [Man57, Tho54], as was mentioned in the introduction. As the α particle is strongly bound, it is feasible for the protons and neutrons of the parent nucleus to combine themselves in stable clusters substructures within the nucleus [Fre07]. As these clusters are stable, they can survive for a long time. The preformed α clusters propagate unperturbed within the parent nucleus and interact with the daughter nucleus via the Coulomb interaction. In the first approximation, they are considered as a separate physical system with no internal structure neglecting any internal correlation between the paired nucleons. This is the phenomenological approach that Gamow [Gam28], Condon and Gurney [GC29] and Preston [Pre47] took in their work.

The formation of α particles at the nuclear surface is favored in the nuclear theory, due to the stability and large excitation energy (around 20.2 MeV) of the α particle [TWH92, Moh08]. However, the formation of the α clusters in the nucleus was not fully understood in phenomenological models, until the microscopic considerations between the nucleons of the parent nucleus were taken into account. Brink and Castro found that the formation of nucleon clustering in the parent nucleus is favored by energetic constrains [BC73]. In their work, the formation of α clusters in nuclear matter was studied by considering a lattice of α particles, and considering the possible correlations between the preformed α clusters within the lattice. Comparing the plane wave model for nuclear matter with the α clustering lattice model, Brink and Castro found that for the normal density of nuclear matter, the correlation effects that allow the formation of clusters do not play a role in the interior region of the parent nucleus, only on its surface. When the nuclear density decreases to one third of the normal nuclear matter density, there is a phase transition to the lattice structure, favoring the condensation of α clusters on the parent nucleus surface, as Brink and Castro concluded in their work [BC73].

The most natural way of describing the rate of α cluster formation in the nuclear matter is by by introducing the concept of a preformation probability that can be calculated for every α decaying system [Fre07]. Preformation probabilities are determined by microscopic interactions between the nucleons in the range where the strong interaction dominates over the Coulomb force between the protons of the α cluster and the daughter nucleus. In the first model that included microscopic interactions between the nucleons of the parent nucleus by Thomas [Tho54], the preformation probability of the α cluster in the parent nucleus is defined as the projection of the total wavefunction of the parent nucleus on the final state corresponding to the α cluster-daughter nucleus system. In some models, the preformation probabilities are fitted from experimental data of scattering reactions, reproducing the spontaneous α decay lifetimes [XR05]. In others, the preformation probability is calculated from microscopic considerations from the definition by Thomas including the definition of the final state as a superposition of the nuclear single shell model and the state of the daughter nucleus-α cluster physical system, [VLL92]. The theoretical calculation

of lifetimes depends on the value of the preformation probabilities. For simplicity in some models, the preformation probability is taken as unity, but this can lead to discrepancies with respect to the experimental lifetimes.

In general, the lifetimes of the α emitting nuclei in the three naturally radioactive chains are many orders of magnitude longer than the typical times of nuclear motion scale (around 10^{-21} seconds). In that sense, the state of the nucleus can be considered stationary. The lifetimes of the α emitters follow a semiempirical rule, which comes from the dynamics of the α decay. This semi-empirical law, called the Geiger-Nuttall law, determines the relation between the released α particle energy with the decay half life [GN11, GN12, ME69],

$$\log \Gamma = a + b \log\big(R_\alpha\big). \tag{2.1}$$

Here, a and b are empirical constants that are found from logarithmic plots of experimental data. R_α represents the linear range, and it is "a direct measure of the α energy " [ME69]. In his work, Geiger was able to find a direct relation between R_α and the initial velocity of the particle, known as Geiger's rule,

$$R_\alpha = c_1 v_\alpha^3, \tag{2.2}$$

here c_1 is a proportionality constant.

One of the most successful results achieved by the phenomenological model of Gamow [Gam28], and Condon and Gurney [Gam28] was the reproduction of the Geiger-Nuttall law, Eq. (2.1). By making the assumption that the α particle is preformed within the nucleus and then escapes the nucleus entirely, the initial state of the α particle can be considered quasistationary (QS). In consequence, the α decay is the perfect example of the decay of a QS state via tunneling.

2.1. Phenomenological Gamow model and the description of the α decay by tunneling

The α decay process is considered to be a two step process. Firstly, the α particle is preformed on the surface of the parent nucleus. The radius of the parent nucleus is defined as [PB75]

$$R_{\mathrm{p}} = c_0 A_p^{\frac{1}{3}}. \tag{2.3}$$

Here c_0 is a constant that is fitted from experimental data in order to get the correct lifetimes. Its value oscillates between 1.2 and 1.5 fm. A_p is the number of nucleons of the parent nucleus. The α particle is assumed to be a boson, and its inner structure is neglected. Once the α particle is preformed with a probability given by the preformation factor[1] P_α, the nuclear decay is reduced to a two body problem. The fundamental properties of the α decay can then be determined from the dynamics of the α particle as it tunnels through the potential barrier formed from the interaction between the daughter nucleus and the α preformed cluster.

Initially, the preformed α particle is confined in a spherically symmetric potential well that describes the mean-field nuclear potential. The α particle has an initial

[1]The definition of the preformation factor is still a matter of controversy.

energy E, related with the Q_α value of the nuclear process,

$$Q_\alpha = m\mathrm{p} - m_\alpha - m_\mathrm{d}, \tag{2.4}$$

with m_α, m_d and m_p being the masses of the α particle, the daughter and the parent nuclei, respectively. The spontaneous α decay cannot occur as long as the mass of the products of the decay is larger than the mass of the parent nucleus. That means that the Q_α value of the spontaneous decay is greater than zero. Due to the short range of the nuclear forces, the nuclear interaction is assumed to vanish outside of the surface of the parent nucleus. Therefore, in this model there is no intermediate region where the nuclear and Coulomb interaction overlap, and the tunneling barrier suffers a discontinuity at the R_p. At large distances, the Coulomb force dominates the interaction between the preformed cluster and the daughter nucleus system.

There are some microscopical models in which the interactions between the nucleons of the α cluster and the daughter nucleus are considered, and the densities of the nuclear matter need to be defined for the cluster and the daughter nucleus [BMP92, XR05]. Mean-field potentials can be added to represent the microscopic properties of the interaction, allowing higher accuracies to be achieved in the calculations of the lifetimes, [ICLD91, OR07]. This parametrization of the nuclear densities allows effects like Pauli blocking between the nucleons or deformation of the parent nucleus to be included, as was introduced by Xu and Ren, [XR06]. If the microscopic interactions between the nucleons of the parent nucleus are included in the characterization of the mean nuclear potential, the tunneling barrier traversed by the α particle is smooth, and the discontinuity in the parent radius R_p disappears. Including such microscopic considerations into phenomenological models leads to improvements in the theoretical estimate of the lifetime of the α emitters, as shown by Xu and Ren [XR05] and Basu [Bas03] amongst others.

In this thesis, we work with the precluster model, a phenomenological model based on the approach proposed by Gamow and Condon and Gurney. We do not consider the microscopic features of the interaction between the nucleons of the α particle and the daughter nucleus for simplicity. If an effect of the laser upon α lifetimes is seen, the calculation can later be performed including microscopic considerations.

The α particle spends most of the lifetime of the decay process, bouncing back and forth inside the potential well, with a frequency identified as the "assault frequency". The assault frequency is given by,

$$\nu_\mathrm{assault} = \frac{\hbar\kappa_\mathrm{well}}{2m_\mathrm{r}R_\mathrm{p}}, \tag{2.5}$$

where κ_well is the wavenumber of the α particle confined in the nuclear potential well and m_r is the reduced mass of the α cluster-daughter nucleus system,

$$m_\mathrm{r} = \frac{m_\alpha m_\mathrm{d}}{m_\mathrm{d} + m_\alpha}. \tag{2.6}$$

Here, m_α is the mass of the α particle, whereas m_d is the mass of the daughter nucleus.

The Coulomb potential forms a barrier that the α particle classically cannot pass, since it does not have enough energy to overcome it. However, Gamow, Condon and Gurney used the concept of quantum tunneling in order to explain the release of

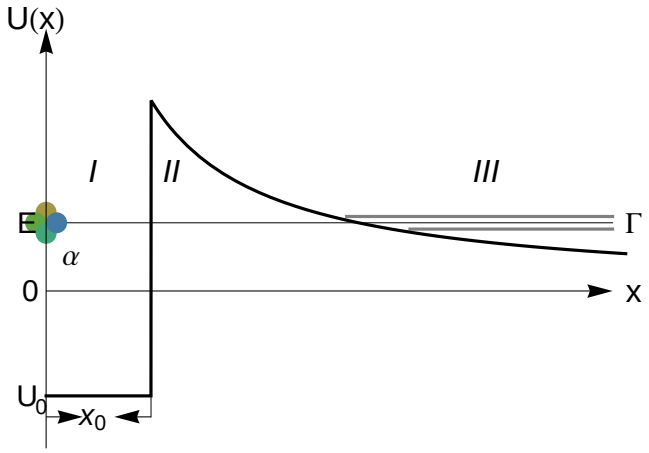

Figure 2.1: Sketch of the phenomenological model of the α decay, proposed by Gamow in 1928 and Condon and Gurney, [Gam28, GC29]. The α particle is preformed in the surface of the parent nucleus, and eventually tunnels through the barrier formed by the Coulomb potential.

the α particle. Since the potential barrier has a finite height, the initial state of the system is a QS state, rather than a bound one. The α particle tunnels through the barrier when the α decay occurs, and the penetrability through the Coulomb barrier is proportional to the tunneling probability.

As the parent nucleus is assumed to be spherical, the rotational and vibrational degrees of freedom are neglected in the phenomenological model, such that the deformations of the parent nucleus are not taken into account in the dynamics of the α decay [PB75]. When the system is assumed to be spherically symmetric, there is an additional term that appears naturally in the time-independent Schrödinger equation, which corresponds to the so called "centrifugal barrier". This additional term increases the tunneling barrier the particle traverses when the relative angular momentum L between the components of the physical system is not zero. As Marmier defined it in his book, the physical meaning of the centrifugal barrier is associated with "a rotational energy related to the motion of colliding particles about their common center of mass", [ME69]. It is written as $L(L+1)/2m_{\mathrm{r}}r^2$. Consequently for $L = 0$, the centrifugal barrier vanishes.

Some α emitters are characterized by an even number of protons and neutrons and decay into the ground state of even-even nuclei. Since the angular momentum of the α particle is zero in its ground state, the centrifugal barrier is defined in terms of the relative angular momentum between the α particle and the daughter nucleus. Therefore, if the relative angular momentum is zero, there is no effective contribution of the centrifugal barrier and the tunneling barrier is only given by the superposition of the nuclear interaction and the Coulomb potential.

2.1.1. Solution of the tunneling problem through a Coulomb barrier

According to what Gamow, Condon and Gurney proposed in their model, the α decay rate is proportional to the tunneling probability of the α particle tunneling through the Coulomb barrier. The tunneling probability can be found using different

approaches. Due to the analytical properties of the Coulomb barrier and the range of energies of the α particle, semiclassical methods like the Wentzel-Krammers-Brillouin method (WKB) have proved to be accurate in the theoretical calculation of lifetimes of α emitters, as it will be discussed later in this chapter.

The wavefunction of the physical system is found from the Schrödinger equation. If the α particle in the potential well is a QS state, then the physical considerations that must be taken into account in order to determine the total state of the system are

- the wave function of the QS state $\psi_\alpha(x,t)$ must be regular at the origin,
- the QS wave function must represent an outgoing wave at $x \gg x_0$, in the asymptotic limit where $x \to \infty$.

The decay rates can be found using the exact calculation of the tunneling probability through a Coulomb barrier. We start from the time-independent Schrödinger equation, as it was written in the book "Nuclear Physics" by Srivastava [Sri06],

$$-\frac{\hbar^2}{2m_\mathrm{r}}\nabla^2\psi_\alpha(r) + \Big(V(r) - E\Big)\psi_\alpha(r) = 0, \tag{2.7}$$

and using the assumption that the parent nucleus is spherically symmetric, the radial part of the wave function ψ_α takes the form

$$\frac{d^2u_l}{dr^2} + \frac{2m_\mathrm{r}}{\hbar^2}\Big(E - V(r) - \frac{L(L+1)\hbar^2}{2m_\mathrm{r}r^2}\Big)u_l(r) = 0. \tag{2.8}$$

The total wavefunction of the preformed α cluster-daughter nucleus system takes the form

$$\psi_\alpha(r) = \frac{u_l(r)}{r}Y_{lm}(\theta,\varphi). \tag{2.9}$$

The equation of the radial component $u_l(r)$, Eq. (2.8) is exactly the one-dimensional Schrödinger equation for an effective potential given by $V(r) + \frac{L\left(L+1\right)\hbar^2}{2m_\mathrm{r}r^2}$. The second term is the centrifugal barrier described earlier in this chapter. Taking $\rho = k_0 r$, with $k_0^2 = 2m_\mathrm{r}E/\hbar^2$, Eq. (2.8) can be written as [Sri06]

$$\frac{d^2u_l}{d\rho^2} + \left(1 - \frac{\eta}{\rho} - \frac{L\Big(L+1\Big)\hbar^2}{2m_\mathrm{r}r^2}\right)u_l = 0. \tag{2.10}$$

Here, $\eta = \left(\frac{2Ze^2}{\hbar}\right)\sqrt{m_\mathrm{r}/E}$. The dynamics of the α particle after leaving the barrier is determined by the Coulomb interaction. In consequence, the solutions of Eq. (2.10) are written in terms of the regular and irregular Coulomb functions $F_l(\rho)$ and $G_l(\rho)$. Asymptotically, at large r, the Coulomb functions have the following behavior [AS64, Sri06]

$$F_L(\rho) \underset{r\to\infty}{\to} \sin\Big(\rho - \eta\log(2\rho) - \frac{L\pi}{2} + \mathrm{arg}\Gamma\big(L+1+i\eta\big)\Big), \tag{2.11}$$

$$G_L(\rho) \underset{r\to\infty}{\to} \cos\Big(\rho - \eta\log(2\rho) - \frac{L\pi}{2} + \mathrm{arg}\Gamma\big(L+1+i\eta\big)\Big). \tag{2.12}$$

As mentioned previously, the radial part of the wavefunction at large distances is expected to take the form of outgoing waves. This corresponds to the Sommerfeld

radiation condition. The outgoing solution can be expressed without any difficulty in terms of the Coulomb functions [Sri06]

$$u_l(\rho) = C_0\Big(G_L(\rho) + iF_L(\rho)\Big). \tag{2.13}$$

The regular Coulomb function vanishes at the origin, and, "increases as a function of the distance inside the Coulomb barrier" as Delion explained in his review [Del10]. On the other hand, the irregular Coulomb function diverges at the origin, but decreases with distance, and asymptotically vanishes at large distances. Alternatively, the wavefunction outside of the barrier can be expressed in terms of the Hankel functions $H_l^{(-)}(\eta,\rho)$ and $H_l^{(+)}(\eta,\rho)$ [Del10]

$$u_l(\rho) = \frac{i\exp(i\delta_l(E))}{2}\Big(H_l^{(-)}(\eta,) - S_l(E)H_l^{(+)}(\eta,)\Big). \tag{2.14}$$

In this definition, the function $\delta_l(E)$ is the scattering phaseshift, and the term $S_l(E)$ is the scattering matrix, which has all the physical information of the physical transition from the initial to the final state. There is a strict relation between the scattering phaseshift and the S matrix from quantum scattering theory [BPZ69, Del10]

$$S_l(E) = \exp(2i\delta_l(E)). \tag{2.15}$$

The S matrix has well defined properties from the behavior of the solutions of the Schrödinger equation,

$$\begin{aligned} S_l(E) &= \Big(S_l^{-1}(E)\Big)^*, \\ S_l(k_0(E)) &= \Big(S_l^{-1}(-k_0(E))\Big). \end{aligned} \tag{2.16}$$

Using the continuity of the wavefunction and its derivative at $r = x_0$, a condition on the radial part of the wavefunction inside the well (region I in Fig. 2.1) [Sri06]

$$\frac{x_0}{u_l(x_0)}\frac{du_l(x)}{dx}\Big|_{x=x_0} = \frac{k_0x_0\Big(G_l'(x_0) + iF_l'(x_0)\Big)}{G_l(x_0) + iF_l(x_0)}. \tag{2.17}$$

The tunneling barrier determines three different regions, as depicted in Fig. 2.1. The wavefunction takes a particular analytical form depending on the properties of the potential $V(r)$ in that region. In [Win54], the author used the fact that when the α particle is not close to a turning point, the Coulomb functions can be written as,

$$G_L(\rho) = |\Phi(\rho)|^{-\frac{1}{4}}\exp\big(\omega(\rho)\big), \tag{2.18}$$

$$F_L(\rho) = \frac{1}{2}|\Phi(\rho)|^{-\frac{1}{4}}\exp\big(-\omega(\rho)\big). \tag{2.19}$$

In the expression above, the following quantities have been defined

$$|\Phi(\rho)| = \frac{2\eta}{\rho} + \frac{\Big(L+\frac{1}{2}\Big)^2}{\rho^2} - 1, \tag{2.20}$$

$$\omega\big(\rho\big) = \int_\rho^{\frac{2k_0Z}{E}} |\Phi(\xi)|^{\frac{1}{2}}d\xi. \tag{2.21}$$

The first term $2\eta/\rho$ corresponds to the effective potential the α particle tunnels through. There is a distinction between the usual form of the centrifugal barrier, and the one that appears in Eq. (2.21). The numerator in the L depending term corresponds to a modification implemented by Langer [Lan37]. The Langer modification to the centrifugal barrier will be explained in detail in the description of the semiclassical methods, later on in this chapter.

The asymptotic forms of the Coulomb functions, Eq. (2.18) show the exponential decreasing of the real part of the radial wavefunction $u_l(r)$, inside the barrier. The imaginary part of the radial wavefunction, given by the regular Coulomb function $F_L(r)$ increases with the distance and $|\Phi(\rho)|$ becomes negative in the limit where $\rho \to \infty$. It can be seen that the radial wavefunction has an oscillating behavior, representing traveling waves. Taking the derivative of the Coulomb functions,

$$G_L(\rho) = -\frac{1}{4}|\Phi(\rho)|^{-\frac{5}{4}} \exp\big(\omega(\rho)\big)\frac{d|\Phi(\rho)|}{d\rho} + |\Phi(\rho)|^{\frac{1}{4}} \exp\big(\omega(\rho)\big)|\frac{d|\Phi(\rho)|}{d\rho}, \tag{2.22}$$

$$F_L(\rho) = -\frac{1}{8}|\Phi(\rho)|^{-\frac{5}{4}} \exp\big(-\omega(\rho)\big)\frac{d|\Phi(\rho)|}{d\rho} - \frac{1}{2}|\Phi(\rho)|^{\frac{1}{4}} \exp\big(-\omega(\rho)\big)\frac{d|\Phi(\rho)|}{d\rho}, \tag{2.23}$$

the logarithmic derivative of the wavefunction can be found explicitly, according to Eq. (2.17). The logarithmic derivative evaluated at x_0 takes the form

$$\frac{x_0}{u_l(x_0)}\frac{du_l(x)}{dx}\Big|_{x=x_0} = k_0 x_0 \frac{d|\Phi(\rho)|}{d\rho}\left[-\frac{|\Phi(\rho)|^{-1}}{4} + \frac{1 - \frac{i\exp\left(-2\omega(\rho)\right)}{2}}{1 + \frac{i\exp\left(-2\omega(\rho)\right)}{2}}\right]. \tag{2.24}$$

The expression above is exactly the same expression Preston derived in his work on α decay, [Pre47]. Defining $\gamma = \frac{1}{4}|\Phi(\rho)|^{\frac{-3}{2}}\frac{d|\Phi(\rho)|}{d\rho}$, the logarithmic derivative is given by

$$\frac{x_0}{u_l(x_0)}\frac{du_l(x)}{dx}\Big|_{x=x_0} = -k_0 x_0 \left[\frac{|\Phi(\rho)|^{\frac{1}{2}}\Big(\big(1+\gamma\big) - \frac{i\big(1-\gamma\big)\exp(-2\omega)}{2}\Big)}{1 + \frac{i\exp(-2\omega)}{2}}\right]\Bigg|_{x_0}. \tag{2.25}$$

If k_0 is real, Eq. (2.24) cannot be satisfied. The condition on the internal wavefunction in region I demands that this should be regular in the origin. The continuity of the wavefunction and its derivative at the radius where the Coulomb potential is the only interaction is only fulfilled by a complex wavenumber, [Del10]. The imaginary part of the energy is associated with the decay rate of the QS, Γ, such that the total energy the tunneling particle has is

$$E_T = E - \frac{i\Gamma}{2}. \tag{2.26}$$

Those states with complex energies are called "Gamow states" (GS). Since the QS states are identified with resonant states, the GS are associated with resonant poles of the S matrix, located in the second Riemannian or "unphysical" sheet of the complex energy plane, where $\mathrm{Im}(E_T) \leq 0$. The time evolution of the GS follows an exponential decay law, well known in the decay of QS states.

If $\Gamma \ll E$, then the logarithmic derivative of the wavefunction in the region I can be

expanded as

$$\begin{aligned}&\frac{x_0}{u_l^{\mathrm{I}}(x_0)}\frac{du_l^{\mathrm{I}}(x)}{dx}\Big|_{x=x_0}= \\ &\left(\frac{x_0}{u_l^{\mathrm{I}}(x_0)}\frac{du_l^{\mathrm{I}}(x)}{dx}\Big|_{x=x_0}\right)\Bigg|_{E=E}-\frac{i\Gamma}{2}\frac{d}{dE}\left(\frac{x_0}{u_l^{\mathrm{I}}(x_0)}\frac{du_l^{\mathrm{I}}(x)}{dx}\Big|_{x=x_0}\right)\Bigg|_{E=E}\end{aligned} \tag{2.27}$$

The real part of the Eq. (2.24) must be equal to the real part of Eq. (2.27). Thus,

$$\left(\frac{x_0}{u_l^{\mathrm{I}}(x_0)}\frac{du_l^{\mathrm{I}}(x)}{dx}\Big|_{x=x_0}\right)\Bigg|_{E=E}=-\frac{k_0x_0|\Phi(\rho)|^{\frac{1}{2}}\left(1+\gamma-\frac{\exp\left(-4\omega(\rho)\right)\left(1-\gamma\right)}{4}\right)}{1+\frac{\exp\left(-4\omega(\rho)\right)}{4}}. \tag{2.28}$$

From the imaginary part of the logarithmic derivative of the wavefunction, we find that

$$\Gamma=\left[\frac{d}{dE}\left(\frac{x_0}{u_l^{\mathrm{I}}(x_0)}\frac{du_l^{\mathrm{I}}(x)}{dx}\Big|_{x=x_0}\right)\Bigg|_{E=E}\right]^{-1}\frac{2k_0x_0|\Phi(\rho)|^{\frac{1}{2}}\gamma\exp\left(-2\omega(\rho)\right)}{1+\frac{\exp\left(-4\omega(\rho)\right)}{4}}. \tag{2.29}$$

If $f_l'=\frac{\hbar}{m_{\mathrm{r}}x_0^2}\left[\frac{d}{dE}\left(\frac{x_0}{u_l^{\mathrm{I}}(x_0)}\frac{du_l^{\mathrm{I}}(x)}{dx}\Big|_{x=x_0}\right)\Bigg|_{E=E}\right]$, Eq. (2.29) takes the form

$$\Gamma=\frac{2\hbar k_0\exp\left(-2\omega(\rho)\right)}{m_{\mathrm{r}}x_0}\left[\frac{f_l'^{-1}|\Phi(\rho)|^{\frac{1}{2}}\gamma}{1+\frac{\exp\left(-4\omega(\rho)\right)}{4}}\right]. \tag{2.30}$$

The parameter α is introduced such that,

$$\tan^2(\alpha)=|\Phi(\rho)|. \tag{2.31}$$

The parameter α in the expression above can be evaluated at $\rho=k_0x_0$,

$$\tan^2(\alpha_R)=\frac{\eta}{k_0x_0}+\frac{\left(L+\frac{1}{2}\right)^2}{\left(k_0x_0\right)^2}-1. \tag{2.32}$$

Replacing the parametrization (2.31) in Eq. (2.33) we obtain

$$\Gamma=\frac{2\hbar k_0\exp\left(-2\omega(\rho)\right)}{m_{\mathrm{r}}x_0}\left[\frac{f_l'^{-1}\tan\left(\alpha\right)\gamma}{1+\frac{\exp\left(-4\omega(\rho)\right)}{4}}\right]. \tag{2.33}$$

In the case of $L=0$, when the centrifugal barrier vanishes and the tunneling barrier is only given by the Coulomb interaction at large distances, the integral ω in Eq. (2.21) can be found easily using the parameterization (2.31). In that case, it was found to be [Pre47, Sri06]

$$\omega(\alpha)=\eta\Big(2\alpha-\sin(2\alpha)\Big). \tag{2.34}$$

The integral ω in the expression above, defined in Eq. (2.21) is known as the reduced action. The factor $2\omega(\alpha)$ that appears as the argument of the exponential function

in the width, Eq. (2.33) has been called the "Gamow factor", G. Each one of the factors in the definition of the width can be explained physically. If

$$\frac{1}{C_2} = \frac{f_l'^{-1}\gamma}{1+\frac{\exp\left(-4\omega(\rho)\right)}{4}},$$

Eq. (2.33) takes exactly the same form of the α decay rate shown in the Eqs. $(11-14)$ of the book by Preston and Bhaduri, "Structure of the nucleus", [PB75]. C_2 depends on the inside wavefunction factor $f_l'(x)$ and the factor $2\hbar k_0/m_{\rm r}x_0C_2$ can be assumed as the assault frequency of the α particle before tunneling through the Coulomb barrier. The factor C_2 is defined by Preston and Bhaduri as [PB75],

$$C_2 = \frac{2}{R}\frac{\int_0^{x_0}|u_l(r)|^2dr}{|u_l(r)|^2}. \tag{2.35}$$

The exponential factor $\exp(-G)$ is evaluated on the tunneling barrier and was introduced from the definition of the asymptotic behavior of the Coulomb functions, Eq. (2.18). In most text books, the exponential factor is associated with the penetrability through the Coulomb potential and is proportional to the tunneling probability of the α particle through the barrier. Consequently, the change in the width Γ comes mainly from the penetrability of the α particle.

2.2. Semiclassical methods

In the α decay, the usual energies of the α particle are not close to the top or the bottom of the barrier. At these energies, the rate of change of the de Broglie wavelength $\lambda_{\rm DB}$,

$$\lambda_{\rm DB} = \frac{\hbar^2}{\sqrt{2m_{\rm r}\left(\frac{Z_\alpha Z_d e^2}{x}-E\right)}}, \tag{2.36}$$

with respect to the distance $d\lambda_{\rm DB}/dx$ is extremely small, as is depicted in Fig. 2.2. For distances closer to the outer turning point, however, the rate of change of the de Broglie wavelength increases dramatically. The almost negligible change in $\frac{d\lambda_{\rm DB}}{dx}$ far away from the turning points for the tunneling barrier allows us to express the wavefunction of the α cluster-daughter nucleus system via semiclassical methods, such as the WKB method [Wen26, Kra26, Bri26, Jef25, Raz03, GP90] or the Two Potential Approach method (TPA) [GK87] in its semiclassical limit. We now describe the generalities of two of the semiclassical methods most commonly used to find the spontaneous α decay lifetimes.

2.2.1. WKB method and tunneling

The WKB method was proposed by Wentzel and Brillouin separately [Wen26, Bri26] in order to find the solution of the Schrödinger equation, using the approximations introduced by Jeffreys [Jef25]. The authors considered at first the one-dimensional time-independent Schrödinger equation, although later on, several works have extended the application of the WKB method for multidimensional systems [Ran77].

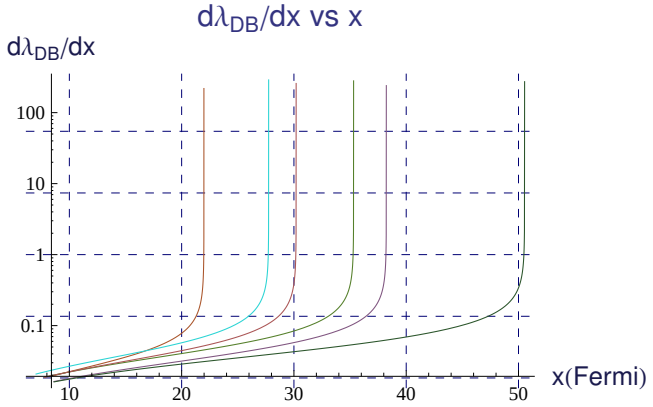

Figure 2.2: Change in the de Broglie wavelength as a function of the distance, for the tunneling barrier of some α emitters.

The wavefunction $\Psi(x)$ is initially defined in terms of the phase $S(x)$, such that $\Psi(x) = \left(\frac{dS(x;\hbar)}{dx}\right)^{-\frac{1}{2}} \exp\left(-\frac{i}{\hbar}S(x;\hbar)\right)$, [GP90]. As the phase of the wave function depends on the $\hbar$ parameter, an expansion of the phase in terms of $\hbar$ can be performed, in the limit where $\hbar \to 0$,

$$S(x;\hbar) = \sum_{n=0}^{\infty} \hbar^{2n} S_n(x). \tag{2.37}$$

Replacing the wave function in the one-dimensional time-independent Schrödinger equation, we find a system of differential equations for $S_n(x)$. The first two terms of the expansion can be found by solving the set of differential equations,

$$\left[S_0'(x)\right]^2 = 2m\left[V(x) - E\right], \tag{2.38}$$

$$2\left[S_0'(x)S_1'(x)\right] - \left[S_0'(x)\right]^{\frac{1}{2}} \frac{d^2\left[S_0'(x)\right]^{-\frac{1}{2}}}{dx^2} = 0. \tag{2.39}$$

The first term of the expansion of the phase $S(x;\hbar)$ can be identified with the Hamilton-Jacobi generating function, as the first expression in Eq. (2.38) is the classical Hamilton-Jacobi equation

$$H(q,p) + \frac{\partial S_{\mathrm{HJ}}}{\partial t} = 0. \tag{2.40}$$

In the context of the Hamilton-Jacobi theory, the generating function S_{HJ} is associated with the classical action. The conjugated momentum is expressed in terms of S_{HJ} by

$$p = \frac{\partial S_{\mathrm{HJ}}}{\partial x}. \tag{2.41}$$

In the limit of $\hbar \to 0$, only the first terms of the expansion Eq. (2.37) are significant. In consequence, it is enough to consider the first two terms of the expansion, in order to find the wavefunction, according to the chosen ansatz. In this limit, the wavefunction takes the following form

$$\Psi_{\pm\mathrm{WKB}}(x) = \frac{1}{\sqrt{k(x)}} \exp\left(\pm\frac{i}{\hbar}\int_x dx' k(x')\right), \qquad k(x) = \sqrt{\frac{2m}{\hbar^2}\Big(V(x) - E\Big)}. \tag{2.42}$$

After some quantum mechanics operations [GP90], the wavefunction can be found for the three different regions: before(I in Fig. 2.1), inside(II in Fig. 2.1) and after the barrier(III in Fig. 2.1), [Raz03]

$$\Psi_{\mathrm{WKB}}(x) = \begin{cases} N\sin(Kx) & 0 \le x \le x_0, \\ \frac{N}{\sqrt{k(x)}}\Big(Ae^{\int_{x_0}^{x}|k(x')|dx'} + Be^{-\int_{x_0}^{x}|k(x')|dx'}\Big) & x_0 \le x \le x_{\mathrm{TP}}, \\ \frac{NC}{\sqrt{k(x)}}e^{\,i\int_{x_{\mathrm{TP}}}^{x}k(x')dx' - \frac{i\pi}{4}} & x_{\mathrm{TP}} \le x < \infty. \end{cases} \tag{2.43}$$

Here, $K = \sqrt{\frac{2m_{\mathrm{r}}}{\hbar^2}\Big(E + U_0\Big)}$ and $k(x) = \sqrt{\frac{2m_{\mathrm{r}}}{\hbar^2}\Big(V(x) - E\Big)}$.

Looking at the expression above, we can distinguish some features depending on the region where the wavefunction is defined. Inside the barrier, the wavefunction decreases exponentially. Outside of the barrier, following the Sommerfeld radiating condition, the wavefunction describes an outgoing wave. The additional phase in the wavefunction outside the barrier comes from the connection formulas that are used in the WKB method to find the analytic form of the wavefunctions in each one of the regions. N is found from the normalization condition imposed on the wavefunction, assuming that there is only one α particle confined in the potential well,

$$N^2\int_0^{x_0}\big|\Psi_{\mathrm{WKB}}(x)\big|^2dx = 1. \tag{2.44}$$

The continuity of the wavefunction and its derivative allows us to express the constant coefficients A, B and C in terms of the barrier parameters. The penetrability in the semiclassical theory is defined as $\sigma = \int_{x_0}^{x_{\mathrm{TP}}}k(x')dx'$. In the limit where $\exp\big(-2\sigma\big) \ll 1$, a condition on K can be found from the continuity of the wavefunction, Eq. (2.43), [Raz03]

$$\tan\big(Kx_0\big) + \frac{K}{\sqrt{\frac{2m_{\mathrm{r}}}{\hbar^2}\Big(E - \frac{\eta_\alpha}{x_0}\Big)}} = 0. \tag{2.45}$$

However, as was mentioned in the last section of this chapter, the only possibility to fulfill the continuity conditions of the wavefunction is by assuming an initial complex eigenenergy of the tunneling particle, $E = E_r - \frac{i\Gamma}{2}$. Taking the complex wavenumber in the potential well region, $K = K_r - i\Delta K_i$, and expanding the right half side of Eq. (2.45), a condition on the imaginary part of the wave number ΔK_i can be found in terms of K_r [Raz03]

$$\Delta K_i = \frac{K_r}{x_0\sqrt{\frac{2m_{\mathrm{r}}}{\hbar^2}\Big(E - \frac{\eta}{x_0}\Big)}}. \tag{2.46}$$

We replace the last expression, Eq. (2.46) in the complex energy that characterizes the QS state $E = \frac{\Big(K_r - i\Delta K_i\Big)^2}{2m_{\mathrm{r}}} - U_0$, finding the width of the nuclear resonance, [Raz03, Elt65]

$$\Gamma = \frac{2K_r^2}{m_{\mathrm{r}}x_0\Big|\sqrt{\frac{2m_{\mathrm{r}}}{\hbar^2}\Big(E - \frac{\eta}{x_0}\Big)}\Big|}\exp\big(-2\sigma\big). \tag{2.47}$$

The exponential factor determined by the continuity of the wavefunction in the outer turning point $x_{\rm TP}$ is exactly the same one that was found in Eq. (2.33). The exponent of the exponential function -2σ is the Gamow factor, defined in the last subsection.

2.2.1.1. Langer modification and the centrifugal barrier

The WKB wavefunction brings some problems of convergence near the origin. In the vicinity of the turning points, the semiclassical expansion of the wavefunction in terms of the classical action is not accurate, as the change in de Broglie wavefunction is not negligible any more, see Fig. 2.2. Langer introduced a transformation to modify the spherically symmetric radial wavefunction [Lan37] in the presence of a Coulomb attractive potential. The purpose of this transformation is to describe a spherically symmetric system in terms of a one-dimensional wavefunction. It does not only reduce the degrees of freedom of the physical system, but it also solves the problem of the convergence of the wavefunction in the origin.

When the physical system is interacting with a central potential, there is an additional term in the radial Schrödinger equation, which is proportional to the angular momentum L, as it was explained earlier in this chapter. The centrifugal barrier increases the tunneling barrier in the case of quantum tunneling, as long as the relative angular momentum is not zero. However, with the centrifugal barrier taking the form of $L(L+1)/r^2$, the WKB wavefunction does not vanishes asymptotically in the origin, as is expected, but it becomes singular in that limit. While Krammers was historically the first one to introduce a modification in the centrifugal barrier, in order to solve the asymptotic behavior of the semiclassical wavefunction, [Kra26], the explanation of the modification in the centrifugal barrier comes by Langer [Lan37]. Langer proposed a transformation in order to get rid of the singularity of the semiclassical wavefunction. Since there is a singularity in the origin, the wavefunction calculated with the usual effective potential was not the physical wavefunction. A new variable x and a new wavefunction Ψ were introduced such that [Lan37, CnC07]

$$\frac{r}{r_0} = \exp\Big(\frac{x}{x_0}\Big), \qquad u_l(r) = \frac{r}{r_0}\Psi(x). \tag{2.48}$$

Here, Ψ is the radial wavefunction, solution of the radial Schrödinger equation, Eq. (2.10). Doing the corresponding substitutions in the radial Schrödinger equation, Eq. (2.10), an equivalent differential equation is found for the new wavefunction as a function of the new coordinate [Lan37, CnC07]

$$\begin{aligned} &\frac{d^2\Psi(x)}{dx^2} + (Q_1(x))^2\Psi(x) = 0, \qquad \text{with} \\ &Q_1(x) = \sqrt{\left[\frac{2m_{\rm r}}{\hbar^2}\left(E - V(x)\right)\left(\frac{r_0}{x_0}\right)^2 \exp\left(\frac{2x}{x_0}\right)\right] - \frac{\left(L+\frac{1}{2}\right)^2}{x_0^2}}. \end{aligned} \tag{2.49}$$

Rewriting the last expression in the original radial coordinates, the wave number $Q_1(x)$ takes a familiar form, [Lan37, CnC07]

$$Q_2(r) = \frac{r}{r_0}\exp\left(-\frac{x}{x_0}\right) = \sqrt{\frac{2m_{\rm r}}{\hbar^2}\left(E - \frac{\eta}{r}\right) - \frac{\left(L+\frac{1}{2}\right)^2}{r^2}}. \tag{2.50}$$

The new wavenumber is essentially the same as the old wave number $k(x)$, with the substitution of the numerator of the centrifugal number term by $\left(L+\frac{1}{2}\right)^2$. The radial dependence of the centrifugal barrier is exactly the same as the one in the radial Schrödinger equation, Eq. (2.10).

The transformation (2.48) does not change the Gamow factor defined earlier. Thus, the reduced action and the penetrability remains unchanged, [CnC07]

$$\int_{x_0}^{x_{\mathrm{TP}}} k(x)dx = \int_{r_0}^{r_{\mathrm{TP}}} Q_2(r)dr. \tag{2.51}$$

The exponential factor of the width depends highly on the turning points, but the fact that the Gamow factor remains unchanged under the transformation of coordinates implies that the difference between the turning points of the two wavenumbers is negligible. This statement is especially true in the s wave tunneling, $L = 0$. In that case, there is no centrifugal barrier, but the new turning point calculated using the modified centrifugal barrier by the Langer transformation is slightly different from the one of the Coulomb barrier. However, the difference between the outer turning points is negligible compared with the dimensions of the Coulomb barrier. Hence, the outer turning point is the same as in the case when there is no centrifugal barrier at all.

In this thesis, we work with nuclear resonances whose ground states have zero angular momentum. In consequence, the Langer modification in the centrifugal barrier is not considered in the wavenumber $k(x)$.

2.2.2. Quasiclassical limit of the Two Potential approach

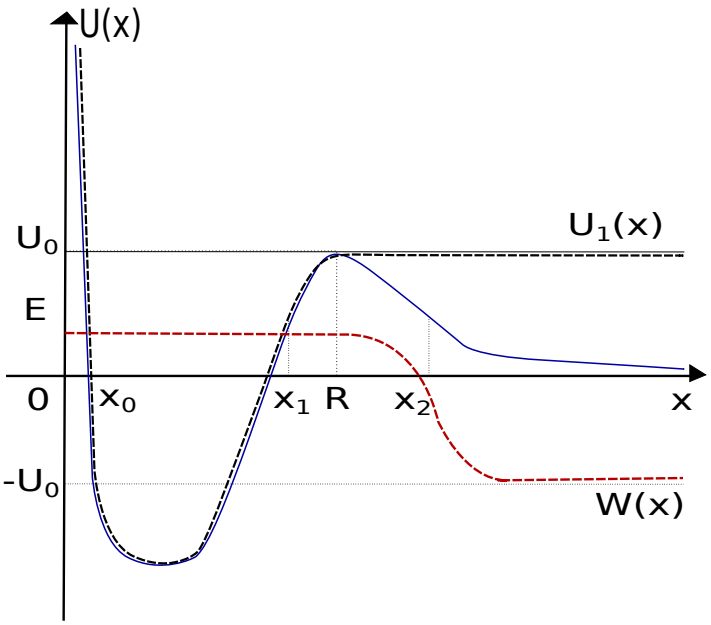

Figure 2.3: Two Potential Approach (TPA).

In 1987, Gurvitz and Kalbermann proposed a approach to the problem of the decay of a QS state [GK87]. Initially, the QS state is confined by the potential $U(x)$

between the turning points x_0 and x_1. Eventually it tunnels through the barrier, as the potential $U(x)$ has a finite height U_0 at $x = R$. The outer classical turning point is x_2, so the wavefunction in the region $x_1 \leq x \leq x_2$ is exponentially suppressed. After the barrier, the physical system goes into the continuum, and the wavefunction takes the form of an outgoing wave.

Gurvitz and Kalbermann took initially a quasibound rather than a QS state. In the limit, the energy of a quasibound state E_0 is close to the energy of the decaying QS state E. Accordingly, the wavefunction of the quasibound state was assumed to have almost the same form of the wavefunction of the QS state, if its decay rate is smaller than its energy $\Gamma \ll E$. In order to express the quasibound behavior of the physical system, the total potential $U(x)$ is split in two potential functions $U_1(x)$ and $W(x)$ (see Fig. 2.3). The potential $U_1(x)$ is a binding potential, given by

$$U_1(x) = \begin{cases} U(x), & \text{for } x_0 \leq x \leq x_1, \\ U_0 & \text{for } x \geq x_1. \end{cases} \tag{2.52}$$

The other potential $W(x)$ corresponds to the transition to the continuum and is defined as [Del10, GK87, Gur88]

$$W(x) = \begin{cases} 0, & \text{for } 0 \leq x \leq R, \\ U(x) - U_0 & \text{for } r \geq R. \end{cases} \tag{2.53}$$

The initial quasibound state $\big|\Psi_0\big\rangle$ is an eigenstate of the Hamiltonian $\mathcal{H}_0 = \hat{p}^2/(2m) + U_1(x)$, with the corresponding energy of the quasibound state E_0. At the initial time $t = 0$, the initial state is perturbed as the transition to the continuum $W(x)$ is considered. Since the new Hamiltonian is $H = \mathcal{H}_0 + W(x)$, the initial state is no longer an eigenstate of the total Hamiltonian. The new eigenstate is expanded in terms of the bound eigenfunctions $\{\Phi_k(x)\}$ of the Hamiltonian $\mathcal{H}_0$ [GK87]

$$\Psi_1(x,t) = b_0(t) \exp\left(-\frac{iE_0 t}{\hbar}\right) \Psi_0(x) + \frac{1}{(2\pi)^3} \int d^3k b_k(t) \exp\left(-\frac{iE_k t}{\hbar}\right) \Phi_k(x). \tag{2.54}$$

The wavefunction $\Psi_1(x,t)$ is replaced in the time-dependent Schrödinger equation. A set of coupled differential equations are found for the set of coefficients $\{b_k(t)\}$, $k = 0, 1, \ldots$ As the total wavefunction at $t = 0$ is $\Psi_0(x)$, the initial conditions of the coefficients are exactly $b_0(0) = 1$ and $b_k(0) = 0$, for all $k = 1, 2, \ldots$ In order to recover the description of the QS state, Gurvitz and Kalberman imposed that the coefficient $b_0(t)$ must drop as $\exp\big(-\Gamma t\big)$ for large times, [GK87]. In this way, the evolution of the physical state follows the exponential decay law, according to the theory of QS states. The set of differential equations that represents the evolution of the wavefunction $\Psi_1(x,t)$ in Eq. (2.54) is

$$\begin{aligned} i\frac{db_0}{dt} &= b_0(t)\langle\Psi_1|W(x)|\Psi_1\rangle \\ &\quad + \frac{1}{\big(2\pi\big)^3} \int d^3k \tilde{b_k}(t) \exp\left[\frac{i\big(E_0 + U_0 - E_k\big)}{\hbar}\right] \langle\Psi_1|W(x)|\Phi_k\rangle, \\ i\frac{d\tilde{b_k}}{dt} &= b_0(t)\langle\Phi_k|W(x)|\Psi_1\rangle \exp\left[\frac{i\big(E_k - E_0 - U_0\big)t}{\hbar}\right] \\ &\quad + \frac{1}{(2\pi)^3} \int d^3k' \tilde{b'_k}(t) \exp\left[\frac{i\big(E_k - E_{k'}\big)}{\hbar}\right] \langle\Phi_k|\tilde{W(x)}|\Phi_{k'}\rangle. \end{aligned} \tag{2.55}$$

Here, $b_k(t) = \tilde{b_k}(t)\exp\big(-iE_0/\hbar\big)$.

As it can be seen in Fig. 2.3, the perturbation $W(x)$ does not vanish at large distances. Instead, it takes a constant value $-U_0$. Gurvitz and Kalbermann argued that the perturbation $W(x)$ should be shifted in order to avoid any singularity in the transition matrix elements describing transitions between continuum and continuum [GK87]. The shifted perturbation $\tilde{W(x)}$ is defined as

$$\tilde{W}(x) = W(x) + U_0. \tag{2.56}$$

From the expression above, it can be seen that the new defined perturbation $\tilde{W}(x)$ vanishes asymptotically as $x \to \infty$. Using this method, Gurvitz and Kalberman were able to reproduce the Fermi Golden rule, by neglecting the first term that corresponds to transition between the eigenstates of the total Hamiltonian, [GK87]. In order to obtain the width of the QS state, a Laplace transformation of the b_0 differential equation in Eq. (2.55) is done, expressing the coefficient $b_0(t)$ in the energy domain $b_0(\epsilon)$. The coefficient $b_0(\epsilon)$ is found in terms of the operator $\tilde{G}$ as

$$b_0(\epsilon) = i\frac{1}{\Big(\epsilon - \langle\Psi_1|W(x)|\Psi_1\rangle - \langle\Psi_1|W(x)\tilde{G}W(x)|\Psi_1\rangle\Big)}. \tag{2.57}$$

Here, $\tilde{G}$ in Eq. (2.57) follows the expression [GK87]

$$\tilde{G} = \frac{\Big(1 + \tilde{W}(x)\tilde{G}\Big)\left(1 - |\Psi_1\rangle\langle\Psi_1|\right)}{\epsilon + E_0 + U_0 - \mathcal{H}_0}. \tag{2.58}$$

Eq. (2.57) shows that the coefficient b_0 has a pole at some energy $\epsilon = \epsilon_0$. Gurvitz and Kalbermann demonstrated in their work that this pole ϵ_0 is located in the second Riemannian sheet in the complex energy plane, where $\mathrm{Im}(\epsilon) \leq 0$. Their result confirmed the resonant behavior of the wavefunction Ψ_0. Accordingly, the width of the QS state is defined as usual,

$$\Gamma = 2\mathrm{Im}\big(\epsilon_0\big). \tag{2.59}$$

Gurvitz and Kalbermann performed an expansion of the radial part of the wavefunction $\Psi_1(x,t)$ in partial waves, finding the following expression for the complex pole of b_0

$$\epsilon_0 = \int_R^\infty |\varphi_1(x)|^2 W(x)dx + \int_R^\infty dx \int_R^\infty \varphi_1(x)W(x)\tilde{G}(E,x,x')W(x')\varphi(x'), \tag{2.60}$$

where $E = E_0 + \epsilon_0$, [GK87].

The operator $\tilde{G}$ is approximated in terms of the Green's function $G_{\tilde{W}} = \Big(E + \nabla^2/(2m) - \tilde{W}\Big)^{-1}$. The main difference between the operator $\tilde{G}$ in Eq. 2.58 and the Green function $G_{\tilde{W}}$ comes in the projection operator on the wavefunction Ψ_1, $|\Psi_1\rangle\langle\Psi_1|$. However, when the integration is performed to calculate ϵ_0, the integrating domain starts at R, where the contribution given by the projection operator is not significant. As the shifted perturbation $\tilde{W}(x)$ takes the value of $U(x)$, for every $x \geq R$, the substitution of $\tilde{G}$ by $G_{\tilde{W}}$ is justified.

The Green's function $G_{\tilde{W}}$ is defined in terms of the regular and irregular wavefunctions of the Hamiltonian $\mathcal{H}_{\tilde{W}} = -\nabla^2/(2m) + \tilde{W}(x)$,

$$G_{\tilde{W}}(E_0, r, r') = -\frac{2m}{rr'k}\xi_k^{(+)}(r_>)\xi_k(r_<). \tag{2.61}$$

Here, ξ_k is the regular eigenstate of the Hamiltonian $\mathcal{H}_{\tilde{W}}$ and $\xi_k^{(+)}$ represents the outgoing eigenstate. Furthermore, $k = \sqrt{2mE_0}$ is the wavenumber of the quasibound state.

The width in Eq. (2.59) is found by replacing Eq. (2.61) in Eq. (2.60). The total decay rate Γ, calculated by the TPA, is

$$\Gamma_{TPA} = \frac{4m}{\hbar^2 k}\Big|\int_R^\infty \varphi_1(x)W(x)\xi_k(x)dx\Big|^2. \tag{2.62}$$

2.2.2.1. Quasiclassical limit of the Two Potential Approach

Although the exact solution of the decay rate is expressed by Eq. (2.62), in many works the calculation of the widths of the α emitters is taken in the semiclassical limit. In the quasiclassical limit, the width (2.62) can be expressed in a similar form to the WKB result, in terms of the penetrability of the α particle through the barrier. In the semiclassical limit, the radial part of the quasibound wavefunction $\varphi_1(x)$ is given by [GK87]

$$\varphi_1(x) = \frac{\sqrt{N}}{2\sqrt{\alpha}}\exp\Big(-\int_{x_1}^R \big|k(x)\big|dx\Big). \tag{2.63}$$

Here, $k(x) = \sqrt{\frac{2m}{\hbar^2}\Big(E_0 - U(x)\Big)}$ is the wavenumber of the tunneling particle and N is a factor that can be obtained from the normalization [GK87]

$$N\int_{x_0}^{x_1}\frac{1}{k(x)}\cos^2\left(\int_{x_0}^{x_1}k(x')dx' - \frac{\pi}{4}\right) = 1. \tag{2.64}$$

The regular wavefunction $\xi_k(x)$ was defined by the authors [GK87] in Eq. (2.62) in the quasiclassical limit similarly to the way $\varphi_1(x)$ was defined. Replacing the wavefunctions to calculate the decay rate Γ we obtain

$$\Gamma_{\mathrm{TPA}} = N\frac{\hbar^2}{4m}\exp\Big(-2\int_{x_1}^{x_2}k(x)dx\Big). \tag{2.65}$$

The exponential term in Eq. (2.65) is the penetrability through the classically forbidden region between the classical turning points x_1 and x_2, as it is shown in Fig. 2.3. The definition of the decay rate (2.65) has been used in several works in order to calculate the decay rates and lifetimes of α emitting nuclei, [BMP92, BCM92, BJMP96, BM89, KCn07, XR05]. The agreement between the decay rates calculated by Eq. (2.65) and the experimental results is determined by the characteristics of the considered tunneling barrier in each one of the approaches that have been proposed to obtain the theoretical lifetimes.

2.3. The precluster model

Here we describe the characteristics of the phenomenological model proposed by Buck *et al.* [BMP91] based on the one introduced by Gamow [Gam28] and Condon and Gurney [GC29].

In the precluster model, the preformed α particle follows two different orbits around the daughter nucleus. The orbits are characterized by different values of the so called "global quantum number", $\mathcal{G}$. Macroscopically, $\mathcal{G}$ can be understood as a large quantum number corresponding to the macroscopic situation where the nucleons of the α particle occupy states above the Fermi surface of the daughter nucleus [BMP91, BMP90b, BM89]. Taking into account the Pauli exclusion of the nucleons in the α cluster-daughter nucleus system, $\mathcal{G}$ is chosen in such a way that they obey the Wildermuth condition [BMP91, TWP62], $\mathcal{G} \leq 2n + L$. Here, n is the quantum number of relative motion, associated with the number of internal nodes of the radial wavefunction. L is the relative angular momentum between the α particle and the daughter nucleus.

In order to study the correlations between $\mathcal{G}$ and the lifetimes of even-even nuclei with $76 \leq Z \leq 100$, being Z the proton number of the parent nucleus, Buck *et al.* use the phenomenological model proposed by Gamow [Gam28] and Condon and Gurney [GC29]. The tunneling barrier that the α particle tunnels through is given by

$$V(x_1) = \begin{cases} -U_0 & \text{for } 0 \leq x_1 \leq x_0, \\ \frac{Z_\alpha Z e^2}{x_1} & \text{for } x_1 \geq x_0. \end{cases} \tag{2.66}$$

Here, $Z_\alpha = 2$ is the proton number of the α particle. The values of x_0 and U_0 are fitted such that they reproduce the experimental lifetimes of even-even α emitters. Furthermore, x_0 is expressed in terms of the mass number of the parent nucleus A as

$$x_0 = c_1 A^{\frac{1}{3}}. \tag{2.67}$$

The orbits of the α decay must follow the well known Bohr-Sommerfeld quantization condition,

$$\int_0^{x_0} \sqrt{\frac{2m_\mathrm{r}}{\hbar^2}\Big(E + U_0 - \frac{Z_\alpha Z e^2}{x}\Big)}\,dx = \Big(\mathcal{G} + 1\Big)\frac{\pi}{2}. \tag{2.68}$$

Buck *et al.* [BMP91, BJMP96] suggested a value of $\mathcal{G} = 22$ for nuclei with proton number Z in the studied region. The change in the global number corresponding to different orbits is $\Delta\mathcal{G} = 2$. The value of U_0 is fixed and c_1 can be found using the Bohr-Sommerfeld condition, Eq. (2.68) for a single value of $\mathcal{G}$. In the semiclassical approximation, the width, or the field-free decay rate is

$$\Gamma = \frac{P\hbar^2 K}{2m_\mathrm{r} x_0} \exp\big(-2W_\mathrm{red}\big). \tag{2.69}$$

where P is the α particle formation probability. The reduced action from the WKB method in the exponential term of Eq. (2.69) is

$$W_\mathrm{red} = \int_{\mathrm{x_0}}^{\frac{Z_\alpha Z e^2}{\mathrm{x_0}}} k(x)dx. \tag{2.70}$$

K and $k(r)$ in Eq. (2.69) and Eq. (2.70) are the wavenumbers in the internal and barrier regions, respectively,

$$K = \sqrt{\frac{2m_{\rm r}}{\hbar^2}\Big(E + U_0 - \frac{Z_\alpha Z e^2}{x_0}\Big)/\hbar^2} \quad \text{and} \quad k(x_1) = \sqrt{\frac{2m_{\rm r}}{\hbar^2}\Big(\frac{Z_\alpha Z e^2}{x_1} - E\Big)/\hbar^2}. \tag{2.71}$$

In their calculations, Buck *et al.* [BMP91, BMP90b] took the preformation factor P as 1, in order to adjust the minimum set of parameters. In order to find the value of the depth of the nuclear potential well, Buck *et al.* minimized the square deviations of the logarithms of the calculated lifetimes using Eq. (2.69) from the experimental values. In that sense, the parameters of the model are chosen in order to fit the experimental data. Buck *et al.* kept the depth of the nuclear potential well U_0 in all cases as 135.6 MeV.

For most of the medium-mass and heavy α emitters considered by Buck *et al.* , the theoretical calculated lifetimes have a difference of a factor of 2 σ or better compared to the experimental values. Some of the lightest nuclei have theoretical values with a difference of a factor of 3 σ, compared with the experimental lifetimes. The discrepancy has been explained by the preformation probability of the α particle in the parent nucleus. In some works, for instance Xu and Ren [XR05], the preformation factor P takes a different value, between 0 and 1, depending on the value of the global quantum number $\mathcal{G}$. The value of the preformation factor in that work is fitted in order to reproduce the experimental results of the medium-mass lifetimes, with proton numbers between 52 and 82. The global quantum number was also modified by Buck *et al.* in their calculations, in order to obtain an adequate description of the lifetimes of the lightest nuclei, compared with the value that $\mathcal{G}$ takes for some heavier nucleus like Po or Rn. The success of the precluster model is attributed by the authors to the values of the nuclear potential well radius x_0 and the behavior of the α-core wavefunction. In the case of the radius x_0, the chosen values correspond to the formation of a quasibound state at the exact energy that the α particle must have in order to be released by the parent nucleus, for a fixed depth of the nuclear potential well. Besides, the spherically symmetric α-core wavefunction contains many nodes, such that the values that the global quantum number $\mathcal{G}$ takes are large. The large number of nodes in the wavefunction agrees with the expectations of the preformation of the α cluster from valence nucleons, according to the authors of Ref. [BMP91]. The simplicity of the precluster model allows us to understand the dynamics of the α decay in a transparent way, and the quantitative results show a satisfactory agreement with the experimental lifetimes of the medium-mass α emitting nuclei.

2.4. Barrier parameterization for laser-assisted α decay

In the present Chapter, we have reviewed some of the simplest phenomenological models that describe in a transparent way the physical concepts behind the spontaneous emission of an α particle by an unstable nucleus. Among the models presented in this Chapter, we put an emphasis in the precluster model proposed by Buck *et al.* [BMP90a, BMP91]. Despite the simple assumptions assumed in the development of the precluster model by Buck *et al.* , the α decay lifetimes calculated using this formalism are close to the experimental results within a factor of 2 or 3 σ. The

agreement with the experimental lifetimes is remarkable, given the phenomenological character of the model and the lack of consideration of microscopic interactions in the α particle-daughter nucleus physical system.

From the spontaneous α decay rate calculated by the precluster model (2.69), we can see that the α decay lifetimes depend on the parameters that define the tunneling barrier and the nuclear potential well, U_0 and x_0. For the calculations of the lifetimes, Buck *et al.* in their work [BMP91] fitted the values of those parameters from available experimental α decay data in order to reproduce some of the fundamental properties of the parent nuclei. We take the same set of parameters, U_0, x_0 and E, that Buck *et al.* listed in their work to define the tunneling barrier and the energy of the α particle for every medium-mass α emitter we study in the present thesis.

Once we have defined the tunneling barrier that the α particle traverses in the spontaneous α decay, our purpose is to study the dynamics of the tunneling α particle in the presence of a laser field. Starting from the field-free decay rate calculated in the precluster model, Eq. (2.69) and considering that the initial state of the preformed α cluster is QS, we develop a method that allows us to study in depth the process of emission of α particle in the presence of a strong laser field. Although the laser-assisted tunneling (LAT) of QS states has been studied in other fields, such as the photon-assisted transport in semiconductor nanostructures [PA04], to the best of our knowledge no one has developed a method to describe the dynamics of the LAT of an α particle through the Coulomb barrier. In the next chapters, starting from a well known approach in strong-field laser-matter interaction, the Strong-Field Approximation, and the definition of the field-free decay rate for a QS state, we develop a general method to study the laser-assisted decay of QS states by studying the dynamics of a tunneling particle in the presence of a strong laser field. Our goal is to apply our formalism to the particular case of the laser-assisted α decay of several α emitting nuclei.

CHAPTER 3

LASER-ASSISTED DECAY OF QUASISTATIONARY STATES

In this Chapter we develop a novel approach to study the laser-assisted decay of quasistationary (QS) states, by extending well known methods used to study the physics of strong laser field-matter interactions. The physics of the spontaneous emission of an α particle has been well studied using the phenomenological methods reviewed in the last Chapter. However, the influence of a direct interaction with a strong laser field during the α decay of medium-mass and heavy nuclei is still an open question that has not been studied. To develop an approach that allows us to study the laser-assisted α decay, we start by reviewing the fundamental features of one of the most successful methods in the description of laser-induced processes in the multiphoton regime, the Strong-Field Approximation (SFA). Since the tunneling mechanism plays a significant role in the description of the field-free α decay, a formulation of SFA that involves the dynamics of the tunneling particle in terms of complex classical trajectories, known as the imaginary time method (ITM), is used to study the transition between the initial QS state and the continuum in the presence of a strong laser field. To describe the laser-assisted decay of an initial QS state, we implement a modification of the ITM formulation of SFA that takes into account the properties of the wavefunction of the QS state, the prefactor of the field-free decay rate of the QS state and the dynamics of the decaying system in the presence of the strong laser field. The method described here allows us to study any laser-assisted decay process whose initial state is QS. In particular, it is a suitable formalism to describe the laser-assisted tunneling (LAT) of the α particle through the Coulomb barrier.

Among the proposals to modify the α decay rates, the direct interaction between the α emitter and a strong laser field has been overlooked over the past years, as available experimental facilities did not have the strong enough lasers to affect the systematics of the spontaneous α decay. However, in recent years, due to the development of new experimental facilities aiming at higher intensities and photon energies, the scenario of direct interaction between nucleus and laser beams cannot be ruled out anymore.

To the best of our knowledge, until now, no theoretical model has been developed to address laser-assisted α decay. However, other laser-assisted phenomena, such as the bremsstrahlung in external electromagnetic fields [BF66, V.97], the photon-assisted transport (PAT) or laser-assisted β decay [NR64] have been studied in other fields of physics. In particular, theoretical tools such as the Floquet method have been applied to the description of PAT, which can be described as a LAT of an initial QS state [PA04]. The laser-assisted decay of QS states can be understood as an example of LAT of an initial QS state, due to the close relation between tunneling and decay.

The Floquet method has been applied extensively in strong-field atomic physics and can be used to study the LAT of a QS state. The Floquet approach is known to be efficient when the characteristic number of absorbed or emitted photons is not very large. However, when a large number of photons is involved, it becomes more cumbersome numerically. Another successful method developed in strong-field atomic physics and relevant in the semiclassical domain (where a typical number of photons is at least of the order of ten and can easily reach hundreds and even thousands) is the SFA. SFA has been extensively used to determine the laser-induced ionization rates, providing a simple and natural description of strong-field laser-atom interactions that in many cases is fully analytical. In particular, there is a formulation of SFA in terms of complex classical trajectories, which characterizes in a transparent way the physics of tunneling in the presence of a strong laser field for laser-induced processes. This formulation is known as ITM. This method was introduced in the early days of strong-field physics [PP67, PKP68] to give a physically transparent formulation of SFA. In addition, the ITM also provides an efficient way to consider significant effects that the plain SFA misses in its original formulation.

However, if SFA is directly applied on the LAT of an initial QS state, some fundamental problems in the definition of the transition amplitude appear due to the behavior of the initial state. For a QS state, the transition amplitude defined by the plain formulation of SFA does not converge due to the asymptotic behavior of the initial wavefunction. This is due to the fact that for a QS state, the initial state is described in terms of a Gamow wavefunction with an associated complex energy. The QS wavefunction takes the asymptotic form of the wavefunction of a free particle at large distances and it is not normalizable. Thus, the transition amplitude defined in terms of the initial and the final wavefunction in the SFA diverges in consideration of the asymptotic behavior of the initial QS state.

In order to solve this problem, we develop here a general and accessible theoretical description of the laser-assisted decay of QS in the presence of intense electromagnetic fields. The general idea of SFA is adopted and modified using ITM for the description of the LAT of an initial QS state. Our approach recovers specific results of Ivlev *et al.* in Ref. [IM85], who were the first authors to propose the ITM for the description of the tunneling of free particles through a potential barrier in the presence of an oscillating electric field. Furthermore, our formalism provides not only qualitative but also quantitative tunneling probabilities that agree with exact numerical calculations, compared with the results by Ivlev *et al.* [IM85]. In particular, the laser-assisted α decay can be studied in depth using our extended SFA formalism to investigate laser-assisted decay of QS states, calculating the spectrum of the tunneling α particle and the laser-assisted lifetimes for medium-mass and heavy nuclei.

In this Chapter, we start by describing in detail the extensions of SFA for the laser-assisted decay of QS states. Firstly, we introduce SFA in general form (to see a

further discussion of methods in strong fields, see [Rei92]). Later on, we discuss the formulation of the SFA in terms of subbarrier trajectories in complex times, known as the Imaginary Time Method (ITM). Using the ITM formulation, an extension of the method to take into account LAT of QS states is developed. Atomic units $m_e = \hbar = 1$ are used throughout this Chapter.

3.1. Strong-field approximation matrix element for quasistationary states

3.1.1. Strong-Field Approximation

We start from a short summary of the SFA that describes ionization from true bound states. Within the SFA, the transition amplitude between an atomic bound state $|\Psi_0\rangle$ of binding energy $E_0 \equiv -I$ and a continuum state $|\Psi_{\vec{p}}\rangle$ with an asymptotic momentum $\vec{p}$ is given by

$$M_{\rm SFA}(\vec{p}) = -i \int_{-\infty}^{+\infty} \langle \Psi_{\mathbf{p}} | \hat{V}(t) | \Psi_0 \rangle dt \,, \tag{3.1}$$

where the final state is approximated by the Volkov function,

$$\Psi_{\mathbf{p}}(\mathbf{r}, t) = \frac{1}{(2\pi)^{3/2}} \exp\left\{ i\mathbf{v}_{\mathbf{p}}(t) \cdot \mathbf{r} - i \int_{-\infty}^{t} \varepsilon_{\mathbf{p}}(t') dt' \right\} \tag{3.2}$$

and

$$\varepsilon_{\mathbf{p}}(t) = \mathbf{v}_{\mathbf{p}}^2(t)/2, \quad \text{with} \quad \mathbf{v}_{\mathbf{p}}(t) = \mathbf{p} + \mathbf{A}(t)/c$$

are the electron time-dependent kinetic energy and velocity in the electromagnetic field, respectively, described by the vector potential $\mathbf{A}(t)$. $\hat{V}(t)$ is the interaction operator of the electron with the field of the electromagnetic wave and c the speed of light. In the dipole approximation, the electric field $\mathcal{E}(t) = -\partial_t \mathbf{A}/c$ and the vector potential depend only on time. It is convenient to simplify the notation by using the field-induced momentum rather than the vector potential, $\mathbf{p}_F(t) = \mathbf{A}(t)/c$.

Amplitude in Eq. (3.1) is relevant under the semiclassical conditions:

$$K_0 = \frac{I}{\omega} \gg 1 \,, \qquad F = \frac{\mathcal{E}_0}{\mathcal{E}_{\rm ch}} \ll 1 \,, \tag{3.3}$$

where $\mathcal{E}_0$ is the electric field amplitude, $\mathcal{E}_{\rm ch} = (2I)^{3/2}$ is the characteristic atomic field (for the ground state of hydrogen $\mathcal{E}_{\rm ch} = m_e^2 e^5/\hbar^4 = 5.14 \times 10^9 \mathrm{V/cm}$) and ω is the laser frequency. The first strong inequality in Eq. (3.3) shows that the minimal number of photons required for ionization is large, hence the coupling is essentially nonlinear. The second inequality guarantees that the spatial scale on which the ionization amplitude forms is large in comparison with the atomic size (see a detailed discussion in Refs. [Pop04, PPB08, PB08]). Another frequently used dimensionless combination known as the Reiss parameter [Rei80] is proportional to the ratio of

the ponderomotive energy $U_p = \langle \mathbf{p}_F^2(t) \rangle_T / 2$ (where T is the optical period) to the photon energy. For the linearly polarized monochromatic field this reads

$$z_F = \frac{4U_p}{\omega} = \frac{\mathcal{E}_0^2}{\omega^3} = 8F^2 K_0^3 \,. \tag{3.4}$$

For ionization of atoms and positive ions by intense infrared and optical lasers, the conditions Eq. (3.3) are usually well satisfied and $z_F \gg 1$. The integrand in Eq. (3.1) is then a rapidly oscillating function of time, so we use the saddle-point method in order to calculate the integral in Eq. (3.1). We expand the time-oscillating integrand in the vicinity of the solution of the saddle-point equation, given by

$$\partial_t S_0(\mathbf{p}, t_0) = \mathbf{v}_\mathbf{p}^2(t_0)/2 + I = 0 \,. \tag{3.5}$$

Here, the function S_0 is the argument of the time-oscillating function in the integrand. It is the defined as the classical action

$$S_0(\mathbf{p}, t) = \int_t^{+\infty} \left\{ \mathbf{v}_\mathbf{p}^2(t')/2 + I \right\} dt'. \tag{3.6}$$

The amplitude can be written as a sum of contributions from all relevant stationary points $t_0(p)$,

$$M_{\mathrm{SFA}}(\mathbf{p}) = \sqrt{-2\pi i} \sum_\alpha \mathcal{P}(\mathbf{p}, t_{0\alpha}) \frac{\exp\left(-iS_0(\mathbf{p}, t_{0\alpha})\right)}{\sqrt{\partial_t^2 S_0(\mathbf{p}, t_{0\alpha})}} \,, \tag{3.7}$$

and the pre-exponential factor $\mathcal{P}$ is the spatial matrix element of the interaction operator $\hat{V}$. The differential ionization rate is given by the squared modulus of Eq. (3.7).

In the case of nonlinear ionization, all roots of the saddle point equation, Eq. (3.5) are complex due to the initial bound state of the electron. Consequently, the phase $S_0(\mathbf{p}, t_0)$ in Eq. (3.7) is a complex quantity with a numerically large and negative imaginary part. That guarantees that the saddle point method can be used. The ionization rate under conditions Eq. (3.3) appear to be a highly nonlinear function of the laser field strength.

In the case of ionization, the form of this nonlinear dependence is quantified by the value of the Keldysh parameter [Kel65]

$$\gamma = \frac{\sqrt{2I}\omega}{\mathcal{E}_0} \equiv \frac{1}{2K_0 F} \tag{3.8}$$

which is the ratio of the characteristic atomic momentum $\kappa_0 = \sqrt{2I}$ to the field momentum $p_F = \mathcal{E}_0/\omega$. Since the final state is approximated by the plane wave Eq. (3.2), the prefactor $\mathcal{P}$ in Eq. (3.7) can be expressed via the Fourier transform of the bound state atomic wave function $\phi_0(\mathbf{r})$. For practical calculations, this means that the prefactor is a weak function of the final momentum and the field and atomic parameters compared with the highly nonlinear exponential, so that one may safely replace it by a constant as long as photoelectron momentum distributions and not the total ionization rates, are considered. Moreover, in the above formulation of the SFA, the so-called plain SFA, the expression of the prefactor is anyway incorrect, except for the case of ionization from a short-range well. The simplest form of the SFA transition

amplitude is therefore given by Eq. (3.7) with $\mathcal{P} = \text{const}$. On the qualitative level this rough approximation is in many cases sufficient. Strictly speaking, the SFA provides a quantitatively correct description of nonlinear ionization only for the exceptional case of a particle bound by a zero-range potential. For short-range potentials, it is still a good approximation if the interaction operator $\hat{V}(t)$ is taken in the length gauge [BMB05]. For atoms, where the electron-core interaction potential always presents a long-range Coulomb tail, the SFA prefactor $\mathcal{P}$ is essentially wrong in any gauge. In this case, to calculate it correctly and bring the SFA back to the quantitative level of description, the technique of Coulomb corrections was developed. For further details we refer the reader to Refs. [PMPB08, PMPB09, PPB08, PB08, SSI08].

3.1.2. Modified SFA for quasistationary states

Let us now turn to the case when not a bound but a QS state is subject to an intense laser pulse. One would then expect the appearance of an above-threshold ionization (ATI)-like photoelectron spectrum with the significant difference that now the initial state energy $E_0 \equiv {p_0}^2/2 > 0$ so that there is no gap between the initial state and the continuum. As a result, laser photons can also be emitted, not only absorbed, and the net number of absorbed photons can also be zero. Figure 4.1 sketches this qualitative difference between photoelectron spectra for stationary and QS states. Nevertheless, in strong fields we expect that the typical number of photons involved in the interaction is anyway large, hence SFA-like approaches should be suitable also for the description of ionization from QS states. With this assumption, we can introduce the amplitude of laser-assisted decay replacing the bound state wave function $|\Psi_0\rangle$ in Eq. (3.1) by the QS state (Gamow's wave function)

$$\Psi_0(\mathbf{r}, t) = \phi_0(\mathbf{r}) e^{-iEt}, \qquad E \equiv E_0 + iE_0' = E_0 - i\Gamma/2 = \frac{{p_0}^2}{2} - ip_0 p_0' \,.$$

Here E_0 is the real part of the complex energy and Γ is the width that determines the decay rate. Following a common width limitation in the theory of QS states, we consider $\Gamma \ll E_0$. If an even stronger limitation is satisfied and the width is small compared with all other characteristic frequencies of the problem, we may disregard the factor $\exp(-\Gamma t/2)$ in the integrand. Then the SFA ionization amplitude differs from the one for the true bound state in the spatial wave function of the initial state $\phi_0(\mathbf{r})$ and by the fact that the initial state energy E_0 lies in the continuum.

This straightforward application of the SFA leads, however, to some difficulties, namely:

1. The spatial matrix element is divergent due to the exponential divergence of the spatial wave function of the QS state,

$$\phi_0(\mathbf{r}) \sim e^{ip_0 r + p_0' r} \to \infty, \qquad r \to \infty, \qquad p_0' \approx \Gamma/2p_0 \,.$$

   This asymptotic exponential divergence at large distances well known in the theory of QS [BPZ69, R.91], originates from the approximate treatment of the decaying state as a stationary state and was noted in the pioneering work of Gamow [Gam28].

2. Even if the phase is large and the saddle point method is applicable, the saddle-points are real (since $E_0 > 0$ and we omit $\Gamma \ll E_0$ in the saddle-point equation) and the stationary phase is also real. The field parameters then enter the tunneling probability only via the pre-exponential factor. In other words, the transition amplitude does not demonstrate the nonlinear dependence on the laser field strength and frequency typical for strong field phenomena. This means that even in a very weak field the probability of detecting the outgoing particle with an energy considerably different from E_0 is not small, i.e. the field-free tunneling exponent does not emerge in the limit $\mathcal{E}_0 \to 0$. Obviously, such a conclusion cannot be correct.

Although the exponential divergence of QS state wavefunctions is itself not surprising and follows from the definition of a QS state, for the calculation of norms and matrix elements containing these divergent factors a regularization method is needed. Such a method was first proposed by Zeldovich [Zel61]. However, for our purposes we will not use any regularization but apply instead another method for reconstruction of the correct prefactor, as explained in the following.

The origin of the second difficulty becomes clear if we consider the structure of the continuum for the system shown in Figure 4.1. For simplicity, in the following we refer to a 1D system. At large distances the eigenfunctions are superpositions of the incoming and the outgoing plane waves:

$$\phi_p(x) = e^{-ipx} + F(p)e^{ipx}, \qquad x \to \infty, \qquad E = p^2/2$$

while inside the well, $x \leq a$,

$$\phi_p(x) \sim A(p) \sin\left(\int_0^x v(p,x')dx'\right), \qquad v(p,x) = \sqrt{p^2 - 2U(x)}\,.$$

For the momenta in the narrow vicinity of the QS state, $p \simeq p_0$, the absolute value of the coefficient $A(p)$ depends strongly on p having a sharp maximum at $p = p_0$. For eigenstates whose energy is sufficiently different from E_0,

$$|E - E_0| \gg \Gamma\,, \qquad 0 < E < U_0\,, \tag{3.9}$$

the wave function inside the well is exponentially small,

$$A(p) \simeq e^{iW_0(p)}\,, \qquad W_0(p) = \int_{a(p)}^{b(p)} v(p,x)dx\,. \tag{3.10}$$

Here $a(p)$ and $b(p)$ are the turning points of classical motion, hence the action W_0 taken over the classically forbidden region is a purely imaginary value and $iW_0 < 0$. The coefficient $A(p)$ is the semiclassical probability amplitude (calculated with exponential accuracy) of the particle to tunnel through the barrier formed by the potential $U(x)$. Thus, for continuum states satisfying Eq. (3.9) the correct spatial matrix element should contain an exponentially small factor Eq. (3.10), whereas the SFA matrix element calculated with a plane wave final state function does not present this feature. We come to the conclusion that the problem with the SFA applied to QS states is that its plane wave final state Volkov function differs from the correct

continuum wave function exponentially, exactly in that part of the position space that contributes most to the spatial matrix element.

Taking this into account we may formulate how one should modify the SFA matrix element to make it appropriate also for the description of LAT from QS states; the spatial matrix element should be replaced according to

$$\sqrt{-2\pi i}\,\langle\phi_p|V(x,t)|\phi_0\rangle/\sqrt{\partial_t^2 S_0(p,t_{0\alpha})} \to A(v_p)\mathcal{P}(v_p,t)\,, \tag{3.11}$$

where $A(v_p)$ is given by Eq. (3.10), v_p is the instant velocity $v_p(t) = p + p_F(t)$ and the new prefactor $\mathcal{P}(v_p,t)$ will be defined below. Then, instead of Eq. (3.7) we obtain

$$M_{\rm SFA}(p) = \sum_\alpha \mathcal{P}(v_p,t_{0\alpha}) \exp\left[iW_0(v_p) - iS_0(p,t_{0\alpha})\right]\,. \tag{3.12}$$

The action $W_0(v_p)$ is complex and describes the field-free tunneling through the potential barrier $U(x)$. The action $S_0(p,t_0)$ is real (just as the saddle point t_0) and therefore accounts for the effect of the laser field on the particle after the tunneling. Thus, in this approximation the laser field only changes the particle's energy on its way from the tunneling exit to a detector. In other words, S_0 accounts for the kinematic effect of the laser field that redistributes the particles in the energy space not affecting the total decay probability. This corresponds to the "exclusive" regime of interaction, addressed in the introduction of the present thesis [NR64, BMSS83, BSS84a, BSS84b]. At first sight, the tunneling exponent is affected by the laser field via the fact that the field-free action W_0 is now taken at the instant velocity v_p at the saddle point. However, according to the saddle point equation Eq. (3.5) $v_p(t_0) = p_0$, so that $W_0(v_p) = W_0(p_0)$ and the laser field dependence vanishes.

We can now translate this formal description of the matrix element Eq. (3.12) into a simple physical picture which would allow us to determine the correct prefactor $\mathcal{P}(p,t)$. The particle tunnels through the potential barrier the same way as it would without the laser field. At some time instant t_0, it emerges in the classically allowed domain having the initial velocity $v(t_0) = p_0$ and starts its motion in the laser field[1]. Then its final energy is given by

$$E = p^2/2 = (p_0 - p_F(t_0))^2/2, \tag{3.13}$$

so that each initial time t_0 corresponds to a certain final energy. The inverse function $t_0(E)$ is not necessarily single-valued. In the linearly polarized monochromatic field with

$$\mathcal{E}(t) = \mathcal{E}_0\cos\omega t\,, \qquad p_F(t) = -p_F\sin\omega t\,, \quad p_F = \mathcal{E}_0/\omega \tag{3.14}$$

we have $E_{\max} = (p_0 + p_F)^2/2$ and $E_{\min} = (p_0 - p_F)^2/2$ or zero; the spectrum consists of ATI-like peaks between the classical boundaries (CB) $E_{\min} \le E \le E_{\max}$. The magnitudes of the ATI-like peaks vary slowly with the energy via the prefactor in Eq. (3.12). Outside the CB, the spectrum vanishes abruptly.

Within the picture described by Eq. (3.12), penetration of the particle through the well and its subsequent evolution are independent. Then the probability to tunnel out during the time interval dt_0 is given by

$$dw(t_0) = R_0 dt_0 = R_0\left|\frac{dt_0}{dp}\right|dp\,, \tag{3.15}$$

[1]Here we assume that the potential well is a short-range one.

where $R_0 = \mathcal{P}_0^2 \exp(-2\mathrm{Im}W_0)$ is the field-free tunneling rate and the derivative $dp/dt_0 = -\dot{p}_F(t)$ is calculated from Eq. (3.13). Note that we assume here that the tunneling probability can be written as a continuous function of the particle asymptotic momentum p. In reality, the spectrum consists of a discrete comb of peaks corresponding to absorption or emission of an integer number of laser photons. Our assumption thus implies that the characteristic number of peaks L in the spectrum is large, $L \gg 1$. According to Eq. (3.13), there are two limiting cases defined by the ratio between the field-free electron asymptotic momentum p_0 and the field momentum p_F. If $p_F \ll p_0$ then the classical boundaries of the spectrum are approximately $E_0 \pm p_0 p_F$ so that the number of peaks is $L \simeq p_0 p_F/\omega$. For stronger fields where $p_F \gg p_0$ the energy scale is determined by the ponderomotive energy and the number of peaks is of the order of the Reiss parameter Eq. (3.4). As will be discussed in the next section, for field values for which L is not much greater than unity, the approximation of the continuous spectrum contradicts energy conservation requirements. As a result, the total rate can only be calculated with some numerical error.

The distribution Eq. (3.15) is divergent at the CBs $p = p_{\max/\min}$ where we have $dp/dt_0 = 0$. Such an integrable divergence near the CBs is typical for SFA-based descriptions, occurring at the final momenta for which the saddle-point method does not work due to cancelation of the second derivative of the action. This does not affect the total probability but renders the momentum distribution incorrect in the vicinity of CBs. To avoid this problem, the term that is proportional to the third derivative of the action has to be accounted for in the phase decomposition near the saddle point. The divergence is then replaced by a local maximum of the spectrum at the CB [GP99, FSB02] with a relative height of the order of $z_F^{1/3}$, where z_F is the Reiss parameter Eq. (3.4).

In the simplest form, this regularization procedure reduces to the replacement

$$\left|\frac{dt_0}{dp}\right| \to \frac{1}{\sqrt{(dp/dt_0)^2 + \beta^2}}. \tag{3.16}$$

The ratio between the value of the spectrum at the local maximum of the spectrum and the corresponding value at the CB is

$$\frac{w_{\mathrm{CB}}}{w_{\max}} = z_F^{\frac{1}{3}}. \tag{3.17}$$

At the CB, the derivative of the final momentum respect to the initial time of motion outside the barrier t_0 is zero So, in accordance to Eq. (3.16), the value of the spectrum in the CB is proportional to

$$w_{\mathrm{CB}} \propto \left|\beta\right|^2. \tag{3.18}$$

Since $|\beta| \ll \frac{dp}{dt_0}\Big|_{\max}$, the spectrum at the local maximum is proportional to

$$w_{\max} = \left|\sqrt{\frac{dp}{dt_0}\Big|_{\max}}\right|^{-2}. \tag{3.19}$$

Replacing Eqs. (3.18) and (3.19) in Eq. (3.17), we find the value of the regularization constant β, which is

$$\beta = z_F^{-\frac{1}{3}} \left|\sqrt{\frac{dp}{dt_0}\Big|_{\max}}\right|^2. \tag{3.20}$$

Next, we take into account that usually there is more than one solution to the saddle-point equation, so that several $t_{0\alpha}$, $\alpha = 1, 2, ...$ correspond to the same final energy. This leads to a coherent sum over all saddle-point solutions.

The momentum distribution takes then the form:

$$\begin{aligned} dw(p) &= |M(p)|^2 \, dp \,, \\ M(p) &= \sum_{\alpha} \frac{\mathcal{P}_0 \exp\left[iW_0(v_p) - iS_0(p, t_{0\alpha})\right]}{\sqrt{dp/dt_0 + i\beta}}\Bigg|_{t=t_{0\alpha}} . \end{aligned} \tag{3.21}$$

Clearly, this result misses two effects: (i) the influence of the laser field on the subbarrier motion is not accounted for and (ii) in the classically allowed domain, the effect of the potential $U(x)$ is disregarded. The former effect becomes more and more significant when the laser intensity grows, whereas the latter is particularly important for potentials with a long-range tail, e.g. for the Coulomb potential. In a latter subsection of this Chapter, we reformulate the amplitude Eq. (3.21) using the ITM and show that this new formulation provides a straightforward way to account for the two missing effects.

3.2. Imaginary Time Method

The ITM is a modification of the method of complex classical trajectories by Landau [Lan32, LL77]. In his work, Landau used the method complex classical trajectories in order to find the quasi-classical matrix element of an operator $\hat{f}$, defined as $\int_{-\infty}^{\infty} \psi_f^*(x)\hat{f}(x)\psi_i(x)dx$. The initial and final states, $\psi_i(x)$ and $\psi_f(x)$ take the form of semiclassical wavefunctions, which are quickly oscillating in the quasi-classical limit. Consequently, the matrix representation of the operator $\hat{f}$ is a quickly oscillating exponential integral. In his calculations, Landau assumed that the x variable is complex, displacing the path of integration off the real axis where the matrix element is evaluated into the upper half-plane. The choice of the path of integration depends on the form of the potential $U(x)$, which defines the wavefunctions of the initial and final state, via the Schrödinger equation [LL77]. The classical trajectories are found by solving the classical equations of motion. There is only one path that describes the transition, which is characterized by an intermediate point "q_0". This point was called by Landau the "transition point". The path of the transition between the initial and the final state is chosen such that it crosses the "transition point". The classical action, $S(q_1, q_2)$, from the initial position q_1 to the final one q_2 is evaluated on this path. If there are more than one transition points, the trajectory must be chosen such that the classical action takes its smallest absolute value. The transition probability is calculated with exponential accuracy as [LL77]

$$w \approx \exp\Big(-2\mathrm{Im}\big(S(q_1, q_0) + S(q_0, q_2)\big)\Big). \tag{3.22}$$

As the potential $U(x, t)$ depends explicitly on time, the energy is no longer conserved. For a slowly changing potential, described by a broad and smooth tunneling barrier, the semiclassical approximation is valid. In the semiclassical limit, the main contribution to the transition probability comes from the extremal trajectory, the path that minimizes the classical action $S(q_0, q_1, t)$, [Pop05, Pop04]. It was suggested by Popov that it is necessary to consider a narrow bundle of classical trajectories, described in

imaginary time, close to the extremal trajectory, and find the second order correction to the classical action [Pop04]. This can be done by starting from the definition of the definition of the semiclassical time-dependent wavefunction, [Pop04],

$$\psi(\mathbf{p},t) = -i\int_{-\infty}^{t} dt_1 \exp\big(-iEt_1\big)\int d\mathbf{r}\, G(\mathbf{p},t;\vec{r}_1,t_1)U(r_1)\varphi_0(r_1), \tag{3.23}$$

where $\vec{p}$ is the final momentum that characterizes the final state and $\varphi_0(r)$ is the radial component of the initial bound state wavefunction. Furthermore, $G(\mathbf{p},t;\vec{r}_1,t_1)$ is the semiclassical Green function, defined by Feynman as [Fey48, FH65]

$$G(\mathbf{r},t;\vec{r}_1,t_1) = \frac{\theta\Big(t-t_1\Big)}{2\pi i\big(t-t_1\big)^{\frac{3}{2}}}\exp\left[iS\left(\mathbf{r},t;r_1,t_1\right)\right]. \tag{3.24}$$

Here $\theta\Big(t-t_1\Big)$ is the Heaviside step function.

A Fourier transform is performed on the semiclassical operator in Eq. (3.24), expressing the propagator in the mixed representation, position-momentum, [Pop04]

$$G(\mathbf{r},t;\vec{r}_1,t_1) \approx \frac{1}{\Big(2\pi\Big)^{\frac{3}{2}}}\exp\left\{i\left[S\left(\mathbf{p},t;\mathbf{r}_1,t_1\right)-\mathbf{p}\cdot\mathbf{r}\right]\right\}. \tag{3.25}$$

The classical action $S(\mathbf{p},t;\mathbf{r}_1,t_1)$ in Eq. (3.25) is evaluated on the calculated subbarrier trajectories, determined by the initial conditions, $\mathbf{r}(t_1)=\mathbf{r}_1$ and $\mathbf{p}(t)=\mathbf{p}$. The time-dependent wavefunction can be expressed by replacing the semiclassical Green function, Eq. (3.25) in the integral definition of the wavefunction, Eq. (3.23). As a consequence, the exponential integral oscillates quickly, due to the large values that the action takes on the complex trajectories [Pop05]

$$\psi(\mathbf{p},t) = \frac{\exp\Big(-iEt\Big)}{\big(2\pi i\big)^{\frac{3}{2}}}\int_{-\infty}^{t} dt_1 d\mathbf{r}_1 \exp\Big(iW(\mathbf{p},t;\mathbf{r}_1,t_1)\Big)U(r_1)\varphi_0(r_1). \tag{3.26}$$

Here $W(\mathbf{p},t;\mathbf{r}_1,t_1)$ is the classical action, which takes the form [Pop04]

$$W(\mathbf{p},t;\mathbf{r}_1,t_1) = \int_{t_1}^{t}\left[\mathcal{L}(t')+E\right]dt' - \mathbf{p}\cdot\mathbf{r}. \tag{3.27}$$

The function $\mathcal{L}(t')$ is the classical Lagrangian of the tunneling particle, interacting with a external field,

$$\mathcal{L}(t') = \frac{m_e\dot{\mathbf{r}}^2}{2} + e\mathbf{r}\cdot\mathcal{E}(t). \tag{3.28}$$

The integral in Eq. (3.26) is calculated using the saddle-point method. In order to find the points whose contribution is larger in the calculation of the integral, we solve the following differential equation [Pop05]

$$\frac{dW}{dt} = -\mathcal{L}(t_{1\alpha}) - E. \tag{3.29}$$

The initial conditions at the instant when the subbarrier motion starts are [Pop05]

$$\mathbf{p}^2(t_0) = -2E, \qquad \mathbf{r}(t_0) = 0, \tag{3.30}$$

assuming that the tunneling particle, i.e. an electron, is located at the origin. To obtain the final velocity and position of the particle after leaving the barrier, Popov calculated the variation of the action W in the vicinity of the extremal trajectory. From the variational formalism, two boundary conditions that are the key elements in the ITM are found

$$\mathrm{Im}(\mathbf{r}(0)) = \mathrm{Im}(\dot{\mathbf{r}}(0)) = 0. \tag{3.31}$$

By convenience, the instant when the particle leaves the barrier is taken as zero. But in general, the initial time when the particle starts its motion after the barrier ϕ_0 can take any positive real value, $\phi_0 \in \mathbb{R}^+$. The conditions in Eq. (3.31) together with the classical equations of motion in complex time specify the extremal trajectory that the particle follows during its subbarrier motion.

The evaluation of the action W in Eq. (3.27) gives a complex quantity, whose imaginary part is related with the dynamics of the tunneling particle traversing the barrier. If there is only one saddle-point solution of the Eq. (3.29), the tunneling probability is [Pop05]

$$w \propto \exp\Big(-2\mathrm{Im}(W)\Big). \tag{3.32}$$

For photo-ionization, Popov showed that the tunneling probability depends sharply on the electric field strength [Pop05]. Eq. (3.32) shows the qualitative behavior of the rate. For some atomic systems in which the prefactor in front of the exponential function in Eq. (3.32) depends strongly on the final momentum of the tunneling particle, the behavior of the rate is also strongly influenced by the momentum-dependent prefactor, the missing proportionality constant in the Eq. (3.32). Following the ITM, a new version of the transition amplitude in Eq. (3.7) can be reformulated in terms of the trajectories in complex times.

3.2.1. Imaginary time method for quasistationary states

We have introduced the ITM following the method developed by Popov, [Pop05, Pop04], in the last subsection. With this formalism, we are able to describe the dynamics of the tunneling particle, e.g. electron, while it is traversing the barrier. If we do not have an initial bound state, but QS, the transition amplitude must be modified, in order to take into account continuum-continuum transitions. With that goal in mind, we reformulate the transition amplitude in the plain SFA formalism, Eq. (3.21) in terms of classical complex trajectories in this subsection.

In accordance to the Eq. (3.31), a trajectory $x_0(t)$ can be found along which the particle starts its motion at the complex time instant $t = t_s$ inside the well, $x(t_s) = 0$, having the energy $E = v^2(t_s)/2 = E_0$ and arrives at $x = b$ when $t = t_0$. Here $b = b(E_0)$ is the outer classical turning point, $U(b) = E_0$. The trajectory satisfies the Newton equation

$$\ddot{x} = \dot{v} = -\partial U/\partial x\,. \tag{3.33}$$

The exit point $x = b$ is separated from the well by the classically forbidden region. Thus, the solution of Eq. (3.33) satisfying the assigned initial conditions only exists in complex time, $t = t_0 + i\tau$. The action W_0 in Eq. (3.10) and Eq. (3.21) can be represented as

$$W_0(p_0) = \int_{t_s}^{t_0} (\mathcal{L} + E_0)dt - p_0 b\,, \tag{3.34}$$

where $\mathcal{L} = v^2/2 - U(x)$ is the field-free Lagrange function. Since the particle moves in complex time, $t \in [t_s, t_0]$, its velocity is imaginary, whereas the coordinate is real. At the exit $x(t_0) = b$ all quantities become real. To solve Eq. (3.33), one has to consider t_0 as an external parameter and τ_0 can be found from the initial condition $x_0(t_s = t_0 + i\tau_0) = 0$.

After the exit, when time becomes real $t \geq t_0$, the particle moves under the action of the laser field. The respective trajectory satisfies another Newton equation

$$\ddot{x} = \dot{v} = \dot{p}_F(t)\,, \qquad v(t_0) = p_0\,, \qquad x(t_0) = b \tag{3.35}$$

with the solution

$$x(t) = b + p(t - t_0) + G(t) - G(t_0)\,, \qquad G(t) = \int_0^t p_F(t')dt'\,. \tag{3.36}$$

The condition $\dot{x}(t_0) = p_0$ then specifies t_0 to be a function of the final momentum, p. The following algebra

$$\begin{aligned} -S_0 &= -\int_{t_0}^{+\infty} \left(v^2/2 - E_0 + \frac{d}{dt}vx - \frac{d}{dt}vx \right) dt = \\ &= \int_{t_0}^{+\infty} \left(v^2/2 + \dot{v}x + E_0 \right) dt - vx|_{t\to+\infty} + vx|_{t=t_0}\,, \end{aligned}$$

allows to represent the action S_0 in a form identical to that of Eq. (3.34). Thus, the exponential in Eq. (3.12) can be rewritten as $\exp(iW)$ where

$$W = \int_{t_s}^{+\infty} (\mathcal{L} + E_0)dt - vx|_{t\to+\infty} \tag{3.37}$$

is the classical action calculated along the complex trajectory selected described above. This is the basic result of the ITM [Pop05].

The focal point of this subsection is using ITM to generalize the transition amplitude given in plain SFA, Eq. (3.21). Indeed, one can calculate the function Eq. (3.37) accounting for both the binding potential and the field of the electromagnetic wave, i.e. evaluating the trajectory $x(t)$ from the equation

$$\ddot{x} = \dot{v} = -\partial U/\partial x + \dot{p}_F(t) \tag{3.38}$$

with initial and boundary conditions

$$x(t_s) = 0\,, \qquad v^2(t_s)/2 = E_0\,, \qquad v(t \to \infty) = p\,. \tag{3.39}$$

Except for the simplest model systems, a solution to Eqs. (3.38) and (3.39) can only be found numerically or by iteration with respect to one of the two fields. However, even in first-order perturbation theory, it is possible to account for the nonlinear effect of an intense laser field on tunneling. Indeed, if in some part of the position space the laser field is small compared with the binding force (or vice versa), corrections to trajectory δx and to the action δW can be derived perturbatively. These corrections

must remain small compared to the respective unperturbed values, $|\delta W| \ll |W|$, to justify the application of perturbation theory. However, since under semiclassical conditions Eq. (3.3) the action is numerically large, the condition

$$1 \ll |\delta W| \ll |W| \tag{3.40}$$

is typically fulfilled. This means that even a perturbative correction due to the presence of another (e.g. laser) field can cause a substantial modification of the spectra. The regime where such a semiclassical perturbation theory for the action is relevant fulfills for a variety of strong field problems [PP67, PMPB08, PMPB09, PPB08, PB08].

The correction δW consists of two parts: one due to the functionally different action that accounts for the additional interactions, and the other related to the modification of the trajectory. In the literature the first correction has been better studied than the second. In particular, in the work of Ivlev and Melnikov [IM85] presenting the first ITM treatment of LAT, only the first correction was accounted for.

To summarize, by taking into account both potential and laser fields, the differential probability of observing the electron with the asymptotic momentum p takes the form Eq. (3.21) with the amplitude

$$M(p) = \sum_{\alpha} \frac{\mathcal{P}_0(v(t_{0\alpha}))\exp(iW(p,t_{s\alpha}))}{\sqrt{dp/dt_{0\alpha} + i\beta}}\,, \tag{3.41}$$

with $W(p, t_{s\alpha})$ calculated along Eqs. (3.37) and (3.39). This distribution is the key part of our modified method to describe laser-assisted decay of QS states. It is the main result of the present Chapter. The transition amplitude $M(p)$ in Eq. (3.41) includes both the field-free and the LAT and accounts for the redistribution of the particle momenta due to the laser field after exiting the barrier. It is relevant under conditions Eq. (3.3) with the additional requirement that the number of ATI-like peaks in the spectrum should be large to keep Eqs. (3.15) and (3.16) valid, i.e. $p_0 p_F \gg \omega$ or $z_F \gg 1$. Integration over the final momenta of the particle at the detector provides the total tunneling probability. In Appendix C, it is shown that the field-free decay rate follows from Eq. (3.41) in the weak field limit $\mathcal{E}_0 \to 0$, in the case of a monochromatic field. In the next Chapter, we present a test case for the method developed here that can be treated analytically, namely LAT through a rectangular barrier.

A remaining important question is what happens to the spectrum for increasingly thick barriers up to the limit of a true bound state. For an infinitely thick barrier, the field-free decay vanishes and only ATI is possible. An examination of the equations of motion and the action considered above shows that those trajectories that correspond to the final energy $p^2/2 > U_0$ survive for the infinite barrier and the respective ionization probability is nonzero. This will result in a common ATI spectrum. We can therefore state that the present formulation contains contributions from both the laser-assisted and laser-induced processes. These contributions can be distinguished according to the type of trajectories: trajectories that vanish for an infinitely thick barrier are responsible for LAT. One should note, however, that this classification is only qualitative, since both families of trajectories depend continuously on the barrier width.

CHAPTER 4

LASER-ASSISTED TUNNELING THROUGH A RECTANGULAR BARRIER

As a test case, in this Chapter the method developed in Chapter 3 is used to determine the spectra and total decay rates for the laser-assisted tunneling (LAT) through a one-dimensional rectangular barrier. We start by considering the tunneling rate of a QS state in the presence of a static laser field, using ITM. The subbarrier trajectories and the classical action are calculated and the total decay rate is determined. In order to show the consistency of the ITM, we compare the analytic results obtained by ITM with the WKB method. A monochromatic laser pulse is considered and we calculate the final momentum distribution and the laser-assisted decay rate for two different sets of parameters of rectangular barriers. We show that depending on the parameters, two regimes of decay can be realized in the laser-assisted decay of QS states. These two regimes, referred as "inclusive" and "exclusive", were described qualitatively in several works of laser-assisted decay of particles [NR64, BMSS83, BSS84a, BSS84b]. Finally, the LAT in the presence of a short laser pulse is considered and the tunneling spectrum is determined. In order to prove the accuracy of our method, we compare our results with exact numerical solutions of the time-dependent Schrödinger equation (TDSE). The outcome of this comparison is an excellent quantitative agreement. The results presented in this Chapter have been published in [CnPBP11].

In this Chapter, we consider a test case of LAT through a one-dimensional barrier that admits an analytical solution. Due to its simplicity, we cosider the problem of the LAT through a one-dimensional rectangular barrier. Initially, the state of the particle is described as QS in a one-dimensional rectangular well of extension a, as the one depicted in Fig. 4.1. For the simplicity of the calculations, a is taken as zero. Our initial QS state has the an energy E_0 and a width Γ, with $\Gamma \ll E_0$. In the case of spontaneous decay of the QS state, the spectrum of the tunneling particle has the form of a single narrow line centered at the real part of the QS state energy, E_0. If the barrier is infinite, the initial state is then bound rather than QS. The spectrum in the presence of a monochromatic laser field when the barrier is infinite is an ATI

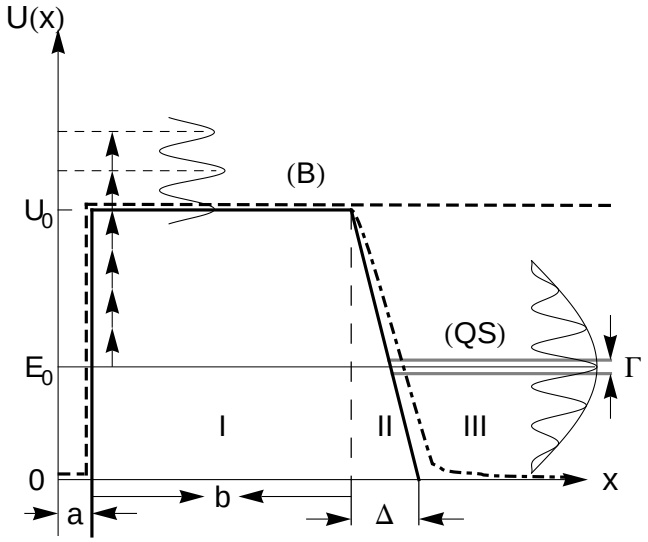

Figure 4.1: Sketch of 1D short range potential $U(x)$ including the potential well ($0 \leq x \leq a$) and rectangular barrier (I). A smooth boundary to the rectangular barrier, including the triangular barrier of width Δ (II), is shown by the dashed-dotted line. Qualitative photoelectron spectra for strong-field ionization from a true bound state (B) and a QS state (QS) are presented. Dashed line: the infinite barrier used to obtain numerically with the help of the Schrödinger equation the ground-state wavefunction of the particle inside the well. For such a barrier with $b = \infty$, only the ATI spectrum (B) is present [CnPBP11].

spectrum, consisting of several discrete maxima separated by the photon energy of the incoming laser (see Fig. 4.1).

The rectangular barrier has the thickness b, as depicted in Fig. 4.1. In order to study the LAT through the rectangular barrier, we introduce an additional triangular barrier with a negligible width Δ after the rectangular barrier (region II in Fig. 4.1), smoothing the tunneling barrier traversed by the particle. By the introduction of the triangular barrier, we are able to avoid the discontinuity in the tunneling barrier that affects the velocity of the tunneling particle at $x = b$, where the potential $U(x)$ vanishes.

We start by studying the LAT in the presence of a static field $\mathcal{E}_0$, following ITM. Next, the LAT of the QS state in the presence of a time-dependent monochromatic laser pulse given by $\mathcal{E}(t) = \mathcal{E}_0 \cos\big(\omega t\big)$ is studied, using the method we developed in Chapter 3. And finally, we investigate the LAT in the presence of a short pulse, of the form $\mathcal{E}(t) = \mathcal{E}_0 \sin^2\big(\omega t/(2n_p)\big) \cos\big(\omega t\big)$. The spectrum and the laser-assisted decay rates are calculated for the LAT in the presence of the monochromatic and the short pulse laser fields, in order to see qualitatively and quantitatively the role of the laser in the LAT of a QS state. The test case of the LAT through a rectangular barrier studied in this Chapter helps us to explore the systematics of our method developed in Chapter 3 when applied to the laser-assisted decay of QS states. We will use our formalism to investigate laser-assisted α decay, the main aim of the present thesis, in the next Chapter. Atomic units are used throughout this Chapter, so that $m_e = \hbar = 1$.

4.1. Field-free tunneling rate via ITM

Initially, we consider the field-free tunneling of a particle through a rectangular barrier by the ITM formalism. In this particular case the solution is trivial, since there is no force acting on the tunneling particle: for arbitrary ϕ_0 (time when the particle leaves the classically forbidden region), there is a single trajectory

$$x_0(\varphi) = i(\kappa_0/\omega)(\varphi - \varphi_s) \ , \quad \psi \in [\psi_0, 0] \ , \quad \psi_0 = b\omega/\kappa_0 \ ,$$
$$x_0(\varphi) = b + (p_0'/\omega)(\varphi - \phi_0) \ , \quad \varphi \in [\phi_0, +\infty) \ . \tag{4.1}$$

Here and below we use *dimensionless time* $\varphi = \omega t' = \phi_0 + i\psi(t')$. Correspondingly, $\varphi_s = \phi_0 + i\psi_0$ and $\omega t_0 = \phi_0$.

For a time-independent tunneling barrier, there is only one solution of the saddle-point equation, Eq. (3.29). The field free action can be found via the classical action defined Eq. (3.34). Correspondingly, we find that the field-free action is

$$W_0 = ib(\kappa_0 - p_0') \ , \tag{4.2}$$

with $\kappa_0^2 = 2(U_0 - E_0)$ and $p_0' = \sqrt{2E_0}$. The field-free action via ITM coincides with the reduced action calculated by the semiclassical WKB method. This result shows the consistency of the method for the field-free tunneling through the rectangular barrier. Now, we come to investigate the field-assisted tunneling in the presence of a static electric field.

4.2. Laser-assisted tunneling for a static electric field

We consider the tunneling of a particle through a rectangular barrier, interacting with a constant electric field $\mathcal{E}_0$. Since the barrier is static, the WKB method explained in Chapter 2 can be used to find the tunneling probability.

Firstly, we use the WKB method to find the penetrability through the modified tunneling barrier including the interaction with the static electric field $\mathcal{E}_0$. Then, we use the ITM to find the tunneling probability by calculating the subbarrier trajectories in complex times and determining the classical action. We eventually show the equivalence between the two methods, as the reduced action in the argument of the exponential factor in the WKB method corresponds to the classical action calculated on the subbarrier trajectories in ITM, Eq (3.34). In that sense, we are able to show the validity of ITM in the semiclassical regime.

4.2.1. Tunneling calculated via WKB method

In the WKB method, the penetrability through the tunneling barrier is calculated in terms of the reduced action, as was outlined in Chapter 2,

$$|T|^2 = \exp\Big(-2\int_0^b \sqrt{2\Big(U(x) - E_0\Big)}dx\Big). \tag{4.3}$$

For a static electric field, the potential is given by $U(x) = U_0 - x\mathcal{E}_0$. Replacing the potential $U(x)$ in Eq. (4.3), and performing a substitution of variables, it is

straightforward to find the penetrability in terms of the electric field $\mathcal{E}_0$, the energy of the tunneling particle E_0, the height of the rectangular barrier U_0 and its length b. The obtained penetrability is

$$\int_0^b \sqrt{2m\Big(U(x)-E_0\Big)} = \frac{2\sqrt{2}}{3\mathcal{E}_0}\Big(\big(U_0-E_0\big)^{\frac{3}{2}} - \big(U_0-E_0-\mathcal{E}_0 b\big)^{\frac{3}{2}}\Big). \tag{4.4}$$

This expression should be compared to the ITM result.

4.2.2. Calculation of the tunneling decay rate using ITM

Now, we use ITM in order to calculate the penetrability. The subbarrier trajectories are determined by solving the Newton equation in complex time. Then, the classical action is found along the calculated trajectories.

According to ITM, we start with the Newton equation in complex time that describes the dynamics of the tunneling particle in the subbarrier region,

$$\frac{d^2x}{d\varphi} = \frac{p_F}{\omega}, \tag{4.5}$$

with $p_F = \mathcal{E}_0/\omega$. Initially, the particle is found at $x(t_s) = a$. The initial conditions when the particle starts its motion in the subbarrier region are

$$dx/dt'(\varphi_s) = i\kappa_0, \quad \text{with} \quad \kappa_0^2 = 2\big(U_0 - E_0\big), \quad \text{and} \quad x(\varphi_s) = 0. \tag{4.6}$$

Integrating Eq. (4.5), we find the complex velocity of the tunneling particle through the rectangular barrier,

$$\frac{dx}{dt'}(\varphi) = i\kappa_0 + p_F(\varphi - \varphi_s), \qquad \varphi \in \mathbb{C}. \tag{4.7}$$

Afterwards, we find the position of the particle by integrating the velocity in the expression above. The position $x(\varphi)$ is given by

$$x(\omega) = i\frac{\kappa_0}{\omega}\big(\varphi-\varphi_s\big) + \frac{p_F}{2}\big(\varphi-\varphi_s\big)^2. \tag{4.8}$$

At $x = b$, there is a discontinuity in the tunneling barrier that affects the dynamics of the tunneling particle. In order to avoid the discontinuity, we smooth out the tunneling potential by introducing an additional potential in the form of a triangular barrier, as depicted in Fig. 4.1. The additional triangular barrier, $U_1(x)$ is defined as

$$U_1(x) = \begin{cases} 0 & \text{for } x \le b, \\ U_0 - \frac{U_0}{\Delta}(x-b) & \text{for } b \le x \le b+\Delta. \end{cases} \tag{4.9}$$

At $\varphi = \varphi_s' = \phi_0 + i\psi_0'$, the particle leaves the rectangular barrier, and enters in the region II inside the triangular barrier, as shown in Fig. 4.1, defined in Eq. (4.9). If we evaluate the position of the particle in Eq. (4.8) at $\varphi = \varphi_s'$, we obtain the following relation,

$$b = -\frac{\kappa_0}{\omega}\big(\psi_0' - \psi_0\big) - \frac{p_F}{2\omega}\big(\psi_0' - \psi_0\big)^2. \tag{4.10}$$

The velocity of the particle at the end of the subbarrier motion is found from Eq. (4.7), at $\varphi = \varphi_s'$. This is the initial velocity of the particle when it starts to move inside the triangular barrier (4.9), and is given by

$$\frac{dx}{dt'}\Big|_{\varphi=\varphi_s'} = i\kappa_0 + ip_F\big(\psi_0' - \psi_0\big). \tag{4.11}$$

Now that we have connected the motion between the region I and II (see Fig. 4.1), we can find the trajectories that the particle follows inside the triangular barrier. The Newton equation has an additional term, which comes from the definition of the additional potential, Eq. (4.9). The equation of motion is written as

$$\frac{d^2x_{II}}{\varphi^2} = \frac{p_F}{\omega} + \frac{U_0}{\omega^2\Delta}. \tag{4.12}$$

Integrating the expression above we can find the position and the velocity of the particle traversing the triangular barrier, which are

$$\begin{aligned}
\frac{dx_{II}}{dt'}(\varphi) &= i\kappa_0 + ip_F\big(\psi_0' - \psi_0\big) + p_F(\varphi - \varphi_s') + \frac{U_0}{\omega^2\Delta}\big(\varphi - \varphi_s'\big), \\
x_{II}(t') &= b + \frac{p_F}{2\omega}\big(\varphi - \varphi_s'\big)^2 + \frac{U_0}{2\omega^2\Delta}\big(\varphi - \varphi_s'\big)^2 \\
&\quad + \frac{1}{\omega}\bigg(\Big(i\kappa_0 + ip_F\big(\psi_0' - \psi_0\big)\Big)\big(\varphi - \varphi_s'\big)\bigg).
\end{aligned} \tag{4.13}$$

When $\varphi = \phi_0$, the particle leaves the barrier and starts its motion in real time (region III in Fig. 4.1). Evaluating the Eqs. (4.13), we are able to determine the velocity and the position of the particle at the end of the classically forbidden region. We find that

$$\frac{dx_{II}}{dt'}\Big|_{\varphi=\phi_0} = i\kappa_0 - i\frac{U_0\psi_0'}{\Delta\omega^2} - ip_F\psi_0, \tag{4.14}$$

$$x_{II}\big|_{\varphi=\phi_0} = b - \frac{p_F(\psi_0')^2}{2\omega} - \frac{U_0(\psi_0')^2}{\Delta\omega^2} + \frac{\psi_0'}{\omega}\bigg(\kappa_0 + \frac{\mathcal{E}_0}{\omega}\big(\psi_0' - \psi_0\big)\bigg). \tag{4.15}$$

In accordance to ITM, the velocity of the particle once it leaves the tunneling barrier must be real. Thus, the imaginary part of the velocity in region II, given by the first expression in Eq. (4.14) is zero. This condition allows us to find an expression for the time of flight of the particle inside the triangular barrier ψ_0'/ω in terms of the time of flight inside the rectangular barrier, ψ_0, the electric field $\mathcal{E}_0$ and κ_0. The time of flight inside the triangular barrier is

$$\psi_0' = \frac{\omega\Delta}{U_0}\left(\kappa_0 - p_F\psi_0\right). \tag{4.16}$$

It can be seen in the equation above that in the limit where $\Delta \to 0$, the time of flight inside the triangular barrier ψ_0'/ω vanishes and the original rectangular barrier is recovered.

Replacing Eq. (4.16) in the final position of the particle after leaving the barrier, Eq. (4.14), we find that the particle leaves the barrier at

$$x_{II}\big|_{\varphi=\phi_0} = b + \frac{p_F\omega\Delta^2}{2U_0^2}\Big(\kappa_0 - p_F\psi_0\Big). \tag{4.17}$$

In consequence, in the limit where $\Delta \to 0$, the final position of the particle coincides with the position where the rectangular barrier comes to an end, as expected.

Now, once the particle leaves the barrier, its velocity is zero, in accordance to Eq. (4.14), and its dynamics are described in real time. Outside the barrier, the particle interacts with the static electric field and the force related with the triangular barrier U_1. The dynamics of the particle are determined by these two forces in the time interval $[\phi_0/\omega, \phi_1/\omega]$. Afterwards, the particle is affected only by the interaction with the static field. The equation of motion in the interval $[\phi_0, \phi_1]$ takes the same form as Eq. (4.12). The velocity and the position for $t \in [\phi_0, \phi_1]$ are expressed as

$$\frac{dx_{\triangle}}{dt'} = p_F(\varphi - \phi_0) + \frac{U_0}{\omega^2 \Delta}(\varphi - \phi_0), \qquad \varphi \in [\phi_0, \phi_1], \tag{4.18}$$

$$x_{\triangle} = b + \frac{p_F \omega \Delta^2}{2U_0^2}\Big(\kappa_0 - p_F \psi_0\Big) + \frac{p_F}{2\omega}(\varphi - \phi_0)^2 + \frac{U_0}{2\Delta\omega^2}(\varphi - \phi_0)^2. \tag{4.19}$$

At $\varphi = \phi_1$, the position of the particle is $b + \Delta$. Evaluating the equations above at $\varphi = \phi_1$, we can find an expression for ϕ_1

$$(\phi_1 - \phi_0) = \omega \sqrt{\left(\Delta - \frac{\mathcal{E}_0 \Delta^2}{2U_0^2}\Big(\kappa_0 - \omega p_F \psi_0\Big)\right)\left(\frac{\omega p_F}{2} + \frac{U_0}{2\Delta}\right)^{-1}}. \tag{4.20}$$

As expected, in the limit $\Delta \to 0$, ϕ_1 goes to ϕ_0.

Now, we calculate the classical action defined by Popov in [Pop05], Eq. (3.27), on the classical trajectories, Eqs. (4.7), (4.8) . The particle position, Eq. (4.8), and the velocity, Eq. (4.7), are complex inside the barrier. As Popov explained in [Pop05], for a static case, there is only one solution to the saddle-point equation, Eq. (3.29). So, there is no interference between the trajectories described by the particle for a single saddle-point solution.

In the case of the static field, the tunneling rate is expressed as the exponential function of the imaginary part of the action, Eq. (3.32), taking the same form that Popov found in [Pop05]. In consequence, to find the tunneling rate, it is enough to evaluate the classical action on the trajectories inside the barrier, Eqs. (4.7) and (4.8).

Replacing the trajectories Eqs. (4.8) and (4.7) in the definition of the classical action in Eq. (3.27), we find that the imaginary part of the classical action W takes the form

$$\mathrm{Im}(W) = \frac{p_F^2 \psi_0^3}{6\omega} - \frac{\kappa_0 p_F \psi_0^2}{2\omega} - \frac{2\kappa_0^2 \psi_0}{\omega}. \tag{4.21}$$

The imaginary part of the classical action W is expressed in terms of the time of flight of the particle through the rectangular barrier ψ_0/ω. In order to compare the result in Eq. (4.21) with Eq. (4.4), we need to express ψ_0 in terms of the parameters of the rectangular barrier, b, U_0 and the electric field $\mathcal{E}_0$. We recall the definition of the traversal time, by Büttiker and Landauer [BL82], which is associated with the time that the tunneling particle spends inside the barrier. The traversal time through a rectangular barrier like the one in Fig. 4.1 was defined by Büttiker and Landauer as

$$\tau_t = \int_0^b \frac{dx}{\sqrt{2\Big(U(x) - E_0\Big)}}. \tag{4.22}$$

In the case of the tunneling through a rectangular barrier in the presence of a static electric field, the traversal time in Eq. (4.22) takes the form

$$\tau_t = \frac{\sqrt{2}}{\mathcal{E}_0}\Big(\sqrt{U_0 - E_0} - \sqrt{U_0 - E_0 - b\mathcal{E}_0}\Big). \tag{4.23}$$

We identify the traversal time in Eq. (4.22) with the time of flight through the rectangular barrier, ψ_0/ω.

Replacing the definition of ψ_0/ω given by Eq. (4.22) in our result, Eq. (4.21), we find that the imaginary part of the action W takes the following form

$$\mathrm{Im}(W) = \frac{2\sqrt{2}}{3\mathcal{E}_0}\Big(\big(U_0 - E_0\big)^{\frac{3}{2}} - \big(U_0 - E_0 - b\mathcal{E}_0\big)^{\frac{3}{2}}\Big). \tag{4.24}$$

This is exactly the same result that we obtained using the WKB method, Eq. (4.4). The equivalence between our ITM result and the WKB reduced action shows the consistency of the ITM for a time-independent barrier.

4.3. Laser-assisted tunneling for a monochromatic pulse

Following the calculation of the decay rate of a particle tunneling through a rectangular barrier shown in the last section of this Chapter, we consider now the LAT of the particle in the case of an external monochromatic laser field.

According to the ITM, one has to find trajectories which start at $t' = t_s$ from inside the well, $x(t_s) = 0$, its kinetic energy is $v^2(t_s)/2 = E_0 - U_0 \equiv -\kappa_0^2/2$ so that $v(t_s) = i\kappa_0$. The velocity is imaginary in complex time and becomes real since the evolution of the dynamics of the tunneling barrier is described in real time when the particle leaves the barrier. Afterwards, the particle only interacts with the laser field, $\mathcal{E}(t') = \mathcal{E}_0 \cos(\omega t')$ and the trajectory followed by the particle is real. At a final time, the laser field is switched off adiabatically, such that particle arrives at the detector having a final momentum p.

We start showing the calculations of the subbarrier trajectories and the dynamics outside of the rectangular barrier in the case of the monochromatic laser field. Next, the total classical action W is determined on the trajectories previously calculated. From the classical action, defined in Eq. (3.34), the transition amplitude $M(p)$ is found by Eq. (3.41), in accordance to the method we have developed in Chapter 3. Finally, the laser-assisted differential decay rate and the total decay rate are calculated.

Now we should find the trajectories in the presence of the monochromatic laser field. As it was discussed in Section 4.2, the tunneling barrier has a discontinuity at $x = b$. In order to calculate the trajectories, we introduce an additional potential that smooths the total tunneling barrier, see Fig. 4.1. This additional potential is a triangular barrier with a negligible width Δ, defined in Eq. (4.9). Thus, the subbarrier trajectories are calculated for both the rectangular and the triangular barrier. When the particle leaves the classically forbidden region at the time ϕ_0/ω, the dynamics of the tunneling particle are described in real time, in accordance to ITM. The particle initially interacts with the force due to the triangular barrier and the

monochromatic field up to a time ϕ_1/ω. At that time, the triangular barrier vanishes and consequently, the only force acting on the particle is due to the monochromatic laser field. Finally, at $\varphi = \omega t_F$, the electric field is switched off adiabatically and the particle with final momentum p, is measured in a detector far away from the rectangular barrier.

We start with the calculation of the trajectories inside the rectangular barrier, region I in Fig. 4.1. Inside the rectangular barrier, the dynamics of the particle are studied in complex times, in accordance to ITM. The equation of motion in region I takes the form

$$\frac{d^2x^{\mathrm{I}}}{d\varphi^2} = \frac{p_F}{\omega}\cos(\varphi), \quad \text{with } \varphi = \phi_0 + i\psi, \psi \in [\psi_0', \psi_0]. \tag{4.25}$$

We find the subbarrier trajectories by solving the equation above. Under the rectangular barrier, the trajectory is given by

$$v^{\mathrm{I}}(\varphi) = \kappa_0(i - \gamma^{-1}(\sin(\varphi) - \sin(\varphi_s))) \ , \tag{4.26}$$

and

$$x^{\mathrm{I}}(\varphi) = b\{\mu(i\gamma + \sin(\varphi_s))(\varphi - \varphi_s) + \mu(\cos(\varphi) - \cos(\varphi_s))\} \ . \tag{4.27}$$

Here two dimensionless parameters are introduced

$$\gamma = \kappa_0\omega/\mathcal{E}_0, \quad \mu = \mathcal{E}_0/\omega^2 b, \tag{4.28}$$

which determine the relative strength and frequency of the external field. Note that γ in (4.28) has the same physical meaning as the Keldysh parameter [Kel65], i.e. the ratio of the "atomic" momentum κ_0 to the field induced momentum p_F.

In the region II, as is shown in Fig. 4.1, we replace the discontinuous potential by a smooth one, namely, the dashed line where the potential drops down to zero on the width Δ, defined in Eq. (4.9). The tunneling particle enters the triangular barrier at φ_s', the time when $\mathrm{Re}x^I[\varphi_s'] = b$, and leaves the tunneling region at $\varphi = \phi_0$. In region II, the equation of motion is given by

$$\frac{dx^{\mathrm{II}}}{d\varphi} = \frac{U_0}{\Delta} + p_F\cos(\varphi), \quad \text{with } \varphi = \phi_0 + i\psi, \psi \in \left[\psi_0', 0\right] \tag{4.29}$$

In the intermediate region II the solution is

$$\begin{aligned} v^{\mathrm{II}}(\varphi) &= v^{\mathrm{I}}(\varphi_s') - p_F(\sin(\varphi) - \sin(\varphi_s')) + (F_0/\omega)(\varphi - \varphi_s') \ , \quad F_0 = U_0/\Delta \ , \\ x^{\mathrm{II}}(\varphi) &= x^{\mathrm{I}}(\varphi_s') + (p_F/\omega)(\cos(\varphi) - \cos(\varphi_s')) + (F_0/2\omega^2)(\varphi - \varphi_s')^2 \ . \end{aligned} \tag{4.30}$$

The dynamics of the particle outside of the barrier is determined by the Newton equations in real time. Between $\varphi = \phi_0$ and $\varphi = \phi_1$, the tunneling particle dynamics are described in real time and the particle feels the forces by the triangular barrier and the time-dependent monochromatic field. We detail the calculations of the trajectories in this time interval in Appendix B. Later on, as $\varphi \geq \phi_1$, the particle only interacts with the laser field, since there is no other time-independent potential $U(x) = 0$. The calculated trajectories in that region take the form

$$v^{\mathrm{III}}(\varphi) = v_0 - p_F(\sin(\varphi) - \sin(\phi_0)) \ , \quad \rightarrow \ p = v_0 + p_F\sin(\phi_0), \tag{4.31}$$

$$x^{\mathrm{III}}(\varphi) = x^{\mathrm{I}}(\phi_0) + p/\omega(\varphi - \phi_0) + (p_F/\omega)(\cos(\varphi) - \cos(\phi_0)) \ . \tag{4.32}$$

Here v_0 is the velocity of the particle after leaving the triangular barrier. As the particle only interacts with the electric field, the equation of motion has exactly the same functional form as the ones inside the rectangular barrier. The main difference comes with the initial time of the motion, which is $t = \phi_0$ in region III. In consequence, the subbarrier trajectories follow Eq. (4.26) and Eqs. (4.27). The time interval when the motion of the particle after the barrier takes place starts at $t' = \phi_0/\omega$ up to the final time t_F, when the particle reaches the detector. At $t' = t_F$, when the final momentum p is measured, the electric field has been switched off adiabatically.

For a time-dependent field, there is more than a single solution of the saddle-point equation, Eq. (3.29). Accordingly, for every value of final energy $E_F = p^2/2$ there are two different initial times of the motion in real time, ϕ_{0_1}/ω and ϕ_{0_2}/ω. The associated trajectories that the particle follows after the barrier are completely different. Yet, the final energy measured at t_F, when the particle reaches the detector, is exactly the same.

Matching the solutions in the domains I, II and III, we can find the constant v_0 as a function of the other parameters. We show in the Appendix B that the sharper the slope is, $\Delta \to 0$ the closer the time instant $\varphi_s' = \phi_0 + i\psi_0'$ to ϕ_0. Consequently, the time of flight of the particle inside the triangular barrier ψ_0' goes to 0, as well as the time spent by the particle outside of the triangular $\phi_1 - \phi_0$.

Decomposing the equations with respect to $\psi_0' \ll 1$ we obtain:

$$\begin{aligned} v_0 = \Big\{ \left(p_0'\right)^2 + 2\kappa_0 p_F \cos(\phi_0)\sinh(\psi_0) + p_F^2[(\cosh(\psi_0)-1)^2\sin^2(\phi_0) \\ - \cos^2(\phi_0)\sinh^2(\psi_0)] \Big\}^{\frac{1}{2}} \ . \end{aligned} \tag{4.33}$$

Then the two equations determining the initial time φ_s are:

$$b = (\kappa_0/\omega)\psi_0 - (p_F/\omega)\cos(\phi_0)(\cosh(\psi_0) - 1 - \psi_0\sinh(\psi_0)) \ , \tag{4.34}$$

$$p = v_0(\varphi_s) + p_F\sin(\phi_0) \ . \tag{4.35}$$

The first equation arises from the requirement that the particle escapes from the barrier when time arrives on the real axis, $\varphi = \phi_0$. At the same time, the imaginary part of the trajectory becomes a nonzero constant, in the general case

$$\mathrm{Im}\left[x\left(\varphi \geq \phi_0\right)\right] \equiv X_0 = (\mathcal{E}_0/\omega^2)\sin(\phi_0)\left[\sinh(\psi_0) - \psi_0\cosh(\psi_0)\right] \ .$$

For the most probable trajectories corresponding to $\phi_0 = 0,\ \pi$, $X_0 = 0$. Eqs. (4.35) can be solved analytically in the limit of weak field, $\mu \ll 1$, or low-frequency field $\gamma \ll 1$, while in general case numerical solution is required. We detail the calculation in the weak field in Appendix C. The low frequency limit approaches the case of a static electric field, see the results detailed in Section 4.2.

Note that solutions do not exist for all values of the final momentum and for arbitrary parameters μ and γ. Indeed, from the second equation of Eq. (4.35) it is clear that the final momentum is determined by the time instant ϕ_0/ω when the particle is released from the barrier and its initial velocity v_0. Thus, it cannot have an arbitrary value, since the width of the momentum space available is determined roughly by the field momentum, $p_{\mathrm{max,min}} \approx p_0' \pm p_F$. Another restriction comes from the fact that Eqs. (4.27) and (4.30) assume that the instant kinetic energy at the exit is below the instant barrier height, $v_0^2 < 2(U_0 - \mathcal{E}_0 b\cos(\phi_0))$. This imposes a condition on

the electric field, $\mathcal{E}_0 b < \kappa_0^2/2$. In the opposite case, Eqs. (4.27) and (4.30) for the trajectories and Eqs. (4.35) for the initial time should be generalized.

In the limit of the rectangular barrier, $\Delta \to 0$, the domain II vanishes and the action is determined by trajectories Eq. (4.27) and (4.32) and the Lagrange function

$$\mathcal{L} = \dot{x}^2/2 + \mathcal{E}_0 x \cos(\varphi) - U_0 \theta(b - x) \ . \tag{4.36}$$

Here, $\theta(x)$ is the step function.

Initially, we find the action evaluated on the classical trajectories during the subbarrier motion, i.e., from $\varphi_s = \phi_0 + i\psi_0$ to $\varphi_f = \phi_0$. From the definition of the classical action inside the barrier, Eq. (3.34), we can identify the three main contributions to the action: the kinetic energy, the stationary tunneling barrier and the interaction with the monochromatic laser field. The final time of integration in Eq. (4.37) is only the real part of φ, ϕ_0, which is the time when the particle leaves the rectangular barrier. We show in depth the calculations of the three contributions to the action in Appendix D. Since we have expressed the subbarrier trajectories in terms of the dimensionless parameter φ, we use the Leibniz rule to perform a simple substitution of variables,

$$W_0 = \frac{1}{\omega} \int_{\phi_0 + i\psi_0}^{\phi_0} \left[\frac{1}{2} \Big(\omega \frac{dx}{d\varphi}(\varphi) \Big)^2 - (U_0 - E_0) + \omega p_F x(\varphi) \cos(\varphi) \right] d\varphi. \tag{4.37}$$

With the trajectories outside the barrier given by Eq. (4.32), we can find the action on the trajectories in real time as

$$W_{\text{out}} = \frac{1}{\omega} \int_{\phi_0}^{t_F} \left[\frac{1}{2} \Big(\omega \frac{dx}{d\varphi}(\varphi) \Big)^2 + E_0 + \omega p_F x(\varphi) \cos(\varphi) \right] d\varphi. \tag{4.38}$$

Now that the action outside the barrier has been found, Eq. (4.38), the total action is defined by ITM, Eq. (3.37) as

$$W = W_0 + W_{\text{out}} - \big(xp\big)\big|_{t'=t_F}. \tag{4.39}$$

This is the classical action that enters in the definition of the transition amplitude $M(p)$, Eq. (3.41).

In the weak field regime, $\mu \ll 1$ or $\nu = \mathcal{E}_0 b/\kappa_0^2 \ll 1$, the result in Eq. (4.39) can be simplified by keeping only terms linear to $\mathcal{E}_0$. Then, the action has the form

$$\begin{aligned} W_\alpha(p) &= i\kappa_0 b \left(1 + \frac{\mathcal{E}_0 b \cos(\phi_{0\alpha})}{2\kappa_0^2} + \frac{p_0 \mathcal{E}_0 \psi_{00}^3 \sin(\phi_{0\alpha})}{3\kappa_0 b \omega^2} \right) + \frac{p_0(p - p_0)}{\omega} \phi_{0\alpha} \\ &+ \psi_{00} \frac{\mathcal{E}_0 b^2 \sin(\phi_{0\alpha})}{2\kappa_0} - pb + p_F b \sin(\phi_{0\alpha}) + \frac{\kappa p_F}{\omega} \cos(\phi_{0\alpha}) \,, \end{aligned} \tag{4.40}$$

with $\psi_0 \approx \psi_{00} = b\omega/\kappa_0 \ll 1$.

We show schematically the dynamics of the tunneling particle during its subbarrier motion and after leaving the barrier in Fig. (4.2). Now that we have calculated the total action, we can determine the differential decay rate.

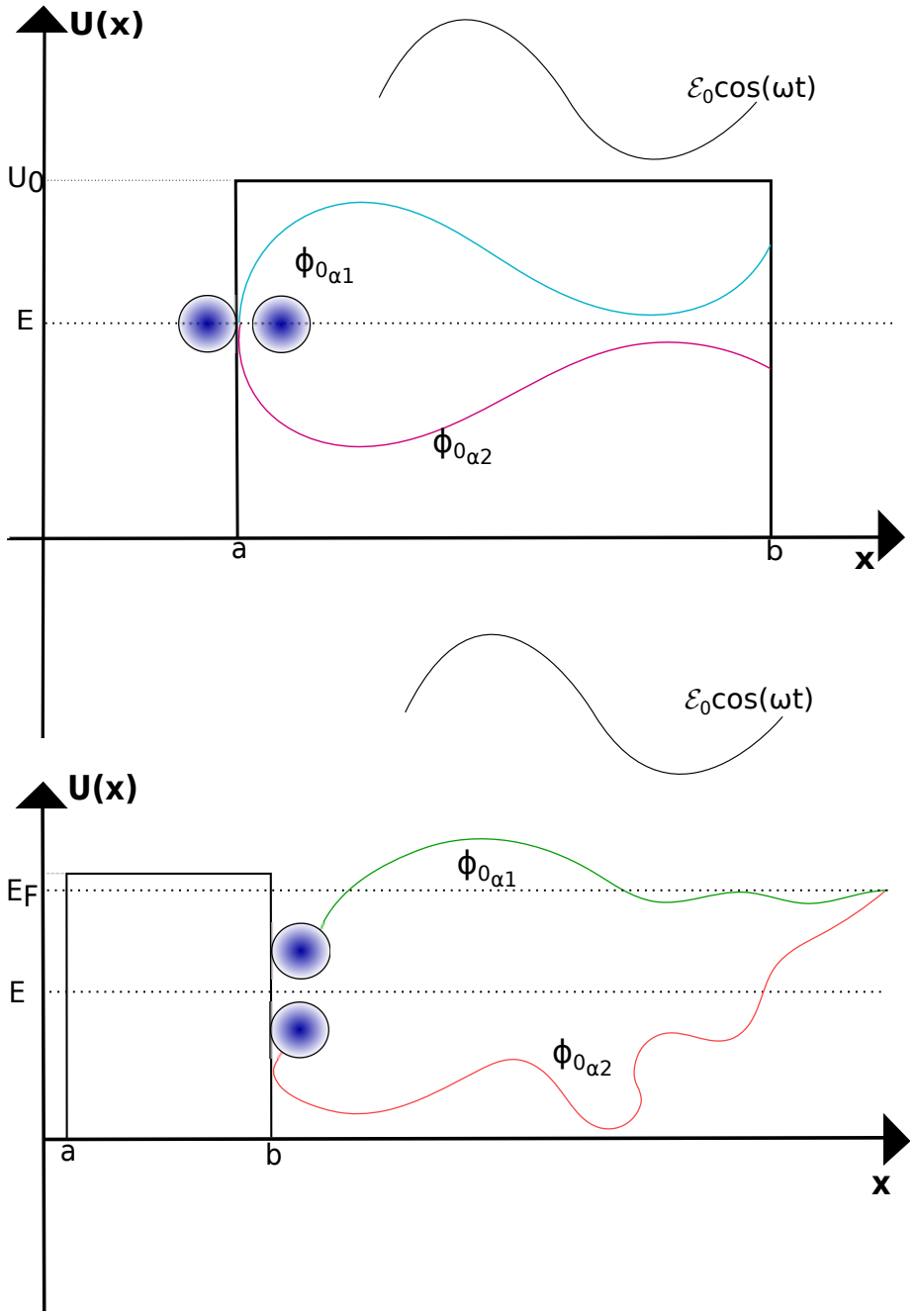

Figure 4.2: Qualitative picture of the motion inside (above) and outside the barrier (below) for different solutions of the saddle-point equation. The electric field outside of the barrier (thin black line) is switched off adiabatically. Each subbarrier trajectory corresponding to the same final energy E_F is related to a solution of the saddle-point equation, $\phi_{0_{\alpha 1}}$ and $\phi_{0_{\alpha 2}}$. The associated trajectories are shown (blue and red, for the subbarrier motion and red and green lines, for the motion outside the barrier). If we are in the "inclusive" regime, the laser does affect the dynamics of the subbarrier motion of the tunneling particle. On the other hand, in the "exclusive" regime, the laser only affects the dynamics of the particle outside of the barrier. On its way to the detector, the tunneling particle only interacts with the laser field. The two trajectories for a single E_F are added coherently in accordance to Eq. (3.41).

4.2.2.1. Differential decay rate

We can obtain the differential decay rate from the transition amplitude in Eq. (3.41). First of all, we need to calculate the regularization constant β in the denominator of the transition amplitude for the rectangular barrier. We can find the exact value of β by replacing the definition of p, given in Eq. (4.31) and the Reiss parameter z_F in Eq. (3.4), in Eq. (3.20). For the rectangular barrier, β takes the form

$$\beta_{rb} = \omega \mathcal{E}_0^{\frac{1}{3}}. \tag{4.41}$$

For the monochromatic field (3.14) all periods are equivalent, so that there are only two essentially different solutions, all the others being obtained by a $2\pi k$ translation, for all $k \in \mathbb{Z}$. The distinction between the solutions of the two saddle-point equation for a final energy comes in the two possible values of the action W. A schematic picture of the dynamics of the particle on its way to the detector is shown in Fig. 4.2. The sum of the action $W(\mathbf{p}_k)$ over all laser periods is expressed as [PP10]

$$\begin{aligned}\sum_{k=-\infty}^{\infty} \exp\Big[-iW(\mathbf{p}_k)\Big] &= \sum_{k=-\infty}^{\infty} \exp\Big[i\frac{2\pi k}{\omega}\big(\frac{p^2}{2} + U_p - E_0 - k\big)\Big] \\ &= \omega \sum_{k=-\infty}^{k} \delta\Big(\frac{p^2}{2} + U_p - E_0 - k\omega\Big).\end{aligned} \tag{4.42}$$

Here we have used the fact that

$$\sum_{k=-\infty}^{\infty} \delta(x-k) = \sum_{k=-\infty}^{k} \exp\big(2\pi i k x\big). \tag{4.43}$$

As it can be seen in Eq. (4.42), the summation over all periods gives the factor $\omega\,\delta(p^2/2 - E_0 + U_P - j\omega)$, which expresses energy conservation.

Replacing the value of β_{rb}, Eq. (4.41) and the Eq. (4.42), in the modified transition amplitude (3.41), we find the transition amplitude $M(p)$ for the tunneling through a rectangular barrier in the presence of a monochromatic laser field,

$$M(p) = \omega \sum_{k=-\infty}^{\infty} \sum_{\alpha} \frac{\mathcal{P}_0\left[v(t_{0\alpha})\right] \exp\left[iW\left(p, t_{s\alpha}\right)\right]}{\sqrt{dp/dt_{0\alpha} + i\beta_{rb}}} \delta\left(\frac{p^2}{2} + U_p - E_0 - k\omega\right). \tag{4.44}$$

In Eq.(3.21) we have shown that the differential rate dw/dp is given by the modulus squared of the transition amplitude $|M(p)|^2$. From Eq. (4.44), we see that the transition amplitude has a quadratic Dirac delta distribution $\delta\Big(\frac{p^2}{2} + U_p - E_0 - l\omega\Big)^2$. The quadratic Dirac delta term can be expressed in terms of the observation time $T = t'_F \gg \phi_0/\omega$ as follows

$$\delta\left(\frac{p^2}{2} + U_p - E_0 - k\omega\right)^2 = \frac{T}{2\pi}\delta\left(\frac{p^2}{2} + U_p - E_0 - k\omega\right).$$

In consequence, the differential decay rate R over the whole observation time $T = t_F$ for the LAT through the rectangular barrier in the presence of a monochromatic laser field is given by

$$dR = \frac{dw(p)}{T} = \sum_k \omega^2 \frac{\delta(p - p_k)}{2\pi p_k} \frac{8\kappa_0^3 p_0}{\kappa_0^2 + p_0^2} \left| \sum_{\alpha=1,2} \frac{\exp\left(iW(p, t'_{s\alpha})\right)}{\sqrt{dp/dt_{0\alpha} + i\beta_{rb}}} \right|^2 dp\,, \tag{4.45}$$

where $p_k = \sqrt{p_0^2 - p_F^2/2 + 2k\omega}$ are the momenta corresponding to the ATI-like peaks. Here we have taken into account that the prefactor $\mathcal{P}_0$ corresponding to the field-free rate $R_0 = \mathcal{P}_0^2 \exp(-2\kappa_0 b)$ is given (in the narrow well limit $\kappa_0 a \ll 1$) by

$$\mathcal{P}_0^2 = \frac{8\kappa_0^3 p_0}{\kappa_0^2 + p_0^2}\,. \tag{4.46}$$

For the action (4.40), the probability vanishes in the limit $b \to \infty$. This, however cannot be consistent with the existence of ATI for an infinitely thick barrier. The apparent paradox can be solved if we take into account that the results of this subsection are found by assuming that the particle escapes from under the barrier at its right edge, $x = b$. This is, however, true only when $\mathcal{E}_0 b \leq U_0 - E_0$. Clearly, with increasing barrier thickness b, this condition will be violated for any given field amplitude and trajectories that escape through the tilted part of the barrier will come into play. Along such trajectories, the action becomes b-independent and virtually identical to the case of common ATI.

4.4. Laser-assisted tunneling for a few-cycles pulse

Considering instead of the monochromatic field a few-cycle laser pulse, we calculate the trajectories inside and outside the rectangular barrier. We calculate the total decay rate and the spectra using a six-cycle pulse of the form

$$\mathcal{E}(t) = \mathcal{E}_0 \sin^2\left(\frac{\omega t}{2n_p}\right)\cos(\omega t)\,, \qquad n_p = 6. \tag{4.47}$$

The initial conditions of the subbarrier motion are given in Eq. (4.6). The equation of motion in the classically forbidden region takes the form

$$\frac{d^2x^{\mathrm{I}}}{d\varphi^2} = \frac{p_F}{\omega}\sin^2\left(\frac{\varphi}{2n_p}\right)\cos(\varphi), \qquad \varphi = \phi_0 + \psi \in \mathbb{C} \quad \text{and} \quad \psi \in [0, \psi_0]. \tag{4.48}$$

Using trigonometric functions properties, the last expression can be written as

$$\frac{d^2x^{\mathrm{I}}}{d\varphi^2} = \frac{p_F}{2\omega}\cos(\varphi) - \frac{p_F}{4\omega}\cos\left[\left(1 + \frac{1}{n_p}\right)\varphi\right] - \frac{p_F}{4\omega}\cos\left[\left(1 - \frac{1}{n_p}\right)\varphi\right]. \tag{4.49}$$

The equation above shows that the short pulse in Eq. (4.47) can be taken as a superposition of three monochromatic pulses with different frequencies. Accordingly, the total subbarrier trajectory is the superposition of the trajectories calculated for the three monochromatic pulses. Solving Eq. (4.49), the trajectories under the rectangular barrier are found in terms of the dimensionless parameter φ and take

the form

$$\frac{dx^{\mathrm{I}}}{dt'} = i\kappa_0 - \frac{p_F}{2}\left[\sin(\varphi) - \sin(\varphi_s)\right] + \frac{p_F n_p}{4\big(n_p+2\big)}\left\{\sin\left[\frac{\varphi\big(n_p+2\big)}{n_p}\right] - \sin\left[\frac{\varphi_s\big(n_p+2\big)}{n_p}\right]\right\} + \frac{p_F n_p}{4\big(n_p-2\big)}\left\{\sin\left[\frac{\varphi\big(n_p-2\big)}{n_p}\right] - \sin\left[\frac{\varphi_s\big(n_p-2\big)}{n_p}\right]\right\}, \tag{4.50}$$

$$\begin{aligned} x^{\mathrm{I}} =& \big(\varphi-\varphi_s\big)\left\{i\frac{\kappa_0}{\omega} + \frac{p_F\sin(\varphi_s)}{2\omega} - \frac{p_F n_p}{4\omega\big(n_p+2\big)}\sin\left[\frac{\varphi_s(n_p+2)}{n_p}\right] - \frac{p_F n_p}{4\omega\big(n_p-2\big)}\sin\left[\frac{\varphi_s(n_p-2)}{n_p}\right]\right\} - \frac{p_F}{2\omega}\left[\cos(\varphi)-\cos(\varphi_s)\right] \\ &+ \frac{p_F n_p^2}{4\omega\big(n_p+2\big)^2}\left\{\cos\left[\frac{\varphi\big(n_p+2\big)}{n_p}\right] - \cos\left[\frac{\varphi_s\big(n_p+2\big)}{n_p}\right]\right\} \\ &+ \frac{p_F n_p^2}{4\omega\big(n_p-2\big)^2}\left\{\cos\left[\frac{\varphi\big(n_p-2\big)}{n_p}\right] - \cos\left[\frac{\varphi_s\big(n_p-2\big)}{n_p}\right]\right\}. \end{aligned} \tag{4.51}$$

Similarly to the case of the monochromatic laser field in Section 4.3, we introduce an additional potential to smooth the rectangular barrier and avoid the discontinuity at $x = b$. The trajectories inside the region II take the form

$$\begin{aligned} v^{\mathrm{II}}(\varphi) =& v^{\mathrm{I}}(\varphi_s') - \frac{p_F}{2}\left[\sin(\varphi) - \sin(\varphi_s')\right] + \frac{p_F n_p}{4\big(n_p+2\big)}\left\{\sin\left[\frac{\varphi\big(n_p+2\big)}{n_p}\right] - \sin\left[\frac{\varphi_s'\big(n_p+2\big)}{n_p}\right]\right\} + \frac{p_F n_p}{4\big(n_p-2\big)}\left\{\sin\left[\frac{\varphi\big(n_p-2\big)}{n_p}\right] - \sin\left[\frac{\varphi_s'\big(n_p-2\big)}{n_p}\right]\right\} \\ &+ \frac{F_0}{\omega}\left(\varphi-\varphi_s'\right), \qquad F_0 = U_0/\Delta\ , \end{aligned} \tag{4.52}$$

$$\begin{aligned} x^{\mathrm{II}}(\varphi) =& x^{\mathrm{I}}(\varphi_s') + \left\{\frac{v^{\mathrm{I}}(\varphi_s')}{\omega} + \frac{p_F}{2\omega}\sin(\varphi_s') - \frac{p_F n_p}{4\omega\big(n_p+2\big)}\sin\left[\frac{\varphi_s'\big(n_p+2\big)}{n_p}\right] - \frac{p_F n_p}{4\omega\big(n_p-2\big)}\sin\left[\frac{\varphi_s'(n_p-2)}{n_p}\right]\right\}\big(\varphi-\varphi_s'\big) - \frac{p_F}{2\omega}\left[\cos(\varphi)-\cos(\varphi_s')\right] \\ &+ \frac{p_F n_p^2}{4\omega\big(n_p+2\big)^2}\left\{\cos\left[\frac{\varphi\big(n_p+2\big)}{n_p}\right] - \cos\left[\frac{\varphi_s'\big(n_p+2\big)}{n_p}\right]\right\} \\ &+ \frac{p_F n_p^2}{4\omega\big(n_p-2\big)^2}\left\{\cos\left[\frac{\varphi\big(n_p-2\big)}{n_p}\right] - \cos\left[\frac{\varphi_s'\big(n_p-2\big)}{n_p}\right]\right\} \\ &+ \frac{F_0}{2\omega^2}\left(\varphi-\varphi_s'\right)^2\ . \end{aligned} \tag{4.53}$$

Here, $\varphi_s' = \phi_0 + i\psi_0'$.

In the limit where the triangular barrier in Eq. (4.9) disappears and since $\mathrm{Re}\left[x^{\mathrm{I}}\varphi_s\right] = b$, we can find an expression for ψ_0 in terms of ϕ_0, the barrier parameters b, κ_0 and the field momentum p_F, similar to the one we found for the monochromatic case,

Eq. (4.34),

$$
\begin{aligned}
b = & \frac{p_F}{2\omega}\left[\cosh(\psi_0) - 1 - \psi_0\sinh(\psi_0)\right] \\
& - \frac{p_F n_p}{4\omega(n_p-2)}\cos\left(\frac{\phi_0 n_p}{n_p-2}\right)\left\{\frac{n_p}{n_p-2}\left[\cosh\left(\frac{\psi_0 n_p}{n_p-2}\right)-1\right] - \psi_0\sinh\left(\frac{\psi_0 n_p}{n_p-2}\right)\right\} \\
& - \frac{p_F n_p}{4\omega(n_p+2)}\cos\left(\frac{\phi_0 n_p}{n_p+2}\right)\left\{\frac{n_p}{n_p+2}\left[\cosh\left(\frac{\psi_0 n_p}{n_p+2}\right)-1\right] - \psi_0\sinh\left(\frac{\psi_0 n_p}{n_p+2}\right)\right\} \\
& + \frac{\kappa_0\psi_0}{\omega}\ .
\end{aligned}
\tag{4.54}
$$

At $\varphi = \phi_0$, the motion in real time starts. In accordance to ITM, the imaginary part of the velocity evaluated at that time is zero. Evaluating Eq. (4.52) at $\varphi = \phi_0$, we find an expression for the time of flight of the tunneling particle through the triangular barrier, ψ_0', region II in Fig. 4.1. The time of flight ψ_0' is

$$
\begin{aligned}
\psi_0' = \frac{\omega\Delta}{U_0}\Bigg\{ & \kappa_0 - \frac{p_F}{2}\cos(\phi_0)\sinh(\psi_0) + \left[\frac{p_F n_p}{4\big(n_p-2\big)}\cos\left(\frac{\phi_0 n_p}{n_p-2}\right)\sinh\left(\frac{\psi_0 n_p}{n_p-2}\right)\right] \\
& + \left[\frac{p_F n_p}{4\big(n_p+2\big)}\cos\left(\frac{\phi_0 n_p}{n_p+2}\right)\sinh\left(\frac{\psi_0 n_p}{n_p+2}\right)\right]\Bigg\}\ .
\end{aligned}
\tag{4.55}
$$

As expected, in the limit $\Delta \to 0$, the time of flight of the tunneling particle through the triangular barrier vanishes. The imaginary part of the position of the particle at $\varphi = \phi_0$ is

$$
\begin{aligned}
\mathrm{Im}\left[x^{\mathrm{II}}(\varphi=\phi_0)\right] = & \frac{p_F}{2\omega}\sin(\phi_0)\left[\sinh(\psi_0) - \psi_0\cosh(\psi_0)\right] \\
& - \frac{p_F n_p^2}{4\omega\big(n_p-2\big)^2}\sin\left(\frac{\phi_0 n_p}{n_p-2}\right)\left[\sinh\left(\frac{\psi_0 n_p}{n_p-2}\right) - \frac{(n_p-2)\psi_0}{n_p}\cosh\left(\frac{\psi_0 n_p}{n_p-2}\right)\right] \\
& - \frac{p_F n_p^2}{4\omega\big(n_p+2\big)^2}\sin\left(\frac{\phi_0 n_p}{n_p+2}\right)\left[\sinh\left(\frac{\psi_0 n_p}{n_p+2}\right) - \frac{(n_p+2)\psi_0}{n_p}\cosh\left(\frac{\psi_0 n_p}{n_p+2}\right)\right].
\end{aligned}
\tag{4.56}
$$

The trajectories that the particle follows outside the barrier are determined by solving the Newton equation, for $\varphi \geq \phi_1$,

$$
\begin{aligned}
v^{\mathrm{III}}(\varphi) = v_0 - \frac{p_F}{2}\left[\sin(\varphi) - \sin(\phi_0)\right] & + \frac{p_F n_p}{4(n_p-2)}\left[\sin\left(\frac{n_p\varphi}{n_p-2}\right) - \sin\left(\frac{n_p\phi_0}{n_p-2}\right)\right] \\
& + \frac{p_F n_p}{4(n_p+2)}\left[\sin\left(\frac{n_p\varphi}{n_p+2}\right) - \sin\left(\frac{n_p\phi_0}{n_p+2}\right)\right],
\end{aligned}
\tag{4.57}
$$

$$
\begin{aligned}
x^{\mathrm{III}}(\varphi) = b &+ \mathrm{Im}\left[x^{\mathrm{II}}(\varphi=\phi_0)\right] \\
&+ \left(\varphi-\phi_0\right)\left[\frac{v_0}{\omega}+\frac{p_F}{2\omega}\sin(\phi_0)-\frac{p_F n_p}{4\omega(n_p-2)}\sin\left(\frac{n_p\phi_0}{n_p-2}\right)\right. \\
&\left.-\frac{p_F n_p}{4(n_p+2)}\sin\left(\frac{n_p\phi_0}{n_p+2}\right)\right]-\frac{p_F}{2\omega}\left(\cos(\varphi)-\cos(\phi_0)\right) \\
&+\frac{p_F n_p^2}{4\omega\left(n_p-2\right)^2}\left[\cos\left(\frac{\varphi n_p}{n_p-2}\right)-\cos\left(\frac{\phi_0 n_p}{n_p-2}\right)\right] \\
&+\frac{p_F n_p^2}{4\omega\left(n_p+2\right)^2}\left[\cos\left(\frac{\varphi n_p}{n_p+2}\right)-\cos\left(\frac{\phi_0 n_p}{n_p+2}\right)\right] \ .
\end{aligned}
\tag{4.58}
$$

Here, v_0 is the velocity of the particle after leaving the triangular barrier.

For a short pulse there are several solutions of the saddle-point equation, Eq. (3.29). The number of solutions of the saddle-point equation is related by the number of cycles n_p. In our calculations, we consider $n_p = 6$. We have twelve saddle-points in this particular case. Accordingly, for every value of final energy $E_F = p^2/2$ there are twelve different initial times of the motion in real time, which is a significant difference with respect to the monochromatic laser field, with only two solutions of the saddle-point equation.

As it was shown for the monochromatic field, the trajectories in the domains I, II and III are connected at $\varphi = \varphi_s$ and $\varphi_s = \varphi_s'$. The constant v_0 is found as a function of the other parameters. In the case of the short pulse, when the time of flight through the triangular barrier $\psi_0' \ll 1$, the velocity v_0 is:

$$
\begin{aligned}
v_0 = \Bigg\{ & 2U_0 + \Big\{ \frac{p_F}{2}\left[\cosh(\psi_0)-1\right]\sin(\phi_0) \\
&-\frac{p_F n_p}{4\left(n_p-2\right)}\sin\left(\frac{n_p\phi_0}{n_p-2}\right)\left[\cosh\left(\frac{n_p\psi_0}{n_p-2}\right)-1\right] \\
&-\frac{p_F n_p}{4\left(n_p+2\right)}\sin\left(\frac{n_p\phi_0}{n_p+2}\right)\left[\cosh\left(\frac{n_p\psi_0}{n_p+2}\right)-1\right]\Big\}^2 \\
&-\left[\kappa_0-\frac{p_F}{2}\cos(\phi_0)\sinh(\psi_0)+\frac{n_p p_F}{\left(n_p-2\right)}\cos\left(\frac{n_p\phi_0}{n_p-2}\right)\sinh\left(\frac{n_p\psi_0}{n_p-2}\right)\right. \\
&\left.+\frac{n_p p_F}{\left(n_p+2\right)}\cos\left(\frac{n_p\phi_0}{n_p+2}\right)\sinh\left(\frac{n_p\psi_0}{n_p+2}\right)\right]^2\Bigg\}^{\frac{1}{2}} \ .
\end{aligned}
\tag{4.59}
$$

The final momentum after the electric field has been switched off is written in terms of v_0 as

$$
p = v_0(\varphi_s) - \frac{p_F}{2}\sin(\phi_0) + \frac{p_F n_p}{4\left(n_p-2\right)}\sin\left(\frac{n_p\phi_0}{n_p-2}\right) + \frac{p_F n_p}{4\left(n_p+2\right)}\sin\left(\frac{n_p\phi_0}{n_p+2}\right) \ . \tag{4.60}
$$

The classical action is calculated on the subbarrier trajectories, Eq. (4.51), and the trajectories outside the barrier, Eqs. (4.57) and (4.58) in an identical way as it was

calculated for the monochromatic laser field, i.e.,

$$W_0 = \frac{1}{\omega}\int_{\phi_0+i\psi_0}^{\phi_0}\left\{\frac{1}{2}\left[\frac{dx^{\mathrm{I}}}{dt'}(\varphi)\right]^2 - (U_0 - E_0) + \omega p_F x^{\mathrm{I}}(\varphi)\sin^2\left(\frac{\varphi}{2n_p}\right)\cos(\varphi)\right\}d\varphi, \tag{4.61}$$

$$W_{\mathrm{out}} = \frac{1}{\omega}\int_{\phi_0}^{\omega t_F}\left\{\frac{1}{2}\left[\frac{dx^{\mathrm{III}}}{dt'}(\varphi)\right]^2 + E_0 + \omega p_F x^{\mathrm{III}}(\varphi)\sin^2\left(\frac{\varphi}{2n_p}\right)\cos(\varphi)\right\}d\varphi. \tag{4.62}$$

The total action is found using Eq. (4.39). From the calculated total action along the trajectories that the particle follows, we can determine the transition amplitude via Eq. (3.41).

For the short pulse, the transition amplitude $M(\mathbf{p})$ consists of up to $2n_p$ coherent contributions, corresponding to the $2n_p$ saddle-point solutions. The spectrum of Dirac-delta functions in Eq. (4.45) is replaced by a comb of broadened ATI-like maxima between E_{min} and E_{max}. In consequence, the differencial decay rate per pulse takes the form

$$\frac{dw(p)}{dp} = \frac{8\kappa_0^3 p_0}{\kappa_0^2 + p_0^2}\left|\sum_{\alpha=1}^{2n_p}\frac{\exp\left(iW(p,t_{s\alpha})\right)}{\sqrt{dp/dt_{0\alpha} + i\beta_{rb}}}\right|^2 . \tag{4.63}$$

4.5. Numerical results

As numerical examples we first consider tunneling through two rectangular barriers of parameters $U_0 = 3.0,\ b = 3.0$ and $U_0 = 4.0,\ b = 10.0$ assisted by a monochromatic laser field with frequency $\omega = 0.1$. The action W and the rate R are obtained using the expressions given in Eq. (4.45) and Appendix D. We first calculate the trajectories that the particle follows inside and outside the barrier according to ITM. For each energy between the classical boundaries (CB), E_{min} and E_{max}, we have two different solutions of the saddle-point equation. The solutions are associated with trajectories starting inside the well at times $\varphi_{s\alpha}$ with $\alpha = 1, 2$. We present the results of the initial time of the motion outside of the barrier ϕ_0, as a function of the final energy E_F, for three different field intensities, $\mathcal{E}_0 = 0.02$, 0.05 and 0.12 a.u. in Fig. 4.3. We can distinguish a local maximum and a local minimum in Fig. 5.9, associated with the CB. As it was mentioned earlier in this chapter, the range of final energies E_F is restricted between the CB. The time of flight of the tunneling particle inside the rectangular barrier is calculated from Eq. (B.4). The deformed ellipse-like shape that the imaginary part of the initial dimensionless parameter ψ_0 takes as a function of the final energy E_F in Fig. 4.4 shows the distinction between the solutions of the saddle-point solutions for a final energy of the tunneling particle E_F. For a single final energy, there are two associated values of the imaginary part of the initial complex dimensionless "time", ψ_0. This parameter is related to the time of flight of the tunneling particle traversing the rectangular barrier. In consequence, for a single value of E_F there are two possible trajectories that the tunneling particle follows in the subbarrier region. In addition, we can see in Figs. 5.9 and Fig. 4.4 that for higher laser field intensities, the range of values that the time of flight ψ_0 takes increases and the ellipse-like shape increases its size. When the final energies take closer values to the CB, the difference between the solutions of the saddle-point equation is smaller.

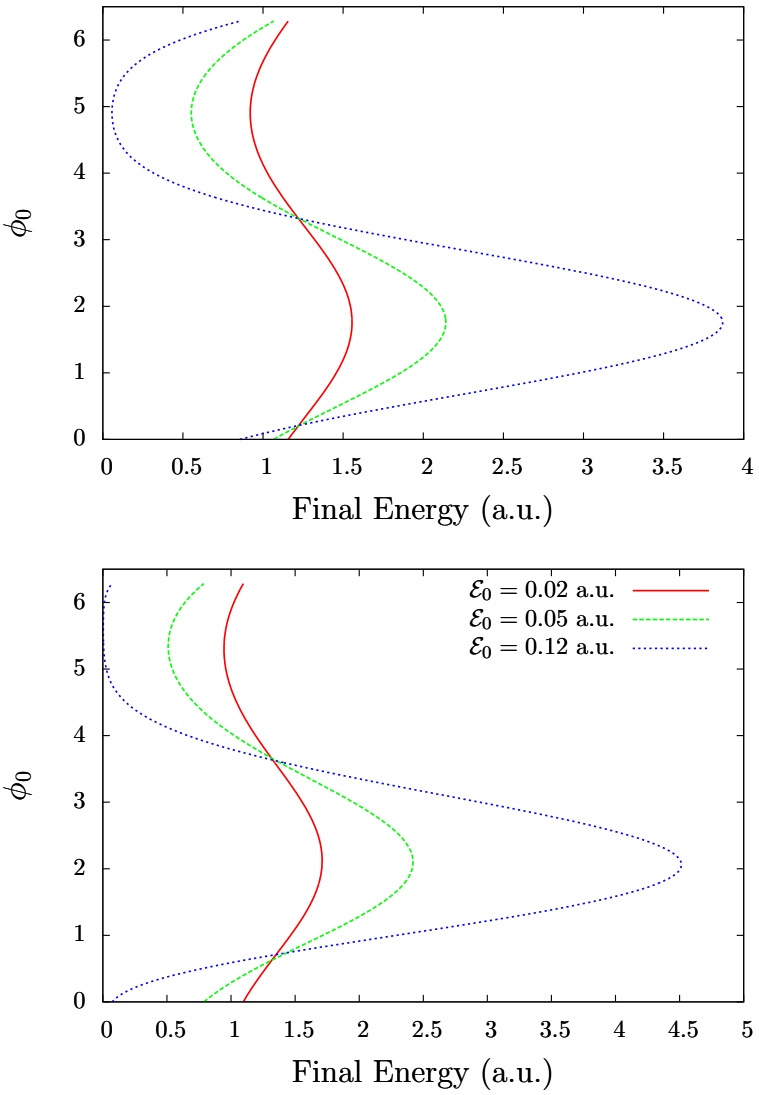

Figure 4.3: Real part of the initial complex dimensionless parameter $\mathrm{Re}\,(\varphi_s) = \phi_0$ as a function of the final energy E_F for three electric fields $\mathcal{E} = 0.02$, 0.05 and 0.12 of frequency $\omega = 0.1$ for the thin rectangular barrier ($U_0 = 3.0$, $b = 3.0$, $E_0 = 1.217$, $\omega = 0.10$) above and thick rectangular barrier ($U_0 = 4.0$, $b = 10.0$, $E_0 = 1.302$) below.

In Fig. 4.5 we present the imaginary part of the action Im(W) and the spectrum of the LAT as a function of the final energy E_F for three different field amplitudes $\mathcal{E}_0$. As a consequence of the difference between the values of the time of flight ψ_0/ω and ϕ_0, the imaginary part of the action has two values for a single final energy, determining two different branches. The spectrum consists of several ATI-like maxima whose positions are dictated by the energy conservation conditions in Eq. (4.45). In the case of the thin barrier with $b = 3$, the LAT occurs mostly field-free, and the main effect of the laser is to change the particle momentum after the barrier exit. By comparing the results for different field intensities in Figure 4.5b, we observe that the spectra become narrower with the decrease of $\mathcal{E}_0$, approaching the Lorenzian shape of the field-free decay rate. Furthermore, the ratios between the field-free and LAT probabilities do not vary much for the considered field amplitudes $R_{0.02}/R_0 = 0.41$,

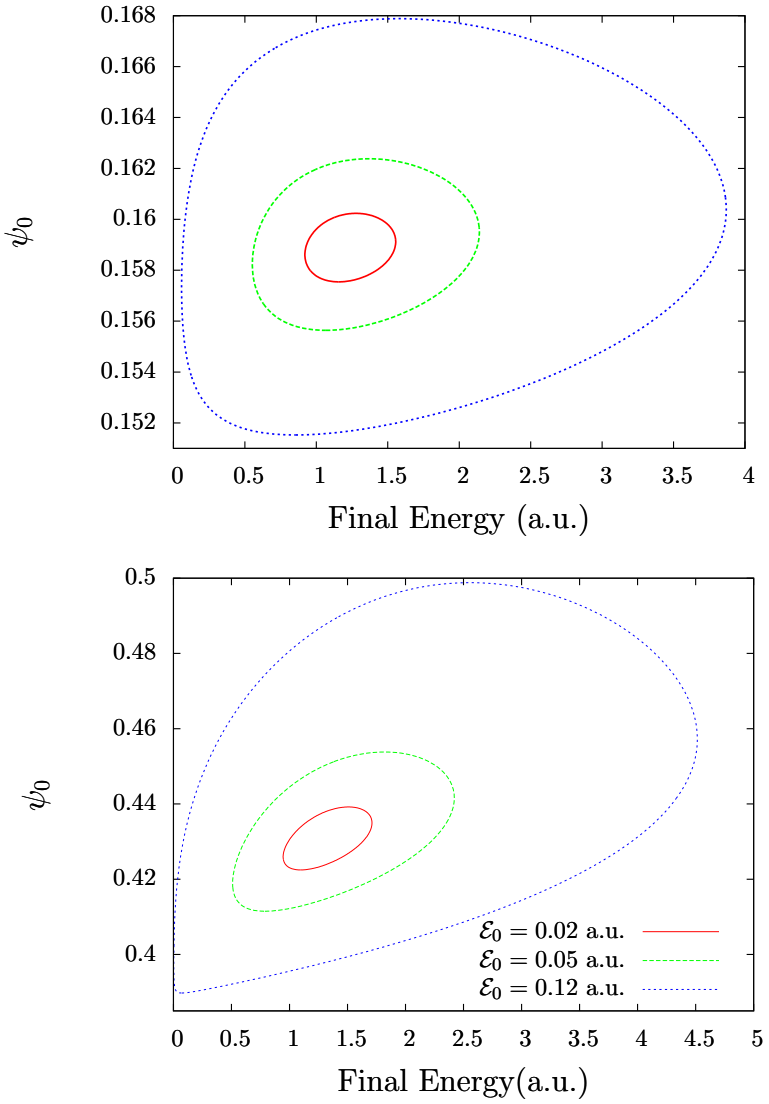

Figure 4.4: Imaginary part of the initial complex dimensionless parameter $\mathrm{Im}\,(\varphi_s) = \psi_0$ as a function of the final energy E_F for three electric fields $\mathcal{E} = 0.02$, 0.05 and 0.12 of frequency $\omega = 0.1$ for the thin rectangular barrier ($U_0 = 3.0$, $b = 3.0$, $E_0 = 1.217$, $\omega = 0.10$) above and thick rectangular barrier ($U_0 = 4.0$, $b = 10.0$, $E_0 = 1.302$) below.

$R_{0.05}/R_0 = 0.62$ and $R_{0.12}/R_0 = 0.89$. Note that for these parameters, the large number of ATI-like maxima condition $p_0 p_F \gg \omega$, necessary to justify the momentum distribution along Eq. (3.15) is not fulfilled. As a consequence, our distribution loses a part of the tunneled particles, and the laser-assisted to field-free decay ratios are less than unity. Due to this effect, it is more informative to consider as reference the laser-assisted rate at the lowest field intensity. This gives us $R_{0.12}/R_{0.02} \approx 2$, showing that the laser field of the amplitude $\mathcal{E}_0 = 0.12$ only enhances the total decay rate by the factor of 2 for this barrier width.

In contrast, for the thick barrier of width $b = 10$, corresponding to a very small field-free decay rate, the "inclusive" regime is achieved, in which the laser has a substantial effect also on the tunneling rate itself. Here, the ratios of the field-free

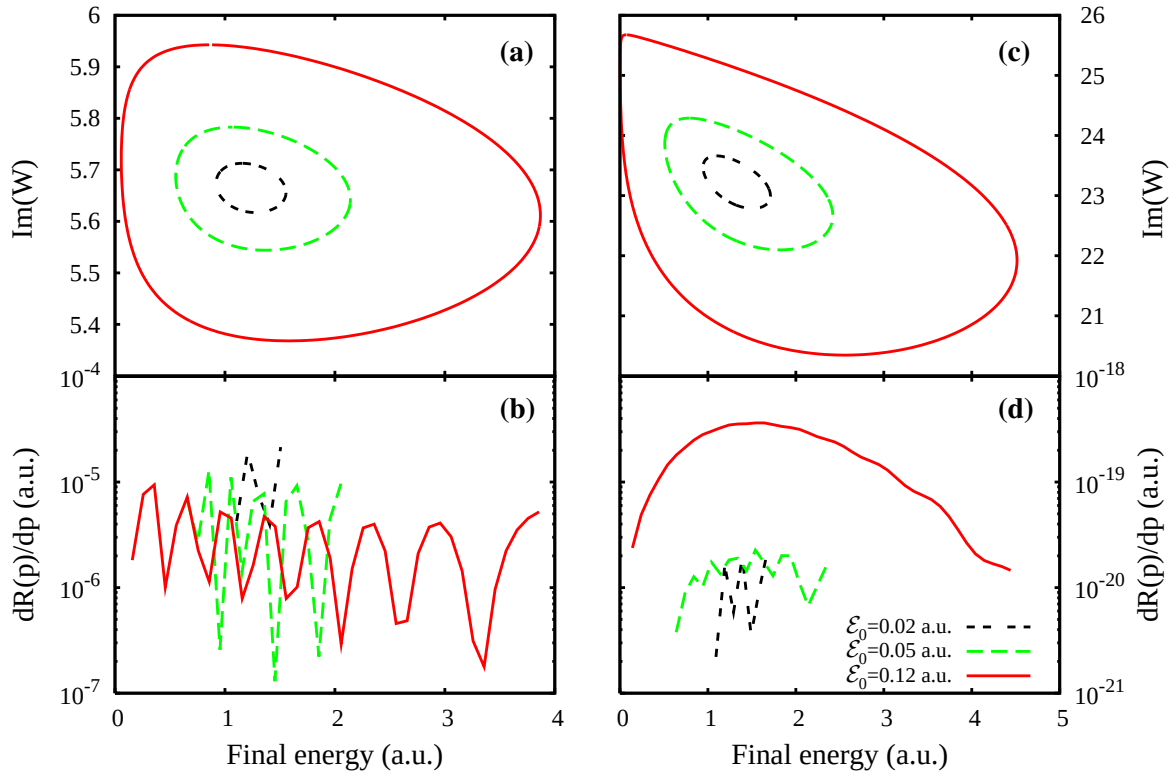

Figure 4.5: Imaginary part of the action $\mathrm{Im}(W)$ (a), (c) and the spectra (b), (d) as a function of the the final energy $E = p^2/2$ for two sets of parameters: $U_0 = 3.0$, $b = 3.0$, $E_0 = 1.217$, $\omega = 0.10$, (a)-(b) and $U_0 = 4.0$, $b = 10.0$, $E_0 = 1.302$, $\omega = 0.10$, (c)-(d). Each panel shows three curves for $\mathcal{E}_0 = 0.02$ (black double-dashed line), $\mathcal{E}_0 = 0.05$ (dashed green line) and $\mathcal{E}_0 = 0.12$ (solid red line).

and LAT probabilities are $R_{0.02}/R_0 = 0.72$, $R_{0.05}/R_0 = 1.94$ and $R_{0.12}/R_0 = 58.17$, extending over almost two orders of magnitude with the increasing field.

Thus, our method described in Chapter 3 reproduces important qualitative conclusions of the earlier studies on laser-assisted decay of elementary particles which holds also for the laser-assisted decay of QS states[NR64, BSS84b, BSS84a, BMSS83]. Namely that depending on the parameters, there are two different regimes of decay: "exclusive", when *the spectrum is strongly affected without a modification of the total decay rate* (the thin barrier) and "inclusive", when *the rate of decay and the spectrum are strongly modified by the laser field* (the thick barrier). The physical difference between the two regimes becomes clear if we notice that for a strong modification of the spectrum no high-field intensity is actually needed, but only a large quiver (ponderomotive) energy. The latter can be achieved at low laser frequencies. A relatively weak but low-frequency laser field strongly affects the kinematics of the charged particle, accelerating or decelerating it after decay. This changes the final energy at the detector with almost no effect on the total decay probability.

In contrast, in the "inclusive" regime, the particle's dynamics on the short-time scale corresponding to the subbarrier motion is also influenced, modifying the total probability. This indeed requires high laser field strengths. The particular expression of the critical field that delimits the "inclusive" regime depends on the investigated system.

In the case of the monochromatic case, we find a true criterion in the weak-field limit corresponding to the "exclusive" regime, from Eq. (4.40). We introduce the parameter μ_{ext} defined such that in the "inclusive" regime (thick barrier)

$$\mu_{ext} = \kappa_0 b \frac{\mathcal{E}_0 b}{\kappa_0^2} \gg 1 \ . \tag{4.64}$$

On the other hand, the "exclusive" regime requires $\mu_{ext} \ll 1$ and holds for the first set of parameters.

Under the further simplification that only the most probable trajectory is considered (i.e. $\phi_0 = 0$ or π) and the real part of the action is disregarded (no interference), the result of Ivlev and Melnikov is recovered [IM85]. It should be noted however that the result of Ivlev and Melnikov in [IM85] is more general than the one of this section, since the former does not assume the potential to be a rectangular barrier.

In Figs. 4.6 and 4.7, we have considered the case of the thin barrier with $b = 3$ for different laser field amplitudes and frequencies such that the field momenta are $p_F = 1$. We calculate the dimensionless parameter ψ_0 as a function of the final energy and the initial dimensionless parameter ϕ_0 related to the instant when the particle leaves the barrier. The ratio of the different field frequencies can be identified from the spectra. The total tunneling rate is increasing with increasing the field, with $R_{0.1}/R_0 = 0.74$, $R_{0.2}/R_0 = 0.91$ and $R_{0.3}/R_0 = 1.56$.

4.5.1. Few-cycle laser pulse

For the few-cycle laser pulse, defined by Eq. (4.47) the spectrum of Dirac-delta functions will be replaced by a comb of broadened ATI-like maxima between $E_{\min}$ and $E_{\max}$. Spectra obtained using the extended ITM for a six-cycle pulse for the

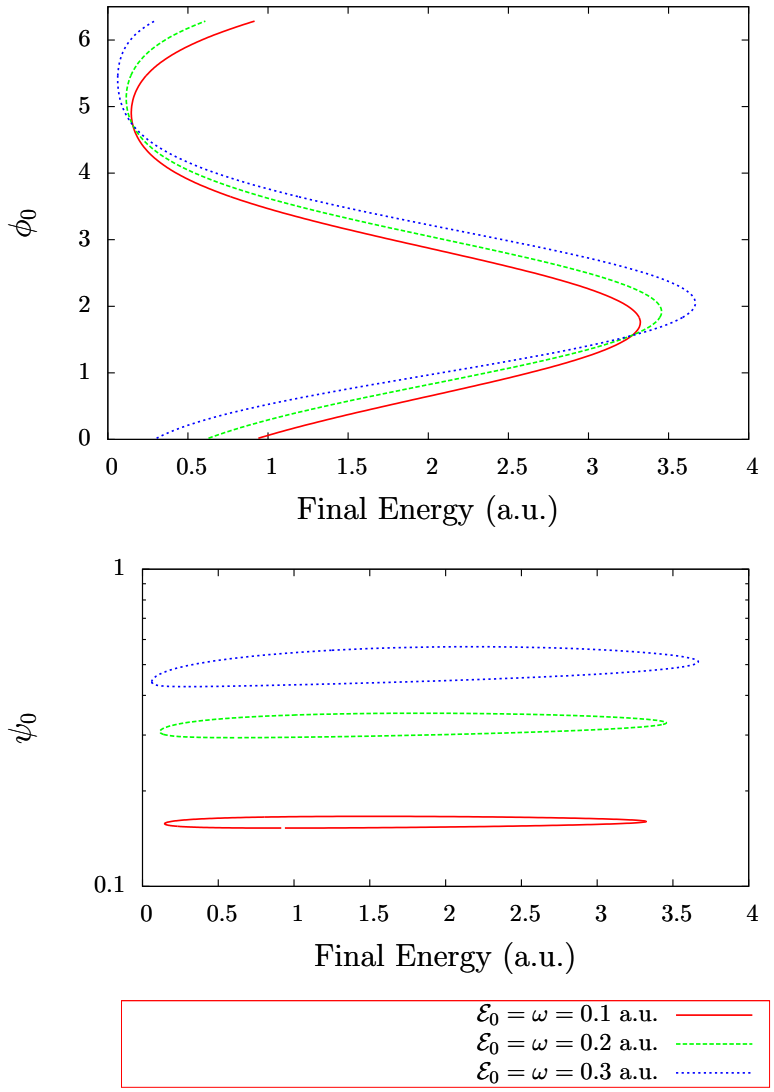

Figure 4.6: Real and imaginary part of the initial dimensionless parameter φ_s, ϕ_0 (above) and ψ_0 (below) calculated for monochromatic fields with various frequencies and field momenta $p_F = 1$ for the thin barrier considered in Figure 4.5. The field amplitudes and frequencies are $\mathcal{E}_0 = 0.1$ and $\omega = 0.1$ (black double-dashed line), $\mathcal{E}_0 = 0.2$ and $\omega = 0.2$ (green dashed line) and $\mathcal{E}_0 = 0.3$ and $\omega = 0.3$ (red solid line), respectively.

parameters previously addressed in the text are presented in Fig. 4.8. Here the amplitude consists of up to $2n_p$ coherent contributions that produce the interference pattern of the spectra.

The broad ATI-like maxima can be observed best for the thick barrier case in Fig. 4.8d, where the absolute values of the two contributions from a given laser period differ substantially and smear out the interference. Unlike the case of tunneling assisted by a monochromatic field where the differential rate $dR(p)$ is calculated, the spectra in Fig. 4.8 present the differential probability $dw(p)/dp$. The differential decay rate $w(p)/dp$ per pulse duration delivers approximately the decay rate.

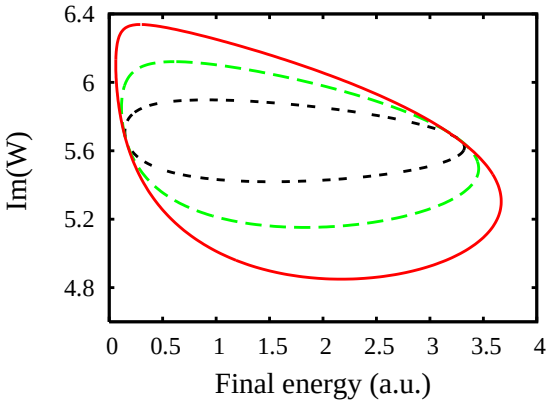

Figure 4.7: Imaginary part of the action (left) and laser assisted decay spectra (right) calculated for monochromatic fields with various frequencies and field momenta $p_F = 1$ for the thin barrier considered in Figure 4.5. The field amplitudes and frequencies are $\mathcal{E}_0 = 0.1$ and $\omega = 0.1$ (red solid line), $\mathcal{E}_0 = 0.2$ and $\omega = 0.2$ (green dashed line) and $\mathcal{E}_0 = 0.3$ and $\omega = 0.3$ (blue dashed line), respectively.

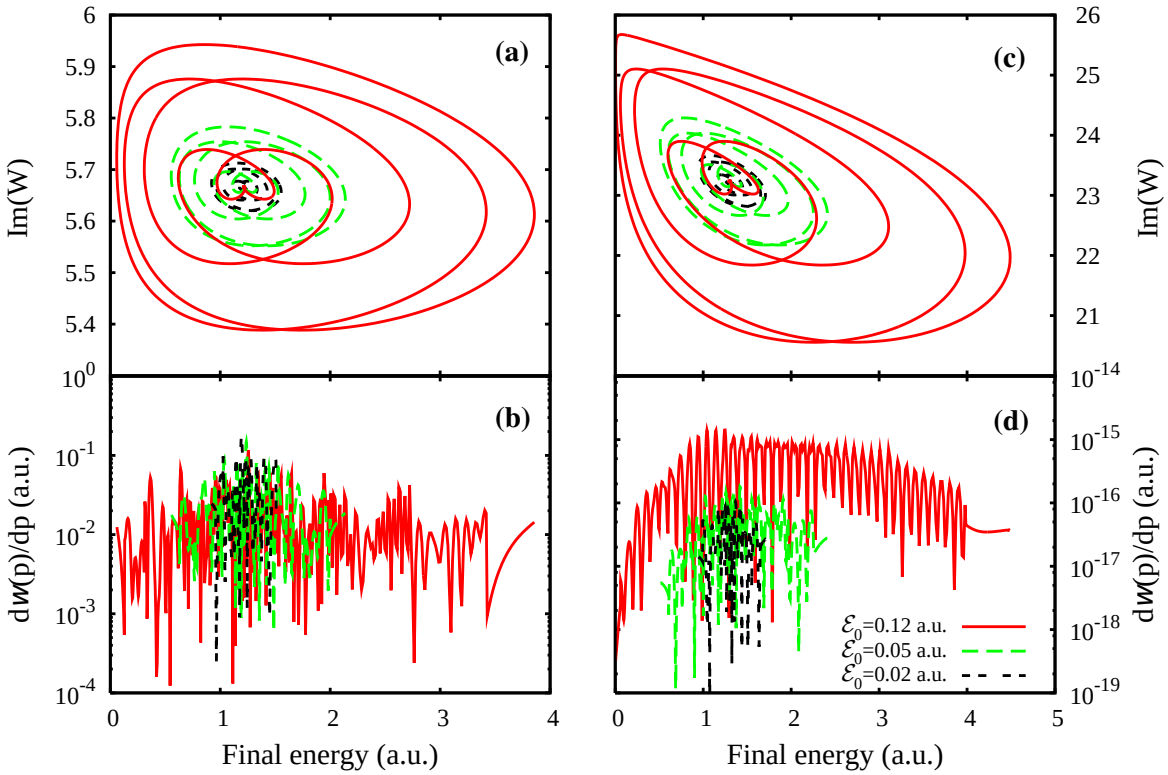

Figure 4.8: Imaginary part of the action (a), (c) and laser assisted decay spectra (b), (d) calculated for a finite pulse of the form (4.47) for the two barrier parameter sets of Figure 4.5 and fields of frequency $\omega = 0.1$ and amplitudes $\mathcal{E}_0 = 0.02,\ 0.05,\ 0.12$.

4.5.2. Comparison with numerical results of the time-dependent Schrödinger equation

In order to check the accuracy of our approach, we compared the obtained spectra with accurate numerical results of the TDSE. For the test case of the rectangular barrier, we have calculated exact numerical spectra using a one-dimensional version of the QPROP Schrödinger solver [BK06], which propagates the wavefunction in real time on a spatial grid. For the numerical simulations, the width of the potential well (in which $U = 0$) needed to be specified and was chosen as $a = \pi/2$. We first obtained the ground state wavefunction for the particle inside the well of height U_0=3 and $b \to \infty$, i.e., a barrier of infinite width, as depicted by the dashed line in Fig. 4.1. The ground state energy on the numerical grid of spacing $\Delta x = 0.1$ was $E_0 = 1.24$. At time $t = 0$, the infinite barrier was replaced by a barrier of finite width $b - a = 4$, keeping the height constant. As a consequence, tunneling occurs for $t > 0$. The sudden switch from the infinite to the finite barrier disturbs the trapped electron and leads to a short time interval of transient tunneling dynamics before a constant free-tunneling rate is established. However, this time interval of a few atomic units is much shorter than the pulse duration so that it did not make a difference whether the six-cycle laser pulse of the form (4.47) and frequency $\omega = 0.057$ (Ti:Sa laser) was switched on at $t = 0$ or with a delay. In any case, the numerical grid was big enough to support the entire wavefunction during the propagation time without reflections off the grid boundary. The electron spectra were calculated using the window operator technique (see, e.g., [BK06]) and normalized to the field-free decay.

In Fig. 4.9, we compare the obtained tunneling probabilities for a barrier of thickness $b - a = 4$, height $U_0 = 3$ and initial particle energy $E_0 = 1.24$ under the action of fields of amplitudes $\mathcal{E}_0$=0.02 (Fig. 4.9a) and $\mathcal{E}_0$=0.005 (Fig. 4.9b). The spectra agree well both qualitatively and quantitatively for final energies within the CB, with the ITM results slightly higher than the TDSE ones. From a comparison of the two field-free decay rates, we observe that the fitted from the TDSE results are always smaller than the calculated R_0. This behavior is related to TDSE numerics requirements, which cannot handle the very thin potential well limit $a \to 0$.

The ITM approach delivers spectra that vanish abruptly beyond the CB and cannot reproduce the shoulders visible in the TDSE results. As already discussed in Chapter 3, the saddle-point method is actually not applicable in the form described here outside the CB. The correct approach requires us to include the term proportional to the third derivative of the action in the phase decomposition near the saddle-point [FSB02, GP99]. For broad spectra, the contribution of the shoulders outside the CB is not significant and our approach provides reliable results. The contribution of the shoulders increases for narrow spectra, as one can see comparing Figs. 4.9a and 4.9b.

We further compare the ITM and TDSE results for a thicker barrier with $b - a = 6$ and field amplitude $\mathcal{E}_0$=0.05 in Fig. 4.9c. Here the agreement is less accurate at small energies $E < 0.8$, where the ITM results are about one order of magnitude higher than the TDSE ones. Since ITM delivers a momentum spectrum, the variable transformation $dE = pdp$ introduces a divergence for asymptotic momenta approaching the origin. However, for energies close to the initial particle energy and larger, the ITM agrees well with the TDSE. We conclude that the ITM provides not only qualitative but also quantitative results for LAT of QS states within the semiclassical parameter regime.

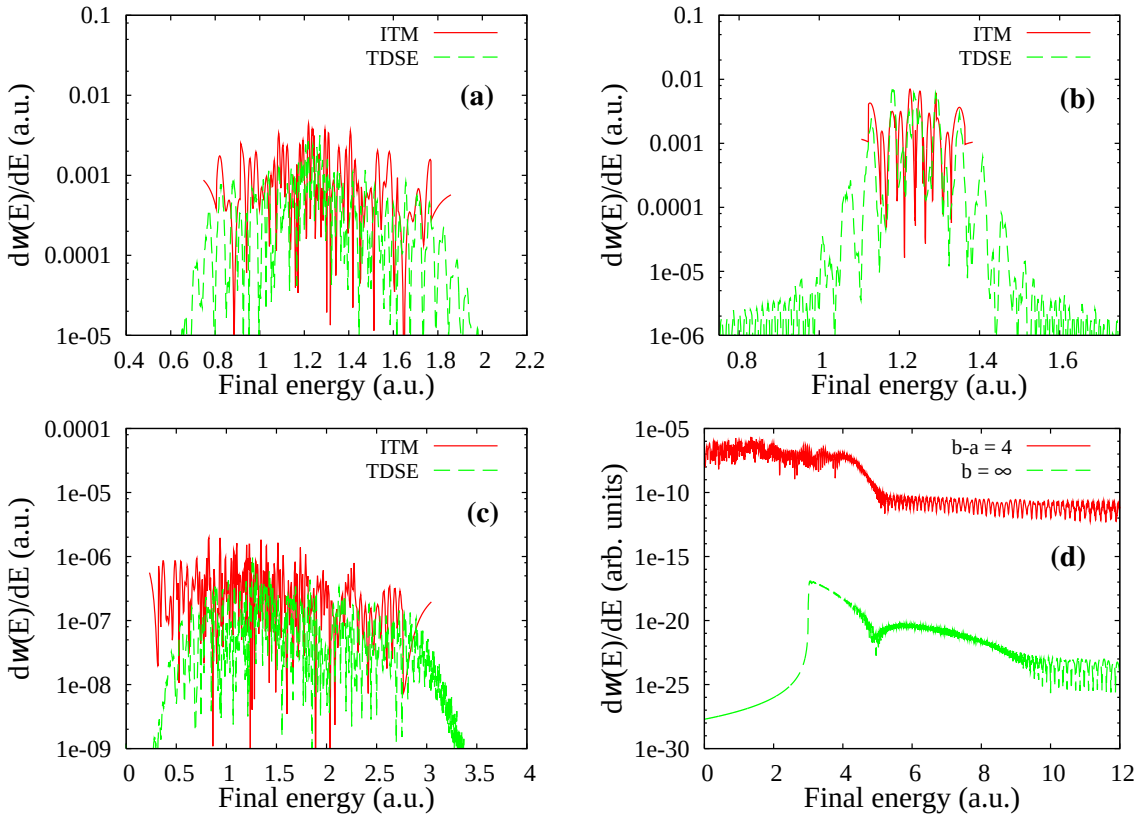

Figure 4.9: (a),(b),(c) Tunneling probabilities $dw(E)/dE$ for rectangular barriers of widths $b-a=4$ (a), (b), and $b-a=6$ (c) as a function of the final energy: the present ITM calculation (solid red line) and numerical solution of the TDSE (green dashed line). The laser field parameters are $\omega=0.057$ and (a) $\mathcal{E}_0$=0.02, (b) $\mathcal{E}_0$=0.005 and (c) $\mathcal{E}_0$=0.05. (d) Comparison between LAT through the finite barrier considered in (a) under the action of a field of amplitude $\mathcal{E}_0$=0.075 (solid red line) and ATI for $b=\infty$ in the same field (green dashed line).

Note that in all numerical examples considered in this Chapter, two effects were disregarded in the ITM. Firstly, in our analytical formulae trajectories that escape through the tilted barrier are not accounted for, so that the contribution that turns in the limit $b \to \infty$ into ATI is missing. For the parameters we have chosen, this contribution can be safely neglected. For demonstration, we show in Fig. 4.9d the LAT spectrum calculated numerically using the TDSE for the barrier parameters of panel (a) under the action of a laser field of amplitude $\mathcal{E}_0 = 0.075$ and compare it with ATI through an infinite barrier ($b = \infty$) of the same height. We can see that for the chosen parameters, the ATI probability is many orders of magnitude smaller than LAT one. Secondly, the theory does not take into account that the electron can be driven back to the barrier and rescatter absorbing or emitting additional photons. As is known from the literature, rescattering leads to the formation of one or more plateaus in the spectrum, with the characteristic number of peaks given by the Reiss parameter Eq. (3.4). The same effect can also be interpreted as multiphoton stimulated bremsstrahlung [BF66]. For our calculations, we have selected the parameters such that in all cases $p_0 > p_F$ and rescattering plays no significant role. The rescattering plateau can be reproduced by TDSE calculations covering the higher field amplitude domain $p_F > p_0$, which was, however, not considered in this thesis.

CHAPTER 5

LASER-ASSISTED α DECAY

With the help of the method developed in Chapter 3 for the laser-assisted decay of QS states, we study the effect of an incoming laser field on the decay of some medium-mass and heavy α emitting nuclei. In particular, we focus on changes in the lifetimes and the final momentum distribution of the α particle. Following the precluster model in one-dimension proposed by Buck et al. *[BMP90a, BMP91], we assume that the parent nucleus is described by a spherical preformed α cluster, initially confined in a nuclear potential well. The emission of the α particle corresponds to its tunneling through the Coulomb potential barrier. The interaction with the external laser field is taken as a perturbation compared with the Coulomb force between the protons of the parent nucleus and introduces a correction on the field-free trajectories that the α particle follows inside the barrier. In the low-frequency limit, the monochromatic laser field can be taken as static. Using ITM, the correction on the trajectories are determined by solving the classical equations in complex time and the penetrability of the α particle through the Coulomb barrier in the presence of a static field is calculated. A comparison with the results obtained via the WKB method shows complete agreement. For the more general case of a monochromatic laser field, the total decay rates and numerical values of the laser-assisted lifetimes for several laser intensities are calculated. We compare our theoretical results with the available experimental field-free lifetime and determine the recollision threshold for the laser field.*

In the precluster model, the parent nucleus is taken as a preformed α cluster-daughter nucleus system. The preformed α cluster is initially confined in a potential well with depth $-U_0$, which is taken as the mean field nuclear potential that the nucleons of the parent nucleus experience. The nuclear interaction is short-ranged, so the potential well has a finite length x_0. For distances larger than x_0, the total interaction is the Coulomb force between the protons of the components of the physical system. In consequence, the tunneling barrier that the α particle traverses during the decay process is the Coulomb potential, exactly as the phenomenological model proposed by Gamow, Condon and Gurney (see Fig. 2.1). The α particle is moving around the daughter nucleus in an orbit characterized by the global quantum number $\mathcal{G}$, expressed in terms of the principal quantum number n, which corresponds to the

number of nodes of the radial wavefunction of the α cluster-daughter nucleus system and the relative angular momentum of the α cluster-daughter nucleus system L as $\mathcal{G} = 2n + L$.

Buck *et al.* calculated the lifetimes of medium-mass and heavy α emitting nuclei with $50 \geq Z \geq 82$ using the semiclassical version of the TPA, Eq. (2.65) and considering a constant value of the depth of the nuclear potential $U_0 = 135.6$ MeV. Then, the radius x_0 can be obtained from the well known Bohr-Sommerfeld quantization condition, Eq. (2.68) in order to reproduce the experimental lifetimes for each one of the nucleus they study. With those values, the theoretical lifetimes for α emitters are calculated, showing a difference of a factor of 2 or 3 σ with respect to the experimental results. Later on, Buck *et al.* used the same precluster model to find the lifetimes of other α emitting nucleus, considering different nuclear potentials, such as more realistic analytic potentials with parameters, fitted in order to reproduce the experimental lifetimes [BMP92, BJMP96]. They showed that the difference between the lifetimes calculated with the new analytic nuclear potential and the phenomenological model including the nuclear potential well was not significant. Assuming the phenomenological model, it is not possible to obtain more information about the nuclear properties that depend on the correlation between the nucleons of the parent nucleus. Although the nuclear potential well is not the most realistic model to describe the interaction between the nucleons, the results obtained by considering the tunneling barrier with the nuclear potential well are not far from the experimental lifetimes.

We choose the precluster model with a nuclear potential well to represent the α emitter since it gives an insightful and comprehensive phenomenological description of the mechanism of the α decay. Due to the spherical symmetry of the α cluster-daughter nucleus physical system, we treat the laser-assisted α decay as the LAT of the α particle through the one-dimensional Coulomb barrier. We did not consider any deformation on the parent or the daughter nuclei. Hence, the tunneling barrier is only described in the radial coordinate. The calculation of the lifetimes in the precluster model are done in the semiclassical limit, by using the definition of the width from the TPA, Eq. (2.65). The parameters that define the Coulomb barrier for specific medium-mass and heavy α emitters can be found in Ref. [BMP91]. This gives us a complete description of the Coulomb barrier for the nuclei we study in this Chapter in the field-free case.

We start by studying the spontaneous α decay in the frame of ITM. Initially, we use the Hamilton-Jacobi theory, in order to find a parametrization of the subbarrier trajectories that the α particle follows. Once we find the subbarrier trajectories, the classical action on the parameterized trajectories is calculated, obtaining the penetrability of the α particle through the Coulomb barrier. We compare the classical action obtained using ITM with the reduced action that can be calculated from the WKB method. The complete agreement shows the consistency of the ITM.

Next, we focus on the problem of laser-assisted α decay. We initially consider tunneling assisted by a static laser field. The interaction with the laser field is taken as a perturbation, so it only introduces a correction on the field-free trajectories. We find the correction introduced by the static laser field, and then, determine the classical action based on the total trajectories including the corrections, in accordance to ITM. Since the barrier is static, there is only one solution to the saddle-point equation, Eq. (3.29). In consequence, there is no interference between the different

trajectories that the α particle follows through the modified tunneling barrier. We are able to find the laser-assisted lifetimes by calculating the penetrability through the modified tunneling barrier including the dipole interaction with the static laser field in Eq. (2.69). The laser-assisted lifetimes are compared with the lifetimes obtained using the WKB method with perfect agreement for several medium-mass and heavy parent nuclei. The static field case is the low-frequency limit of the monochromatic laser field. In that sense, our results with the static electric field serves as a benchmark to the calculation of the laser-assisted lifetimes in the presence of a monochromatic field.

As a further step, we consider tunneling assisted by a monochromatic laser field. In this case, the tunneling barrier is time-dependent, and we use the method we proposed in Chapter 3 to study the dynamics of the laser-assisted decay of QS states. Analogously to the static field case, we find the correction to the subbarrier trajectories that are calculated by ITM. After leaving the classically forbidden region, the α particle interacts with the incoming electric field on its way to the detector, where the final momentum is measured. The monochromatic laser field is switched off by introducing an exponentially decaying electric field amplitude, which eventually makes the field vanish at a distance far away from the outer turning point of the Coulomb barrier. Following our method, we calculate the trajectories outside the barrier, and determine the transition amplitude as it was done in the case of the LAT through the rectangular barrier in Chapter 4.

In the case of the monochromatic laser field, there are two solutions of the saddle point equation. Therefore, the trajectories corresponding to a same final energy must be added coherently and the transition amplitude $M(\mathbf{p})$ can be calculated by Eq. (3.41). The main difference with respect to the tunneling through the rectangular barrier comes from the prefactor $\mathcal{P}_0$ in Eq. (3.41), which we take from the definition of the field-free decay rate by Buck *et al.* [BMP91], Eq. (2.69), and the regularization constant β in Eq. (3.41). In order to find the correct form of β, we use the definition we have introduced in Chapter 3, Eq. (3.20), from the works of Popruzhenko and Goreslavskii on the behavior of the angular distribution near the CB, [GP99, FSB02]. Then, the laser-assisted decay rate is calculated from the definition of the differential decay rate in terms of the transition probability, $dw/dp = |M(\mathbf{p})|^2$. We show the behavior of the imaginary part of the action, which describes the dynamics of the α particle during its subbarrier motion and find the laser-assisted lifetimes for several nuclei, comparing our results with the field-free lifetimes calculated by Buck *et al.* in Ref. [BMP91]. At high-intensity fields, recollision with the Coulomb barrier occurs. While this case is not the main topic of this thesis, we do find the recollision threshold intensities and study the behavior of the semiclassical action with increasing fields. We show qualitatively that, when the intensities of the laser field are close to the recollision limit, there are more than two solutions of the saddle-point equation for a range of energies between the CB. The calculation of the recollision spectrum is however not included at the present stage of the developed formalism.

5.1. Field-free parametrization

Here, we discuss the field-free α tunneling through the barrier in the spontaneous α decay. In accordance to the precluster model, the nuclear potential is a potential well

of depth U_0 and length x_0 (see Fig. 2.1). The nuclear interaction is a short-ranged one, which dominates at distances shorter than the radius of the parent nucleus x_0. Meanwhile, the main contribution to the tunneling barrier at large distances compared with x_0 comes from the Coulomb barrier. Since the angular momenta of the parent and the daughter nuclei are zero, the relative angular momentum L of the α cluster-daughter nucleus system is also zero. In consequence, the centrifugal barrier $L(L+1)/m_{\rm r}x^2$ does not contribute to the effective tunneling barrier the α particle traverses. As it was mentioned in Chapter 2, m_r is the reduced mass of the α cluster-daughter nucleus system, Eq. (2.6).

Initially, the position and velocity of the α particle are

$$x_1(\varphi_s) = x_0, \qquad \frac{dx_1}{dt'}(\varphi_s) = i\sqrt{\frac{2}{m_{\rm r}}\Big(\frac{Z_\alpha Z e^2}{x_0} - E\Big)}. \tag{5.1}$$

We introduce the dimensionless time parameter $\varphi = \phi_0 + i\psi(\xi) = \omega t'$. Here $\varphi_s = \phi_0 + i\psi_0 = \omega t'_s$ is the initial complex and dimensionless parameter when the α particle starts its motion under the Coulomb barrier. Z and Z_α are the proton numbers of the daughter nucleus and the α particle, respectively.

As the Coulomb potential dominates at long distances, the outer classical turning point of the tunneling barrier is the same outer turning point in the case of a Coulomb barrier, namely $x_{TP} = Z_\alpha Z e^2/E$. In order to find the subbarrier trajectories, we can use the Hamilton-Jacobi theory. Knowing that the Hamiltonian of the α cluster-daughter particle system is time-independent, the total energy is conserved

$$H = \frac{p^2}{2m_{\rm r}} + \frac{Z_\alpha Z e^2}{x_1} = E. \tag{5.2}$$

From the Hamilton-Jacobi theory, the characteristic function is related to the canonical momentum as

$$p = \frac{dW_{\rm HJ}}{dx_1}. \tag{5.3}$$

The time-dependent characteristic Hamilton-Jacobi function $S_{\rm HJ}(x_1, t')$ is defined as $S_{\rm HJ}(x_1, t') = W_{\rm HJ}(x_1) - E(t' - t'_s)$.

Using the energy conservation, we are able to find the one-dimensional Hamilton-Jacobi function, which is

$$W_{\rm HJ}(x_1) = i\int_{x_1}^{x_0} \sqrt{2m_{\rm r}\big(\frac{Z_\alpha Z e^2}{x} - E\big)}\,dx. \tag{5.4}$$

A property of the total characteristic Hamilton-Jacobi function in the case of stationary potentials is used in order to find the subbarrier trajectories. Taking into account that

$$\frac{\partial S_{\rm HJ}(x_1, t')}{\partial E} = 0, \tag{5.5}$$

we can find a relation that expresses the time spent by the particle inside the barrier in terms of the position of the α particle,

$$t' = t'_s - i\sqrt{\frac{m_{\rm r}}{2}}\int_{x_0}^{x_1} \frac{dx}{\sqrt{\frac{Z_\alpha Z e^2}{x} - E}}. \tag{5.6}$$

In order to solve the integral equation above, we can define a parameterized form of the subbarrier trajectories. The parameterized position $x_1(\xi)$ and time $t'(\xi)$

$$\begin{aligned} x_1(\xi) &= \frac{Z_\alpha Z e^2}{E}\sin^2\left(\frac{\xi}{2}\right), \qquad \text{for } \xi_0 \le \xi \le \xi_F, \\ t'(\xi) &= \frac{1}{\omega}\Big(\phi_0 + i\psi_0\Big) - \frac{i}{2E}\sqrt{\frac{m_\mathrm{r} Z_\alpha^2 Z^2 e^4}{2E}}\left[\xi - \xi_0 - \sin(\xi) + \sin(\xi_0)\right], \end{aligned} \tag{5.7}$$

follow the field-free trajectory found from the Hamilton-Jacobi theory, Eq. (5.6).

Using the initial conditions in Eq. (5.1) and the parametrization (5.7), we find the initial value of ξ, ξ_0 when the α particle starts its tunneling through the barrier. We also find its final value ξ_F when the particle leaves the barrier and starts its motion in real time,

$$\xi_0 = 2\arcsin\left(\sqrt{\frac{x_0}{Z Z_\alpha e^2}}\right), \qquad \xi_F = \pi. \tag{5.8}$$

Evaluating Eq. (5.7) at the instant when the particle leaves the Coulomb potential, we find the time of flight spent by the α particle traversing the tunneling barrier,

$$\frac{\psi_0}{\omega} = \frac{1}{2E}\sqrt{\frac{m_\mathrm{r} Z_\alpha^2 Z^2 e^4}{2E}}\big(\xi_F - \xi_0 + \sin(\xi_0)\big). \tag{5.9}$$

From the field-free parameterizations in Eq. (5.7), we calculate the subbarrier velocity of the α particle in terms of the parameter ξ,

$$\frac{dx_1}{dt'}(\xi) = i\sqrt{\frac{2E}{m_\mathrm{r}}}\cot\Big(\frac{\xi}{2}\Big). \tag{5.10}$$

Evaluating the Eq. above at $\xi = \xi_F$, we can see that the velocity of the α particle after leaving the barrier is zero.

In accordance to ITM, the classical action in Eq. (3.34) is calculated on the field-free parameterized trajectories in Eq. (5.7). We find that the classical action takes the form

$$W_0 = i\sqrt{\frac{m_\mathrm{r} Z_\alpha^2 Z^2 e^4}{2E}}\left[\xi_F - \xi_0 - \sin\big(\xi_F\big) + \sin\big(\xi_0\big)\right]. \tag{5.11}$$

The action calculated by the ITM, Eq. (5.11) can be compared with the reduced action W_red found via the WKB method, Eq. (2.70). We replace the parametrization of the spatial coordinate $x_1(\xi)$ as it was defined in Eq. (5.7) in Eq. (2.70). After a simple change of variables, and the integral Eq. (2.70) takes the form

$$W_\mathrm{red} = i\sqrt{\frac{m_\mathrm{r} Z_\alpha^2 Z^2 e^4}{2E}}\left(\xi_F - \xi_0 - \sin\big(\xi_F\big) + \sin\big(\xi_0\big)\right), \tag{5.12}$$

which is exactly the same result obtained by the ITM in the field-free case, Eq. (5.11). This shows the consistency of the ITM in the semiclassical limit for the spontaneous α decay.

5.2. Laser-assisted tunneling for a static electric field

After studying the spontaneous α decay via ITM and finding the parameterized field-free subbarrier trajectories $x_1(\xi)$, Eq. (5.7), we focus on the study of the laser-assisted α decay. Initially, we consider the case of a constant electric field interacting with the α emitter. A static electric field can be taken as the low-frequency limit of the monochromatic laser field. Thus, the study of the assistance of the α decay by a static field can give us a benchmark to understand the laser-assisted α decay in the presence of the monochromatic laser field. With the introduction of the interaction of the static electric field, the total tunneling barrier is written as

$$V_{\rm st}(x) = \frac{Z_\alpha Z e^2}{x} - Z_\alpha x e \mathcal{E}_0. \tag{5.13}$$

Here $\mathcal{E}_0$ is the static electric field.

With the tunneling barrier given by Eq. (5.13), the outer turning point is found by the condition $V_{\rm st}(x_{\rm TP}) = E$. Solving the quadratic equation, the outer classical turning point in the case of the electric static field $\mathcal{E}_0$ is

$$x_{\rm TP} = \frac{E}{Z_\alpha e \mathcal{E}_0}\Big(\sqrt{1 + \frac{4 Z Z_\alpha e^3 \mathcal{E}_0}{E^2}} - 1\Big). \tag{5.14}$$

The interaction with the static laser field can be taken as a perturbation to the Coulomb force between the protons of the α cluster and the daughter nucleus. In consequence, the external electric field introduces a small correction x_{2s} on the field-free subbarrier trajectories, Eq. (5.7). The position of the α particle inside the barrier in terms of the parameter ξ is given by

$$x_{\rm st}(\xi) = x_1(\xi) + x_{2s}(\xi), \qquad \xi_0 \le \xi \le \xi_F. \tag{5.15}$$

Due to the perturbative character of the interaction with the external field, $x_{2s} \ll x_1$ during the subbarrier motion.

The initial conditions of the corrections on the trajectories $x_{2s}(t'(\xi))$ must follow

$$x_{2s}(\xi_0) = 0, \qquad \frac{dx_{2s}}{dt'}(\xi_0) = 0. \tag{5.16}$$

In accordance to the ITM, the dynamics of the α particle is defined by the classical equations of motion in complex time,

$$m_{\rm r}\left(\frac{d^2 x_1}{dt'^2} + \frac{d^2 x_{2s}}{dt'^2}\right) = \frac{Z Z_\alpha e^2}{(x_1 + x_{2s})^2} + Z_\alpha e \mathcal{E}_0. \tag{5.17}$$

The correction on the field-free trajectories follows $x_{2s}(\xi) \ll x_1(\xi)$, for all $\xi_0 \le \xi \le \xi_F$. We expand the interaction force between the α cluster and the daughter nucleus around the field-free trajectory $x_1(\xi)$ up to the first leading order in $x_{2s}(\xi)$, neglecting the other higher order contributions,

$$m_{\rm r}\frac{d^2 x_{2s}}{dt'^2} \approx -2\frac{Z Z_\alpha e^2 x_{2s}(\xi)}{x_1^3(\xi)} + Z_\alpha e \mathcal{E}_0. \tag{5.18}$$

Using the field-free parametrization of the complex time in terms of ξ in Eq. (5.7), we can find a set of coupled differential equations that determines the correction on the subbarrier trajectories $x_{2s}(\xi)$ as a function of the parameter ξ,

$$\begin{aligned} \frac{dx_{2s}}{d\xi} &= -i\sqrt{\frac{m_{\rm r}Z_\alpha^2Z^2e^4}{2E^3}}\sin^2\left(\frac{\xi}{2}\right)\frac{dx_{2s}}{dt'}(\xi), \\ m_{\rm r}\frac{d}{d\xi}\left(\frac{dx_{2s}}{dt'}\right) &= i\sqrt{\frac{m_{\rm r}Z_\alpha^2Z^2e^4}{2E^3}}\sin^2\left(\frac{\xi}{2}\right)\left[2\frac{Z_\alpha^2Z^2e^4x_{2s}(\xi)}{(x_1(\xi))^3} - Z_\alpha e\mathcal{E}_0\right]. \end{aligned} \tag{5.19}$$

The set of differential equations (5.19) is solved numerically, with the initial conditions Eq. (5.16). As the dynamics of the α particle under the barrier is described in complex times, the set of equations Eq. (5.19) shows a complex value of the correction to the final velocity, $dx_{2s}/dt'(\xi_F)$. Since the final velocity in the field-free case is zero, the total velocity of the particle after leaving the barrier is complex.

This however contradicts the ITM requirement that the initial velocity of the tunneling particle after the barrier must be real. In order to obtain a real initial velocity outside of the barrier, a correction in the time of flight of the α particle in the field-free case due to the presence of the electric field, $\psi_0/\omega \to \psi_0/\omega + \Delta\psi/\omega$ has to be accounted for. This correction corresponds to a similar correction in the final value of the parameter $\xi_F \to \xi_F + \Delta\xi$. We can write the relation between $\Delta\psi_0$ and $\Delta\xi$ as

$$\Delta\psi_0 = -\psi_0 + \frac{1}{2}\sqrt{\frac{m_{\rm r}Z_\alpha^2Z^2e^4}{2E^3}}\left[\xi_F + \Delta\xi_F - \xi_0 - \sin(\xi_F + \Delta\xi_F) + \sin(\xi_0)\right]. \tag{5.20}$$

Taking into account that $\xi_F = \pi$ and the definition of the time of flight through the Coulomb barrier, Eq. (5.9), we obtain for the imaginary part of the initial complex dimensionless parameter ψ_0

$$\Delta\psi_0 = \frac{\omega}{2}\sqrt{\frac{m_{\rm r}Z_\alpha^2Z^2e^4}{2E^3}}\big(\Delta\xi + \sin(\Delta\xi)\big). \tag{5.21}$$

We can find explicitly $\Delta\xi$ using the fact that $\mathrm{Im}\left[dx_1/dt'(\xi_F + \Delta\xi) + dx_{2s}/dt'(\xi_F)\right] = 0$. The field-free velocity, Eq. (5.10), has to be evaluated accordingly at the corrected parameter $\xi = \xi_F + \Delta\xi$

$$\frac{dx_1}{dt'}(\xi_F + \Delta\xi) = -i\sqrt{\frac{2E}{m_{\rm r}}}\tan\frac{\Delta\xi}{2}. \tag{5.22}$$

Replacing the expression above in the final velocity of the α particle, we can find the expression of the correction

$$\Delta\xi = 2\arctan\left[\frac{1}{\sqrt{2m_{\rm r}E}}\mathrm{Im}\big(\frac{dx_{2s}}{dt'}(\xi)\big|_{\xi=\xi_F}\big)\right]. \tag{5.23}$$

The total classical action is calculated on the subbarrier field-free trajectories (5.7) and the corrections introduced by the static field from the Newton equations in Eq. (5.19). We can separate the action inside the barrier in three different contributions: the analytic field-free action evaluated on the corrected final parameter $\xi_F + \Delta\xi$, Eq. (5.11), the action depending on the corrections on the trajectories due to the external field (x_{2s} and dx_{2s}/dt') and a mixed term. We consider the perturbations introduced by the static field up to linear terms in $\mathcal{E}_0$. Any other terms proportional to higher orders of $\mathcal{E}_0$ are neglected.

In the first contribution, the field-free classical action Eq. (5.11) is evaluated on the final value of the parameter, $\xi_F + \Delta\xi$, as

$$W_0 = i\mu_1\big[\xi_F + \Delta\xi - \xi_0 + \sin(\xi_F + \Delta\xi) - \sin(\xi_0)\big], \tag{5.24}$$

with $\mu_1 = \sqrt{\frac{m_r Z_\alpha^2 Z^2 e^4}{2E}}$.

With the modification of the field-free action given in the equation above, the classical action $W_{\rm st}$ takes the form

$$\begin{aligned} W_{\rm st} = W_0 &- \frac{2i\mu_1\mathcal{E}_0}{E}\int_{\xi_0}^{\xi_F} x_1(\xi)\sin^2\Big(\frac{\xi}{2}\Big)d\xi - \frac{2i\mu_1\mathcal{E}_0}{E}\int_{\xi_0}^{\xi_F} x_{2s}(\xi)\sin^2\Big(\frac{\xi}{2}\Big)d\xi \\ &- \frac{i\mu_1}{E}\left[\int_{\xi_0}^{\xi_F}\frac{m_r}{2}\Big(\frac{dx_{2s}}{dt'}(\xi)\Big)^2\sin^2(\tfrac{\xi}{2})d\xi + Z_\alpha Z e^2\int_{\xi_0}^{\xi_F}\frac{x_{2s}(\xi)}{x_1(\xi)^2}\sin^2(\tfrac{\xi}{2})d\xi\right] \\ &- \frac{i\mu_1 m_r^2}{E}\int_{\xi_0}^{\xi_F}\Big(\frac{dx_1}{dt'}(\xi)\frac{dx_{2s}}{dt'}(\xi)\Big)\sin^2(\tfrac{\xi}{2})d\xi. \end{aligned} \tag{5.25}$$

The width of the nuclear resonance can be found in the semiclassical limit by TPA, Eq. (2.65), replacing the reduced action $W_{\rm red}$ in Eq. (2.69) by the classical action $W_{\rm st}$ in Eq. (5.25). Since the tunneling barrier is stationary, there is only one solution to the saddle-point equation. Thus, there is no interference between the subbarrier trajectories that the α particle follows, and the momentum distribution corresponds to the spectrum of the QS state, i.e., a single narrow line centered at the energy E of the α particle.

5.3. Laser-assisted α decay for a monochromatic laser field

Once we have studied the α decay in the presence of an external constant electric field, we investigate the laser-assisted α decay, considering a monochromatic laser field of the form

$$\mathcal{E}(\varphi) = \mathcal{E}_0\cos\big(\varphi\big). \tag{5.26}$$

Following ITM, the dynamics of the α particle in the classically forbidden region is described in complex times, starting at $\varphi_s = \omega t'_s = \phi_0 + i\psi_0$. In the absence of an external electric field, the α particle follows the trajectories in Eq. (5.7) and leaves the Coulomb barrier at $\varphi = \omega t' = \phi_0$. The field-free trajectories must be corrected because of the interaction with the monochromatic laser field as in the case of the static field in Section 5.2.

Once the α particle moves in real time outside the barrier, the α particle interacts with the daughter nucleus via the Coulomb force between the protons and the monochromatic laser field. We eventually switch off the monochromatic electric field adiabatically, so that the final momentum p can be measured at a detector at a time $t'_{\rm F}$ large compared with the pulse duration $T = \frac{2\pi}{\omega}$, and a distance far away from the outer turning point of the Coulomb barrier.

Initially, we study the dynamics of the subbarrier motion in complex times. We calculate the corrections to the trajectories introduced by the monochromatic laser

field. The classical action is calculated on the field-free trajectories, Eq. (5.7) and the corrections by the laser field. Next, the trajectories of the α particle outside the barrier are calculated in accordance to the ITM. We determine the classical action outside the barrier and finally the laser-assisted differential decay rate is found from the transition amplitude $M(\mathbf{p})$ in Eq. (3.41) using the prefactor of the field-free decay rate in Eq. (2.65).

5.3.1. Inside the barrier

Here, we study the tunneling of the α particle inside the barrier. We use the field-free parameterized trajectories in Eq. (5.7) and find the correction on the field-free trajectories due to the interaction with the monochromatic laser field. In order to fulfill the requirements imposed by ITM, a correction on the final parameter ξ_F must be introduced, following the calculations in the static field case, Section 5.2.

Next, the classical action is evaluated on the total subbarrier trajectories in accordance to ITM. We see that there are three main contributions to the classical action, and the calculations of each one of them are detailed. Finally, we find an expression for the classical action inside the barrier that can be solved partly analytically and partly numerically.

5.3.1.1. Correction on the field-free trajectories

In the presence of the laser field, the position of the α particle is expressed as the sum of the field-free parameterized coordinate $x_1(t'(\xi))$, Eq. (5.7) and a small correction to the trajectories $x_2(t'(\xi))$ as we have shown in Eq. (5.15) for the static field case,

$$x = x_1(t'(\xi)) + x_2(t'(\xi)). \tag{5.27}$$

The initial conditions of the corrections on the trajectories $x_2(t'(\xi))$ are defined exactly as the ones for the static field case, Eq. (5.16)

$$x_2(\xi_0) = 0, \qquad \frac{dx_2}{dt'}(\xi_0) = 0, \qquad \text{for } \xi_0 \leq \xi \leq \xi_F. \tag{5.28}$$

In accordance to ITM, the dynamics of the α particle is defined by classical equations of motion in complex time,

$$m_\mathrm{r}\left(\frac{d^2x_1}{dt'^2} + \frac{d^2x_2}{dt'^2}\right) = \frac{ZZ_\alpha e^2}{(x_1+x_2)^2} + Z_\alpha e\mathcal{E}_0\cos(\omega t'). \tag{5.29}$$

As the correction introduced by the laser field is assume to act only as a small perturbation, $x_2(\xi) \ll x_1(\xi)$, we expand the interaction around the field-free trajectory $x_1(\xi)$, as we did in the case of the static field, Eq. (5.18)

$$m_\mathrm{r}\ddot{x}_2 \approx -2\frac{ZZ_\alpha e^2 x_2(\xi)}{x_1^3(\xi)} + Z_\alpha e\mathcal{E}_0\cos(\omega t). \tag{5.30}$$

In accordance to Eq. (5.7), $x_2(\xi)$ can also be expressed in terms of the parameter ξ, as $dt'/d\xi = -i\sqrt{m_\mathrm{r}Z^2Z_\alpha^2e^4/2E^3}\sin^2(\xi/2)$. The last expression can be written as a

set of two coupled first-order differential equations

$$\begin{aligned}\frac{dx_2}{d\xi} &= -i\sqrt{\frac{m_{\rm r}Z_\alpha^2Z^2e^4}{2E^3}}\sin^2\left(\frac{\xi}{2}\right)\frac{dx_2}{dt'}(\xi),\\ m_{\rm r}\frac{d}{d\xi}\left(\frac{dx_2}{dt'}\right) &= i\sqrt{\frac{m_{\rm r}Z_\alpha^2Z^2e^4}{2E^3}}\sin^2\left(\frac{\xi}{2}\right)\left[2\frac{Z_\alpha^2Z^2e^4x_2(\xi)}{x_1^3(\xi)} - Z_\alpha e\mathcal{E}_0\cos\big(\omega t'(\xi)\big)\right].\end{aligned} \tag{5.31}$$

While the correction to the field-free velocity, calculated using Eqs. (5.31), takes a complex value at $\xi=\xi_F$, the field-free velocity of the α particle is zero at the end of the barrier. In consequence, the total velocity of the α particle in the presence of the monochromatic laser field is complex, contradicting the requirements of ITM. For the imaginary part of the total velocity of the α particle at the end of the subbarrier motion to be zero, we introduce a correction to the field-free time of flight of the α particle through the Coulomb barrier $\psi_0/\omega \to \psi_0/\omega + \Delta\psi_0/\omega$. This correction corresponds to a correction to the final value of the parameter $\xi_F \to \xi_F + \Delta\xi$. We find the connection between the corrections on the time of flight ψ_0 and the parameter ξ_F in Eq. (5.20). If we evaluate the field-free velocity dx_1/dt' on the modified final parameter $\xi = \xi_F + \Delta\xi$, we can guarantee that the field-free velocity becomes complex. That gives us the condition determining the correction $\Delta\xi$, such that $\mathrm{Im}\left[dx_1/dt'(\xi_F+\Delta\xi) + dx_2/dt'\right] = 0$, see Eq. (5.23).

The action is calculated along the modified trajectories in Eqs. (5.7), (5.27) and (5.31). The classical action inside the barrier is defined as

$$\begin{aligned}W_{\rm ins} = \int_{\frac{\phi_0+i\psi_0}{\omega}}^{\frac{\phi_0}{\omega}} dt'\Bigg\{&\frac{(m_{\rm r}(\dot{x_1}(t')+\dot{x_2}(t'))^2)}{2} - \frac{Z_\alpha Ze^2}{(x_1(t')+x_2(t'))}\\ &+Z_\alpha e\mathcal{E}_0\left[x_1(t')+x_2(t')\right]\cos(\omega t') + E\Bigg\}.\end{aligned} \tag{5.32}$$

We can separate the action inside the barrier into three different contributions as we show in the static field case: the analytic field-free action evaluated from $\xi = \xi_0$ to $\xi = \xi_F + \Delta\xi$, Eq. (5.11), the action depending on the corrections on the trajectories due to the external field (x_2 and dx_2/dt') and a mixed term. We consider the perturbations introduced by the laser field up to linear terms in $\mathcal{E}_0$, neglecting higher order contributions.

The first contribution to the classical action comes from the field-free parameterized trajectories (5.7). The field-free classical action W_0 in Eq. (5.11) is evaluated on the corrected final parameter, $\xi_F + \Delta\xi$, as

$$W_0 = i\mu_1\left[\xi_F + \Delta\xi - \xi_0 + \sin(\xi_F+\Delta\xi) - \sin(\xi_0)\right], \tag{5.33}$$

with $\mu_1 = \sqrt{m_{\rm r}Z_\alpha^2Z^2e^4/2E}$.
The action term in Eq. (5.32) that stands for the interaction with the laser field and depends on the field-free trajectory $x_1(\xi)$ takes the form

$$W_1 = -\frac{2i\mu_1\mathcal{E}_0}{E}\int_{\xi_0}^{\xi_F} x_1\big(\xi\big)\cos\left[\omega t'(\xi')\right]\sin^2\Big(\frac{\xi}{2}\Big)d\xi. \tag{5.34}$$

The second contribution to the action comes from the terms proportional to the correction on the trajectories $x_2(\xi)$ due to the laser field. This term can be expressed

as

$$W_2 = -\frac{i\mu_1}{E}\left\{\int_{\xi_0}^{\xi_F}\frac{m_\mathrm{r}}{2}\left[\frac{dx_2}{dt'}(\xi)\right]^2\sin^2\left(\frac{\xi}{2}\right)d\xi + Z_\alpha e\mathcal{E}_0\int_{\xi_0}^{\xi_F}x_2(\xi)\cos\left[\omega t(\xi)\right]\sin^2\left(\frac{\xi}{2}\right)d\xi\right\}. \tag{5.35}$$

The zero order term of the expansion is the Coulomb potential calculated on the field-free trajectories. The first perturbation term is a mixed term, proportional to $x_2(\xi)/\left[x_1(\xi)\right]^2$. This term corresponds to the third contribution to the classical action, Eq. (5.32),

$$W_3 = -\frac{i\mu_1 Z_\alpha Z e^2}{E}\int_{\xi_0}^{\xi_F}\frac{x_2(\xi)\sin^2\left(\frac{\xi}{2}\right)}{x_1(\xi)^2}d\xi - \frac{i\mu_1 m_\mathrm{r}^2}{E}\int_{\xi_0}^{\xi_F}\left[\frac{dx_1}{dt'}(\xi)\frac{dx_2}{dt'}(\xi)\right]\sin^2\left(\frac{\xi}{2}\right)d\xi. \tag{5.36}$$

After the total action evaluated on the trajectories inside the barrier has been calculated as $W_\mathrm{ins} = W_0 + W_1 + W_2 + W_3$, we focus on the dynamics of the motion once the particle leaves the barrier.

5.3.2. Motion outside the barrier

With the correction on the time of flight of the tunneling particle through the Coulomb barrier in Eq. (5.23), we can safely say that the velocity of the particle after leaving the tunneling barrier is real. As the motion in the two regions must be connected, the final position that the α particle has once it leaves the barrier is the initial position in the second part of the motion in real time, starting at $\varphi = \phi_0$.

During the motion outside the barrier, the α particle interacts with the monochromatic electric field and the daughter nucleus via the Coulomb force. At a time t'_F, the α particle reaches a detector at a distance far away from the point where it leaves the barrier. Once at the detector, the final momentum of the α particle p is measured. We introduce an exponential damping factor for the field amplitude of the form $f(t') = \mathcal{E}_0\exp\Big(-\Gamma_d\big(t'-\phi_0/\omega\big)/2\Big)$ in order to switch off the electric field adiabatically, such that $\Gamma_d t'_F \gg 1$. The final time of observation t'_F when p is measured is long compared to the time when the particle leaves the Coulomb barrier and starts its motion in real time ϕ_0/ω.

In accordance to ITM, the dynamics of the α particle outside the barrier is determined by the classical equations, now in real time

$$m_\mathrm{r}\frac{d^2\dot{x_3}}{dt'^2} = \frac{Z_\alpha Z e^2}{(x_3(t'))^2} + Z_\alpha e\mathcal{E}_0\exp\left[-\Gamma_d\Big(\frac{\omega t'-\phi_0}{2\omega}\Big)\right]\cos(\omega t'), \quad \text{for } \frac{\phi_0}{\omega} \le t' \le t'_F. \tag{5.37}$$

As a consequence of introducing an exponential damping factor in the amplitude of the monochromatic laser, the interaction of the α particle with the external electric field decreases slowly on its way to the detector. Eventually, the monochromatic electric field vanishes completely. Moreover, since we place our detector far away, the Coulomb interaction with the daughter nucleus is neglected at t'_F. Therefore, the energy of the α particle at t'_F is purely kinetic and remains constant.

Along the trajectories $x_3(t')$ in Eq. (5.37), the action is numerically calculated as

$$W_{\text{out}} = \int_{\frac{\phi_0}{\omega}}^{t'_F} dt' \Bigg\{ \frac{m_{\text{r}}}{2} \left(\frac{dx_3}{dt'} \right)^2 - \frac{Z_\alpha Z e^2}{x_3(t')} + Z_\alpha e \mathcal{E}_0 \exp\left[-\Gamma_d \left(\frac{\omega t' - \phi_0}{2\omega} \right) \right] x_3(t') \cos(\omega t') + E \Bigg\} - x(t'_F) p(t'_F). \tag{5.38}$$

Finally, the total action can be determined:

$$W_{\text{tot}} = W_{\text{ins}} + W_{\text{out}} - \left(x\big|_{t=t'_F} p\big|_{t=t'_F} \right). \tag{5.39}$$

The last term corresponds to the momentum and the position of the α particle when it reaches the detector, and comes from the action in ITM, Eq. (3.37). This is the classical action $W(\mathbf{p}, t_{s\alpha})$ in the definition of the transition amplitude $M(p)$ via our method in Chapter 3, Eq. (3.41).

In order to complete the description of the transition amplitude $M(p)$ for the laser-assisted α decay, we also need to find the prefactor $\mathcal{P}_0$. Since the field-free decay rate of the α decay is given by Eq. (2.69) in the precluster model, we can take the prefactor as $\mathcal{P}_{0\gamma}^2 = P\hbar^2 K / 2m_{\text{r}} x_0$. Here, K is the wavenumber inside the nuclear potential well, $K = \sqrt{\frac{2m_{\text{r}}}{\hbar^2}\left(E + U_0 - \frac{Z_\alpha Z e^2}{x_0} \right)}$. The parameters x_0 and U_0 define the nuclear potential well and the preformation probability of the α particle in the parent nucleus is taken as $P = 1$, following the work of Buck *et al.* [BMP91].

5.3.2.1. Choice of the damping factor Γ_d and t'_F

The numerically calculated trajectories, and hence the total action and the energy spectrum depend on the choice of the damping parameter Γ_d and on t'_F.

It is important to choose the parameters appropriately in order to switch off the electric field such that the dynamics of the α particle are not affected considerably by the exponentially decreasing amplitude of the electric field. Additionally, if the photon energy of the laser field $\hbar\omega$ is small compared with the energy of the α particle, the period of the laser is extremely large compared to the time of flight of α particle through the Coulomb barrier. In that case, the α particle essentially interacts with a static field rather than a time-dependent one. Accordingly, we take a long time of observation t'_F and switch off the electric field smoothly. The value that we choose for Γ_d depends on the characteristics of the tunneling barrier and is nucleus-specific. We impose two conditions on Γ_d, [Pop10]

(i) $\Gamma_d \frac{2\pi}{\omega} \ll 1$, such that all the physical processes taking place in addition to the interaction with the laser field proceed faster than the switching off of the electric field.

(ii) $\Gamma_d t'_F \gg 1$, such that we can guarantee that at t'_F, the electric field has vanished completely, and the final momentum can be measured at the detector.

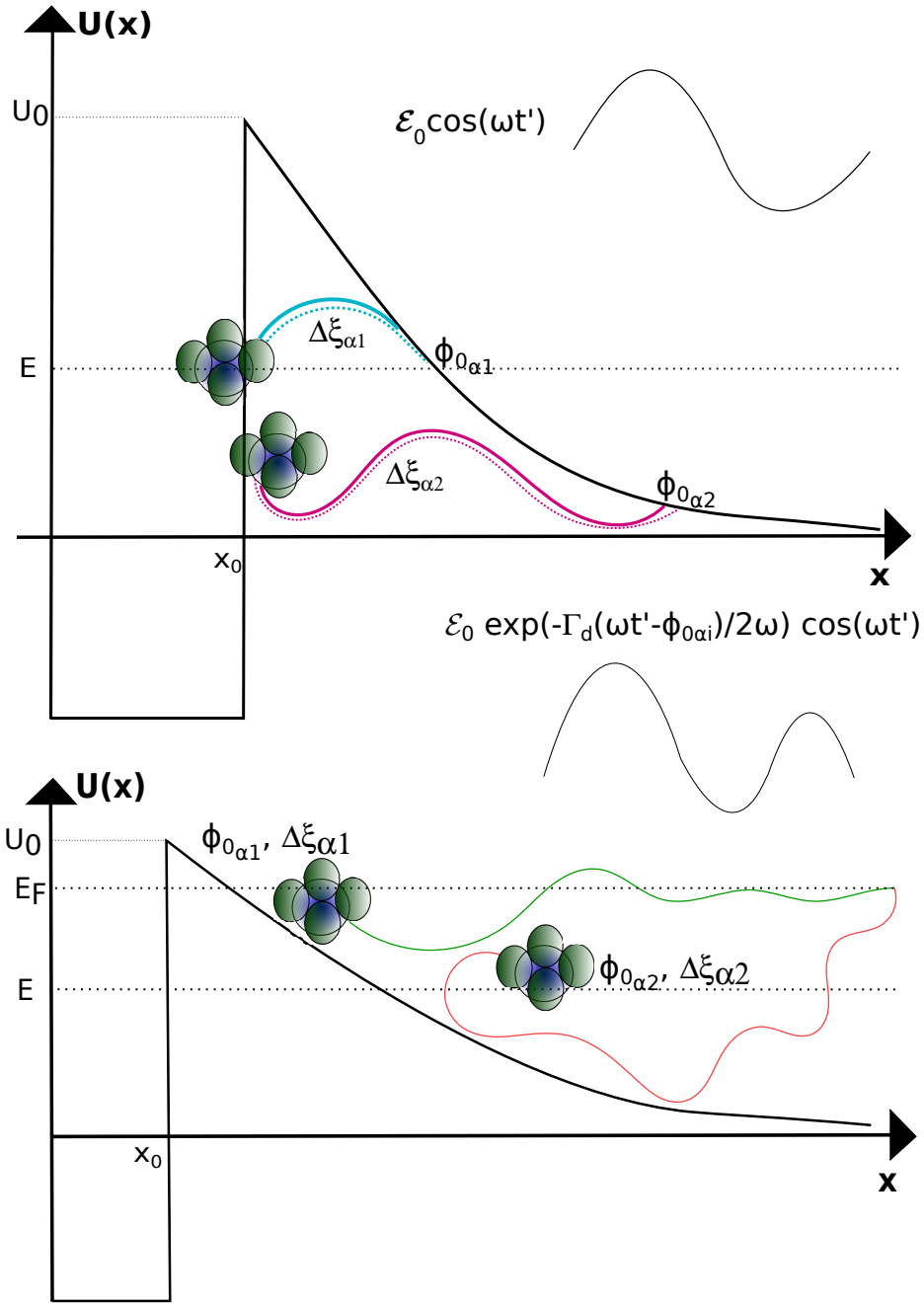

Figure 5.1: Qualitative picture of the LAT of the α particle in the presence of a monochromatic field. The α particle dynamics are shown in the subbarrier region (above) and outside the tunneling barrier (below) for different solutions of the saddle-point equation in the case of the laser-assisted α decay. The electric field outside of the barrier (thin black line) is switched off adiabatically. Similarly to the case of the LAT through the rectangular barrier, each subbarrier trajectory corresponding to the same final energy E_F is related with a solution of the saddle-point equation, $\phi_{0_{\alpha 1}}$ and $\phi_{0_{\alpha 2}}$. The associated trajectories are shown (blue and magenta, for the subbarrier motion and magenta and green lines, for the motion outside the barrier). The two trajectories for a single E_F are added coherently in accordance to Eq. (3.41).

5.3.3. Differential decay rate

In order to obtain the differential decay rate, we follow the procedure developed for the rectangular barrier in the Subsection 4.3.

The regularization constant β in the denominator of the transition amplitude $M(\mathbf{p})$ needs to be specified. Since the corrections on the field-free trajectories $x_2(\xi)$ cannot be found analytically as in the LAT through the rectangular barrier, we can only find β numerically, using its definition in Eq. (3.20), namely, $\beta_\gamma = z_F^{-\frac{1}{3}} \left(dp/dt_0 \big|_{max} \right)$. A schematic picture of the dynamics of the laser-assisted α decay in the presence of a monochromatic field is shown in Fig. 5.1.

We recall that in the case of a monochromatic field Eq. (3.14), all periods were equivalent, so that there were only two essentially different solutions, all the others being obtained by a $2\pi k$ translation, for all $k \in \mathbb{Z}$. In the present case, due to the procedure we have used to switch off adiabatically the monochromatic field, we no longer deal with a monochromatic field. However, since the applied damping factor is very small and therefore the number of periods over which we sum is large, we expect the deviation from the pure monochromatic field case to be very small. Thus following the results in Subsection 4.3, summing over all periods of the monochromatic laser field gives additional Dirac-delta factors in the transition amplitude $M(\mathbf{p})$. For the particular case of the laser-assisted α decay, the transition amplitude $M(\mathbf{p})$ in Eq. (3.41) can be calculated by including the prefactor $\mathcal{P}_{0\gamma}$, the regularization constant β_γ and the Dirac delta of the conservation of energy in the modified transition amplitude in Eq. (3.41). The transition amplitude $M(\mathbf{p})$ takes the form

$$M(p) = \hbar\omega \sum_{l=-\infty}^{l} \delta\Big(\frac{p^2}{2m_\mathrm{r}} + \frac{Z_\alpha^2 e^2 \mathcal{E}_0^2}{4m_\mathrm{r}\omega^2} - E - \hbar l\omega \Big) \sum_\alpha \frac{\mathcal{P}_{0\gamma}^2 \left[v(t_{0\alpha}) \right] \exp\left[iW(p, t_{s\alpha}) \right]}{\sqrt{dp/dt_{0\alpha} + i\beta_\gamma}} \,. \quad (5.40)$$

The second term of the argument of the Dirac delta distribution in the expression above corresponds to the ponderomotive potential U_p felt by the α particle in the presence of the monochromatic laser field.

We can find the differential decay rate dw/dp by taking the modulus square of the transition amplitude $M(\mathbf{p})$ in Eq. (5.40). The differential decay rate is evaluated on the long time of observation $T = t'_F$, as we showed in the case of LAT through the rectangular barrier, Eq. (4.45). In consequence, the differential decay rate dR/dp for the laser-assisted α decay in the presence of a monochromatic laser field is given by

$$dR = \frac{dw(p)}{T} = \sum_j \frac{\delta(p - p_j)}{2\pi p_j} \left(\frac{P\hbar^4 K\omega^2}{2m_\mathrm{r} x_0} \right) \left| \sum_{\alpha=1,2} \frac{\exp\left(iW_\mathrm{tot}(p, t_{s\alpha}) \right)}{\sqrt{dp/dt_{0\alpha} + i\beta_\gamma}} \right|^2 dp \,, \quad (5.41)$$

where $p_j = \sqrt{2m_\mathrm{r} \left(E - Z_\alpha^2 e^2 \mathcal{E}_0^2 / 4m_\mathrm{r}\omega^2 + \hbar j\omega \right) / \hbar^2}$ are the momenta corresponding to the ATI-like peaks.

If we are interested only in the total decay rate (respectively the lifetime of the alpha emitter) instead of the energy spectrum, it is numerically more advantageous to consider the total laser-assisted rate averaged per laser period,

$$R_\mathrm{av} = \left(\frac{P\hbar^4 K\omega}{4\pi m_\mathrm{r} x_0} \right) \int_0^{2\pi} \exp\left\{ \mathrm{Im}\left[W_\mathrm{tot}(p, \phi_{s\alpha}) \right] \right\} d\phi_{s\alpha}. \quad (5.42)$$

The total rate depends on the imaginary part of the action along the trajectories inside the barrier, while the spectrum is mainly influenced by the α particle motion after the barrier exit and its interaction with the laser field outside the barrier. In principle, the integration of the differential decay rate (5.41) over the whole energy spectrum should yield the same result as the averaged rate in (5.42). However, due to the involved numerics for the propagation of the α particle outside the barrier, numerical inaccuracies of the order of the lifetime change due to the laser field occur. We therefore use (5.42) to calculate the laser-assisted α decay lifetime,

$$t_{1/2} = \frac{\hbar \log(2)}{R_{\rm av}}. \tag{5.43}$$

5.3.3.1. Recollision limit

We have found that the external laser field can modify the dynamics of the α particle in the subbarrier region or after leaving the Coulomb barrier on its way to the detector. If we take into account the time-dependent character of the monochromatic field, the interaction of the α particle with the field changes in direction. If the intensity of the incoming laser field is not strong, the dynamics of the α particle are not affected strongly by the change in the change in direction of the electric force. However, there is a particular large intensity at which the effects of the change in direction of the field are no longer negligible. At this limit, the energy of the α particle is twice the drift energy gained by the α particle from the laser field, U_p. This is the *recollision limit*. The change in the direction of force by the laser field modifies the trajectories of the α particle, such that there can be more than two saddle-point solutions for a single value of the final energy.

The recollision limit is satisfied by the following relation

$$E = \frac{Z_\alpha^2 Z^2 e^2}{2m_{\rm r}\mathcal{E}_{0_{rec}}}. \tag{5.44}$$

Although we can explore the dynamics of the LAT of the α particle through the Coulomb barrier for intensities close to the recollision limit, the method we have developed to calculate the laser-assisted decay rates of initial QS does not include the description of recollision processes. Therefore, for intensities close to the recollision limit, we can only show qualitatively the behavior of the most important quantities that characterize the LAT of the α particle through the barrier.

5.4. Numerical results

In the last section, we have found the decay rate in the case of a static electric field by replacing the classical action (5.25) in the definition of the decay rate of the spontaneous α decay for the precluster model, Eq. (2.69). We also used ITM to study the dynamics of the α particle tunneling through the Coulomb barrier in the presence of a monochromatic laser field, and obtained the laser-assisted differential decay rate dR/dp, given in Eq. (5.41). Here, we show the numerical results obtained for some α emitting nuclei (^{106}Te, ^{162}W, ^{150}Dy and ^{238}U), whose field-free lifetimes were calculated theoretically by Buck *et al.* , using the precluster model [BMP91].

5.4.1. Nuclear parameters for different α emitters

In this thesis, we study the laser-assisted α decay of four different medium-mass and heavy nuclei α emitting nuclei, with zero angular momentum in their ground state, $^{106}_{52}$Te, $^{150}_{66}$Dy, $^{162}_{74}$W and $^{238}_{92}$U. We chose these particular cases, since their experimental lifetimes are spread over a long range of values, from a few microseconds up to millions of years. The measured decay lifetimes together with parent and daughter nuclei parameters are presented in Table5.1.

We can characterize the spontaneous α decay following the precluster model, proposed by Buck *et al.* and explained in the section 2.3. We follow the assumptions made by the precluster model in [BMP91], considering the preformation factor as $P = 1$ in the field-free decay rate, Eq. (2.69). The definition of the field-free decay rate given by Buck *et al.* in [BMP90a] can be used to describe the spontaneous α decay since the energy of the α particle is not close to the top or the bottom of the barrier. Following the description of the tunneling barrier in the phenomenological precluster model by Buck *et al.* , we use the parameters found in [BMP91] to characterize the tunneling barrier. The relevant parameters that are necessary to calculate the field-free lifetime in accordance to the precluster model are given in Table 5.1. We also give the theoretical values of the α emitter lifetimes from Ref. [BMP91].

Parent	Daughter	E (MeV)	c_1 (fm)	m_d (MeV)	$t_{1/2}^{\text{exp}}$ (s)	$t_{1/2}^{\text{pm}}(s)$
$^{106}_{52}$Te	$^{102}_{50}$Sn	4.325	1.486	95706	$7(1.7) \times 10^{-5}$	7×10^{-5}
$^{150}_{66}$Dy	$^{146}_{64}$Sm	4.350	1.461	137018	430.2(300)	520
$^{162}_{74}$W	$^{158}_{72}$Hf	5.675	1.432	148316	1.36(6)	2.4
$^{238}_{92}$U	$^{234}_{90}$Th	4.274	1.394	219701	$4.469(3) \times 10^{17}$	4.7×10^{17}

Table 5.1: Nuclear parameters that define the tunneling barrier of the α cluster-daughter nucleus system for the four α emitters studied in this thesis. Here, m_d is the mass of the daughter nucleus, c_1 is the constant that defines the radius of the parent nucleus as $x_0 = c_1 A^{\frac{1}{3}}$. E is the energy of the α particle. The experimental lifetimes are listed for the α emitters. $U_0 = 135.6$ MeV is the depth of the nuclear potential well, following the precluster model by Buck *et al.* in [BMP91]. The experimental lifetimes $t_{1/2}^{\text{exp}}$ and the calculated lifetimes by Buck *et al.* in [BMP91] $t_{1/2}^{\text{pm}}(s)$ are listed above for the four considered α emitters. The mass of the α particle is taken as 3727.379240 MeV, in order to calculate the reduced mass m_{r} according to Eq. (2.6).

5.4.1.1. Tunneling of the α particle in a static field

In the following for exemplification, we detail step by step the numerical results for the LAT dynamics through the Coulomb barrier for the lightest of the considered nuclei, $^{106}_{50}$Te. As it was mentioned in Section 5.3.2, when the frequency of the monochromatic laser field is low, the laser period is far longer than the time of flight of the α particle through the Coulomb barrier. As a consequence, the α particle sees a static barrier. We can take the intensities of an incoming laser field and determine the amplitude of the electric field. In the low-frequency limit, this amplitude is exactly the static field that modifies the decay rate in accordance to what was explained in

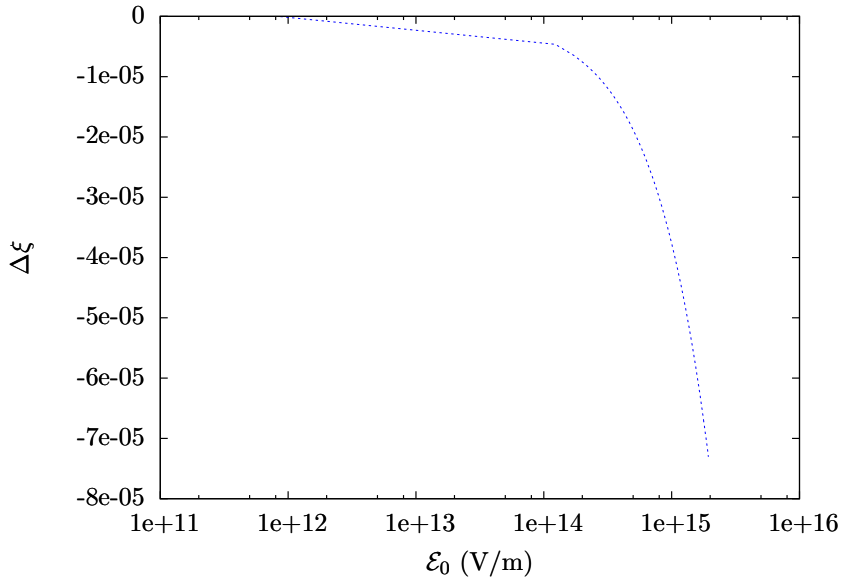

Figure 5.2: Correction on the time of flight of the α particle $\Delta\xi$ as a function of the static electric field $\mathcal{E}_0$ in the case of ^{106}Te.

Section 5.2. Therefore, we use the relation between the intensity I and the magnitude of the electric field $\mathcal{E}_0$ in Eq. (A.2) in order to calculate the field-assisted lifetimes as a function of the intensities, following the ITM field-free subbarrier trajectories, Eq (5.7), the correction on the subbarrier trajectories x_{2s} due to the static field in Eq. (5.19) and the classical action $W_{\rm st}$ in Eq. (5.25).

We have stated earlier in this Chapter that the interaction with the static field only introduces a small change in the time of flight of the α particle. The correction on the final parameter $\xi_F + \Delta\xi$ that determines the end of the subbarrier motion is calculated, according to Eq. (5.23). The results are shown in Fig. 5.2. The magnitude of the correction on the final parameter $\xi_F = \pi$ due to the interaction with the static field is very small compared with the value of ξ_F. It can be seen in Fig. 5.2 that it only affects the fifth decimal of ξ_F. The correction in the time of flight of the α particle, $\Delta\psi_0/\omega$ is also small compared with the time of flight of the α particle, traversing the barrier ψ_0/ω, in accordance to Eq. (5.20). In consequence, the time that the particle spends inside the Coulomb barrier in the presence of the static field is close, but not exactly the same one in the field-free case, Eq. (5.9).

As the stationary tunneling barrier is modified by the presence of the static field, the outer turning point is redefined, as it was shown in Eq. (5.14). With that said, the penetrability of the α particle through the new tunneling barrier changes, as the exponential factor in the decay rate (2.69) is sensitive to the definition of the turning points. We calculate the penetrability and the lifetimes using ITM, Eq. (5.25) and WKB, Eq. (2.70) and compare our results with the field-free lifetime in Fig. 5.3. It can be seen in Fig. 5.3 that the lifetimes calculated using WKB and the lifetimes calculated using ITM coincide. The agreement achieved between the lifetimes calculated via ITM and the WKB method found in $^{106}_{50}$Te is also found for $^{162}_{74}$W (see Fig. 5.4), $^{150}_{66}$Dy (see Fig. 5.5) and $^{238}_{92}$U (see Fig. 5.6).

Moreover, we can see in Figs. 5.3, 5.4, 5.5 and 5.6, that for larger values of the

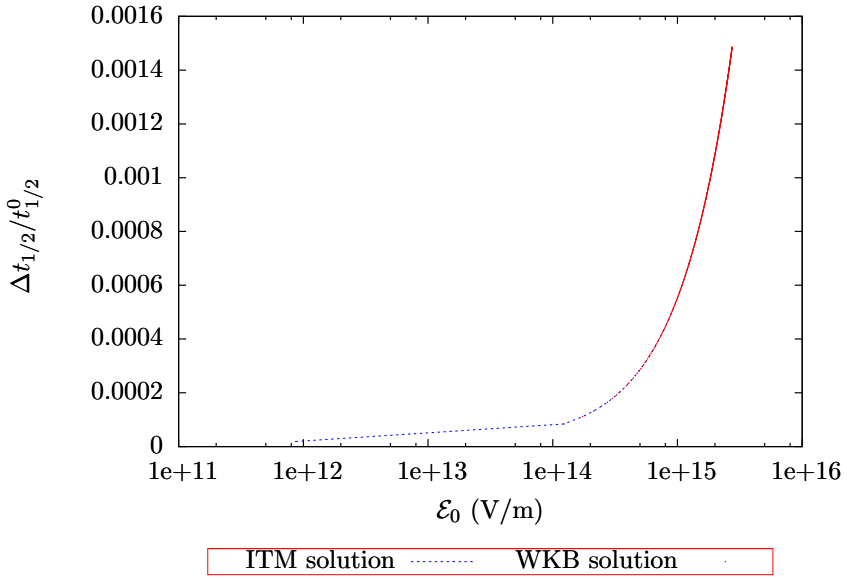

Figure 5.3: Relative modification in the field-assisted lifetimes $\Delta t_{1/2}/t^0_{1/2}$ as a function of the electric field $\mathcal{E}_0$ in the case of ^{106}Te.

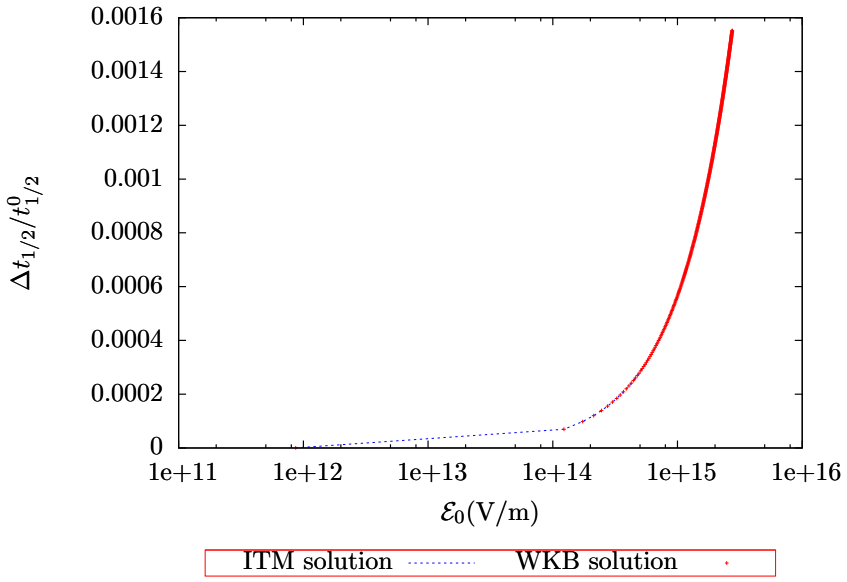

Figure 5.4: Relative modification in the field-assisted lifetimes $\Delta t_{1/2}/t^0_{1/2}$ as a function of the electric field $\mathcal{E}_0$ in the case of ^{162}W.

electric field strength $\mathcal{E}_0$, the field-assisted lifetimes become *shorter* with respect to the field-free lifetime, leading to a slight acceleration of the decay. However, for electric fields with values up to an order of magnitude of 10^{15} V/m, the relative modification in the lifetimes by the interaction with the external field $\Delta t_{1/2}/t^0_{1/2}$ is about 6×10^{-4} in the case of ^{106}Te, with respect to the value $t^0_{1/2}$ calculated via ITM for the field-free decay. For ^{162}W, the relative modification in the field-assisted lifetime for such a strong static field is extremely small, around 7×10^{-4} as in the case of the Tellurium. Similarly, in the cases of ^{150} Dy and ^{238}U, with longer spontaneous

α decay lifetimes, the relative modification $\Delta t_{1/2}/t^0_{1/2}$ in the value of the lifetimes is almost negligible ($\Delta t_{1/2}/t^0_{1/2} = 10^{-3}$ for a electric field strength of 10^{15} V/m), and it increases with the electric field strength. We thus conclude that the dynamics of the α decay during the tunneling through the Coulomb barrier is not only negligibly affected by the presence of the static field and there is no significant change in the spontaneous decay lifetime of the α emitter.

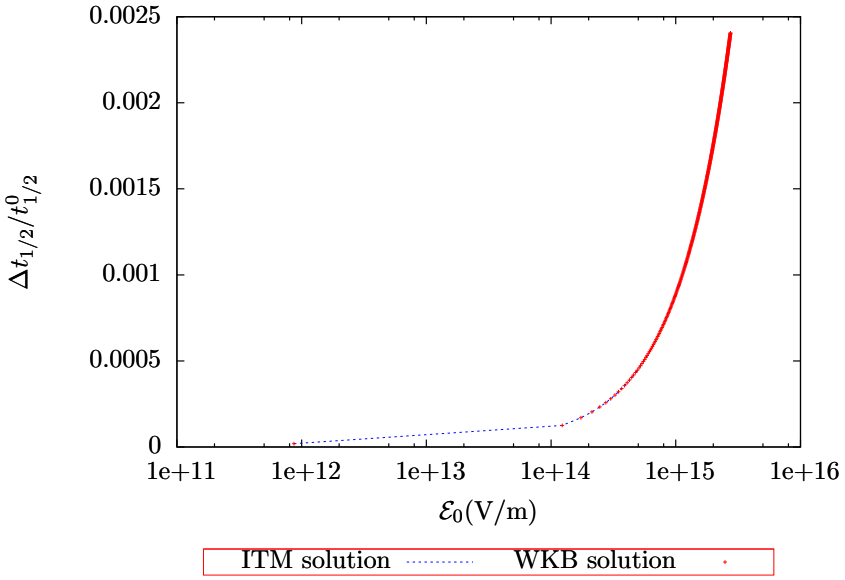

Figure 5.5: Relative modification in the field-assisted lifetimes $\Delta t_{1/2}/t^0_{1/2}$ as a function of the electric field $\mathcal{E}_0$ in the case of ^{150}Dy.

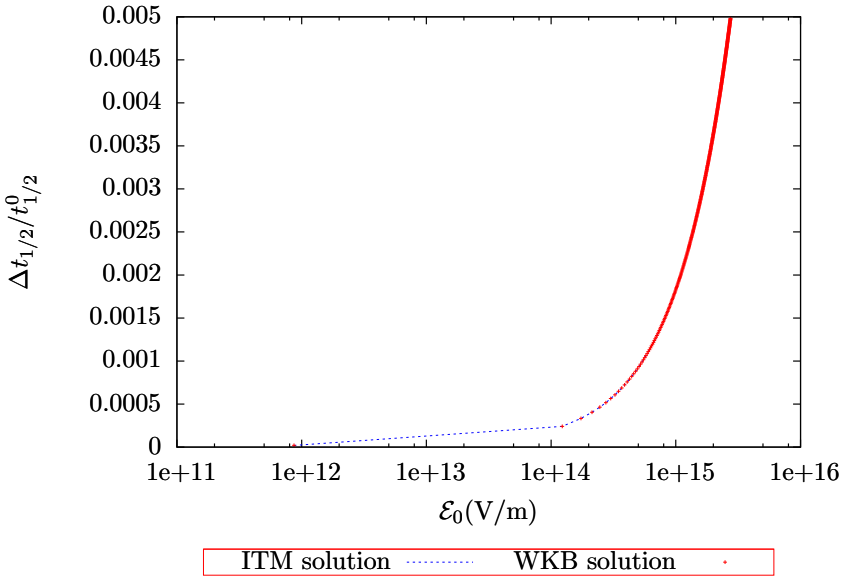

Figure 5.6: Relative modification in the field-assisted lifetimes $\Delta t_{1/2}/t^0_{1/2}$ as a function of the electric field $\mathcal{E}_0$ in the case of ^{238}U.

5.4.1.2. Monochromatic laser field

We now focus on the calculation of the laser-assisted lifetimes in the case of a monochromatic laser field, like the one in Eq. (3.14). Similarly to the static field case, for exemplification we present the LAT results in detail for ^{106}Te. Laser-assisted lifetimes and α particle spectra are calculated for optical and x-ray laser field parameters for all four considered nuclei. We choose the damping parameters Γ_d and the final time t'_F for all nuclei such that we can guarantee that the laser field is switched off adiabatically. For the calculation of the α particle spectrum, we consider a range of laser-field intensities lower than the recollision threshold regime, calculated using Eq. (5.44). The chosen parameters, including the recollision limit for the four α emitters are listed in the Table 5.2. Firstly, we calculate the order of magnitude of

	Optical			**XFEL**	
	Γ_d *(MeV)*	$\omega_{XFEL}t'_F$	I_{rec} *(W/cm^2)*	Γ_d *(MeV)*	$\omega_{opt}t'_F$
$^{106}_{52}$Te	0.00183959	7000	6.36288×10^{22}	0.449678	5000
$^{150}_{66}$Dy	0.0019	7050	6.47281×10^{22}	0.449678	5000
$^{162}_{74}$W	0.0018	7000	8.46149×10^{22}	0.45	5050
$^{238}_{92}$U	0.00183959	7000	6.42375×10^{22}	0.44	5000

Table 5.2: Table of laser parameters. Γ_d and t'_F are the damping parameters introduced to switch off the electric field adiabatically. The considered photon energies are $\hbar\omega_{opt} = 1.55$ eV for the optical laser and $\hbar\omega_{XFEL} = 3$ keV for XFEL. The recollision limit is only meaningful for the optical laser parameters.

the correction to the imaginary part of the initial complex dimensionless parameter ψ_0 introduced by the laser, in accordance to Eqs. (5.20) and (5.23). The results are shown in Fig. 5.7. For ^{162}W, the imaginary part of the initial complex dimensionless parameter ψ_0 takes the value of 0.000135292, and for ^{106}Te, $\psi_0 = 0.000140389$, which are small values compared with $\varphi = 2\pi$. Hence, the field-free time of flight inside the Coulomb barrier, ψ_0/ω for each of the considered α emitters interacting with the monochromatic field is far smaller than the period of the incoming laser field for the optical frequency ω_{opt} and the x-ray ω_{XFEL}.

The ellipse-like shape that the correction $\Delta\psi_0$ takes as a function of the final energy in Figs. 5.7 and 5.8 corresponds to the existence of two solutions of the saddle-point equation, as expected in the case of the monochromatic field. However, the order of magnitude of the corrections are far smaller than the value of ψ_0 in the field-free case, as it can be seen in Fig. 5.7 and 5.8. In consequence, the correction introduced by the laser on the time of flight of the α particle through the barrier is extremely small.

If we look at the final time of the subbarrier motion, ϕ_0/ω as a function of final energy of the α particle E_F (for the optical laser, see Fig. 5.9 and for the x-ray laser field, see Fig. 5.10), we can see that the shape of the function that relates the two variables remains the same, regardless the strength of the electric field. For larger intensities not close to the recollision limit, shown in Table 5.2 for the four α emitting nuclei, the spectrum gets broader as can be seen in Figs. 5.9 and 5.10. For the monochromatic laser field with x-ray $\hbar\omega_{XFEL} = 3$ keV, the recollision threshold intensity take values close to the Schwinger limit. For instance, in the case of ^{106}Te,

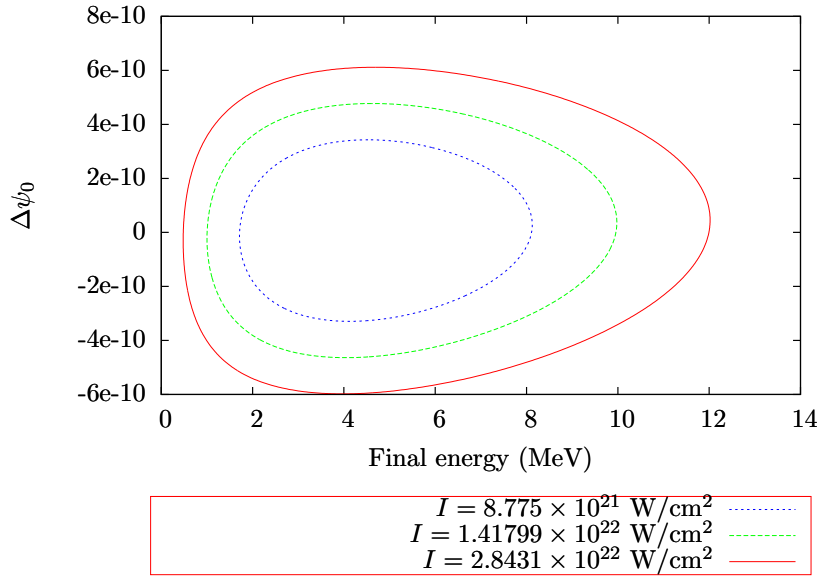

Figure 5.7: Correction $\Delta\psi_0$ on the parameter ψ_0 as a function of the final energy E_F, for a few laser field intensities and $\hbar\omega_{\text{opt}} = 1.55$ eV, in the case of ^{106}Te.

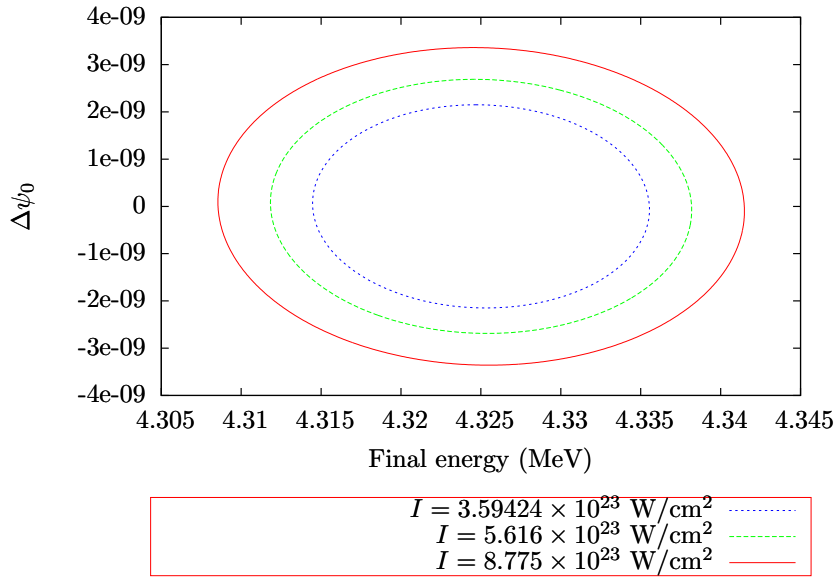

Figure 5.8: Correction $\Delta\psi_0$ on the parameter ψ_0 as a function of the final energy E_F, for a few laser field intensities and $\hbar\omega_{XFEL} = 3$ keV, in the case of ^{106}Te.

the recollision limit that corresponds to a photon energy of 3 keV is 2.38037×10^{29} W/cm^2. Therefore, the recollision effects cannot be observed at this large intensities without modifying completely the structure of the nucleus.

The energy interval delimited by the CB gets larger as the intensity of the monochromatic laser field increases. Furthermore, for the range of intensities that are not close to the recollision limit, there are only two solutions of the saddle-point equation, which determine two different trajectories. The trajectories that are described by the solutions interfere with each other, entering the coherent sum in the definition

of the modified transition amplitude $|M|^2$, Eq.(3.41).

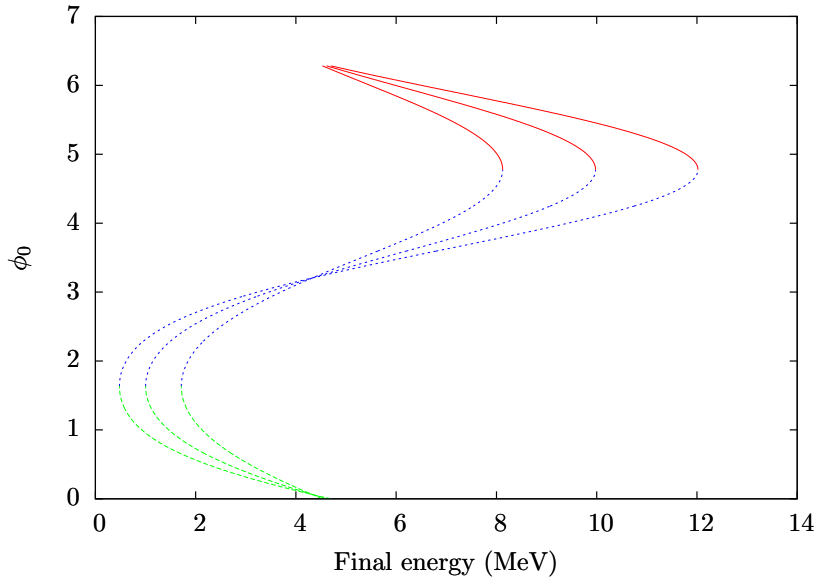

Figure 5.9: Real part of the initial complex dimensionless parameter ϕ_0 as a function of the final energy E_F, for $I = 8.775 \times 10^{21}$, 1.41799×10^{22} and 2.8431×10^{22} W/cm^2 (from left to right) in the case of ^{106}Te. The different trajectory branches are shown with red, blue, and green colors. The photon energy is $\hbar\omega_{opt} = 1.55$ eV.

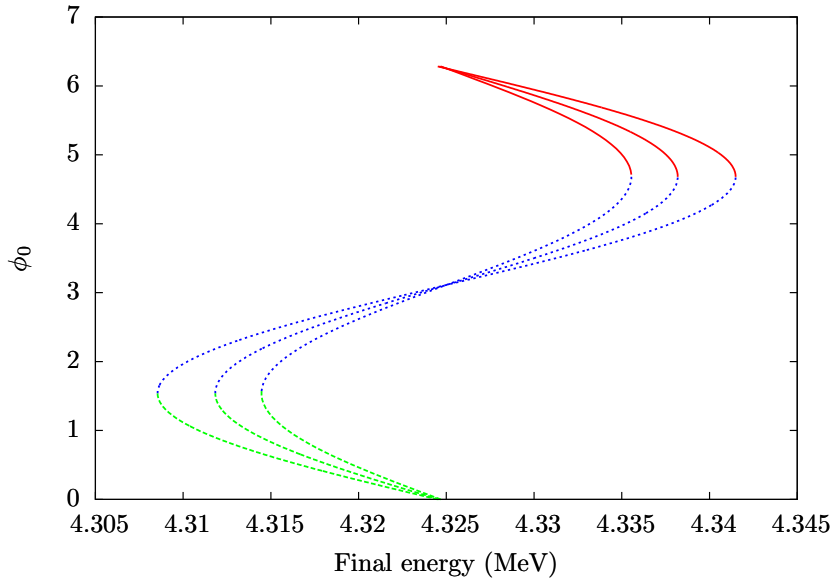

Figure 5.10: Real part of the initial complex dimensionless parameter ϕ_0 as a function of the final energy E_F, for $I = 3.59424 \times 10^{23}$, 5.676×10^{22} and 8.775×10^{23} W/cm^2 (left to right) in the case of ^{106}Te. The different trajectory branches are shown with red, blue, and green colors. The photon energy is $\hbar\omega = 3$ keV

The imaginary part of the total action $W_{\rm tot}$ in Eq. (5.39) as a function of the final energy E_F is given in Figs. 5.11 and Figs. 5.12, for the two considered laser-field parameters. The effect of the laser field is not completely negligible, as the imaginary part of the total action $W_{\rm tot}$ presents two different values for energies within the

CB, that correspond to the two saddle-point solutions. That is the reason why the imaginary part of the total action in Fig. 5.11 has a symmetrical, ellipse-like shape. With increasing intensity, the number of absorbed and emitted photons increases, and the range of energies gets broader. In addition to that, for lower intensities, the maximum and minimum values that $\mathrm{Im}\,(W_{\mathrm{tot}})$ takes are closer. The deformation of the ellipse-like shape comes for larger intensities, in which the difference between the maximum and minimum values of $\mathrm{Im}\,(W_{\mathrm{tot}})$ increases. Note in Fig. 5.11 that the horizontal symmetry axis of the ellipse is exactly the value that the imaginary part of the action W_{tot} takes in the field-free case.

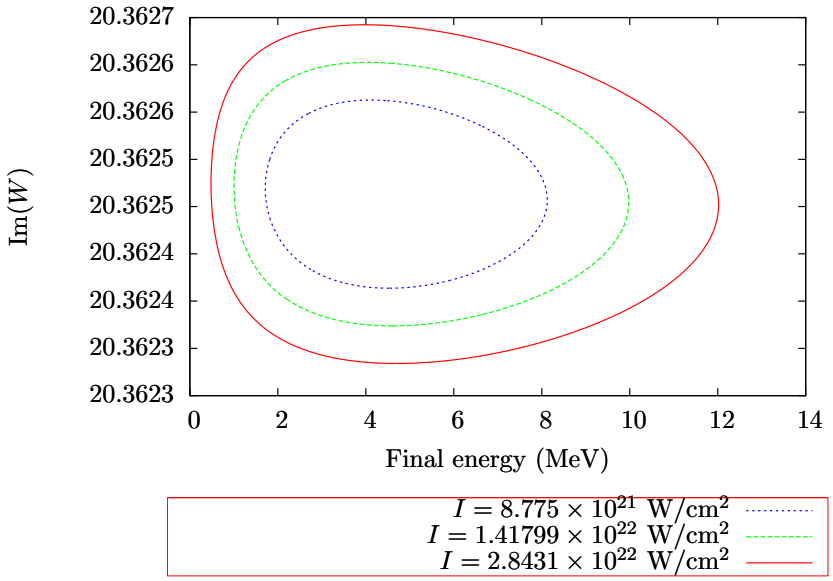

Figure 5.11: Imaginary part of the action $\mathrm{Im}\,(W_{\mathrm{tot}})$ for the laser-assisted α decay of ^{106}Te as a function of the final energy E_F, for a few laser field intensities at $\hbar\omega_{opt} = 1.55$ eV.

However, as we can see in Figs. 5.11 and 5.12, the difference between the maximum value of the imaginary part of the action W_{tot} and its minimum value even for a high laser-field intensity is rather small compared to the value of the imaginary part of the action calculated in the field-free case. As already pointed out, the imaginary part of the classical action W_{tot} characterizes the subbarrier dynamics of the α particle and determines the tunneling rate. In consequence, we can see that the correction on the time of flight introduced by the laser field, and the corrections on the trajectories during the subbarrier motion are small, and have only a weak effect on the dynamics of the α particle inside the Coulomb barrier. The tunneling rate through the Coulomb barrier in the presence of the monochromatic laser field can be calculated by according to the expression (5.42).

In Figs. 5.13 and 5.14, we show the laser-assisted lifetimes in the case of ^{106}Te as a function of several laser intensities. The laser effect is to accelerate the decay. However, the relative modification of the laser-assisted lifetimes is extremely small, on the order of 10^{-8}. Even for large intensities not so far away from the recollision limit for the optical laser, the modification in the lifetimes is only $\Delta t_{1/2}/t^0_{1/2} = \left(t^{\mathrm{LAT}}_{1/2} - t^0_{1/2}\right)/t^0_{1/2} = 4.8 \times 10^{-8}$. For the x-ray laser, the relative change in the

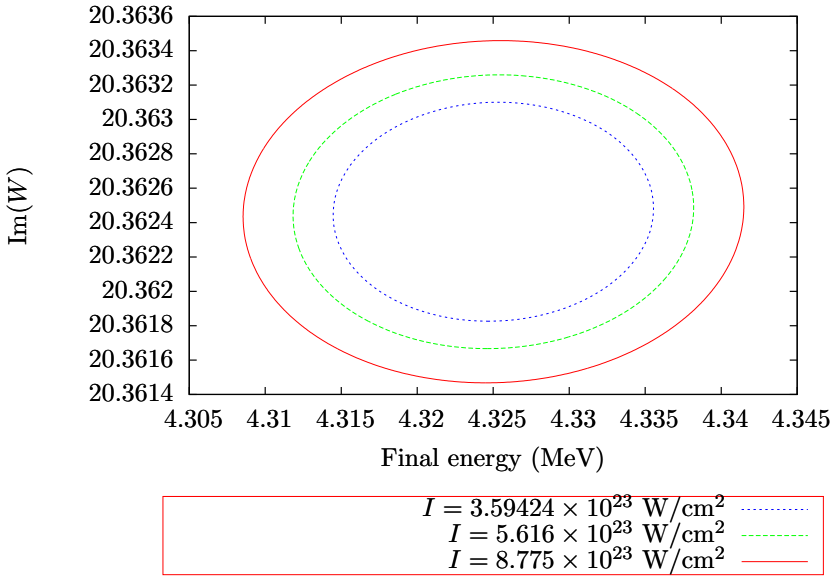

Figure 5.12: Imaginary part of the action $\mathrm{Im}\,(W_{\mathrm{tot}})$ for the laser-assisted α decay of ^{106}Te as a function of the final energy E_F, for a few laser field intensities at $\hbar\omega = 3$ keV.

lifetimes is slightly larger, around 10^{-6}. This difference comes from the range of laser-field intensities that can be used to assist the tunneling of the α particle before the recollision effects take place. While in the case of an optical laser, the recollision phenomena starts occuring around 6×10^{22} W/cm^2 (see Table 5.2), for the x-ray laser, the laser-field intensity can be increased without any consideration of recollision effects. Therefore, the laser-field intensities in the case of the x-ray laser field are significantly larger than the values that the field intensity can take before the recollision occurs in the presence of the optical laser field.

We can compare the modification in the calculated laser-assisted lifetimes respect to the field-free lifetimes obtained for the monochromatic case in Figs. 5.13 and 5.14 with the ones in the case of tunneling in the presence of a static field, 5.3. For the monochromatic laser field, the height of the tunneling barrier oscillates in time due to the time-dependent form of the interaction with the external field, and the tunneling rate is obtained by averaging over one laser period. In comparison, in the presence of a constant electric field, the height of the Coulomb barrier is permanently lowered by the interaction with the field. In consequence, the decrease in the calculated field-assisted lifetimes with respect to the spontaneous α decay lifetime is more significant for the static field than for the monochromatic laser field.

Similarly to the case of ^{106}Te, we found that the relative modifications in the laser-assisted lifetimes for ^{150}Dy have small values as shown in Fig. 5.15 (for optical laser parameters) and Fig. 5.16 (for XFEL parameters). The relative changes in the laser-assisted lifetimes for this particular nucleus take values around 10^{-8} for the optical laser and 10^{-6} in the case when the photon energy of the laser field is $\hbar\omega_{XFEL} = 3$ keV. The same order of magnitude in the relative change of the laser-assisted lifetimes is obtained for the other two α emitting nucleus studied in the present thesis, ^{162}W (see Figs. 5.17 and 5.18) and ^{238}U (Figs. 5.19 and 5.20). Regardless of the differences in the characterization of the tunneling barrier, the dynamics of the α particle during

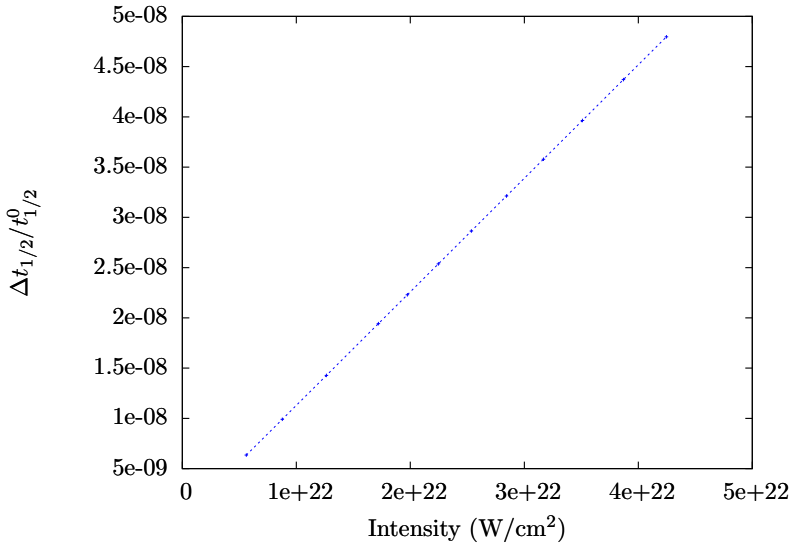

Figure 5.13: Relative modification in the laser-assisted lifetimes $\Delta t_{1/2}/t^0_{1/2} = \left(t^{\mathrm{LAT}}_{1/2} - t^0_{1/2}\right)/t^0_{1/2}$ as a function of the laser intensity I a photon energy $\hbar\omega_{opt} = 1.55$ eV, in the case of ^{106}Te.

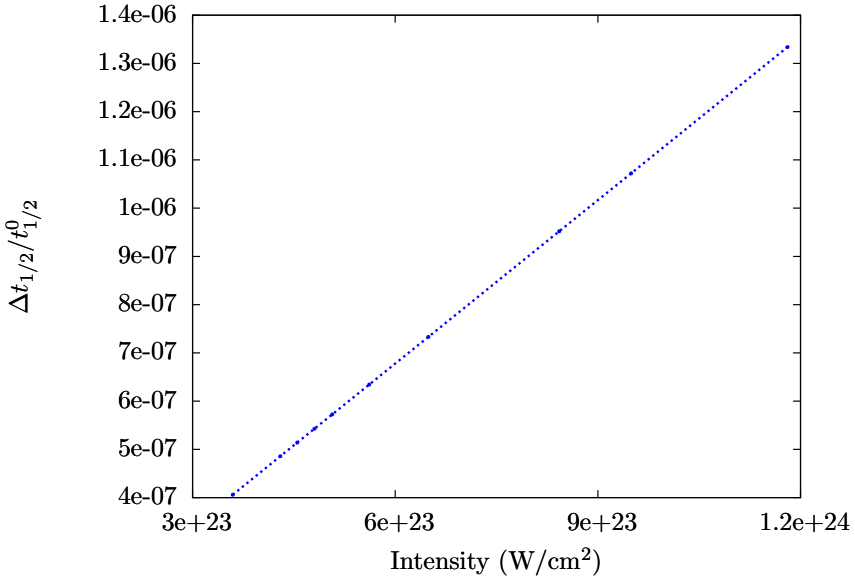

Figure 5.14: Relative modification in the laser-assisted lifetimes $\Delta t_{1/2}/t^0_{1/2} = \left(t^{\mathrm{LAT}}_{1/2} - t^0_{1/2}\right)/t^0_{1/2}$ as a function of the laser intensity I a photon energy $\hbar\omega_{XFEL} = 3$ keV, in the case of ^{106}Te.

the subbarrier motion in the presence of the laser field is essentially the same for the studied α emitters, leading to similar relative modifications of the α decay rate.

Our results for ^{106}Te,^{150}Dy, ^{162}W and ^{238}U thus show that *the direct interaction with the laser field indeed leads to a speed up of α decay, the magnitude of which, however, is very small.* In terms of the exclusive and inclusive parameter regimes defined in Chapter 3, the case of LAT for the four considered α emitters belongs to the exclusive

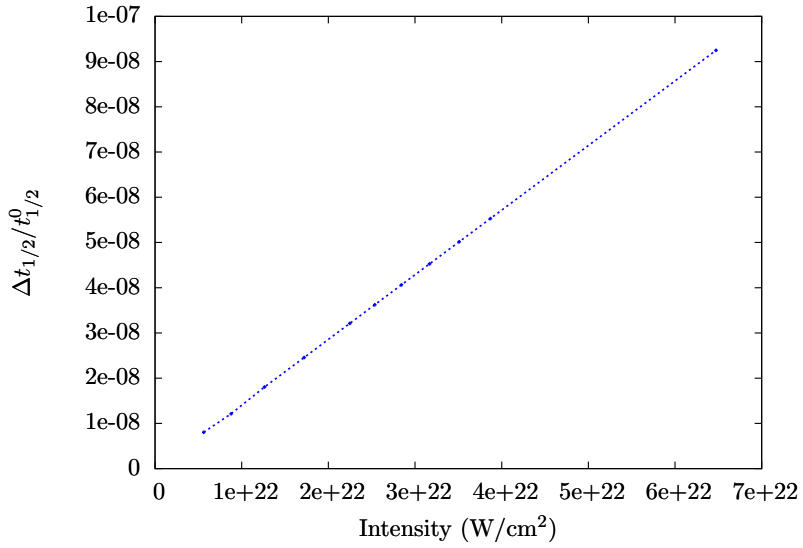

Figure 5.15: Relative modification in the laser-assisted lifetimes $\Delta t_{1/2}/t^0_{1/2} = \left(t^{\mathrm{LAT}}_{1/2} - t^0_{1/2}\right)/t^0_{1/2}$ as a function of the laser intensity I a photon energy $\hbar\omega_{opt} = 1.55$ eV, in the case of ^{150}Dy.

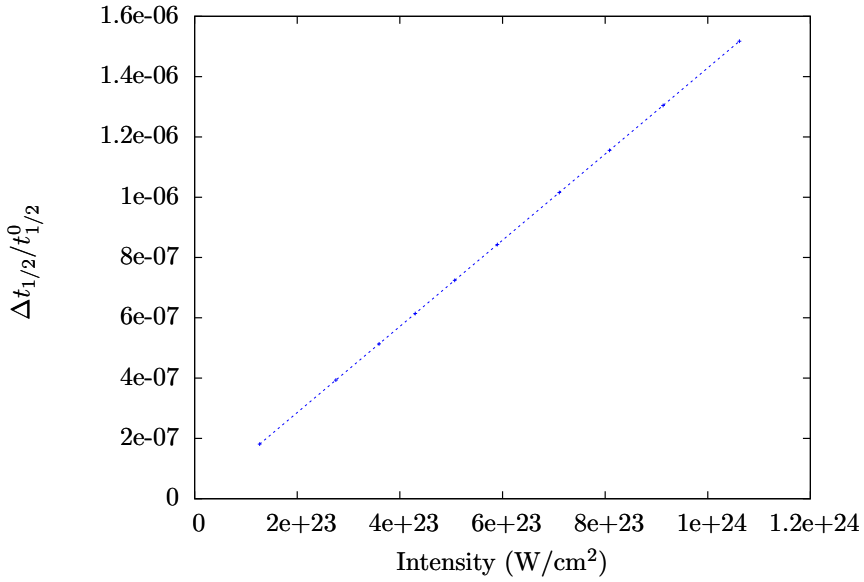

Figure 5.16: Relative modification in the laser-assisted lifetimes $\Delta t_{1/2}/t^0_{1/2} = \left(t^{\mathrm{LAT}}_{1/2} - t^0_{1/2}\right)/t^0_{1/2}$ as a function of the laser intensity I a photon energy $\hbar\omega_{XFEL} = 3$ keV, in the case of ^{150}Dy.

regime, for which the laser has a only a tiny effect on the tunneling through the barrier. However, the spectrum of tunneled particles is changed extensively. As an example, we calculate the value of the parameter μ_{ext} defined in (4.64) for ^{106}Te and obtain a value of $1.00751 \times 10^{-9} \ll 1$, which is deep within the extensive parameter regime. With that said, we can investigate the effect of the monochromatic laser field in the energy spectrum of the α particle.

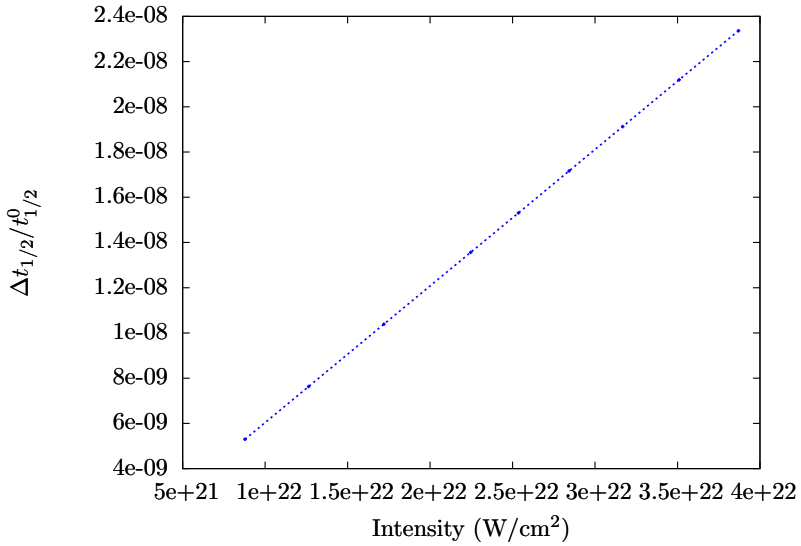

Figure 5.17: Relative modification in the laser-assisted lifetimes $\Delta t_{1/2}/t^0_{1/2} = \left(t^{\rm LAT}_{1/2} - t^0_{1/2}\right)/t^0_{1/2}$ as a function of the laser intensity I a photon energy of 1.55 eV, in the case of ^{162}W.

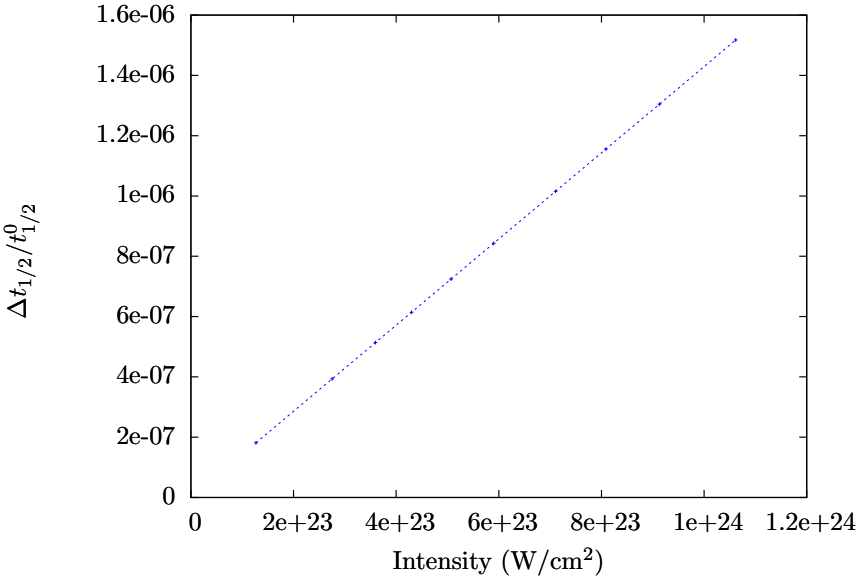

Figure 5.18: Relative modification in the laser-assisted lifetimes $\Delta t_{1/2}/t^0_{1/2} = \left(t^{\rm LAT}_{1/2} - t^0_{1/2}\right)/t^0_{1/2}$ as a function of the laser intensity I a photon energy of 3 keV, in the case of ^{162}W.

We show the differential decay rates dR_l/dp calculated using the expression (5.41) as a function of the final energy in Figs. 5.21, 5.23, 5.25 and 5.27 (optical laser parameters) and Figs. 5.22, 5.24, 5.26 and 5.28 (XFEL laser parameters). The modification in the momentum distribution is more noticeable at larger intensities, as shown in Figs. 5.21- 5.28. The final energy distribution is broadened at larger intensities following the classical boundaries $p_0 \pm p_F$. For lower intensities, the distribution comprises of a narrow region around the energy E of the α particle.

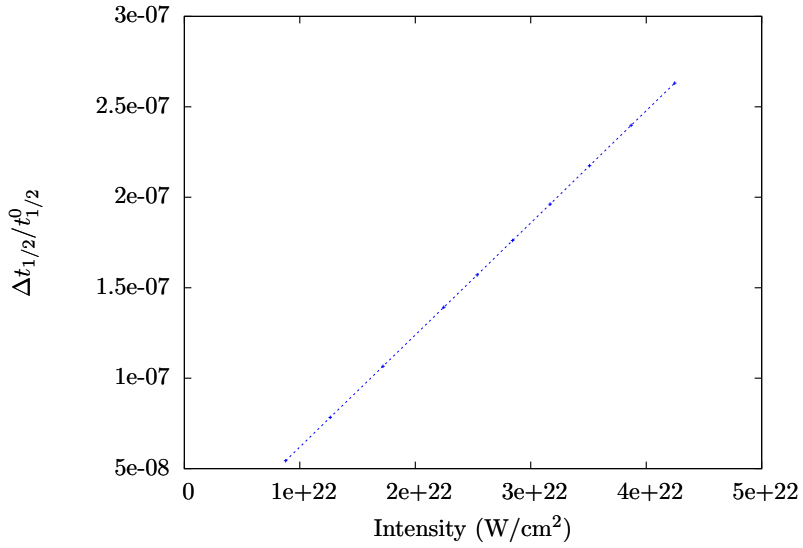

Figure 5.19: Relative modification in the laser-assisted lifetimes $\Delta t_{1/2}/t^0_{1/2} = \left(t^{\mathrm{LAT}}_{1/2} - t^0_{1/2}\right)/t^0_{1/2}$ as a function of the laser intensity I a photon energy of 1.55 eV, in the case of ^{238}U.

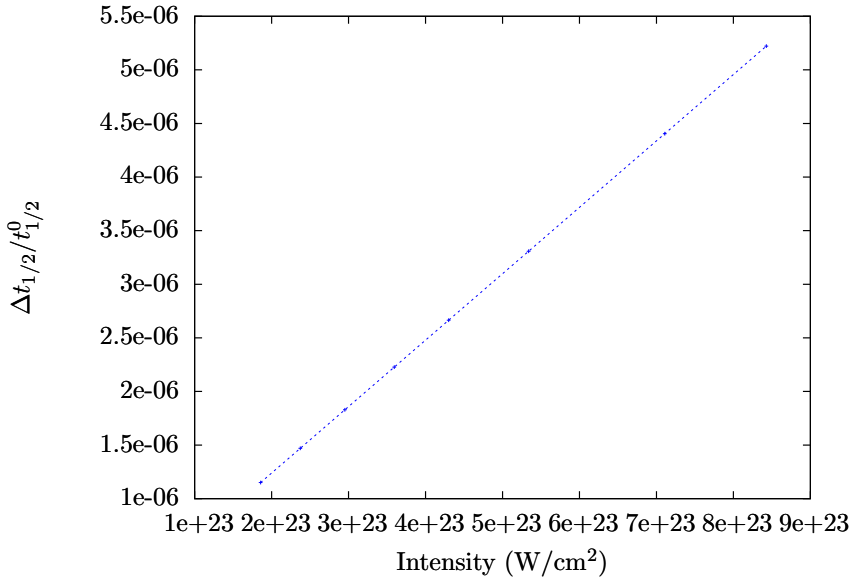

Figure 5.20: Relative modification in the laser-assisted lifetimes $\Delta t_{1/2}/t^0_{1/2} = \left(t^{\mathrm{LAT}}_{1/2} - t^0_{1/2}\right)/t^0_{1/2}$ as a function of the laser intensity I a photon energy $\hbar\omega_{XFEL} = 3$ keV, in the case of ^{238}U.

In the case of the x-ray laser field the number of photons absorbed and emitted by the α particle as it travels to the detector is not as numerous as in the case of the optical laser. However, distinctive features still appear in the spectrum due to the interaction with the high intensity x-ray laser field, similar to the ones observed in the optical laser field case. The distribution gets broader with larger laser-field intensities, corresponding to a larger range of energies between the CB. When the laser-field intensity is lower, the spectrum approaches the field-free limit, characterized by a

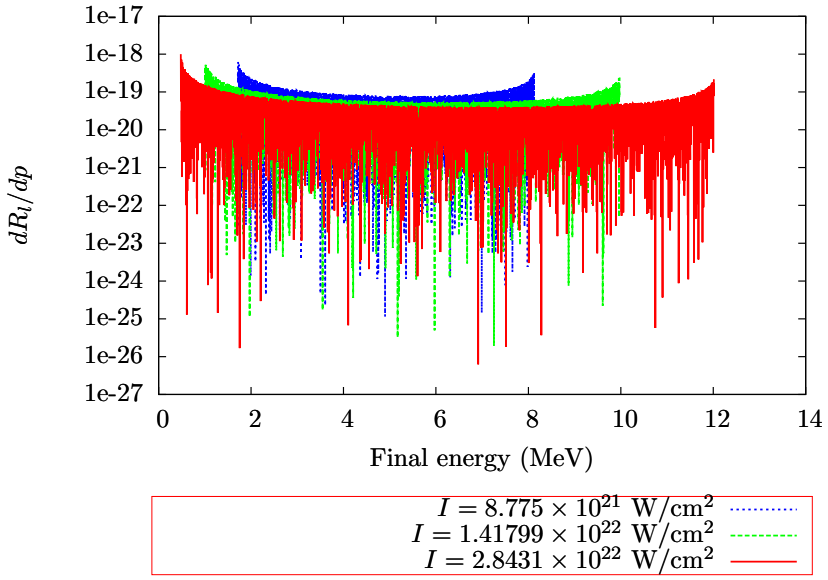

Figure 5.21: Laser-assisted differential decay rate dR_l/dp as a function of the final energy E_l in the case of ^{106}Te at $\hbar\omega_{opt} = 1.55$ eV.

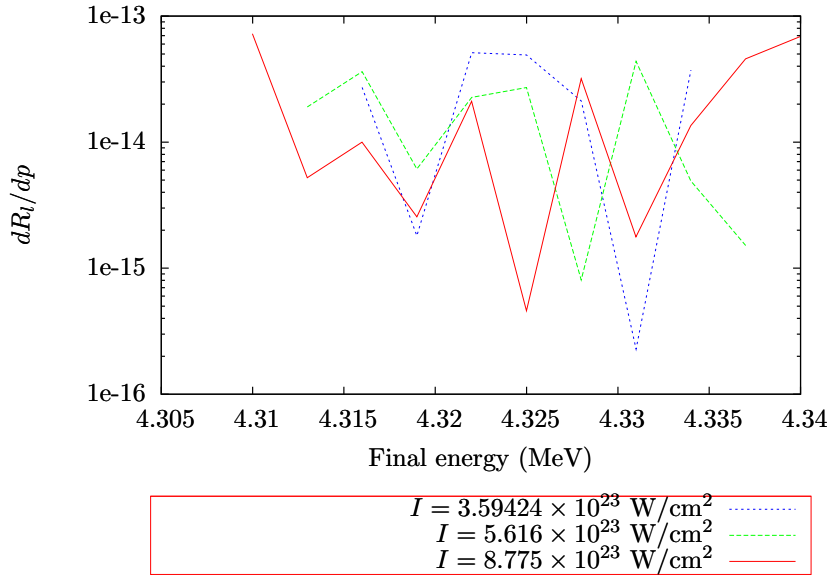

Figure 5.22: Laser-assisted decay rate dR_l/dp as a function of the final energy E_l in the case of ^{106}Te.

narrow distribution centered onn the initial energy E of the α particle.

So far, we here established that the laser-assisted α decay lies deeply within the extensive regime and the laser-assisted α decay lifetimes are not strongly affected by the interaction with the monochromatic field. We have shown that the incoming laser field affects the dynamics of the α particle by modifying its momentum distribution after leaving the barrier for moderate intensities of an optical laser with photon energy $\hbar\omega_{opt} = 1.55$ eV or stronger laser-field intensities for a x-ray laser beam, with photon energy $\hbar\omega_{XFEL} = 3$ keV. At large intensities, recollisions of the α

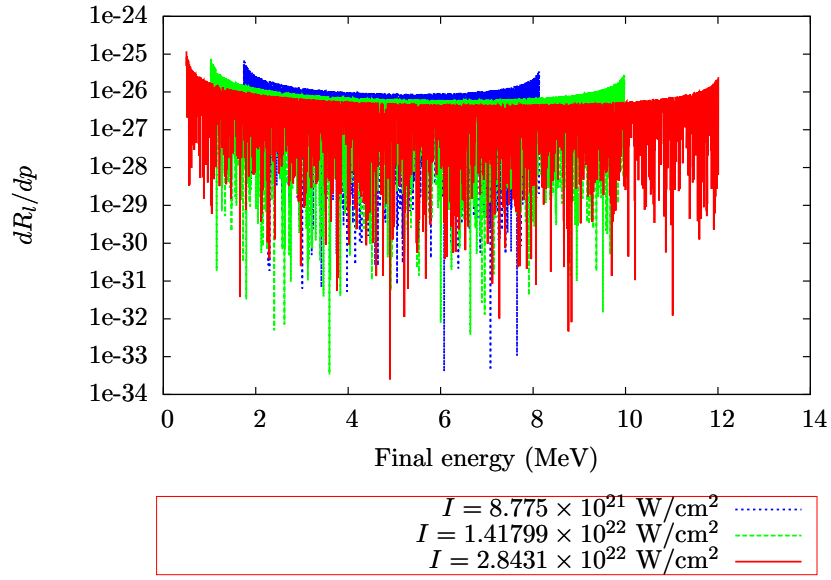

Figure 5.23: Laser-assisted differential decay rate dR_l/dp as a function of the final energy E_l in the case of ^{150}Dy at $\hbar\omega = 1.55$ eV.

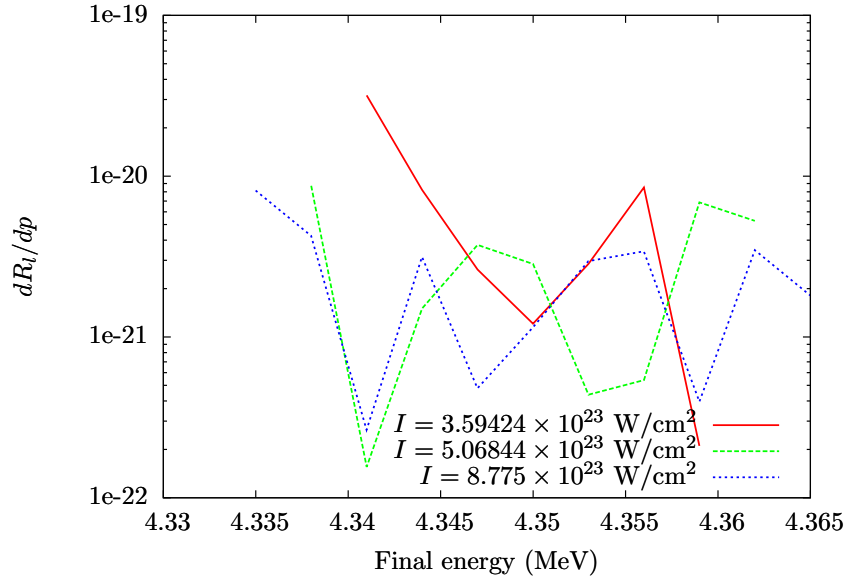

Figure 5.24: Laser-assisted decay rate dR_l/dp as a function of the final energy E_l in the case of ^{150}Dy for a photon energy of 3 keV.

particle with the daughter nucleus may occur. In the case of the x-ray laser field, the phenomenom of recollision is ruled out completely due to the magnitude of the recollision threshold intensity defined in Eq. (5.44). This is not the case for the optical laser, in which the recollision limit is at a high experimentally almost feasible intensity.

Here we present briefly some characteristics of the total action for intensities approaching the recollision threshold from a qualitative perspective. In our numerical calculations, we show that for intensities close to the recollision limit, the change

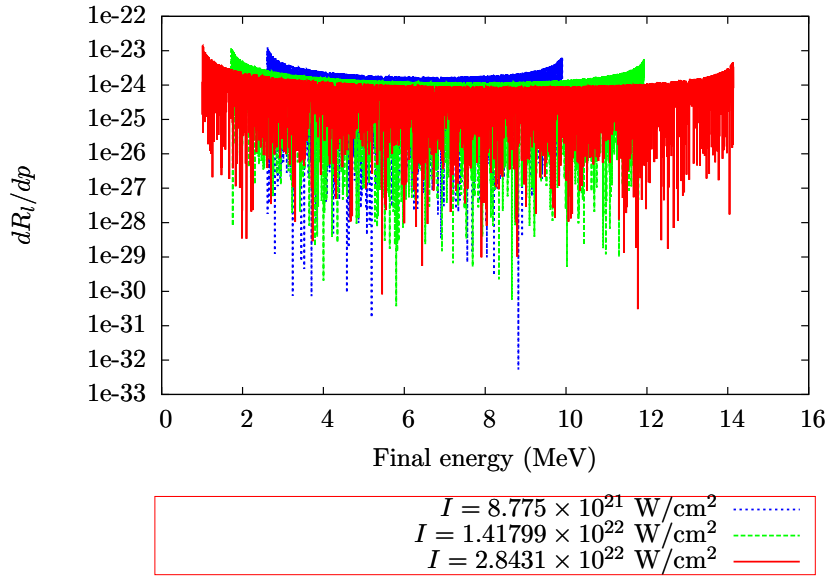

Figure 5.25: Laser-assisted differential decay rate dR_l/dp as a function of the final energy E_l in the case of ^{162}W at $\hbar\omega_{opt} = 1.55$ eV.

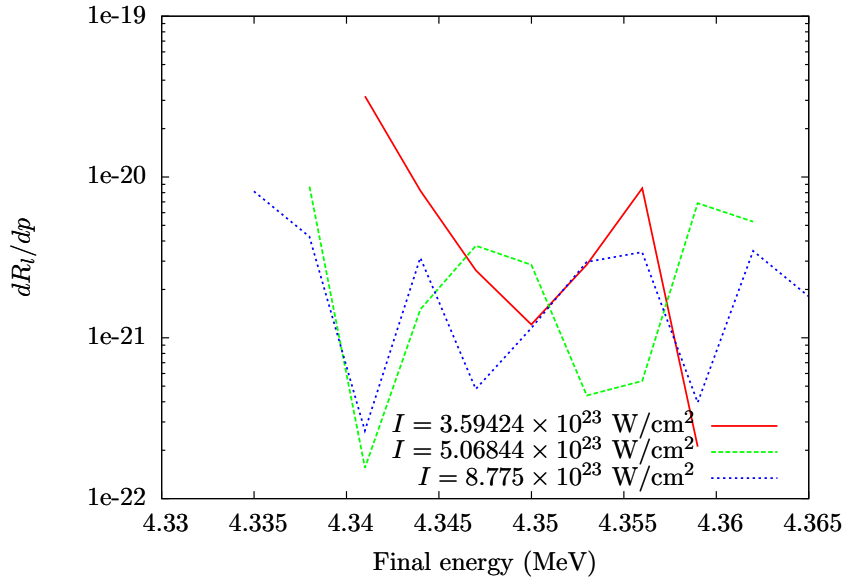

Figure 5.26: Laser-assisted decay rate dR_l/dp as a function of the final energy E_l in the case of ^{162}W for a photon energy $\hbar\omega_{XFEL} = 3$ keV.

in the direction of the monochromatic laser field affects the dynamics of the α particle after the barrier, as shown in Fig. 5.29. We find the trajectories that the α particle follows outside the barrier starting its motion at $\varphi = \phi_0 = 4\pi/5$. The α particle comes back at a later time, rescattering with the daughter nucleus when the laser-field intensities are higher than the recollision threshold laser-field intensity. For laser-field intensities below recollision limit, the change in the direction of the laser field slightly modifies the trajectories of the α particle outside the barrier, but not enough to drive the α particle back to collide with the daughter nucleus. After the initial change in its trajectory, the α particle continues to be accelerated

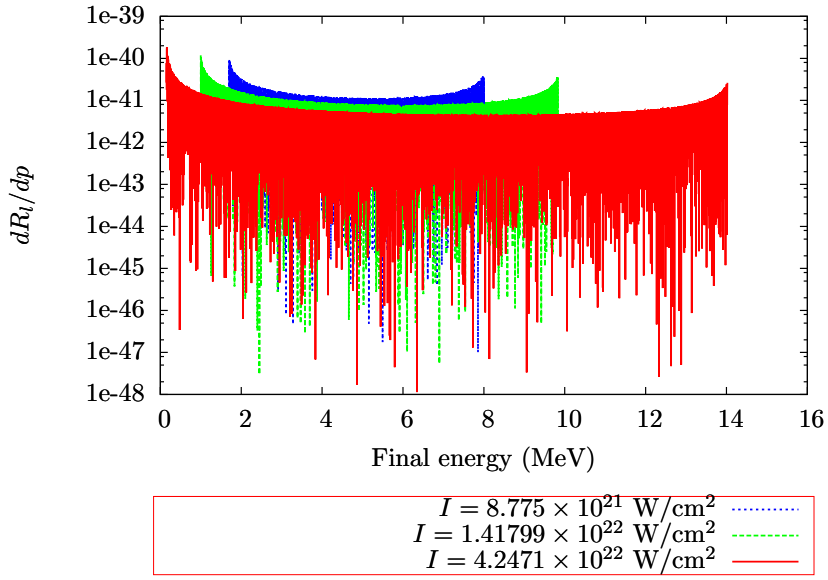

Figure 5.27: Laser-assisted differential decay rate dR_l/dp as a function of the final energy E_l in the case of ^{238}U at $\hbar\omega_{opt} = 1.55$ eV.

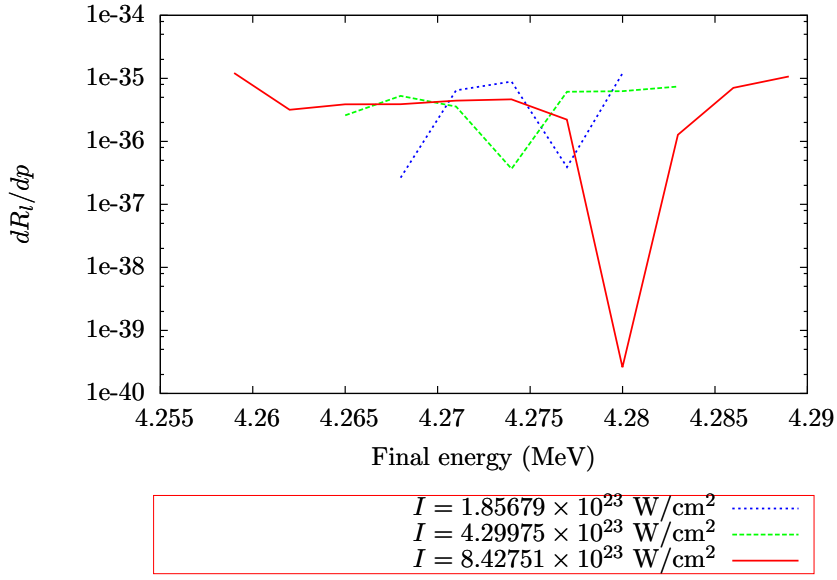

Figure 5.28: Laser-assisted decay rate dR_l/dp as a function of the final energy E_l in the case of ^{238}U for a photon energy $\hbar\omega_{XFEL} = 3$ keV.

by the laser field, far away from the daughter nucleus. For laser-intensities above the laser-field intensity threshold, the change of direction of the monochromatic field affects considerably the dynamics of the α particle. As a consequence, the α particle changes its trajectory. The interaction with the laser field drives back the α particle and finally, it collides with the daughter nucleus before it starts to be driven away from the daughter nucleus by the laser field.

If we compare the behavior of ϕ_0 for low laser field intensities (no recollisions) in Fig. 5.9 with the cases where the recollisions are occurring, shown in Fig. 5.30,

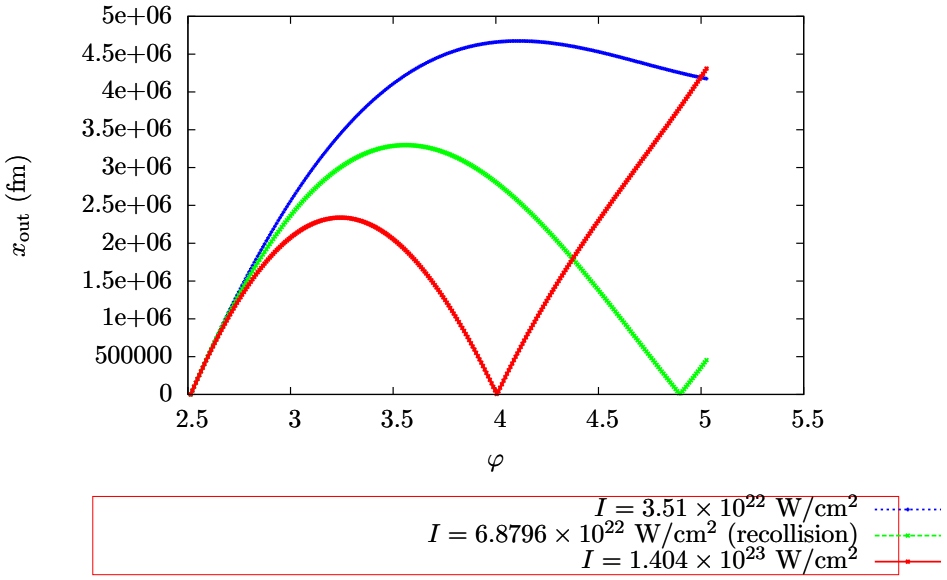

Figure 5.29: Position of the α particle outside the barrier for a single value of the real part of the initial complex dimensionless parameter $\phi_0 = 4\pi/5$ as a function of the dimensionless time parameter φ, for three different intensities: $I = 3.51 \times 10^{22}$ (below the recollision limit, blue line), 6.8796×10^{22} (slightly above the recollision threshold intensity, green line) and 1.404×10^{23} W/cm^2 (above the recollision limit, red line) in the case of ^{106}Te.

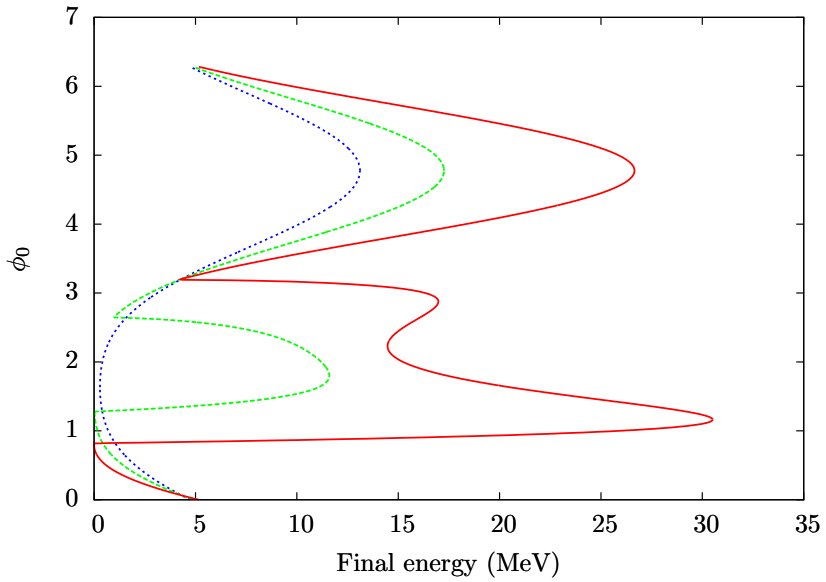

Figure 5.30: Real part of the initial complex dimensionless parameter ϕ_0 as a function of the final energy E_F, for $I = 3.51 \times 10^{22}$ (below the recollision limit, blue line), 6.35912×10^{22} (recollision threshold intensity, green line) and 1.404×10^{23} W/cm^2 (above the recollision limit, red line) in the case of ^{106}Te.

we can identify the distinction in the number of saddle-point solutions, associated with a single final energy. In that sense, we can study qualitatively the recollision dynamics of the α particle. For laser-field intensities close to the recollision intensity

threshold, the number of saddle-point solutions for a value of final energy with the CB increases. In consequence, for a given α particle final energy there can be more than two trajectories that interfere. The shape of the function that expresses the relation between ϕ_0 and the final energy of the α particle changes considerably for laser field intensities close to the recollision limit. Due to the fact that the behavior of the saddle-point solutions is affected at high intensities in the range of the recollision threshold, the imaginary part of the action W_{tot} has a strongly modified shape, as shown in Fig. 5.31. The calculation of the full rescattering spectra requires the summation of all different rescattering trajectories and is beyond the scope of our current calculations. However, our first results for the imaginary part of the action shown in Figs. 5.30 and 5.31 convey the significant effects of the recollision for large intensities.

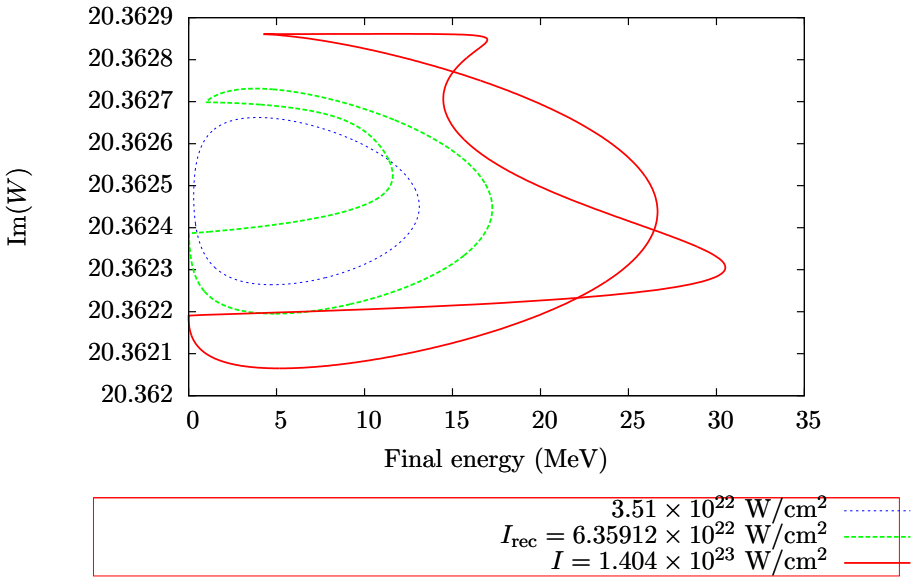

Figure 5.31: Imaginary part of the action W_{tot} as a function of the final energy E_F for three laser intensities: below the recollision threshold intensity (blue line), the recollision limit (green line) and above the recollision threshold intensity (red line) at $\hbar\omega_{opt} = 1.55$ eV.

The qualitative description of recollision in laser-assisted α decay resembles the rescattering of ionized electrons in atomic systems. The recollision of electrons after leaving the atomic potential has led to interesting development in the physics of strong-field laser atomic interactions, such as high harmonic generation [Cor93] and nonsequential double ionization [HVDS08, KI09]. The recollision in atomic systems takes place after the electron tunnels through the Coulomb potential. When the electron is detached from an atom via nonlinear ionization, it is accelerated away from the atom until the field direction is reversed, propelling the released electron back to the atomic system. The electrons are usually emitted along the direction of the laser field. The α decay, on the other hand, occurs mostly spontaneously, such that the α particle is emitted in 4π. Thus, in the case of laser-assisted α decay, only those α particles emitted in a narrow solid angle around the laser field direction will have the possibility to rescatter on the daughter nucleus. Furthermore, we have restricted our present calculations to field intensities below the recollision limit.

A further step to understand the dynamics of the laser-assisted α decay involves first the extension of the one-dimensional treatment to account for recollisions in the spectra. The role of the laser-induced recollisions could offer a possibility to influence the bremsstrahlung emitted during α decay. The bremsstrahlung emitted during the spontaneous α decay is still an intriguing subject and has been extensively studied in the last decade [BdPZ99, DG96, FZ99, PB98, JMT$^+$08, MO03, MOG$^+$09, TNH$^+$99]. The inclusion of recollision effects induced by the interaction with the laser field can have significant effects in the spectrum of radiation emitted after the LAT through the Coulomb barrier has taken place. The determination of the spectrum after the recollision limit and the influence of the recollision of the α particle in the emitted bremsstrahlung of α decay are some of the interesting possibilities that can be explored following the qualitative description of the recollision in the laser-assisted α decay.

CHAPTER 6

CONCLUSIONS AND OUTLOOK

In this thesis we have investigated theoretically the process of laser-assisted α decay. Due to the nature of the initial state, the spontaneous α decay can be considered as a tunneling process of a preformed α particle, described by a QS state, through the Coulomb barrier. In order to investigate the LAT of the α particle, we have developed a general formalism to describe the laser-assisted decay of QS states in the semiclassical parameter regime, extending a well known approach in the physics of nonlinear ionization, namely, the SFA and its formulation in terms of complex trajectories. In order to illuminate the physical essence of the problem and avoid unnecessary technical complications, we have neglected initially some accompanying effects like recollision of the tunneling particle, which can take place at large intensities.

We have tested our method studying the LAT through a rectangular barrier in the presence of a monochromatic laser field and a short pulse. Our results in that particular case demonstrated the existence of two regimes of decay that have been described qualitatively in works on laser-assisted β decay [NR64]: the "exclusive" and "inclusive" regimes. In the exclusive regime, the momentum distribution is strongly affected due to the interaction with the laser field but the total decay rate remains unchanged. Therefore, the laser only plays a role on the dynamics of the tunneling particle after it has left the barrier on its way to the detector. On the other hand, in the "inclusive" regime, both the spectrum and the laser-assisted decay rate are strongly affected by the interaction with the laser field. Thus, the laser field modifies the dynamics of the tunneling particle at all times, during its subbarrier motion and outside the barrier. In order to show the accuracy of our method, we have performed a comparison of the obtained results in the presence of a short pulse using our method with numerical results of the time-dependent Schrödinger equation, showing not only qualitative but also good quantitative agreement.

Using the developed general formalism for laser-assisted decay of QS states, we have investigated the laser-assisted α decay, starting with the tunneling of the α particle through the Coulomb barrier in the presence of a static field for four medium-mass and heavy α emitters with lifetimes ranging from 10^{-5} seconds to millions of years: ^{106}Te, ^{150}Dy, ^{162}W and ^{238}U. The field-assisted tunneling of the α particle through

the Coulomb barrier can be used as a benchmark to characterize the LAT in the presence of a monochromatic electric field, since the static field is the low-frequency limit of the monochromatic field. A comparison of our results for the static field with the ones obtained from the WKB method shows perfect agreement. For the static field, our calculated field-assisted lifetimes show that the field-induced acceleration of the α decay is only of the order of $\Delta t_{1/2}/t_{1/2} = \left(t_{1/2}^{\mathrm{LAT}} - t_{1/2}^{0}\right)/t_{1/2}^{0} = 10^{-3}$ for static fields of electric field strengths of 10^{15} V/m. For a monochromatic field, the laser-assisted lifetime averaged over the laser period is as good as equal to the field-free one, with a relative modification of 10^{-8} for strong optical fields and laser-field intensities of 10^{22} W/cm^2 and 10^{-6} for x-ray coherent fields and laser-field intensities of 10^{24} W/cm^2. However, the spectrum of the emitted α particles in the presence of a monochromatic laser field can be strongly modified, even leading to recollision effects for high intensities.

Although the recollision effects have not been considered in the development of our formalism to study the laser-assisted α decay, we were able to determine the intensity threshold at which the recollision appears. For medium-mass α emitters, we find that the recollision field intensity can be as low as 6×10^{22} W/cm^2, a value soon available at large-scale ultra-intense laser infrastructures. Qualitatively, we show that in the case of recollision, there are more than two saddle-point solutions of the saddle-point equation, associated with trajectories that interfere during the LAT of the α particle. Furthermore, the imaginary part of the action that determines the tunneling rate is strongly modified when the laser field intensities are close or higher than the recollision threshold.

As outlook on future work, it might be possible to investigate further the recollision phenomenon that we described qualitatively in this thesis. In atomic physics, the rescattering of an electron ionized by a laser field leads to the formation of one or more plateaus in the spectrum with the characteristic number of peaks, given by the Reiss parameter, Eq. (3.4). This effect can also be interpreted as multiphoton stimulated bremsstrahlung [BF66], an effect which has not been previously investigated for α decay. Laser-induced recollisions of the α particle with the daughter nucleus would also make a significant contribution to the bremsstrahlung emitted during α decay. The study of the emission of bremsstrahlung radiation in spontaneous α decay has been the subject of intensive research in the last decades [BdPZ99, DG96, FZ99, PB98, JMT$^+$08, MO03, MOG$^+$09, TNH$^+$99], and is still an intriguing concept.

The role of the laser-induced recollisions could offer a possibility to influence the bremsstrahlung emitted during the α decay. The determination of the laser-assisted α decay recollision spectrum in one dimension is a theoretical straightforward step and can be calculated using the formalism presented in this thesis. However, its calculation implies more extensive and cumbersome numerics due to the behavior of the trajectories of the α particle in the recollision limit. Unlike the case of laser-induced ionization of electrons where the electrons are usually emitted along the direction of the laser field, the α particles are emitted in all directions. Thus, in the case of laser-assisted α decay, only those α particles emitted in a narrow solid angle around the laser field direction will have the possibility to rescatter on the daughter nucleus.

Theoretical predictions of the bremsstrahlung radiation in laser-assisted α decay would provide means of further increase our knowledge of the emission of bremsstrahlung

in α decay. In addition, it would provide a useful comparison with the well-understood electron laser-induced rescattering in atomic physics strong-field phenomena, which is the key stone to describe interesting phenomena in the physics of the interaction of atomic systems with strong laser fields, such as high harmonic generation [Cor93] and nonsequential double ionization [HVDS08, KI09]. Ultimately, laser control of α decay bremsstrahlung spectra may provide a useful tool for detection and preparation in nuclear physics.

APPENDIX A

UNITS

Throughout this work, two different set of units have been used. In Chapters 3 and 4 that discuss the laser-assisted decay of a QS state and the test case of laser-assisted tunneling through a rectangular barrier, atomic units (a.u.) are used. In Chapter 5, we use high energy units. In this Appendix, we detail the two systems of units.

A.1. Atomic Units

In the atomic units, the physical constants of length, mass and charge are chosen to be the Bohr radius a_0, the electron mass m_e and the electron charge e. They are all assumed to be 1 as the Plack constant reduced by a factor of 2π, $\hbar$.

The following table shows the conversion of physical quantities from atomic units in SI units, taken from [Het09].

physical quantity	atomic unit [a.u.]	SI units
energy ε	1	$27.21\,\mathrm{eV}$
electric field E	1	$5.14 \times 10^{9}\,\mathrm{V/cm}$
intensity I	1	$3.51 \times 10^{16}\,\mathrm{W/cm^2}$
speed of light c	137.036	$2.99 \times 10^{8}\,\mathrm{m/s}$
time t	1	$24.2 \times 10^{-18}\,\mathrm{s}$
angular frequency ω_0	1	$2.59 \times 10^{17}\,s^{-1}$
length α_0	1	$52.9 \times 10^{-12}\,\mathrm{m}$

The conversion of the electric field E in a.u. of a monochromatic laser field to laser intensities in SI units, is

$$I[\mathrm{W/cm^2}] = 3.51 \times 10^{16} (E_0[\mathrm{a.u.}])^2 \,. \tag{A.1}$$

A.2. High Energy Units (MeV-Fermi)

In order to take into account the natural order of magnitudes of the variables involved in the laser-assisted α decay, we use units of MeV Fermi. The high energy units are summarized in a work by Hartmann *et al.* [HNS91]. We are going to detail the units in the following.

The frequency of the monochromatic laser has been defined in terms of energy units, i.e. MeV. The units of time are MeV^{-1}. A time unit is the time for the light to travel one Fermi [1]. The conversion of time units to MeV corresponds to multiplying by $\hbar c = 197.327\mathrm{MeV\ Fermi}$. This quantity gives the appropriate dimensions of the kinematical variables that define the dynamics of the α particle. The electric charge of the electron is $e^2 = \frac{\hbar c}{137}$. The electric field strength of the laser has units of $\mathrm{MeV}^{\frac{1}{2}}/\mathrm{Fermi}^{\frac{3}{2}}$.

Just to give an idea of the order of magnitude of the electric fields involved, an atomic unit of electric field is $4.29 \times 10^{-10}\mathrm{MeV}^{\frac{1}{2}}/\mathrm{Fermi}^{\frac{3}{2}}$. The electric field force, $e\mathcal{E}_0$, has units of MeV/Fermi.

Since we vary the intensity of the laser, we need to express the intensity I, as a function of the electric force parameter we introduce in the equations of motion. The conversion between the the intensity in SI units, $\mathrm{W/cm^2}$ and the electric field force $e\mathcal{E}_0$ in MeV/Fermi is given by

$$I = 2.64 \times 10^{35} \left(e\mathcal{E}_0\right)^2 . \tag{A.2}$$

[1] 3.33×10^{-24} seconds.

APPENDIX B

INTRODUCTION OF THE TRIANGULAR BARRIER FOR THE LASER-ASSISTED TUNNELING THROUGH A RECTANGULAR BARRIER

For a rectangular barrier, the particle velocity is discontinuous at the barrier exit. In order to avoid this discontinuity, we replace the rectangular barrier by a smooth potential, introducing a triangular barrier after the original rectangular barrier. The additional potential is also a short range potential, dropping linearly from U_0 down to zero on the width Δ, as it is shown in the Fig. (4.1). The tunneling barrier in the region II is

$$V_{\text{triangular}} = -\frac{U_0}{\Delta}\big(x - b - \Delta\big). \tag{B.1}$$

In the limit $\Delta \to 0$, the initial tunneling barrier is recovered.

We assume that the tunneling particle enters in the triangular barrier at $t = t'_s \in \mathbb{C}$, since the particle is still in a forbidden classical region. The initial position and velocity are complex, and are taken as the final velocity and position of the motion through the rectangular barrier. After the particle leaves the triangular barrier at $t' = t''_s$, the time becomes real, and the real physical motion starts, according to ITM. So $\text{Im}\left(\frac{dx}{dt'}\Big|_{t'=t''_s}\right) = 0$.

B.1. Final position and velocity after the rectangular barrier

When the particle leaves the region I, the real component of the position of the particle is known. The velocity can be determined by evaluating the velocity of the tunneling particle, Eq. (4.26) at $\varphi = \varphi'_s = \phi_0 + i\psi'_0$. The initial conditions of the

motion of the particle inside the triangular barrier are

$$\begin{aligned}\mathrm{Re}\left[x^{\mathrm{I}}\right]\Big|_{\varphi=\varphi'_s} &= b,\\ \mathrm{Im}\left[x^{\mathrm{I}}\right]\Big|_{\varphi=\varphi'_s} &= \frac{p_F\sin(\phi_0)}{\omega}\big(-\sinh(\psi_0)-(\psi'_0-\psi_0)\cosh(\psi_0)+\sinh(\psi'_0)\big).\end{aligned} \tag{B.2}$$

Using the last expression, Eq. (B.2), and evaluating the position, Eq. (4.27) at φ'_f, we can find a relation between ψ_0, ψ'_0 and ϕ_0 (the imaginary parts of the complex times and the real part, respectively). This condition is

$$b=\frac{p_F\cos(\phi_0)}{\omega}\Big(\cosh(\psi_0)-\cosh(\psi'_0)+\big((\psi'_0-\psi_0)\sinh(\psi_0)\big)\Big)-\frac{\kappa_0\Big(\psi'_0-\psi_0\Big)}{\omega}. \tag{B.3}$$

In the limit where $\cosh(\psi'_0)\approx 1$, and $\psi'_0\to 0$, the Eq. (B.3) can be written as

$$b=\frac{p_F\cos(\phi_0)}{\omega}\Big(\cosh(\psi_0)-1-\big(\psi_0\sinh(\psi_0)\big)\Big)+\frac{\kappa_0\psi_0}{\omega}. \tag{B.4}$$

Using the initial condition of the velocity of the particle, Eq. (B.2), we can express the imaginary and real parts of the rate of change of the position with respect to the dimensionless parameter,

$$\mathrm{Re}(\frac{dx^{\mathrm{I}}}{d\varphi}\Big|_{\varphi=\varphi'_s})=\frac{p_F\sin(\phi_0)}{\omega}\Big(\cosh(\psi'_0)-\cosh(\psi_0)\Big),$$

and

$$\mathrm{Im}(\frac{dx^{\mathrm{I}}}{d\varphi}\Big|_{\varphi=\varphi'_s})=\frac{\kappa_0}{\omega}-\frac{p_F\cos(\phi_0)}{\omega}\Big(\sinh(\psi_0)-\sinh(\psi'_0)\Big). \tag{B.5}$$

B.2. Equations of motion

During the subbarrier motion throughout the triangular barrier, the tunneling particle experiences an additional force due to the change of the potential barrier in that domain. The equations of motion are determined by the classical dynamics in complex times, in accordance to ITM,

$$\frac{d^2x^{\mathrm{II}}}{dt'^2}=\frac{U_0}{\Delta}+\mathcal{E}_0\cos(\omega t'). \tag{B.6}$$

Introducing the dimensionless parameter φ, the dynamics of the tunneling particle in the region II is determined by the classical equation, which is

$$\frac{d^2x}{d\varphi^2}=\frac{U_0}{\omega^2\Delta}+\frac{p_F\cos(\varphi)}{\omega}. \tag{B.7}$$

Analogously to what has been explained for the rectangular barrier, the position and the velocities of the particle during the subbarrier motion in the region II can be determined by integrating the equations of motion, Eq. (B.7). The dimensionless

parameter runs from the instant at which the particle enters into the triangular barrier ($\varphi'_s = \varphi'_s$) up to when the particle leaves the barrier, and starts its motion in real time ($\varphi_f = \phi_0$). The motion inside the rectangular and the triangular barrier must be connected, such that the initial velocity inside the triangular barrier is the final velocity after the particle leaves the rectangular barrier, $\frac{dx}{d\varphi}\Big|_{\varphi=\varphi'_s}$ (B.5). The change of the position of the particle while it traverses the triangular barrier is expressed as

$$\frac{dx^{\mathrm{II}}}{dt'} = -\frac{p_F \sin(\phi_0)\cosh(\psi_0)}{\omega} + \frac{U_0}{\omega^2\Delta}(\varphi - \varphi'_s) + \frac{p_F \sin(\varphi)}{\omega} + i\Big(\frac{\kappa_0}{\omega} - \frac{p_F \cos(\phi_0)\sinh(\psi_0)}{\omega}\Big). \tag{B.8}$$

The only term that depends on the initial complex time of the subbarrier motion in the region II, ψ'_0, is the linear term which comes from the contribution of the triangular barrier in Eq. (B.8). This is the main difference with respect to the velocity of the particle within the rectangular barrier, Eq. (4.26). In order to find the velocity of the particle, Eq. (B.8) must be multiplied by ω, following the Leibniz rule,

$$\frac{dx^{\mathrm{II}}}{dt'} = \omega \frac{dx}{d\varphi}. \tag{B.9}$$

Once the velocity has been obtained, the position can be found integrating the relation (B.8), from the initial time φ'_s, and taking into account that the initial position in the new motion is the final position once the particle has left the rectangular barrier, (B.2)

$$\begin{aligned} x^{\mathrm{II}}(\varphi) = {} & \Big(b + \frac{p_F \cos(\phi_0)\cosh(\psi'_0)}{\omega}\Big) + i\frac{p_F \sin(\phi_0)}{\omega}\big(-\sinh(\psi_0) - (\psi'_0 - \psi_0)\cosh(\psi_0)\big) \\ & - \Big(\frac{p_F \sin(\phi_0)\cosh(\psi_0)}{\omega} + i\Big(\frac{p_F \cos(\phi_0)\sinh(\psi_0)}{\omega} - \frac{\kappa_0}{\omega}\Big)\Big)(\varphi - \varphi'_s) \\ & + \frac{U_0\big(\varphi - \varphi'_s\big)^2}{2\omega^2\Delta} - \frac{p_F \cos(\varphi)}{\omega}. \end{aligned} \tag{B.10}$$

B.3. Physical motion after the barrier

At the time $t''_s = \phi_0/\omega$, the dynamics of the particle starts in real time. In accordance to ITM, during the real time motion, the velocity and the position of the particle are real measurable quantities, and they must be real. So, $\mathrm{Im}(x(\phi_0)) = Im(\frac{dx}{d\varphi}\big|_{\varphi=\phi_0}) = 0$. We should evaluate the velocity on the final time of the subbarrier motion, Eq. (B.8), and compare it with the condition given by ITM. Doing so, we obtain a relation that allows us to express the value of ψ'_0, the time of flight of the particle through the triangular barrier,

$$\psi'_0 = \frac{m\omega^2\Delta}{U_0}\Big(\frac{\kappa_0}{\omega} - \frac{p_F \cos(\phi_0)\sinh(\psi_0)}{\omega}\Big). \tag{B.11}$$

From Eq. (B.11) it is easy to tell that ψ'_0 is proportional to the width of the triangular barrier Δ. As the width of the barrier goes to 0, the time the particle takes to goes through the triangular barrier goes to 0 as well.

Now, evaluating the position, given by (B.10), at the final dimensionless "time " ϕ_0,

$$\begin{aligned} x^{\mathrm{II}}(\phi_0) = &\big(b + \frac{p_F\cos(\phi_0)\cosh(\psi_0')}{\omega}\big) + i\frac{p_F\sin(\phi_0)}{\omega}\big(-\sinh(\psi_0) - (\psi_0' - \psi_0)\cosh(\psi_0)\big) \\ &- \Big(\frac{p_F\sin(\phi_0)\cosh(\psi_0)}{\omega} + i\big(\frac{p_F\cos(\phi_0)\sinh(\psi_0)}{\omega} - \frac{\kappa_0}{\omega}\big)\Big)(-i\psi_0') \\ &- \frac{U_0\big(\psi_0'\big)^2}{2\omega^2\Delta} - \frac{p_F\cos(\psi_0)}{\omega}. \end{aligned} \tag{B.12}$$

Taking the imaginary part of the last equation, we obtain

$$\mathrm{Im}\left[x^{\mathrm{II}}(\phi_0)\right] \propto -\sinh(\psi_0) + \psi_0\cosh(\psi_0). \tag{B.13}$$

B.4. Final energy at the detector

At a particular real time $t_f' = \phi_1/\omega$, the particle leaves the triangular barrier, and only interacts with the nonstationary laser electric field. At ϕ_1, the position of the tunneling particle is $x(\phi_1) = b + \Delta$. Evaluating the position of the particle, Eq. (B.10) at the final dimensionless "time", $\varphi = \phi_1$, we find an expression in terms of the difference $\phi_1 - \phi_0$,

$$\begin{aligned} \Delta = &\frac{p_F\cos(\phi_0)\cosh(\psi_0')}{\omega} - \frac{p_F(\phi_1-\phi_0)\sin(\phi_0)\cosh(\psi_0)}{\omega} + \frac{\kappa_0\psi_0'}{\omega} \\ &- \frac{p_F\psi_0'\cos(\phi_0)\sinh(\psi_0)}{\omega} + \frac{U_0(\phi_1-\phi_0)^2}{2\omega^2\Delta} - \frac{U_0(\psi_0')^2}{2\omega^2\Delta} - \frac{p_F\cos(\phi_1)}{\omega}. \end{aligned} \tag{B.14}$$

If ψ_0' is expressed in terms of ψ_0 and ϕ_0, Eq. (B.11), and is replaced in the last expression Eq. (B.14), we obtain

$$\begin{aligned} \Delta = &\frac{p_F\cos(\phi_0)\cosh(\psi_0')}{\omega} - \frac{p_F(\phi_1-\phi_0)\sin(\phi_0)\cosh(\psi_0')}{\omega} + \frac{U_0(\psi_0')^2}{2\omega^2\Delta} + \\ &\frac{U_0(\phi_1-\phi_0)^2}{2\omega^2\Delta} - \frac{p_F\cos(\phi_1)}{\omega}. \end{aligned} \tag{B.15}$$

According to Eq. (B.11) in the limit of Δ going to 0, ψ_0' goes to zero as well. Additionally, if ϕ_1 is close to ϕ_0, then $\cos(\phi_1) \approx \cos(\phi_0) - (\phi_1 - \phi_0)\sin(\phi_0)$, and $\cosh(\psi_0') \approx 1 - \frac{(\psi_0')^2}{2}$. Taking the limit of Δ going to 0, in Eq. (B.15), a quadratic equation for $\phi_1 - \phi_0$ can be found, such that

$$\begin{aligned} &\frac{U_0\big(\phi_1-\phi_0\big)^2}{2\omega^2\Delta} - \frac{p_F(\phi_1-\phi_0)\sin(\phi_0)\big(\cosh(\psi_0)-1\big)}{\omega} \\ &+ \left(-\Delta + \Big(\frac{\omega^4\Delta^2}{U_0^2}\big(\frac{U_0}{2\omega^2\Delta} - \frac{p_F\cos(\phi_0)}{\omega}\big)\big(\frac{\kappa_0}{\omega} - \frac{p_F\cos(\phi_0)\sinh(\psi_0)}{\omega}\big)^2\Big)\right) = 0. \end{aligned} \tag{B.16}$$

Solving the quadratic equation, an expression can be found for the difference of the real "times", $\phi_1 - \phi_0$

$$\phi_1 - \phi_0 = \frac{\omega^2\Delta}{U_0}\Bigg(\frac{p_F\sin(\phi_0)\big(\cosh(\psi_0)-1\big)}{\omega} \pm \Bigg[\frac{p_F^2\sin^2(\phi_0)\big(\cosh(\psi_0)-1\big)^2}{\omega^2} + \frac{2U_0}{\omega^2}\Big(1-\big(\frac{\omega^4}{U_0^2}\big(\frac{U_0}{2\omega^2}-\frac{p_F\Delta\cos(\phi_0)}{\omega}\big)\big(\frac{\kappa_0}{\omega}-\frac{p_F\cos(\phi_0)\sinh(\psi_0)}{\omega}\big)^2\big)\Big)\Bigg]^{\frac{1}{2}}\Bigg). \tag{B.17}$$

Simplifying the last equation, a final relation for $\phi_1 - \phi_0$ is

$$\phi_1 - \phi_0 = \frac{p_F\omega\sin(\phi_0)\big(\cosh(\psi_0)-1\big)\Delta}{U_0}\Bigg\{1 \pm \Bigg[1+\Big(\frac{2U_0}{p_F^2\sin^2(\phi_0)\big(\cosh(\psi_0)-1\big)^2}\Big(1-\Big(\frac{\omega^2}{2U_0}\Big(1-\frac{2p_F\omega\cos(\phi_0)\Delta}{U_0}\Big)\Big(\frac{\kappa_0}{\omega}-\frac{p_F\cos(\phi_0)\sinh(\psi_0)}{\omega}\Big)^2\Big)\Big)\Bigg]^{\frac{1}{2}}\Bigg\}. \tag{B.18}$$

As Δ goes to 0, ϕ_1 goes to ϕ_0 as expected.

In order to find the velocity of the particle when it starts its motion in the region III, we evaluate its final velocity inside the triangular barrier at the time $t_s'' = \phi_1/\omega$,

$$v_\infty = -p_F\sin(\phi_0)\cosh(\psi_0) + \frac{U_0(\phi_1-\phi_0)}{\omega\Delta} - \frac{iU_0\psi_0'}{\omega\Delta} + p_F\sin(\phi_1) + i\Big(\kappa_0 - p_F\cos(\phi_0)\sinh(\psi_0)\Big). \tag{B.19}$$

Using ψ_0' from Eq. (B.11), we can see that the imaginary terms vanish and the final velocity of the subbarrier motion is real. Besides, since $\phi_1 - \phi_0$ is approximately zero as $\Delta \to 0$, $\sin(\phi_1)$ can be expanded in a Taylor series around ϕ_0. We take only the first term of the expansion, $\sin(\phi_1) \approx (\phi_1 - \phi_0)\sin(\phi_0)$. Replacing $\phi_1 - \phi_0$ from Eq. (B.18) and taking the limit as Δ goes to 0, the velocity at the final of the triangular barrier is expressed as

$$v_{\phi_1} = \pm p_F\sin(\phi_0)\big(\cosh(\psi_0)-1\big)\Bigg\{\Bigg[1+\Big(\frac{2U_0}{p_F^2\sin^2(\phi_0)\big(\cosh(\psi_0)-1\big)^2}\Big(1-\Big(\frac{\omega^2}{2U_0}\Big(\frac{\kappa_0}{\omega} - \frac{p_F\cos(\phi_0)\sinh(\psi_0)}{\omega}\Big)^2\Big)\Big)\Bigg]^{\frac{1}{2}}\Bigg\}. \tag{B.20}$$

In region III, the dynamics of the particle are only affected by the interaction with the monochromatic electric field. Its velocity as a function of the dimensionless parameter φ is exactly

$$v_{\text{new}} = v_{\phi_1} + p_F\sin(\varphi) - p_F\sin(\phi_1). \tag{B.21}$$

At the time t_{final}, long compared with the time the particle has left the tunneling barrier, $t_s'' = \phi_0/\omega$, the electric field is switched off adiabatically. We can easily find

the velocity that the particle has at t_{final}, which is

$$\begin{aligned} v_\infty = &-p_F \sin(\phi_0) \pm p_F \sin(\phi_0)\big(\cosh(\psi_0) - 1\big) \\ &\times \Bigg\{ \Bigg[1 + \Big(\frac{2U_0}{p_F^2 \sin^2(\phi_0)\big(\cosh(\psi_0) - 1\big)^2} \Big(1 - \Big(\frac{\omega^2}{2U_0} \Big(1 \\ &- \frac{2p_F \cos(\phi_0)\Delta}{\omega U_0} \Big) \Big(\kappa_0 - p_F \cos(\phi_0) \sinh(\psi_0) \Big)^2 \Big) \Big) \Big) \Bigg]^{\frac{1}{2}} \Bigg\}. \end{aligned} \tag{B.22}$$

All the implicit variables that are defined by the dynamics of the particle during its tunneling, ϕ_0, ψ_0 and ψ_0', are now expressed in terms of the measurable final kinetic energy,

$$E_F = \frac{v_\infty^2}{2}. \tag{B.23}$$

APPENDIX C

FIELD-FREE LIMIT FOR THE LASER ASSISTED TUNNELING THROUGH A RECTANGULAR BARRIER

In this Appendix we show that in the weak field limit the field-free decay rate

$$R_0 = \mathcal{P}_0^2 \exp(-2\mathrm{Im}W_0) \tag{C.1}$$

follows from the amplitude (3.41). Quantitatively, the weak field limit is determined by the condition (4.64) [CnPBP11]. Correspondingly, the subbarrier correction to the action is smaller than unity so that the imaginary part of the action is given by the field-free contribution W_0 (3.34). Since the momentum change during the subbarrier motion is also small, the initial velocity at the exit is $v(t_0) = p_0$ and then the final momentum is given by

$$p(t_0) = p_0 + p_F \sin\omega t\,. \tag{C.2}$$

We have assumed here a monochromatic field (3.14) for simplicity. The spectrum consists of $L = 2p_0p_F/\omega \gg 1$ ATI-like peaks with energies between $(p_0+p_F)^2/2$ and $(p_0-p_F)^2/2$. For the given momentum inside this interval, there are two solutions per period, so that

$$\begin{aligned} \omega t_{0n}^{(+)} &= \arcsin\left(\frac{p-p_0}{p_F}\right) + 2\pi n\,, \\ \omega t_{0n}^{(-)} &= \pi - \arcsin\left(\frac{p-p_0}{p_F}\right) + 2\pi n\,. \end{aligned} \tag{C.3}$$

In the limit we consider, the laser field only enters the action via these initial times t_0,

$$\begin{aligned} W &= W_0 + \int_{t_0}^{T} (p^2/2 + E_0)dt - px(T) + p_0 b \\ &= i\mathrm{Im}W_0 + \frac{1}{2}(p_0^2 - p^2)(T - t_0)\,, \end{aligned} \tag{C.4}$$

where T is the large observation time and we take into account that $x(t) \approx b + p(t - t_0)$. The sum over the laser periods gives

$$\sum_{n=0}^{N} \exp\left(i(p^2 - p_0^2)\frac{\pi n}{\omega}\right) \to \sum_j \delta\left(\frac{p^2 - p_0^2}{2\omega} - j\right)\,, \quad N \to \infty\,. \tag{C.5}$$

Then

$$dR = \frac{dw}{T} = \frac{\mathcal{P}_0^2(p_0)}{2\pi p_F}\exp(-2\mathrm{Im}W_0) \times \sum_j \delta\left(\frac{p^2-p_0^2}{2\omega}-j\right)\left|\frac{\exp(ij\omega t_0^{(+)})}{\sqrt{\cos\omega t_0^+}}-\frac{\exp(-ij\omega t_0^{(+)})}{\sqrt{-\cos\omega t_0^+}}\right|^2 dp\,. \quad \text{(C.6)}$$

Under the condition $p_0 p_F/\omega \gg 1$, the number of ATI-like peaks is large and the sum over j can be replaced by an integral which evaluates to 1. The resulting distribution should be integrated over dp within the limits $p_0 \pm p_F$. Taking into account that $\cos\omega t_0^+ = \sqrt{1-(p-p_0)^2/p_F^2}$ and disregarding the rapidly oscillating interference term in the modulus square, we obtain precisely the field-free rate (C.1).

APPENDIX D

THREE CONTRIBUTIONS TO THE SEMICLASSICAL ACTION FOR THE LASER-ASSISTED TUNNELING THROUGH A RECTANGULAR BARRIER

Integration of the kinetic energy

In order to integrate the kinematical term in the Lagrangian, the square of the velocity must be calculated. The velocity has been already calculated for the motion in the rectangular barrier potential, Eq. (4.26). Taking the square of this expression, we obtain

$$\begin{aligned}\left[\omega\frac{dx}{d\varphi}(\varphi)\right]^2 = &-\kappa_0^2 + \frac{2\kappa_0\mathcal{E}_0\cos(\phi_0)\sinh(\psi_0)}{\omega} - \frac{E_0^2\cos^2(\phi_0)\sinh^2(\psi_0)}{\omega^2} \\ &+ \frac{\mathcal{E}_0^2\sin^2(\varphi)}{\omega^2} + \frac{\mathcal{E}_0^2\sin^2(\phi_0)\cosh^2(\psi_0)}{\omega^2} + \frac{2i\kappa_0\mathcal{E}_0\sin(\varphi)}{\omega} \\ &- \frac{2i\mathcal{E}_0^2\cos(\phi_0)\sinh(\psi_0)\sin(\varphi)}{\omega^2} - \frac{2i\kappa_0\mathcal{E}_0\sin(\phi_0)\cosh(\psi_0)}{\omega} \\ &+ \frac{2i\mathcal{E}_0^2\sin(\phi_0)\cos(\phi_0)\sinh(\psi_0)\cosh(\psi_0)}{\omega^2} - \frac{2\mathcal{E}_0^2\sin(\phi_0)\cosh(\psi_0)\sin(\varphi)}{\omega^2}.\end{aligned} \tag{D.1}$$

Here, $\varphi = \phi_0 + i\psi$. Performing the integration of every single term, and multiplying by $\frac{1}{2\omega}$, then

$$\begin{aligned}\frac{1}{\omega}\int_{\varphi_0}^{\phi_0}\frac{1}{2}\left[\omega\frac{dx}{d\varphi}(\varphi)\right]^2 d\varphi = {} & \frac{i(V_0-E)\psi_0}{\omega} - \frac{i\kappa_0\mathcal{E}_0\psi_0\cos(\phi_0)\sinh(\psi_0)}{\omega^2} \\ & + \frac{i\mathcal{E}_0^2\psi_0\cos^2(\phi_0)\sinh^2(\psi_0)}{2\omega^3} - \frac{i\mathcal{E}_0^2\psi_0}{4\omega^3} - \frac{\mathcal{E}_0^2\sin(2\phi_0)}{8\omega^3} \\ & + \frac{\mathcal{E}_0^2\sin(2\phi_0)\cosh(2\psi_0)}{8\omega^3} + \frac{i\mathcal{E}_0^2\cos(2\phi_0)\sinh(2\psi_0)}{8\omega^3} \\ & - \frac{i\mathcal{E}_0^2\psi_0\sin^2(\phi_0)\cosh^2(\psi_0)}{2\omega^3} - \frac{i\kappa_0\mathcal{E}_0\cos(\phi_0)}{\omega^2} \\ & + \frac{i\kappa_0\mathcal{E}_0\cos(\phi_0)\cosh(\psi_0)}{\omega^2} + \frac{\kappa_0\mathcal{E}_0\sin(\phi_0)\sinh(\psi_0)}{\omega^2} \\ & + \frac{i\mathcal{E}_0^2\cos^2(\phi_0)\sinh(\psi_0)}{\omega^3} - \frac{i\mathcal{E}_0^2\cos^2(\phi_0)\sinh(\psi_0)\cosh(\psi_0)}{\omega^3} \\ & - \frac{\mathcal{E}_0^2\cos(\phi_0)\sin(\phi_0)\sin^2(\psi_0)}{\omega^3} - \frac{\kappa_0\mathcal{E}_0\psi_0\sin(\phi_0)\cosh(\psi_0)}{\omega^2} \\ & + \frac{\mathcal{E}_0^2\psi_0\sin(\phi_0)\cos(\phi_0)\sinh(\psi_0)\cosh(\psi_0)}{\omega^3} \\ & + \frac{\mathcal{E}_0^2\sin(\phi_0)\cosh(\psi_0)\cos(\phi_0)}{\omega^3} - \frac{\mathcal{E}_0^2\sin(\phi_0)\cosh^2(\psi_0)\cos(\phi_0)}{\omega^3} \\ & + \frac{i\mathcal{E}_0^2\sin^2(\phi_0)\cosh(\psi_0)\sinh(\psi_0)}{\omega^3}.\end{aligned} \tag{D.2}$$

Taking the imaginary part of the last relation, then the contribution of the kinematic term to the action can be obtained

$$\begin{aligned}\mathrm{Im}\left\{\frac{1}{\omega}\int_{\varphi_0}^{\phi_0}\frac{1}{2}\left[\omega\frac{dx}{d\varphi}(\varphi)\right]^2 d\varphi\right\} = {} & \frac{(V_0-E)\psi_0}{\omega} - \frac{\kappa_0\mathcal{E}_0}{\omega^2}\Big[\psi_0\cos(\phi_0)\sinh(\psi_0) + \cos(\phi_0) \\ & - \cos(\phi_0)\cosh(\psi_0)\Big] + \frac{\mathcal{E}_0^2\psi_0}{2\omega^3}\Big[\cos^2(\phi_0)\sinh^2(\psi_0) \\ & - \sin^2(\phi_0)\cosh^2(\psi_0)\Big] - \frac{\mathcal{E}_0^2\psi_0}{4\omega^3} \\ & + \frac{\mathcal{E}_0^2}{\omega^3}\Big[\cos^2(\phi_0)\sinh(\psi_0) - \cos^2(\phi_0)\sinh(\psi_0)\cosh(\psi_0) \\ & + \sin^2(\phi_0)\cosh(\psi_0)\sinh(\psi_0)\Big] + \frac{\mathcal{E}_0^2\cos(2\phi_0)\sinh(2\psi_0)}{8\omega^3}.\end{aligned} \tag{D.3}$$

The real part of the contribution of the kinematical term is given by

$$\begin{aligned}\mathrm{Re}\left\{\frac{1}{\omega}\int_{\varphi_0}^{\phi_0}\frac{m}{2}\Big(\omega\frac{dx}{d\varphi}(\varphi)\Big)^2 d\varphi\right\} = &-\frac{\mathcal{E}_0^2\sin(2\phi_0)}{8\omega^3}+\frac{\mathcal{E}_0^2\sin(2\phi_0)\cosh(2\psi_0)}{8\omega^3}\\ &+\frac{\kappa_0\mathcal{E}_0\sin(\phi_0)\sinh(\psi_0)}{\omega^2}-\frac{\mathcal{E}_0^2\cos(\phi_0)\sin(\phi_0)\sinh(\psi_0)^2}{\omega^3}\\ &-\frac{\kappa_0\mathcal{E}_0\psi_0\sin(\phi_0)\cosh(\psi_0)}{\omega^2}+\frac{\mathcal{E}_0^2\cos(\phi_0)\sin(\phi_0)\cosh(\psi_0)}{\omega^3}\\ &+\frac{\mathcal{E}_0^2\psi_0\cos(\phi_0)\sin(\phi_0)\sinh(\psi_0)\cosh(\psi_0)}{\omega^3}\\ &-\frac{\mathcal{E}_0^2\sin(\phi_0)\cos(\phi_0)\cosh(\psi_0)^2}{\omega^3}.\end{aligned} \tag{D.4}$$

Contribution of the nonstationary dipole interaction to the action

Once the kinematical contribution has been calculated, Eq. (D.3) the next step is to calculate the dipole interaction contribution to the action. Since the trajectory has been analytically found, Eq. (4.27), then, in accordance to Eq. (4.37), the contribution to the dipole interaction is given by

$$\begin{aligned}\frac{1}{\omega}\int_{\varphi_0}^{\phi_0}\mathcal{E}_0 x^{\mathrm{I}}(\varphi)\cos(\varphi)d\varphi = &\frac{a\mathcal{E}_0\sin(\phi_0)}{\omega}-\frac{a\mathcal{E}_0\sin(\phi_0)\cosh(\psi_0)}{\omega}-\frac{ia\mathcal{E}_0\cos(\phi_0)\sinh(\psi_0)}{\omega}\\ &+\frac{\mathcal{E}_0^2\cos(\phi_0)\cosh(\psi_0)\sin(\phi_0)}{\omega^3}-\frac{\mathcal{E}_0^2\cos(\phi_0)\cosh^2(\psi_0)\sin(\phi_0)}{\omega^3}\\ &-\frac{i\mathcal{E}_0^2\cos^2(\phi_0)\cosh(\psi_0)\sinh(\psi_0)}{\omega^3}-\frac{i\mathcal{E}_0^2\sin^2(\phi_0)\sinh(\psi_0)}{\omega^3}\\ &+\frac{i\mathcal{E}_0^2\sin^2(\phi_0)\sinh(\psi_0)\cosh(\psi_0)}{\omega^3}-\frac{\mathcal{E}_0^2\sin(\phi_0)\sinh^2(\psi_0)\cos(\phi_0)}{\omega^3}\\ &+\frac{\mathcal{E}_0^2\sin(\phi_0)\cos(\phi_0)\cosh(\psi_0)\left[\cosh(\psi_0)-1\right]}{\omega^3}\\ &-\frac{i\mathcal{E}_0^2\sin^2(\phi_0)\cosh(\psi_0)\left[\sinh(\psi_0)-\psi_0\right]}{\omega^3}\\ &-\frac{i\kappa_0\mathcal{E}_0\cos(\phi_0)\left[\cosh(\psi_0)-1\right]}{\omega^2}-\frac{\kappa_0\mathcal{E}_0\sin(\phi_0)\left[\sinh(\psi_0)-\psi_0\right]}{\omega^2}\\ &+\frac{i\mathcal{E}_0^2\cos^2(\phi_0)\sinh(\psi_0)\cosh(\psi_0)\left[\cosh(\psi_0)-1\right]}{\omega^3}\\ &+\frac{\mathcal{E}_0^2\cos(\phi_0)\sin(\phi_0)\sinh(\psi_0)\left[\sinh(\psi_0)-\psi_0\right]}{\omega^3}\\ &+\frac{i\mathcal{E}_0^2\psi_0}{2\omega^3}-\frac{\mathcal{E}_0^2\sin(2\phi_0)}{4\omega^3}+\frac{\mathcal{E}_0^2\sin(2\phi_0)\cosh(2\psi_0)}{4\omega^3}\\ &+\frac{i\mathcal{E}_0^2\cos(2\phi_0)\sinh(2\psi_0)}{4\omega^3}.\end{aligned} \tag{D.5}$$

The imaginary part of the last equation gives the contribution of the dipole interaction to the action

$$\begin{aligned}\mathrm{Im}\left[\frac{1}{\omega}\int_{\varphi_0}^{\phi_0}\mathcal{E}_0 x(\varphi)\cos(\varphi)d\varphi\right] = &-\frac{a\mathcal{E}_0\cos(\phi_0)\sinh(\psi_0)}{\omega} - \frac{\mathcal{E}_0^2\cos^2(\phi_0)\cosh(\psi_0)\sinh(\psi_0)}{\omega^3}\\ &- \frac{\mathcal{E}_0\sin^2(\phi_0)\sinh(\psi)}{\omega^3} + \frac{\mathcal{E}_0^2\sin^2(\phi_0)\sinh(\psi_0)\cosh(\psi_0)}{\omega^3}\\ &- \frac{\mathcal{E}_0^2\sin^2(\phi_0)\cosh(\psi_0)\left[\sinh(\psi_0)-\psi_0\right]}{\omega^3}\\ &- \frac{\kappa_0\mathcal{E}_0\cos(\phi_0)\left(\cosh(\psi_0)-1\right)}{\omega^2}\\ &+ \frac{\mathcal{E}_0^2\cos^2(\phi_0)\sinh(\psi_0)\cosh(\psi_0)\left[\cosh(\psi_0)-1\right]}{\omega^3}\\ &+ \frac{\mathcal{E}_0^2\psi_0}{2\omega^3} + \frac{\mathcal{E}_0^2\cos(2\phi_0)\sinh(2\psi_0)}{4\omega^3}.\end{aligned} \tag{D.6}$$

The real part of the contribution of the dipole interaction is given by

$$\begin{aligned}\mathrm{Re}\left[\frac{1}{\omega}\int_{\varphi_0}^{\phi_0}\mathcal{E}_0 x(\varphi)\cos(\varphi)d\varphi\right] = &\frac{a\mathcal{E}_0\sin(\phi_0)}{\omega} - \frac{a\mathcal{E}_0\sin(\phi_0)\cosh(\psi_0)}{\omega}\\ &+ \frac{\mathcal{E}_0^2\sin(\phi_0)\cos(\phi_0)\cosh(\psi_0)}{\omega^3}\\ &- \frac{\mathcal{E}_0^2\sin(\phi_0)\cos(\phi_0)\cosh(\psi_0)^2}{\omega^3}\\ &- \frac{\mathcal{E}_0^2\sin(\phi_0)\cos(\phi_0)\sinh(\psi_0)^2}{\omega^3}\\ &+ \frac{\mathcal{E}_0^2\sin(\phi_0)\cos(\phi_0)\cosh(\psi_0)\left[\cosh(\psi_0)-1\right]}{\omega^3}\\ &- \frac{\kappa_0\mathcal{E}_0\sin(\phi_0)\left[\sinh(\psi_0)-\psi_0\right]}{\omega^2}\\ &- \frac{\mathcal{E}_0^2\sin(2\phi_0)}{4\omega^3} + \frac{\mathcal{E}_0^2\sin(2\phi_0)\cosh(2\psi_0)}{4\omega^3}.\end{aligned} \tag{D.7}$$

Contribution of the static barrier

The final contribution to the action is given by the time independent terms in the Lagrangian, and the energy that appears in the definition of the action, Eq. (4.37). With that in mind, the third contribution is purely imaginary, so that

$$\frac{1}{\omega}\int_{\varphi_0}^{\phi_0}(E-V_0)d\varphi = \frac{i\psi_0(V_0-E)}{\omega} \tag{D.8}$$

Once the three contributions have been calculated, the total action can be expressed in terms of the complex time variables that determine the subbarrier motion.

APPENDIX E

LOW-FREQUENCY LIMIT EQUIVALENCE WITH STATIC ELECTRIC FIELD

In the low frequency limit, the trigonometric function in the monochromatic field $\mathcal{E}_0 \cos(\omega t')$ can be expandend, leading in the first order to a constant electric field $\mathcal{E}_0$. The equations of motion inside the barrier for a static field are

$$\frac{d^2x^{\mathrm{LF}}}{d\varphi^2} = \frac{\mathcal{E}_0}{\omega^2}. \tag{E.1}$$

The velocity and the position are given by[1]:

$$\frac{dx^{\mathrm{LF}}}{dt'} = i\kappa_0 + \frac{\mathcal{E}_0(\varphi - \varphi_s)}{\omega}, \tag{E.2}$$

and,

$$x^{\mathrm{LF}}(\varphi) = a + \frac{i\kappa_0\big((\varphi - \varphi_s)\big)}{\omega} + \frac{\mathcal{E}_0\big(\varphi - \varphi_s\big)^2}{2\omega^2}. \tag{E.3}$$

We introduce the additional triangular barrier, as detailed in Appendix B. The velocity of the particle entering the triangular barrier is expressed as

$$v_0' = \frac{i}{\omega}\kappa_0 + \frac{i\mathcal{E}_0\big(\psi_s' - \psi_s\big)}{\omega}. \tag{E.4}$$

In the case of the triangular barrier, $V(x) = -\frac{V_0}{\Delta}\big(x - b - \Delta\big)$, the equations of motion take a similar analytic behavior of the ones for a static electric field; the new "field" is the superposition of the constant electric field, and the field created due to the change of the linear potential, such that

$$\mathcal{E}_F = E_0 + \frac{V_0}{\Delta}. \tag{E.5}$$

[1] Using the same initial conditions $\frac{dx^{\mathrm{I}}}{dt'}\big|_{t'=t_s'} = \frac{i\kappa_0}{\omega}$, and $x^{\mathrm{I}}(\psi_0) = a$

Hence, the equation of motion is identically to the constant electric field, with the inclusion of this new field

$$\frac{d^2x^{\mathrm{II}}}{d\varphi^2} = \frac{\mathcal{E}_F}{\omega^2}. \tag{E.6}$$

The velocity and the position in the triangular barrier are given by

$$\frac{dx}{dt'} = i\Big(\kappa_0\frac{\mathcal{E}_0(\psi_0'-\psi_0)}{\omega}\Big) + \frac{V_0(\varphi-\varphi_s')}{\omega\Delta} + \frac{\mathcal{E}_0(\varphi-\varphi_s')}{\omega},$$

and

$$x(\varphi) = b + i\Big(\kappa_0\frac{\mathcal{E}_0(\psi_0'-\psi_0)}{\omega}\Big)(\varphi-\varphi_s') + \frac{V_0(\varphi-\varphi_s')^2}{2\omega\Delta} + \frac{\mathcal{E}_0(\varphi-\varphi_s')^2}{2\omega}. \tag{E.7}$$

At $\varphi = \phi_0$, when the particle exits the barrier, the imaginary part of the velocity goes to zero. The real part of the position is $b+\Delta$. Like in the case of the monochromatic case, the condition on the imaginary part of the final velocity allows to determine the value of ψ_0', the imaginary part of the subbarrier time inside the triangular barrier

$$\kappa_0 + \frac{\mathcal{E}_0(\psi_0'-\psi_0)}{\omega} - \frac{V_0\psi_0'}{\omega\Delta} - \frac{\mathcal{E}_0\psi_0'}{\omega} = 0. \tag{E.8}$$

From this last equation, ψ_0' can be written as

$$\psi_0' = \frac{\omega\Delta}{V_0}\left(\kappa_0 - \frac{\mathcal{E}_0\psi_0}{\omega}\right). \tag{E.9}$$

The requirement on the real part of the final position leads to

$$\Delta = \frac{\kappa_0\psi_0'}{\omega} + \frac{\mathcal{E}_0\psi_0\psi_0'}{\omega^2} - \frac{\mathcal{E}_0\psi_0'^2}{\omega^2} - \frac{V_0\psi_0'^2}{2\omega^2\Delta} + \frac{\mathcal{E}_0\psi_0'^2}{2\omega^2}. \tag{E.10}$$

At the time $\varphi = \phi_1$, the particle leaves the triangular barrier, and starts to interact only with the electric field. The velocity at that particular time is given by:

$$v_{\phi_1} = \frac{V_0(\phi_1-\phi_0)}{\omega\Delta} + \frac{\mathcal{E}_0(\phi_1-\phi_0)}{\omega}. \tag{E.11}$$

The condition on the final position at $\varphi = \phi_1$ is such that the real part must be equal to $b+\Delta$. This provides a relation between $(\phi_1-\phi_0)$ and Δ,

$$\begin{aligned}\Delta = {} & \frac{\psi_0'}{\omega}\kappa_0 + \frac{\mathcal{E}_0\psi_0'^2}{\omega^2} - \\ & \frac{\mathcal{E}_0\psi_0\psi_0'}{\omega^2} + \frac{V_0(\phi_1-\phi_0)^2}{2\omega^2\Delta} + \frac{\mathcal{E}_0(\phi_1-\phi_0)^2}{2\omega^2} - \frac{V_0\psi_0'^2}{2\omega^2\Delta} - \frac{\mathcal{E}_0\psi_0'}{2\omega^2}.\end{aligned} \tag{E.12}$$

Replacing the equation (E.9), into the last expression, an analytic definition for $\phi_1-\phi_0$ can be found,

$$\phi_1 - \phi_0 = \omega\Delta\sqrt{\frac{2}{V_0+\mathcal{E}_0\Delta} - \frac{1}{V_0^2}\left(\kappa_0 - \frac{\mathcal{E}_0\psi_0}{\omega}\right)^2}. \tag{E.13}$$

In the limit$\Delta \to 0$, we obtain for Eq. (E.11)

$$v_{\phi_1} = \sqrt{2V_0\left[1 - \frac{\omega^2}{2V_0}\left(\frac{1}{\omega}\kappa_0 - \frac{\mathcal{E}_0\psi_0}{\omega^2}\right)^2\right]}. \tag{E.14}$$

This final velocity is the initial velocity of the particle after leaving the barrier. Following the same procedure in Appendix B, and since $\phi_1 - \phi_0 \to 0$ as $\Delta \to 0$, the asymptotic velocity of the tunneling particle is

$$v_\infty = -\frac{\mathcal{E}_0\phi_0}{\omega} + \sqrt{2V_0\left[1 - \frac{\omega^2}{2V_0}\left(\frac{\kappa_0}{\omega} - \frac{\mathcal{E}_0\psi_0}{\omega^2}\right)^2\right]}. \tag{E.15}$$

Once this velocity has been calculated, it can be related with the final energy the particle has at the moment when the electric field is switched off,

$$\sqrt{2E_F} = -\frac{\mathcal{E}_0\phi_0}{\omega} + \sqrt{2V_0\left[1 - \frac{\omega^2}{2V_0}\left(\frac{\kappa_0}{\omega} - \frac{\mathcal{E}_0\psi_0}{\omega^2}\right)^2\right]}. \tag{E.16}$$

E.1. Calculation of the total action

There are three contributions to the action: the kinetic part, the dipole interaction and the stationary term.

E.1.1. Kinetic contribution

Since $v = i\kappa_0 + \mathcal{E}_0\left(\varphi - \varphi_s\right)/\omega$, the kinetic energy is given by

$$K(\varphi) = -(V_0 - E) + \frac{i\kappa_0\mathcal{E}_0(\varphi - \varphi_s)}{\omega} + \frac{\mathcal{E}_0^2(\varphi - \varphi_s)^2}{2\omega^2}. \tag{E.17}$$

Integrating over time, the kinetic part of the action is

$$\frac{1}{\omega}\int_{\phi_0 + i\psi_0}^{\phi_0} K(\varphi)d\varphi = \frac{2i\psi_0(V_0 - E)}{\omega} - \frac{i\kappa_0\mathcal{E}_0\varphi_s^2}{2\omega^2} + \frac{i\mathcal{E}_0^2\varphi_s^3}{6\omega^3}. \tag{E.18}$$

Taking the limit $\phi_0 \to 0$, and $\psi_0 \to 0$ simplifies the analytic expression that corresponds to the imaginary part of the kinematical contribution of the action for the case of the monochromatic field, (D.3). In this limit $\cos(\phi_0) \to 1$, $\sin(\phi_0) \to \phi_0 \to 0$, $\cosh(\psi_0) \approx 1 + \frac{\psi_0^2}{2}$, and $\sinh(\psi_0) \approx \psi_0 + \frac{\psi_0^3}{6}$[2]. With these approximations in mind, (D.3) takes the form:

$$\begin{aligned}\mathrm{Im}\left[\frac{1}{\omega}\int_{\phi_0 + i\psi_0}^{\phi_0} K d\varphi\right] \approx{}& \frac{(V_0 - E)\psi_0}{\omega} - \frac{\mathcal{E}_0}{\omega^2}\left(\psi_0^2 + \frac{\psi_0^4}{6} - \frac{\psi_0^2}{2}\right)\kappa_0 \\ &+ \frac{\mathcal{E}_0^2}{2\omega^3}\left(\psi_0^3 + \frac{\psi_0^5}{3} + \frac{\psi_0^7}{36}\right) - \frac{\mathcal{E}_0^2\psi_0}{4\omega^3} + \frac{\mathcal{E}_0^2}{\omega^3}\left(\psi_0 + \frac{\psi_0^3}{6} - \psi_0 - \frac{2\psi_0^3}{3}\right) \\ &+ \frac{\mathcal{E}_0^2\psi_0}{4\omega^3} + \frac{\mathcal{E}_0\psi_0^3}{6\omega^3}.\end{aligned} \tag{E.19}$$

[2]The expansion of ψ_0 is taken only up to the third order.

E.1.2. Dipole interaction

Since the dipole interaction is given by $x(\varphi)\mathcal{E}_0$, and the trajectory has been calculated explicitly, an analytic form of the contribution to the action can be expressed as

$$\frac{1}{\omega}\int_{\phi_0+i\psi_0}^{\phi_0} x(\varphi)\mathcal{E}_0 d\varphi = -\frac{ia\mathcal{E}_0\psi_0}{\omega} - \frac{i\mathcal{E}_0\psi_0^2}{2\omega^2}\kappa_0 + \frac{i\mathcal{E}_0^2\psi_0^3}{6\omega^3}. \tag{E.20}$$

In the limits of $\psi_0, \phi_0 \to 0$, the nonvanishing terms are

$$\begin{aligned}\mathrm{Im}\left[\frac{1}{\omega}\int_{\phi_0+i\psi_0}^{\phi_0} x(\varphi)\mathcal{E}_0 d\varphi\right] = &-\frac{a\mathcal{E}_0\psi_0}{\omega} - \frac{a\mathcal{E}_0\psi_0^3}{6\omega} - \frac{\mathcal{E}_0^2\psi_0}{\omega^3} - \frac{2\mathcal{E}_0^2\psi_0^3}{3\omega^3} - \frac{\mathcal{E}_0\psi_0^2}{2\omega^2}\kappa_0 \\ &+ \frac{\mathcal{E}_0^2}{2\omega^3}\left(\psi_0^3 + \frac{2\psi_0^5}{3}\right) + \frac{\mathcal{E}_0^2\psi_0}{2\omega} + \frac{\mathcal{E}_0^2\psi_0}{2\omega^3} + \frac{\mathcal{E}_0^2\psi_0^3}{3\omega^3}.\end{aligned} \tag{E.21}$$

Reducing the last expression, we obtain

$$\begin{aligned}\mathrm{Im}\left[\frac{1}{\omega}\int_{\phi_0+i\psi_0}^{\phi_0} x(\varphi)\mathcal{E}_0 d\varphi\right] &= -\frac{a\mathcal{E}_0\psi_0}{\omega} - \frac{a\mathcal{E}_0\psi_0^3}{6\omega} - \frac{\mathcal{E}_0\psi_0^2}{2\omega^2}\kappa_0 + \frac{\mathcal{E}_0^2\psi_0^3}{2\omega^3} + \frac{\mathcal{E}_0^2\psi_0^3}{3\omega^3} - \frac{2\mathcal{E}_0^2\psi_0^3}{3\omega^3}. \\ &= -\frac{a\mathcal{E}_0\psi_0}{\omega} - \frac{a\mathcal{E}_0\psi_0^3}{6\omega} - \frac{\mathcal{E}_0\psi_0^2}{2\omega^2}\kappa_0 + \frac{\mathcal{E}_0^2\psi_0^3}{6\omega^3}.\end{aligned} \tag{E.22}$$

E.1.3. Time independent term

In both cases of the time-dependent or static fields, the time-independent term is the same. Its contribution, therefore, does not depend on the approximation and has the exact solution (D.8).

E.1.4. Total action

The total action can be expressed as the sum of the three contributions, Eqs. (D.8), (E.18) and (E.20). Note that, in the case of the constant electric field, the three contributions are purely imaginary, such that the total action is also purely imaginary:

$$W = i\left[\frac{2\psi_0(V_0 - E)}{\omega} - \frac{\kappa_0\mathcal{E}_0\psi_0^2}{\omega^2} - \frac{a\mathcal{E}_0\psi_0}{\omega} + \frac{\mathcal{E}_0^2\psi_0^3}{3\omega^3}\right]. \tag{E.23}$$

In the case of the low frequency approximation, the total action is again identically imaginary, as in the case of the static barrier. However, there is an additional term that comes from the dipole interaction contribution to the action,

$$W = i\left[\frac{2\psi_0(V_0 - E)}{\omega} - \frac{\mathcal{E}_0\psi_0^2}{\omega^2}\kappa_0 - \frac{a\mathcal{E}_0\psi_0}{\omega} - \frac{a\mathcal{E}_0\psi_0^3}{6\omega} + \frac{\mathcal{E}_0^2\psi_0^3}{3\omega^3}\right]. \tag{E.24}$$

The expressions (E.23) and (E.24) are identical in the low-frequency limit, given that $\omega, \psi_0 \to 0$. Under these conditions, the additional term is negligible.

BIBLIOGRAPHY

[ALR87] H. J. Assenbaum, K. Langanke, and C. Rolfs. Effects of electron screening on low-energy fusion cross sections. Z. Phys. A: Hadron Nucl. , 327:461–468, 1987.

[Alt97] M. Altarelli. The european x-ray free electron laser: Technical design report. `http://www.xfel.eu/sites/site_xfel-gmbh/content/e63617/e79991/e68669/european-xfel-tdr_eng.pdf`, 1997.

[AP06] M. Altarelli and Deutsches Elektronen-Synchrotron (Center). X-Ray Free-Electron Laser Project. *XFEL: the European X-ray free-electron laser : technical design report*. DESY (Series). DESY XFEL Project Group, 2006.

[AS64] M. Abramowitz and I. A. Stegun. *Handbook of Mathematical Functions with Formulas, Graphs, and Mathematical Tables*. Dover Publications, New York, 1964.

[Bas03] D. N. Basu. Folding model analysis of alpha radioactivity. J. Phys. G: Nucl. Part. Phys. , 29(9):2079, 2003.

[BC73] D. M. Brink and J. J. Castro. Alpha clustering effects in nuclear matter. Nucl. Phys. A , 216(1):109 – 124, 1973.

[BCM92] Buck B., Merchant A. C., and Perez S. M. Favoured alpha decays of odd-mass nuclei. J. Phys. G: Nucl. Part. Phys. , 18(1):143, 1992.

[BdPZ99] C. A. Bertulani, D. T. de Paula, and V. G. Zelevinsky. Bremsstrahlung radiation by a tunneling particle: A time-dependent description. Phys. Rev. C , 60:031602 – 031606, Aug. 1999.

[BEK06] T. J.. Bürvenich, J. Evers, and C. H. Keitel. Nuclear quantum optics with x-ray laser pulses. Phys. Rev. Lett. , 96:142501 – 142505, Apr. 2006.

[BF66] V. F. Bunkin and M. V. Fedorov. Bremsstrahlung in a strong radiation field. Sov. Phys. JETP , 22:844 – 847, 1966.

[BJMP96] B. Buck, J. C. Johnston, A. C. Merchant, and S. M. Perez. Cluster model of α decay and ^{212}Po. Phys. Rev. C , 53:2841, Jun. 1996.

[BK06] D. Bauer and P. Koval. QPROP: A Schrodinger-solver for intense laser-atom interaction. *Comput. Phys. Commun.*, 174(5):396 – 421, Mar 2006.

[BL82] M. Buttiker and R. Landauer. Traversal time for tunneling. Phys. Rev. Lett. , 49(23):1739 – 1742, 1982.

[BM89] B. Buck and A. C. Merchant. Cluster-Model calculations of exotic decays from heavy-nuclei. Phys. Rev. C , 39(5):2097, May 1989.

[BMB05] D. Bauer, D. B. Milosevic, and W. Becker. Strong-field approximation for intense-laser-atom processes: The choice of gauge. Phys. Rev. A , 72(2), Aug 2005.

[BMP90a] B. Buck, A. C. Merchant, and S. M. Perez. New look at α decay of heavy nuclei. Phys. Rev. Lett. , 65(24):2975 – 2977, Dec 1990.

[BMP90b] B. Buck, A.C. Merchant, and S.M. Perez. New look at alpha decay of heavy nuclei. Phys. Rev. Lett. , 65:2975, 1990.

[BMP91] B. Buck, A. C. Merchant, and S. M. Perez. Ground state to ground state alpha decays of heavy even-even nuclei. J. Phys. G: Nucl. Part. Phys. , 17(8):1223, 1991.

[BMP92] B. Buck, A. C. Merchant, and S. M. Perez. α decay calculations with a realistic potential. Phys. Rev. C , 45(5):2247 – 2253, May 1992.

[BMSS83] W. Becker, G. T. Moore, R. R. Schlicher, and M. O. Scully. A note on total cross-sections and decay-rates in the presence of a laser field. Phys. Lett. A , 94(3 – 4):131 – 134, 1983.

[BPZ69] A. I. Baz, A. M. Perelomov, and Y. B. Zel'dovich. *Scattering, reactions and decay in nonrelativistic quantum mechanics.* Israel Program for Scientific Translations, Jerusalem, 1969. Trans. from the Russian.

[Bri26] L Brillouin. The ondulatory mechanics of Schrodinger; A general method of resolution by successive approximations. *COMPTES RENDUS HEBDOMADAIRES DES SEANCES DE L ACADEMIE DES SCIENCES*, 183:24 – 27, 1926.

[BSS84a] W. Becker, R. R. Schlicher, and M. O. Scully. A no-go theorem concerning the enhancement of Nuclear Decays by intense radiation-fields. Phys. Lett. A , 101(1):58 – 60, 1984.

[BSS84b] W. Becker, R. R. Schlicher, and M. O. Scully. Forbidden Nuclear Beta-Decay in an intense plane-wave field. Nucl. Phys. A , 426(1):125 – 136, 1984.

[CL10] National Nuclear Data Center and Brookhaven National Laboratory. Nudat 2.5: Search and plot nuclear structure and decay data interactively. `http://http://www.nndc.bnl.gov/nudat2/`, 2010.

[CnC07] Héctor Mauricio Castañeda Cortés. Characteristic times in quantum decays. Master's thesis, Universidad de los Andes, Carrera 1 18A-10, Bloque Ip,Bogotá, Colombia, 2007. Director: Dr. Neelima G. Kelkar.

[CnPBP11] H. M. Castañeda, S. V. Popruzhenko, D. Bauer, and A. Palffy. Laser-assisted decay of quasistationary states. New J. Phys. , 13, Jun. 2011.

[Cor93] P. B. Corkum. Plasma perspective on strong field multiphoton ionization. Phys. Rev. Lett. ., 71:1994 – 1997, Sep 1993.

[Del10] D. S. Delion. *Semiclassical Approach*, volume 819 of *Lecture Notes in Physics*. Springer Berlin / Heidelberg, 2010.

[DG96] M. I. Dyakonov and I. V. Gornyi. Electromagnetic radiation by a tunneling charge. Phys. Rev. Lett. , 76:3542 – 3545, May 1996.

[Elt65] L. R. B. Elton. *Introductory nuclear theory, by L. R. B. Elton.* Pitman - London, 2nd ed. edition, 1965. Page 168.

[Eme75] G.T. Emery. Perturbation of nuclear decay rates. *Ann. Rev. Nucl. Sc.*, 22:165, 1975.

[EMVP09] S. Eliezer, J. M. Martinez Val, and M. Piera. Alpha decay perturbations by atomic effects at extreme conditions. Phys. Lett. B , 672:372, 2009.

[EWL04] R. C. Ewing, W. J. Weber, and J. Lian. Nuclear waste disposal-pyrochlore (A(2)B(2)O(7)): Nuclear waste form for the immobilization of plutonium and "minor" actinides. *J. Appl. Phys.*, 95(11, Part 1):5949 – 5971, Jun. 2004.

[Fai73] F. H. M. Faisal. Multiple absorption of laser photons by atoms. J. Phys. B: At. Mol. Opt. Phys. , 6(4):L89, 1973.

[Fey48] R. P. Feynman. Space-time approach to non-relativistic quantum mechanics. Rev. Mod. Phys. , 20:367 – 387, Apr. 1948.

[FH65] R. P. Feynman and A. R. Hibbs. *Quantum Mechanics and Path Integrals.* McGraw-Hill, New York, 1965.

[Fre07] M. Freer. The clustered nucleus - cluster structures in stable and unstable nuclei. *Rep. Prog. Phys.*, 70(12):2149 – 2210, Dec 2007.

[FSB02] C. F. D. Faria, H. Schomerus, and W. Becker. High-order above-threshold ionization: The uniform approximation and the effect of the binding potential. Phys. Rev. A , 66(4), Oct 2002.

[FZ99] V. V. Flambaum and V. G. Zelevinsky. Radiation corrections increase tunneling probability. Phys. Rev. Lett. , 83:3108 – 3111, Oct 1999.

[Gam28] G. Gamow. Zur quantentheorie des atomkernes. Z. Phys. A: Hadron Nucl. , 51:204 – 212, 1928.

[GC29] R. W. Gurney and E. U. Condon. Quantum mechanics and radioactive disintegration. Phys. Rep. , 33(2):127 – 140, Feb 1929.

[GK87] S. A. Gurvitz and G. Kalbermann. Decay width and the shift of a quasistationary state. Phys. Rev. Lett. , 59(3):262 – 265, Jul 1987.

[GMN01] R. Guardiola, I. Moliner, and M. A. Nagarajan. Alpha-cluster model for 8be and 12c with correlated alpha particles. Nucl. Phys. A , 679(3 – 4):393 – 409, 2001.

[GN11] H. Geiger and J. M. Nuttall. The ranges of the alpha particles from various radioactive substances and a relation between range and period of transformation. Philos. Mag. , 22:613 – 621, Jul - Dec 1911.

[GN12] H. Geiger and J. M. Nuttall. The ranges of the alpha particles from uranium. Philos. Mag. , 23:439 – 445, Jan - June 1912.

[GP90] A. Galindo and P. Pascual. *Quantum mechanics*. Number v. 1 in Texts and monographs in physics. Springer-Verlag, 1990.

[GP99] S. P. Goreslavskii and S. V. Popruzhenko. Rescattering and quantum interference near the classical cut-offs. J. Phys. B: At. Mol. Opt. Phys. , 32(19):L531– L538, Oct 1999.

[Gur88] S. A. Gurvitz. Novel approach to tunneling problems. Phys. Rev. A , 38:1747 – 1759, Aug. 1988.

[HDWW53] F. Hoyle, D. N. F. Dunbar, W.A. Wenzel, and W. Whaling. A state in 12c predicted from astrophysical evidence. *Phys. Rev.*, 92:1095, 1953.

[Het09] Hetzheim, H. *Ionization and bound-state relativistic quantum dynamics in laser-driven multiply charged ions*. PhD thesis, Ruprecht-Karls Universität Heidelberg, 2009. Referees: Hon.-Prof. Dr. Keitel, C. H. and Prof. Dr. Ulrich, J. H. .

[HNS91] F. X. Hartmann, D. W. Noid, and Y. Y Sharon. Semiclassical model of Nuclear Energy Transfer by Electronic Motion in Intense Ultrashort - Wavelength Laser Fields. *Laser Phys.*, 5(2):371 – 378, 1991.

[HRG+11] Y. Huismans, A. Rouzee, A. Gijsbertsen, J. H. Jungmann, A. S. Smolkowska, P. S. W. M. Logman, F. Lepine, C. Cauchy, S. Zamith, T. Marchenko, J. M. Bakker, G. Berden, B. Redlich, A. F. G. van der Meer, H. G. Muller, W. Vermin, K. J. Schafer, M. Spanner, M. Yu. Ivanov, O. Smirnova, D. Bauer, S. V. Popruzhenko, and M. J. J. Vrakking. Time-Resolved Holography with Photoelectrons. *Science*, 331(6013), Jan 2011.

[HVDS08] S. L. Haan, J. S. Van Dyke, and Z. S. Smith. Recollision excitation, electron correlation, and the production of high-momentum electrons in double ionization. Phys. Rev. Lett. , 101:113001 – 113005, Sep 2008.

[ICLD91] A. Insolia, P. Curutchet, R. J. Liotta, and D. S. Delion. Microscopic Description of Alpha-Decay of Deformed-Nuclei. Phys. Rev. C , 44(1):545 – 547, Jul. 1991.

[IM85] B. I. Ivlev and V. I. Melnikov. Dramatic stimulation of tunneling by an RF field. *JETP Lett.*, 41(3):142 – 145, 1985.

[JBNW+07] H. B. Jeppesen, J. Byskov-Nielsen, P. Wright, J. G. Correia, L. M. Fraile, H. O. U. Fynbo, K. Johnston, and K. Riisager. Alpha-decay half-life of Fr-221 in different environments. *Eur. Phys. J. A*, 32(1):31, Apr. 2007.

[Jef25] H. Jeffreys. On certain approximate solutions of lineae differential equations of the second order. *P. Lond. Math. Soc.*, s2-23(1):428–436, 1925.

[JMT+08] U.D. Jentschura, A.I. Milstein, I.S. Terekhov, H. Boie, H. Scheit, and D. Schwalm. Quasiclassical description of bremsstrahlung accompanying alpha decay including quadrupole radiation. Phys. Rev. C , 77:014611, 2008.

[KBSR06] K. U. Kettner, H. W. Becker, F. Strieder, and C. Rolfs. High-Z electron screening: the cases V-50(p,n)Cr-50 and Lu-176(p,n)Hf-176. J. Phys. G: Nucl. Part. Phys. , 32(4):489, Apr. 2006.

[KCn07] N. G. Kelkar and H. M. Castañeda. Critical view of WKB decay widths. Phys. Rev. C , 76(6), 2007.

[Kel65] L. V. Keldysh. Ionization in the Field of a Strong Electromagnetic Wave. Sov. Phys. JETP , 20(5):1307, 1965.

[KI09] F. Krausz and M. Ivanov. Attosecond physics. *Rev. Mod. Phys.*, 81:163 – 234, Feb. 2009.

[Kra26] H. A. Kramers. Wellenmechanik und halbzahlige quantisierung. Z. Phys. A: Hadron Nucl. , 39:828 – 840, 1926.

[Lan32] L. D. Landau. *Phys. Z. Sowjetunion*, 1:88, 1932.

[Lan37] R. E. Langer. On the connection formulas and the solutions of the wave equation. Phys. Rep. , 51(8):669 – 676, Apr 1937.

[LL77] L. D. Landau and E. M. Lifshitz. *Quantum Mechanics: Non-relativistic theory*, volume 3 of *Course of Theoretical Physics*. Pergamon Press, Oxford; New York, third edition, 1989, c1977.

[LMM+03] K. W. D. Ledingham, J. Magill, P. McKenna, J. Yang, J. Galy, R. Schenkel, J. Rebizant, T. McCanny, S. Shimizu, L. Robson, R. P. Singhal, M. S. Wei, S. P. D. Mangles, P. Nilson, K. Krushelnick, R. J. Clarke, and P. A. Norreys. Laser-driven photo-transmutation of 129 i, a long-lived nuclear waste product. *J. Phys. D: Appl. Phys.*, 36:L79 – L97, 2003.

[Man57] H. J. Mang. Zur Theorie des Alpha-zerfalls - (Insbesondere der Kerne in der umbegung von PB208). *Z. Physik*, 148(5):582 – 592, 1957.

[Man60] H. J. Mang. Calculation of α-transition probabilities. Phys. Rep. , 119:1069 – 1075, Aug. 1960.

[ME69] P. Marmier and Sheldon E. *Physics of Nuclei and Particles, Volume I.* Academic Press Inc.., 1969.

[MO03] S. P. Maydanyuk and V. S. Olkhovsky. Does sub-barrier bremsstrahlung in α-decay of ^{210}po exist? *Progr. Theoret. Phys.*, 109(2):203 – 211, 2003.

[MOG+09] S.P. Maydanyuk, V.S. Olkhovsky, G. Giardina, G. Fazio, G. Mandaglio, and M. Manganaro. Bremsstrahlung emission accompanying alpha-decay of deformed nuclei. Nucl. Phys. A , 823(1-4):38 – 46, 2009.

[Moh08] P. Mohr. alpha-cluster states in intermediate mass nuclei. *The Open Nuclear and Particle Physics Journal*, 1:1, 2008.

[MPBB06] D. B. Milosevic, G. G. Paulus, D. Bauer, and W. Becker. Above-threshold ionization by few-cycle pulses. J. Phys. B: At. Mol. Opt. Phys. , 39(14):R203 – R262, Jul 2006.

[MSE+03] J. Magill, H. Schwoerer, F. Ewald, J. Galy, R. Schenkel, and R. Sauerbrey. Laser transmutation of iodine-129. *Appl. Phys. B-Laser Opt.*, 77(4):387, Oct. 2003.

[NR64] A. I. Nikishov and V. I. Ritus. Quantum processes in the field of a plane electromagnetic wave and in a constant field. II. *Zh. Eksp. Teor. Fiz.*, pages 1768 – 1781, 1964.

[OR07] P. O. G. Ogunbade and S. A. Rakityansky. New theories of alpha-radioactivity. *S. Afr. J. Sci.*, 103(3 – 4):155 – 158, Mar. - Apr. 2007.

[PA04] G. Platero and R. Aguado. Photon-assisted transport in semiconductor nanostructures. Phys. Rep. -*Review Section of Physics Letters*, 395(1 –2):1 – 157, May 2004.

[PB75] M. A. Preston and R. K. Bhaduri. *Structure of the nucleus, by M. A. Preston and R. K. Bhaduri.* Addison-Wesley Pub. Co., Advanced Book Program, Reading, Mass., 1975.

[PB98] T. Papenbrock and G. F. Bertsch. Bremsstrahlung in α decay. Phys. Rev. Lett. , 80:4141 – 4144, May 1998.

[PB08] S. V. Popruzhenko and D. Bauer. Strong field approximation for systems with Coulomb interaction. J. Mod. Opt. , 55(16):2573 – 2589, 2008.

[PEK08] A. Pálffy, J. Evers, and C. H. Keitel. Electric-dipole-forbidden nuclear transitions driven by super-intense laser fields. Phys. Rev. C , 77:044602 – 044611, Apr. 2008.

[PISG84] D. N. Poenaru, M. Ivascu, A. Sandulescu, and W. Greiner. Spontaneous emission of heavy clusters. J. Phys. G: Nucl. Part. Phys. , 10(8):L183, 1984.

[PKP68] V. S. Popov, V. P. Kuznetsov, and A. M. Perelomov. Quasiclassical Approximation for Nonstationary Problems. Sov. Phys. JETP , 26(1):222, 1968.

[PMPB08] S. V. Popruzhenko, V. D. Mur, V. S. Popov, and D. Bauer. Strong Field Ionization Rate for Arbitrary Laser Frequencies. Phys. Rev. Lett. , 101(19), Nov 2008.

[PMPB09] S. B. Popruzhenko, V. D. Mur, V. S. Popov, and D. Bauer. Multiphoton ionization of atoms and ions by high-intensity X-ray lasers. Sov. Phys. JETP , 108(6):947 – 962, Jun 2009.

[Pop04] V. S. Popov. Tunnel and multiphoton ionization of atoms and ions in a strong laser field (Keldysh theory). *Phys. Usp.*, 47(9):855 – 885, Sep 2004.

[Pop05] V. S. Popov. Imaginary-time method in quantum mechanics and field theory. Phys. At. Nucl. , 68(4):686 – 708, Apr. 2005.

[Pop10] S. V. Popruzhenko. About switching off the field. private communication, Jan. 2010.

[PP67] A. M. Perelomov and V. S. Popov. Ionization of Atoms in an alternating electric field .3. Sov. Phys. JETP , 25(2):336, 1967.

[PP10] A. Pálffy and S. V. Popruzhenko. From amplitude to probability. private communication, Aug. 2010.

[PPB08] S. V. Popruzhenko, G. G. Paulus, and D. Bauer. Coulomb-corrected quantum trajectories in strong-field ionization. Phys. Rev. A , 77(5, Part b), May 2008.

[Pre47] M. A. Preston. The theory of alpha-radioactivity. Phys. Rep. , 71(12):865 – 877, June 1947.

[R.91] Peierls R. *More surprises in theoretical physics.* Princeton: University Press, 1991.

[Ran77] A. Ranfagni. Wkb approximation in multidimensional problems. Phys. Lett. A , 62(6):395 – 396, 1977.

[Raz03] M. Razavy. *Quantum theory of tunneling.* World Scientific Publishing Co. Pte. Ltd., 2003. Chapter 5.

[Rei80] H. R. Reiss. Effect of an intense Electromagnetic-Field on a weakly bound system. Phys. Rev. A , 22(5):1786 – 1813, 1980.

[Rei92] H.R. Reiss. Theoretical methods in quantum optics: S-matrix and keldysh techniques for strong-field processes. *Prog. Quant. Electron.*, 16(1):1 –71, 1992.

[Rut99] E. Rutherford. Uranium radiation. Philos. Mag. , 47:109 – 163, 1899.

[RVB+08] Götz R., C. Vockenhuber, L. Buchmann, R. Woods, C. Ruiz, S. Lapi, and D. Bemmerer. Precise measurement of the β decay and electron capture of ^{22}Na, ^{198}Au, and ^{196}Au in low-temperature metal hosts, and reexamination of lifetime modifications. Phys. Rev. C , 77:065502 – 065508, Jun. 2008.

[S.98] Matinyan S. Lasers as a bridge between atomic and nuclear physics. *Phys. Rep.*, 298(4):199 – 249, 1998.

[SAAH+08] R. Salomaa, P. Aarnio, J. Ala-Heikkila, A. Hakola, and M. Santala. Laser-enhanced radioactive decay and selective transmutation of nuclei revisited. *Energy Convers. Manage.*, 49(7, SI):1910, Jul 2008. 13th International Conference on Emerging Nuclear Energy Systems, Istanbul, TURKEY, JUN 03-08, 2007.

[Sal54] E. E. Salpeter. Electron screening and thermonuclear reactions. *Aust. J. Phys.*, 7(3):373 – 388, 1954.

[SL79] G. R. Satchler and W. G. Love. Folding model potentials from realistic interactions for Heavy-Ion Scattering. Phys. Rep. , 55(3):183, 1979.

[SLZ+10] J. Su, Z. H. Li, L. C. Zhu, G. Lian, X. X. Bai, Y. B. Wang, B. Guo, B. X. Wang, S. Q. Yan, S. Zeng, Y. J. Li, E. T. Li, S. J. Jin, X. Liu, Q. W. Fan, J. L. Zhang, X. Y. Jiang, J. X. Lu, X. F. Lan, X. Z. Tang, and W. P. Liu. Alpha decay half-life of (147)Sm in metal samarium and Sm(2)O(3). *Eur. Phys. J. A*, 46(1):69, Oct 2010.

[Sri06] P. B. B. Srivastava. *Nuclear Physics*. Rastogi Publications, 2006.

[SRSC01] F. Strieder, C. Rolfs, C. Spitaleri, and P. Corvisiero. Electron-screening effects on fusion reactions. *Naturwissenschaften*, 88, 2001.

[SSI08] O. Smirnova, M. Spanner, and M. Ivanov. Analytical solutions for strong field-driven atomic and molecular one- and two-electron continua and applications to strong-field problems. Phys. Rev. A , 77(3), Mar. 2008.

[SSL+07] N. J. Stone, J. R. Stone, M. Lindroos, P. Richards, M. Veskovic, and D. A. Williams. On the absence of appreciable half-life changes in alpha emitters cooled in metals to 1 Kelvin and below. Nucl. Phys. A , 793:1 – 19, Sep. 2007.

[Taj09] T. Tajima. Scientific advisory committee: Report on the eli science. `http://www.extreme-light-infrastructure.eu/reports.php`, 2009.

[Tho54] R. G. Thomas. A formulation of the theory of alpha-particle decay from time-independent equations. *Progr. Theoret. Phys.*, 12(3):253 – 264, 1954.

[TNH+99] N. Takigawa, Y. Nozawa, K. Hagino, A. Ono, and D. M. Brink. Bremsstrahlung in α decay. Phys. Rev. C , 59:R593–R597, Feb. 1999.

[Tul05] J. K. Tuli. *Nuclear Wallet Cards*. Brookhaven National Laboratory, 2005.

[TWH92] D. R. Tilley, H. R. Weller, and G. M. Hale. Energy-levels of Light-Nuclei A = 4. Nucl. Phys. A , 541(1):1 – 104, May 1992.

[TWP62] Y. C. Tang, K. Wildermuth, and L. D. Pearlstein. Interpretation of generalized cluster wave functions. Nucl. Phys. , 32:504 – 509, 1962.

[V.97] Fedorov M. V. *Atomic and Free Electrons in a Strong Light Field*. World Scientific Pub. Co., 1997.

[VLL92] K. Varga, R. G. Lovas, and R. J. Liotta. Absolute alpha-Decay width of Po-212 in a combined shell and cluster model. Phys. Rev. Lett. , 69(1):37, Jul. 1992.

[WE47] E. P. Wigner and L. Eisenbud. Higher angular momenta and long range interaction in resonance reactions. Phys. Rep. , 72:29 – 41, Jul. 1947.

[Wen26] G. Wentzel. Eine verallgemeinerung der quantenbedingungen fr die zwecke der wellenmechanik. Z. Phys. A: Hadron Nucl. , 38:518 – 529, 1926.

[Win54] G. H. Winslow. Alpha-decay theory and a surface well potential. Phys. Rep. , 96:1032–1044, Nov 1954.

[WVB+10] F. Wauters, B. Verstichel, M. Breitenfeldt, V. De Leebeeck, V. Yu. Kozlov, I. Kraev, S. Roccia, G. Soti, M. Tandecki, E. Traykov, S. Van Gorp, D. Zákoucký, and N. Severijns. Half-life of ^{221}Fr in si and au at 4 k and at millikelvin temperatures. Phys. Rev. C , 82:064317, Dec. 2010.

[XR05] C. Xu and Z. Z. Ren. Favored [alpha]-decays of medium mass nuclei in density-dependent cluster model. Nucl. Phys. A , 760(3 – 4):303 – 316, 2005.

[XR06] C. Xu and Z. Z. Ren. New deformed model of alpha-decay half-lives with a microscopic potential. Phys. Rev. C , 73(4), Apr. 2006.

[YPVB10] Tian-Min Yan, S. V. Popruzhenko, M. J. J. Vrakking, and D. Bauer. Low-Energy Structures in Strong Field Ionization Revealed by Quantum Orbits. Phys. Rev. Lett. , 105(25), Dec 2010.

[Zel61] Ya B. Zeldovich. On the theory of Unstable States. Sov. Phys. JETP , 12(3):542 – 545, 1961.

[Zin07] N. T. Zinner. Alpha decay rate enhancement in metals: An unlikely scenario. Nucl. Phys. A , 781(1):81, Jan 2007.

ACKNOWLEDGMENTS

I could start recalling every moment of joy that I have experienced in this three years and all the memories come to my mind like a flashback. The hard moments, the joy of pursuing a dream, all those instants that make this whole experience unique, and a reason to be grateful for.

I would like to thank first Prof. Dr. Christoph H. Keitel, who gave the opportunity to do research for three years in his group and whose kind words were appreciated in those dark moments during the journey. I am definitely in debt with Dr. Adriana Pálffy, my supervisor. I can't thank enough for all the advices, the corrections, the innumerable moments of joy. Dr. Pálffy gave me the opportunity to come to Heidelberg, and made everything that was possible in order to pursue my goals as a physicist. I appreciate each one of our meetings, and it has been an honor to work with you. You have given me the tools to continue my work in science, and I really would like to thank you for your patience in these three years, your support even in the darkest moments. Thank you for the hard work and the energy you put in order to complete the projects that allow me to write this thesis. And thank you specially for the corrections to my english, which I can say it was quite hard to read.

I also would like to thank Dr. Sergei Popruzhenko. His guidance and hard work were inspirational and all his suggestions, ideas and physical discussions gave us a light in those moments when there was no path to follow. I sincerely appreciate each one of the meetings and fruitful discussions about physics and the fact that I could go to you when I have some doubts regarding what I was working on at the moment. Thank you for your prompt reply to my questions, and for all the hard work you did in order to get meaningful results in our project.

I would like to thank Prof. Dr. Dieter Bauer. Thank you for hosting me that week in Rostock, which was a key week for the development of the project. I won't forget that Sergei and you were the first ones who welcomed me back in 2008, in a rainy day, when I come from Colombia, disoriented and with a huge jetlag. Thank you for the hard work and the amazing numerical results that were fundamental in our understanding of the analytical results we got in the LAT through the rectangular barrier.

I would like to thank as well Prof. Dr. Dirk Dubbers for accepting being part of

my Thesis Committee and read the present work. Also, I would like to thank Dr. Sandro Wimberger and Prof. Dr. Klaus Pfleisticker for accepting to be part of my Thesis Committee.

I would like to thank my colleagues from my office: Dr. Mathias Ruf, Dr. Markus Kohler, Anis Dadi, Dr, Hossein Ebadi, Gabor Darvasi and Katja Beckerle, who created a wonderful environment to work in the office. It was a wonderful environment, and I hope I had not disturbed you a lot. In particular, I would like to acknowledge Dr. Kohler and Katja for their help with the abstract in German of the present thesis. I would like to thank Katja for the chocolates specially in the final days of the writing up. I would like to thank Wen-Te Liao, Dr. Sumanta Das as well for the dinners and the conversations. I would like to acknowledge Dr. Selym Villalba. I really enjoy so much the conversations about football, the lunchs we have shared and all the help you gave me, specially during the final part of the present thesis.

Also, I would like to thank Ms. Sibel Babacan, who was really kind, and helpful with all the procedures and burocratic issues. I would like also to thank Peter Brunner and Dominik Hertel, our system administrators, who were eager to solve any kind of problem regarding the cluster or the computers we use.

I also would like to thank Huayu Hu for the kindest words she gave me in moments of need and support. I sincerely hope we can meet in the future again. And also, I would like to greet Dr. Octavian Postavaru, for all the invitations and the conversations. I could not accept all of them, but I really appreciate those moments I could share with you.

In particular, I would like to thank Mari Chikvaidze, Nicolaas Brantjes and Dr. Michael Siomau. It was such a nice privilege to meet you and I am quite grateful to share all this experience with you. Specially, Mari, you have given me the strength when I was lacking of it. One of the most dearest things I have found in this experience is your friendship. I can only express from my bottom of my heart a thank you to you and your wonderful family.

I would like to thank Dr. Neelima Kelkar, who allowed me to take the chance to go abroad. I enjoyed so much working with you, and I will be forever grateful for all your advices and your patience. I have been lucky to have such a wonderful advisor during my Bachelor and Masters, and you are one of the main reasons why I could follow my dreams abroad. I will always be in debt with you.

I also would like to thank my Colombian friends: Ana Lucía, Paola, Camila and Julio. Ana, you have been my best friend for such a long time. And as I have said so many times, I could not consider how this experience would be without you at my side. I sincerely thank you for every advice, every coffee, every moment I have shared with you. I have been blessed to have such a wonderful friend. To Paula, Camila and Julio, thank you for the laughter and those moments I won't ever forget. For the patience in those moments of stress and for bringing a smile whenever I need it. Thank you for the delightful colombian meals.

I would like to thank my friends, Juan Andrés, José Luis, Daniel, Germán David, William Javier, Camilo Andrés, Edgar Mauricio. Specially for those kind words and the patience when the things were not going as good as I wanted to. I would like to specially thank Juan Andrés, José Luis and Germán David who were the biggest

support in those moments of frustration and who gave me the strength to pursue my dreams.

I specially would like to thank my girlfriend, Rowan. You have been an angel that came into my life, and there is not a single moment in which I can't express how happy I am to meet you. Thank you for the proofreading, for the patience you have to endure those long journeys through grammar, for those beautiful smiles you have given me and that became the energy I needed to continue working. Thank you for all the cups of tea and the special moments we have shared, the next more special than the last one. And thank you specially for your support at every single moment.

I would like to share this work in particular with my family. There is not a single moment in which I do not miss those persons who belong in my heart. They are the main reason why I have reached my goals, and I keep going in order to make my dreams come true. I just love you with all my heart, and I am so proud of you.

This work is specially dedicated to my parents, my beloved parents who are the persons I love the most. Regardless of the distance, I have shared every moment and every new experience I have had the privilege to live in this experience. And I am quite grateful about it. I owe everything to them. They are my biggest pride and my joy, the persons I am most proud of. This work is specially dedicated to you. You were the main reason why I am here, and why I decided to follow my dreams. No matter what kind of words can I come with, I would never be able to express my full gratitude towards them. I only wish that this work would make them proud as I am sincerely proud of them.